



รายงานวิจัยฉบับสมบูรณ์

โครงการ เซนเซอร์ทางเคมีและอุปกรณ์อิเล็กทรอนิกส์จากโมเลกุลอินทรีย์

โดย ศาสตราจารย์ ดร. รัชชัย ตันทุลานี

เมษายน 2556

สัญญาเลขที่ RTA5080006

รายงานวิจัยฉบับสมบูรณ์

โครงการ เซนเซอร์ทางเคมีและอุปกรณ์อิเล็กทรอนิกส์จากโมเลกุลอินทรีย์

ศาสตราจารย์ ดร. รัชชัย ตันทุลานี
ภาควิชาเคมี คณะวิทยาศาสตร์ จุฬาลงกรณ์มหาวิทยาลัย

สนับสนุนโดยสำนักงานคณะกรรมการการอุดมศึกษา
และสำนักงานกองทุนสนับสนุนการวิจัย

(ความเห็นในรายงานนี้เป็นของผู้วิจัย สกอ. และ สกว. ไม่จำเป็นต้องเห็นด้วยเสมอไป)

Executive Summary

Objective

To synthesize molecular receptors for cations, anions and amino acids and to gain basic knowledge in ion receptors including the applications of synthesized molecules as sensors using techniques such as ion selective electrode, optode, UV-visible and fluorescence spectrophotometry.

Research results

- Benzothiazole derivatives of calix[4]arene were synthesized and used as ionophores in PVC membrane electrodes. Sensing properties of the electrodes were examined using a potentiometer. The prepared electrodes were able to detect Ag^+ selectively and were used to detect Ag^+ in silver nanoparticles (AgNPs) solution effectively. The electrodes were used to detect glucose employing AgNPs as a redox marker. In addition, PVC optode membranes containing lead ionophores and indicators were used to detect lead ion in water samples using Uv-vis spectrophotometry. This topic produced 4 papers as shown in appendices 1, 3, 6 and 12.
- Derivatives of calix[4]arene containing amidoferrocene were synthesized and employed as anion receptors and sensors. This topic produced 2 papers as shown in appendices 2 and 10.
- Derivative of anthraquinone, naphthoimidazoledione containing boronic acid and BF_2 -curcumin were synthesized and used as anion sensors detecting by Uv-vis and fluorescence spectrophotometers. This topic produced 4 papers as shown in appendices 5, 8, 13 and 15.
- Receptors for tryptophan were synthesized from acridine-based thioureas, steroidal urea and azobenzene. This topic produced 2 papers as shown in appendices 9 and 14.
- Calix[4]arene-based dinuclear copper and zinc complexes were synthesized and used to detect pyrophosphate by indicator displacement assays. This topic produced 3 papers as shown in appendices 4, 7 and 11.

บทคัดย่อ

เลขที่สัญญา: RTA5080006

ชื่อโครงการ: เซนเซอร์ทางเคมีและอุปกรณ์อิเล็กทรอนิกส์จากโมเลกุลอินทรีย์

ผู้ดำเนินการวิจัย:

หัวหน้าโครงการ: ศาสตราจารย์ ดร. ธวัชชัย ตันสุลานี

ภาควิชาเคมี คณะวิทยาศาสตร์ จุฬาลงกรณ์มหาวิทยาลัย

E-mail Address: tthawatc@chula.ac.th

ระยะเวลาดำเนินโครงการ: 31 กรกฎาคม 2550 ถึง 30 กรกฎาคม 2553

วัตถุประสงค์:

สังเคราะห์โมเลกุลรีเซปเตอร์สำหรับแคทไอออน แอนไอออน และ กรดอะมิโน สร้างองค์ความรู้ใหม่ทางด้านไอออนรีเซปเตอร์ รวมทั้งนำโมเลกุลที่สังเคราะห์ได้มาทำเป็นเซนเซอร์โดยใช้เทคนิคไอออนเซเลกทีฟอิเล็กโทรด (ion selective electrode) ออปโทด (optode) ยูวีวิสิเบิลและฟลูออเรสเซนส์สเปกโตรโฟโตเมทรี

ระเบียบวิธีวิจัย:

- การสังเคราะห์สารต่างๆ อาศัยกระบวนการเคมีอินทรีย์สังเคราะห์ แล้วศึกษาสมบัติการเป็นรีเซปเตอร์ของสารที่สังเคราะห์ได้ต่อไอออนและโมเลกุลต่างๆ โดยวิธีโปรตอนเอ็นเอ็มอาร์ไทเทรชัน เทคนิคไซคลิกโวลแทมเมทรี สแควร์เวฟโวลแทมเมทรี เทคนิคยูวีวิสิเบิลและฟลูออเรสเซนส์สเปกโตรโฟโตเมทรี
- นำสารที่สังเคราะห์ได้บางชนิดไปสร้างไอออนเซเลกทีฟเมมเบรนอิเล็กโทรดและออปโทดสำหรับตรวจวัดไอออนของโลหะด้วยวิธีโพเทนชิโอเมทรีและยูวีวิสิเบิลสเปกโตรโฟโตเมทรี
- สารที่สังเคราะห์ได้บางชนิดถูกนำไปพัฒนาเป็นเซนเซอร์สำหรับแอนไอออนด้วยเทคนิคการแทนที่อินดิเคเตอร์

ผลที่ได้รับ:

- ได้ทำการสังเคราะห์อนุพันธ์เบนโซไทอาโซลคาลิกซ์[4]เอรีนชนิดต่างๆ แล้วนำไปเป็นไอโอโนฟอร์ในพีวีซีพอลิเมอร์เมมเบรนอิเล็กโทรด ทำการตรวจวัดกับไอออนโลหะต่างๆ ด้วยโพเทนชิโอมิเตอร์ พบว่าพอลิเมอร์เมมเบรนอิเล็กโทรดที่เตรียมขึ้นมีการเลือกจำเพาะกับโลหะเงินสามารถนำไปตรวจวัดปริมาณไอออนของโลหะเงินในสารละลายอนุภาคนาโนของโลหะเงินได้ผลอย่างดีเยี่ยม ต่อมาได้ประยุกต์ใช้อิเล็กโทรดที่สร้างขึ้นนี้ในการตรวจวัดปริมาณน้ำตาลกลูโคสโดยใช้อนุภาคนาโนของโลหะเงินเป็นตัวให้สัญญาณ นอกจากนี้ยังได้ใช้พีวีซีพอลิเมอร์เมมเบรนออปโทดที่ผสมกับไอโอโนฟอร์สำหรับไอออนโลหะตะกั่วและอินดิเคเตอร์ในการตรวจวัดปริมาณของตะกั่วในตัวอย่างน้ำด้วยยูวีวิสิเบิลสเปกโตรโฟโตเมทรี

- ได้ทำการสังเคราะห์อนุพันธ์ของคาลิกซ์[4]เอรีนที่เชื่อมต่อกับเฟอร์โรซีนเอไมด์ เพื่อใช้เป็นแอนไอออนรีเซปเตอร์และแอนไอออนเซนเซอร์
- ได้ทำการสังเคราะห์อนุพันธ์ของแอนทราควิโนน อนุพันธ์ของ Naphthoimidazoledione ที่เชื่อมกับบอโรนิกแอซิด และอนุพันธ์ BF₂-curcumin เพื่อใช้เป็นแอนไอออนเซนเซอร์ โดยวิธีการตรวจวัดด้วยยูวีวิสิเบิลและฟลูออเรสเซนส์สเปกโตรโฟโตมิเตอร์
- ได้ทำการสังเคราะห์รีเซปเตอร์สำหรับกรดแอมิโนทริปโตเฟน (tryptophan) จากอนุพันธ์ของไทโอยูเรียที่มีแอคริดีน (acridine-based thiourea) และจากอนุพันธ์ของ steroidal urea และเอโซเบนซีน
- ได้ทำการสังเคราะห์อนุพันธ์ไดนิวเคลียร์คอปเปอร์และซิงค์ ซึ่งมีคาลิกซ์[4]เอรีนเป็นโครงสร้างฐาน แล้วนำไปใช้เป็นเซนเซอร์สำหรับไพโรฟอสเฟต (pyrophosphate) ด้วยวิธีการแทนที่อินดิเคเตอร์ (indicator displacement assay)

คำสำคัญ: คาลิกซ์[4]เอรีน ไอออนเซเลกทิฟอิเล็กโทรด ออปโตด การแทนที่อินดิเคเตอร์ แอนไอออนรีเซปเตอร์ เซนเซอร์

Abstract

Project Code: RTA5080006

Project Title: Chemical sensors and electronic devices from organic molecules

Investigator:

Project head: Professor Dr. Thawatchai Tuntulani

Department of Chemistry, Faculty of Science, Chulalongkorn University

E-mail Address: tthawatc@chula.ac.th

Project Period: July 31, 2007 to July 30, 2010

Objectives:

To synthesize molecular receptors for cations, anions and amino acids and to gain basic knowledge in ion receptors including the applications of synthesized molecules as sensors using techniques such as ion selective electrode, optode, UV-visible and fluorescence spectrophotometry.

.

Methodology:

- Syntheses of molecular receptors were carried out by standard organic synthetic methods. Binding properties of receptors towards ions and molecules were studied by NMR titrations, cyclic and squarewave voltammetry, UV-visible and fluorescence spectrophotometry.
- Some synthesized compounds were used as ionophores in ion selective membrane electrodes and optodes employing potentiometry and UV-visible spectrophotometry as detection methods.

- Some synthesized compounds were applied as sensors by employing indicator displacement assays

Results:

- Benzothiazole derivatives of calix[4]arene were synthesized and used as ionophores in PVC membrane electrodes. Sensing properties of the electrodes were examined using a potentiometer. The prepared electrodes were able to detect Ag^+ selectively and were used to detect Ag^+ in silver nanoparticles (AgNPs) solution effectively. The electrodes were used to detect glucose employing AgNPs as a redox marker. In addition, PVC optode membranes containing lead ionophores and indicators were used to detect lead ion in water samples using Uv-vis spectrophotometry.
- Derivatives of calix[4]arene containing amidoferrocene were synthesized and employed as anion receptors and sensors.
- Derivative of anthraquinone, naphthoimidazoledione containing boronic acid and BF_2 -curcumin were synthesized and used as anion sensors detecting by Uv-vis and fluorescence spectrophotometers.
- Receptors for tryptophan were synthesized from acridine-based thioureas, steroidal urea and azobenzene.
- Calix[4]arene-based dinuclear copper and zinc complexes were synthesized and used to detect pyrophosphate by indicator displacement assays.

Keywords: calix[4]arene, ion selective electrode, optode, indicator displacement assay, anion receptor, sensor

เนื้อหางานวิจัยโดยสรุป

ในโครงการนี้มีงานวิจัยที่ประสบความสำเร็จดังต่อไปนี้

- ได้ทำการสังเคราะห์อนุพันธ์เบนโซไทอาโซลคาลิกซ์[4]เอรีนชนิดต่างๆ แล้วนำไปเป็นไอโอโนฟอร์ในพีวีซีพอลิเมอร์กเมมเบรนอิเล็กโทรด ทำการตรวจวัดกับไอออนโลหะต่างๆ ด้วยโพเทนชิโอมิเตอร์ พบว่าพอลิเมอร์กเมมเบรนอิเล็กโทรดที่เตรียมขึ้นมีการเลือกจำเพาะกับโลหะเงิน สามารถนำไปตรวจวัดปริมาณไอออนของโลหะเงินในสารละลายอนุภาคนาโนของโลหะเงินได้ผลอย่างดียิ่ง ต่อมาได้ประยุกต์ใช้อิเล็กโทรดที่สร้างขึ้นนี้ในการตรวจวัดปริมาณน้ำตาลกลูโคสโดยใช้อนุภาคนาโนของโลหะเงินเป็นตัวให้สัญญาณ นอกจากนี้ยังได้ใช้พีวีซีพอลิเมอร์กเมมเบรนออปโตดที่ผสมกับไอโอโนฟอร์สำหรับไอออนโลหะตะกั่วและอินดิเคเตอร์ในการตรวจวัดปริมาณของตะกั่วในตัวอย่างน้ำด้วยยูวีวิสซิบิลิสเปกโทรโฟโตเมทรี มีผลงานตีพิมพ์ 4 เรื่องดังนี้
1. Synthesis of Novel Calix[4]arenes Having Benzothiazolylacetamidoalkoxy Pendants and Their Potential Application as Ag^+ -Selective Electrodes *Bull. Kor. Chem. Soc.* **2008**, 29, 221-224. (ภาคผนวก 1)
 2. New Silver Selective Electrode Fabricated From Benzothiazole Calix[4]arene: Speciation Analysis of Silver Nanoparticles *Sens. Actuat. B-Chem.* **2008**, 134, 377-385. (ภาคผนวก 3)
 3. Novel Potentiometric Approach in Glucose Biosensor Using Silver Nanoparticles as Redox Marker *Sens. Actuat. B-Chem.* **2009** 137, 320-326. (ภาคผนวก 6)
 4. Bulk Optode Sensors for Batch and Flow-through Determinations of Lead Ion in Water Samples *Talanta* **2010**, 82, 660-667. (ภาคผนวก 12)
- ได้ทำการสังเคราะห์อนุพันธ์ของคาลิกซ์[4]เอรีนที่เชื่อมต่อกับเฟอร์โรซีนเอไมด์ เพื่อใช้เป็นแอนไอออนรีเซปเตอร์และแอนไอออนเซ็นเซอร์ มีผลงานตีพิมพ์ 2 เรื่องดังนี้

1. Synthesis and Characterization of Monomeric and Dimeric Structures of Calix[4]arenes Containing Amidoferrocene *J. Chem. Cryst.* **2008**, 38, 363-368.

(ภาคผนวก 2)

2. Structural and Conformational investigations of Chiral bis(phenylamido)ferrocenes by X-ray Crystallography and Density Functional Calculations *J. Mol. Struct.* **2009**, 938, 117-124. (ภาคผนวก 10)

- ได้ทำการสังเคราะห์อนุพันธ์ของแอนทราควิโนน อนุพันธ์ของ Naphthoimidazoledione ที่เชื่อมกับบอโรนิกแอซิด และอนุพันธ์ BF₂-curcumin เพื่อใช้เป็นแอนไอออนเซ็นเซอร์ โดยวิธีการตรวจวัดด้วยวิธีสเปกโตรโฟโตเมตริกและฟลูออเรสเซนส์สเปกโตรโฟโตเมตริก มีผลงานตีพิมพ์ 4 เรื่อง ดังนี้

1. Synthesis, Optical and Electrochemical Properties of New Anion Receptors and Sensors Containing Anthraquinone and Benzimidazole Units *Tetrahedron* **2008**, 64, 10619-10624. (ภาคผนวก 5)

2. A-D-A Sensors Based on Naphthoimidazoledione and Boronic Acid as Turn-On Cyanide Probes in Water *J. Org. Chem.* **2009**, 74, 3919-3922. (ภาคผนวก 8)

3. Synthesis, Photophysical Properties and Cyanide Detection in Aqueous Solutions of BF₂-Curcumin Dyes *Tetrahedron* **2010**, 66, 6217-6223. (ภาคผนวก 13)

4. A Selective Spectrofluorometric Determination of Micromolar Level of Cyanide in Water Using Naphthoquinone Imidazole Boronic-Based Sensors and a Surfactant Cationic CTAB Micellar System *J. Fluoresc.* **2011**, 21, 1179-1187.

(ภาคผนวก 15)

- ได้ทำการสังเคราะห์รีเซ็ปเตอร์สำหรับกรดแอมิโนทริปโตเฟน (tryptophan) จากอนุพันธ์ของไทโอยูเรียที่มีแอคริดีน (acridine-based thiourea) และจากอนุพันธ์ของ steroidal urea และเอโซเบนซีน มีผลงานตีพิมพ์ 2 เรื่อง ดังนี้

1. Synthesis, Optical and Electrochemical Properties of New Anion Receptors and Sensors Containing Anthraquinone and Benzimidazole Units *Tetrahedron* **2008**, 64, 10619-10624. (ภาคผนวก 9)
2. Enantioselective Receptor Based on Steroidal Urea and Azobenzene for L-Tryptophan *Tetrahedron* **2010**, 66, 7423-7428. (ภาคผนวก 14)

- ได้ทำการสังเคราะห์อนุพันธ์ไดนิวเคลียร์คอปเปอร์และซิงค์ ซึ่งมีคาลิกซ์[4]เอรีนเป็นโครงสร้างฐาน แล้วนำไปใช้เป็นเซ็นเซอร์สำหรับไพโรฟอสเฟต (pyrophosphate) ด้วยวิธีการแทนที่อินดิเคเตอร์ (indicator displacement assay) มีผลงานตีพิมพ์ 3 เรื่อง ดังนี้

1. Selective Detection of Pyrophosphate by New Tripodal Amine Calix[4]arene-Based Cu(II) Complexes Using Indicator Displacement Strategy" *Tetrahedron Lett* **2010**, 51, 3398-3402. (ภาคผนวก 11)
2. Synthesis and Crystal Structure Analysis of Thiourea-Pendant Pyridines" *J. Chem. Cryst.* **2009**, 39, 348-352. (ภาคผนวก 7)
3. Diaqua{2,6-bis[N-(2-pyridinylmethyl)carbamoyl]phenolato- K^2O^1, O^2 }zinc(II) *Acta Cryst. E* **2008**, E64, m884-885. (ภาคผนวก 4)

Output ที่ได้จากโครงการ

ผลงานที่ได้รับการตีพิมพ์

ผลการวิจัยได้รับการตีพิมพ์จำนวน 15 เรื่องดังต่อไปนี้

1. Morakot, N.; Ngeontae, W.; Aeungmaitrepirom, W.; Tuntulani, T. "Synthesis of Novel Calix[4]arenes Having Benzothiazolylacetamidoalkoxy Pendants and Their Potential Application as Ag^+ -Selective Electrodes" *Bull. Kor. Chem. Soc.* **2008**, 29, 221-224.
2. Suksai, C.; Leeladee, P.; Jennings, C.; Tuntulani, T.; Kongsaree, P. "Synthesis and Characterization of Monomeric and Dimeric Structures of Calix[4]arenes Containing Amidoferrocene" *J. Chem. Cryst.* **2008**, 38, 363-368.
3. Ngeontae, W.; Janrungroatsakul, W.; Morakot, N.; Aeungmaitrepirom, W.; Tuntulani, T. "New Silver Selective Electrode Fabricated From Benzothiazole Calix[4]arene: Speciation Analysis of Silver Nanoparticles" *Sens. Actuat. B-Chem.* **2008**, 134, 377-385.
4. Suksai, C.; Watchasit, S.; Tuntulani, T.; Pakawatchai, C. "Diaqua{2,6-bis[N-(2-pyridinylmethyl)carbamoyl]phenolato- $\text{K}^2\text{O}^1, \text{O}^2$ }zinc(II)" *Acta Cryst. E* **2008**, E64, m884-885.
5. Wannalerse, B.; Tomapatanaget, B.; Tuntulani, T. "Synthesis, Optical and Electrochemical Properties of New Anion Receptors and Sensors Containing Anthraquinone and Benzimidazole Units" *Tetrahedron* **2008**, 64, 10619-10624.
6. Ngeontae, W.; Janrungroatsakul, W.; Maneewattanapinyo, P.; Egkasit, S.; Aeungmaitrepirom, W.; Tuntulani, T. "Novel Potentiometric Approach in Glucose

Biosensor Using Silver Nanoparticles as Redox Marker" *Sens. Actuat. B-Chem.*

2009 137, 320-326.

7. Suksai, C.; Pakawatchai, C.; Tuntulani, T. "Synthesis and Crystal Structure Analysis of Thiourea-Pendant Pyridines" *J. Chem. Cryst.* **2009**, 39, 348-352.
8. Jamkratoke, M.; Ruangpornvisuti, V.; Tumcharern, G.; Tuntulani, T.; Tomapatanaget, B. "A-D-A Sensors Based on Naphthoimidazoledione and Boronic Acid as Turn-On Cyanide Probes in Water" *J. Org. Chem.* **2009**, 74, 3919-3922.
9. Sirikulajorn, A.; Duanglaor, P.; Ruangpornvisuti, V.; Tomapatanaget, B.; Tuntulani, T. "Tryptophan Receptors Containing Acridine-Based Thiourea" *Supramol. Chem.* **2009**, 21, 486-494.
10. Suksai, C.; Leeladee, P.; Tuntulani, T.; Ruangpornvisuti, V.; Chaichit, N. "Structural and Conformational Investigations of Chiral bis(phenylamido)ferrocenes by X-ray Crystallography and Density Functional Calculations" *J. Mol. Struct.* **2009**, 938, 117-124.
11. Watchasit, S.; Kaowliew, A.; Suksai, C.; Tuntulani, T.; Ngeontae, W.; Pakawatchai, C. "Selective Detection of Pyrophosphate by New Tripodal Amine Calix[4]arene-Based Cu(II) Complexes Using Indicator Displacement Strategy" *Tetrahedron Lett* **2010**, 51, 3398-3402.
12. Baulom, C.; Ngeontae, W.; Nitiyanotakit, S.; Ngamukot, P.; Tuntulani, T.; Aeungmaitrepirom, W. "Bulk Optode Sensors for Batch and Flow-through Determinations of Lead Ion in Water Samples" *Talanta* **2010**, 82, 660-667.

13. Chaicham, A.; Kulchat, S.; Tumcharern, G.; Tuntulani, T.; Tomapatanaget, B.
“Synthesis, Photophysical Properties and Cyanide Detection in Aqueous
Solutions of BF₂-Curcumin Dyes” *Tetrahedron* **2010**, 66, 6217-6223.
14. Sirikulajorn, A.; Tuntulani, T.; Ruangpornvisuti, V.; Tomapatanaget, B.; Davis, A.
P. “Enantioselective Receptor Based on Steroidal Urea and Azobenzene for L-
Tryptophan” *Tetrahedron* **2010**, 66, 7423-7428.
15. Jamkratoke, M.; Tumcharern, G.; Tuntulani, T.; Tomapatanaget, B. “A Selective
Spectrofluorometric Determination of Micromolar Level of Cyanide in Water
Using Naphthoquinone Imidazole Boronic-Based Sensors and a Surfactant
Cationic CTAB Micellar System” *J. Fluoresc.* **2011**, 21, 1179-1187.

ผลงานตีพิมพ์ข้างต้นได้แสดงไว้ในภาคผนวก 1-15 ตามลำดับ

การสร้างนักวิจัยใหม่

ในโครงการนี้ได้เป็นส่วนหนึ่งในสร้างนักวิจัยในสถาบันการศึกษาทั้งภายในและภายนอก

จุฬาลงกรณ์มหาวิทยาลัยดังต่อไปนี้

- ผศ.ดร.บุษยรัตน์ ธรรมพัฒน์กิจ ภาควิชาเคมี คณะวิทยาศาสตร์ จุฬาลงกรณ์มหาวิทยาลัย
- ผศ.ดร.วัลภา เอื้องไมตรีภิมย์ ภาควิชาเคมี คณะวิทยาศาสตร์ จุฬาลงกรณ์มหาวิทยาลัย
- ผศ.ดร.จอมใจ สุกใส ภาควิชาเคมี คณะวิทยาศาสตร์ มหาวิทยาลัยบูรพา
- ผศ.ดร.วิทยา เงินแท้ ภาควิชาเคมี คณะวิทยาศาสตร์ มหาวิทยาลัยขอนแก่น

นอกจากนี้ยังได้สร้างนักวิจัยทั้งในระดับปริญญาโทและเอกประมาณ 10 คน

Synthesis of Novel Calix[4]arenes Having Benzothiazolylacetamidoalkoxy Pendants and Their Potential Application as Ag⁺-selective Electrodes

Neramit Morakot, Wittaya Ngeontae, Wanlapa Aeungmaitrepirom,* and Thawatchai Tuntulani*

Department of Chemistry, Faculty of Science, Chulalongkorn University, Bangkok 10330, Thailand

*E-mail: tthawatc@chula.ac.th

Received September 11, 2007

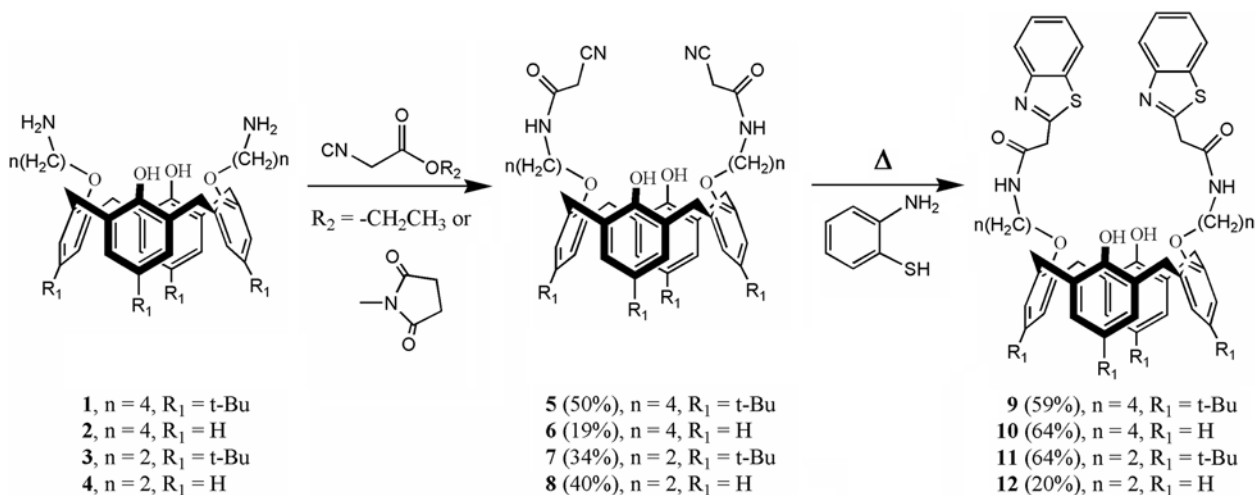
Key Words : Calix[4]arene, Membrane electrode, Ion selective electrode

Calix[4]arenes, a class of macrocyclic compounds, are superb supramolecular building block for fabricating ion and molecular receptors.¹ Appropriately functionalized calix[4]arenes have been used as carriers in ion selective membranes. Predominantly, calixarenes containing ester, ether, carboxylic acid and carbamate have been reported for using as ion-selective electrode (ISE) for alkali metal ions.^{2,3} Only few calixarene derivatives reported by Reinhoudt and Kim have been employed as ISE for heavy metal ions such as Cu²⁺, Hg²⁺ and Cd²⁺.^{4,5} Kimura and coworkers reported calix[4]arene derivatives incorporating substituents such as allyl, benzyl and propargyl groups being used as soft neutral carrier for silver ion sensors.⁶ Mercaptobenzothiazole-appended calix[4]arene was used as Ag⁺-ISE which showed the selectivity towards Ag⁺ with good discrimination against Hg²⁺.⁷

We are interested in the development of new Ag⁺ receptors for use as ionophores in Ag⁺-selective electrodes. Herein, we report syntheses of compounds **9** and **10** bearing two benzothiazolylacetamidobutoxy groups at the narrow rim of *p*-*tert*-butylcalix[4]arene and compounds **11** and **12** consisting of benzothiazolylacetamidoethoxy groups on the narrow rim of calix[4]arene. The preliminary studies using the synthesized compounds for Ag⁺-selective electrodes towards metal ions were carried out to see the effect of substituent groups on sensitivity and selectivity of the ionophore.

Benzothiazolylacetamidoalkoxy calix[4]arenes, **9-12**, have been prepared in two steps as shown in Scheme 1. The first step involved the conversion of amine groups in calix[4]arene derivatives **1-4** into corresponding cyanoacetamido groups. Using modified Salol procedure,⁸ the conversion of compound **1** to compound **5** (50%) was achieved by heating **1** with ethyl cyanoacetate. However, compounds **2-4** could not react with ethyl cyanoacetate to produce compounds **6-8**. Therefore, succinimide cyanoacetate was employed instead. The cyanoacetate ester containing the succinimide group was prepared from reaction of cyanoacetic acid with *N*-hydroxysuccinimide in the presence of dicyclohexylcarbodiimide in dry ethyl acetate. The amines **2-4** were reacted with succinimide cyanoacetate in dry CH₂Cl₂ to give cyanoacetamido compounds **6-8** in 19%, 34% and 40% yields, respectively. The cyanoacetamido compounds **5-8** were then heated with 2-aminothiophenol to give the final products **9-12** in 59%, 64%, 64% and 20% yields, respectively.

All of the compounds showed characteristic peaks of *p*-*tert*-butylcalix[4]arene (or calix[4]arene) building blocks and were in cone conformations which were substantiated by two doublets of the Ar-CH₂-Ar protons (*J* = 13-14 Hz) around 3-4 ppm in ¹H NMR spectra. The benzothiazolylacetamido groups showed two doublets and two triplets of the benzene proton of the benzothiazolyl group, one singlet for the proton in the alpha position of the carbonyl group and



Scheme 1. Synthesis pathway of benzothiazolylacetamidoalkoxycalix[4]arenes **9-12**.

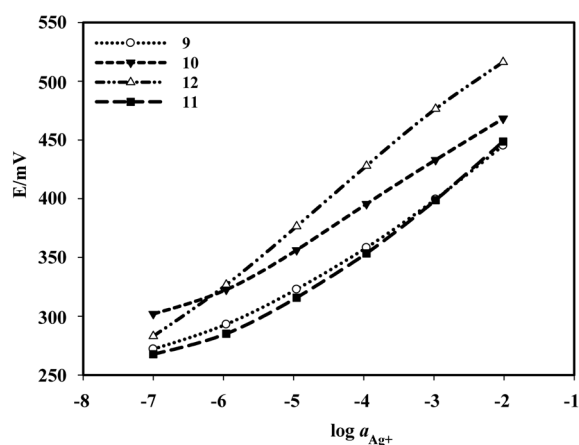


Figure 1. The response of Ag^+ -ISE electrodes preparation from (○) compound **9** (▼) compound **10** (■) compound **11** and (△) compound **12**.

one broad triplet of the amide proton. Mass spectrometry and elemental analysis results also supported the proposed structures of compounds **9-12**.

PVC-based ion-selective membrane electrodes employing benzothiazolylacetamidoalkoxy calix[4]arenes **9-12** as ionophores were prepared using a membrane composition of 1.0: 65.5:33.0:0.5 (ligand:*o*-NPOE:PVC:KTpClPB in weight percent) to determine the potentiometric response for Ag^+ . The calibration plots of the membranes based on compounds **9-12** were obtained by converting the concentration of Ag^+ in each solution into activity using the activity coefficient from the *Debye-Huckel equation*⁸ and plotted against measured emf's. The plots are shown in Figure 1 and slopes, linear range, detection limit and response time are summarized in Table 1. The **12**-ISE's showed response closer to the theoretical slope, 50.5 mV decade⁻¹. The results suggested that the length of the tethers affected Nernstian response towards Ag^+ . Ionophores **11** and **12** with shorter tethers were found to give higher slope than ionophores **9** and **10**. This observation was similar to Ag^+ -ISE using benzothiazolyl-thiaalkoxycalix[4]arene as an ionophore where the longer tethers gave the lower slope.⁷

The potentiometric selectivity coefficients of the ISE were determined by the mixed solution methods. The variation of emf at varying concentration of Ag^+ in interfering ions and the calculated potentiometric selectivity coefficients are shown in Table 2. The selectivity coefficient ($\log K_{\text{Ag},J}^{\text{pot}}$) represents the preference of ISE-**9** through ISE-**12** for Ag^+

Table 2. The potentiometric selectivity coefficients

Ion J	$\log K_{\text{Ag},J}^{\text{pot}}$			
	9	10	11	12
Ag^+	0	0	0	0
Na^+	-3.35	no response	-3.35	no response
K^+	-3.35	no response	-3.37	no response
Ca^{2+}	-4.42	no response	-4.57	no response
Mg^{2+}	no response	no response	-4.48	no response
Cd^{2+}	no response	no response	-4.00	no response
Ni^{2+}	no response	no response	-3.95	no response
Pb^{2+}	-3.41	-3.88	-3.38	-3.98
Cu^{2+}	-3.95	-4.05	-3.99	-4.00
Hg^{2+}	-2.35	-2.70	-2.45	-2.96

over the other cations. The coefficient $K_{\text{Ag},J}^{\text{pot}}$ defines the ability of an ISE to recognize different ions under the same conditions. The smaller the $K_{\text{Ag},J}^{\text{pot}}$ value, the greater the electrode preference for the Ag^+ ion over the interfering ion (J).

It should be seen from Table 2 that among the calix[4]-arene-based ionophores, **10** and **12** lacking of the *tert*-butyl substituents generally gave better potentiometric selectivity coefficients than **9** and **11** containing *tert*-butyl groups. There were a number of examples reported the serious dependence of the response of some carrier based silver membrane electrodes on the amount (by mol) of a ionophore in the membrane phase.¹⁰⁻¹² It is obviously seen that ionophore **12** which possesses the lowest molecular weight shows the highest selectivity coefficients to Ag^+ . Furthermore, all ISE's showed no response or only slight response to interfering alkali, alkali earth and transition metal ions. This can be tentatively rationalized that the four sulfur atoms or two sulfur atoms and two nitrogen atoms on the benzothiazolyl groups of **9-12** participate in the coordination with Ag^+ at the same time. Oxygen atoms on the narrow rim of the calix[4]arene unit did not involve in the coordination sphere because this would lead to the interference of other ions such as Na^+ , K^+ , Mg^{2+} and some other divalent transition cations which had affinity towards hard donors.⁷

In summary, the ionophores **9-12** consisting of benzothiazolylacetamidoalkoxy groups were synthesized. PVC membrane electrodes incorporating such ionophores showed high selectivity and sensitivity towards silver ions, especially ISE-**12**. The studies showed that among calix[4]arene

Table 1. Response parameters of ionophores **9-12**

parameters	Ionophores			
	9	10	11	12
Slope (mV decade ⁻¹)	38.7	38.7	41.9	50.5
Linear range (log a)	-5.3 to -2.0	-6.5 to -2.0	-5.1 to -2.0	-6.9 to -2.2
Detection limit (M)	5.01×10^{-6}	3.16×10^{-7}	7.94×10^{-6}	1.26×10^{-7}
Response time (s)	< 12	< 12	< 12	< 12
Correlation coefficient (r)	0.9988	0.9999	0.9984	0.9999

derivative-ionophores, both *tert*-butyl substituents and the length of the pendant on the narrow rim affected the selectivity and sensitivity of the membranes in which the absence of *tert*-butyl group and shorter length of the pendant groups gave a better membrane electrode.

Experimental Section

Nuclear magnetic resonance (NMR) spectra were recorded on a Varian Mercury Plus 400 nuclear magnetic resonance spectrometer. In all cases, samples were dissolved in deuterated chloroform. The chemical shifts were recorded in part per million (ppm) using a residue proton as internal reference. Elemental analysis was carried out on CHNS/O analyzer (Perkin Elmers PE 2400 series II). ESI mass spectra were recorded on a Micromass Platform II. Compounds **1-4** were prepared according to literature procedure.^{13,14}

5,11,17,23-Tetra-*p*-*tert*-butyl-25,27-bis(cyanoacetamidobutoxy)-26,28-dihydroxycalix[4]arene (5). In a 100 mL one-necked round bottom flask equipped with a magnetic bar, 5,11,17,23-tetra-*p*-*tert*-butyl-25,27-bis(aminobutoxy)-calix[4]arene **1** (0.34 g, 0.42 mmol), ethyl cyanoacetate (0.34 g, 2.9 mmol) were stirred under nitrogen atmosphere and heated gradually to 80 °C for 5 h. The mixture was cooled to room temperature and the residue was solubilized with 10 mL CH₂Cl₂. The solution was chromatographed on a silica column with gradient elution (CH₂Cl₂-ethyl acetate) to give **5** as a white solid after evaporation in 50% yield (0.19 g). Mp 121-122 °C. ¹H-NMR (400 MHz, CDCl₃): δ = 7.52 (s, 2H, NH), 7.26 (s, 2H, ArOH), 7.11 (s, 4H, *m*-HArOH), 6.70 (s, 4H, *m*-HArOCH₂), 4.19 (d, *J* = 14 Hz, 4H_A, ArCH₂Ar), 4.01 (t, *J* = 6 Hz, 4H, CH₂OAr), 3.64 (q, *J* = 6 Hz, 4H, CH₂NH), 3.50 (s, 4H, CH₂CN), 3.39 (d, *J* = 13 Hz, 4H, ArCH₂Ar), 1.96 (t, *J* = 6 Hz, 4H, CH₂CH₂OAr), 1.88 (t, *J* = 6 Hz, 4H, CH₂CH₂CH₂OAr), 1.32 (s, 18H, *t*-C₄H₉), 0.87 (s, 18H, *t*-C₄H₉). ¹³C-NMR (100 MHz, CDCl₃): δ = 162.19, 149.73, 147.64, 142.75, 131.79, 128.13, 125.66, 125.34, 115.63, 39.66, 33.94, 33.85, 31.66, 31.54, 30.87, 27.07, 26.13. MALDI-TOF MS (*m/z*) [M + Na]⁺ = 948.56 (Calcd. 947.56) Anal. Calcd. for C₅₈H₇₆N₄O₆: C, 75.28; H, 8.28; N, 6.06. Found C, 74.19; H, 9.47; N, 5.95.

General procedures for preparation of compounds 6-8. In a 250 mL two-necked round bottom flask equipped with a magnetic bar, succinamide cyanoacetic was dissolved in CH₂Cl₂ and stirred at room temperature under nitrogen atmosphere. A solution of aminoalkoxy calix[4]arene and *N*-ethyl-di-*isopropylamine* in CH₂Cl₂ was added dropwise. The mixture was left stirring for 48 h at room temperature. The solution was extracted with 1 M HCl and washed with water. After drying over anhydrous Na₂SO₄, the organic part was evaporated to dryness under reduced pressure and the product was chromatographed on a silica column with gradient elution (CH₂Cl₂/ethyl acetate) to give benzothiazolylacetamidocalix[4]arene as a white solid after evaporation.

25,27-Bis(cyanoacetamidobutoxy)-26,28-dihydroxycalix[4]arene (6). Yield 19%. Mp 113-115 °C. ¹H-NMR (400 MHz, CDCl₃). δ = 7.48 (s, 2H, ArOH), 7.32 (s, 2H, NH),

7.11 (d, *J* = 8 Hz, 4H, *m*-HArOH), 6.85 (d, *J* = 8 Hz, 4H, *m*-HArOCH₂), 6.76-6.70 (m, 4H, *p*-HArOH and *p*-HArOCH₂), 4.23 (d, *J* = 14 Hz, 4H, ArCH₂Ar), 4.02 (t, *J* = 6 Hz, 4H, CH₂OAr), 3.59 (q, *J* = 6 Hz, 4H, CH₂NH), 3.45 (s, 4H, CH₂CN), 3.43 (d, *J* = 14 Hz, 4H, ArCH₂Ar), 2.05 (t, *J* = 7 Hz, 4H, CH₂CH₂OAr), 1.94 (t, *J* = 7 Hz, 4H, CH₂CH₂NH). ¹³C-NMR (100 MHz, CDCl₃): δ = 162.19, 152.63, 151.90, 132.71, 129.12, 128.77, 128.19, 125.49, 119.81, 115.02, 39.98, 31.34, 27.29, 26.04, 25.94. MALDI-TOF MS [M + Na]⁺ (*m/z*) = 723.97 (Calcd. 723.32). Anal. Calcd. for C₄₂H₄₄N₄O₆·0.5H₂O C, 71.07; H, 6.39; N, 7.89. Found: C, 71.98; H, 6.33; N, 7.99.

5,11,17,23-Tetra-*p*-*tert*-butyl-25,27-bis(acetamidoethoxy)-26,28-dihydroxycalix[4]arene (7). Yield 34%. Mp 271-275 °C (decomposed). ¹H NMR (400 MHz, CDCl₃): δ = 8.63 (t, *J* = 6 Hz, 2H, NH), 8.28 (s, 2H, ArOH), 7.07 (s, 4H, *m*-HArOH), 6.95 (s, 4H, *m*-HArOCH₂), 4.21 (d, *J* = 13 Hz, 4H_A, ArCH₂Ar), 4.11 (t, *J* = 5 Hz, 4H, CH₂OAr), 3.99 (q, *J* = 4 Hz, 4H, CH₂NH), 3.41 (d, *J* = 13 Hz, 4H, ArCH₂Ar), 3.41 (s, 4H, CH₂CN), 1.26 (s, 18H, *t*-C₄H₉), 1.07 (s, 18H, *t*-C₄H₉). ¹³C-NMR (100 MHz, CDCl₃): δ = 161.66, 149.14, 148.47, 148.24, 143.21, 132.76, 127.55, 126.13, 125.77, 114.73, 75.13, 40.03, 34.17, 33.92, 31.92, 31.56, 31.03, 26.14. MALDI-TOF MS [M + Na]⁺ (*m/z*) = 892.49. (Calcd. 891.50). Anal. Calcd. C₅₄H₆₈N₄O₆ C, 74.61; H, 7.89; N, 6.45. Found C, 75.29; H, 7.25; N, 6.66.

25,27-Bis(cyanoacetamidoethoxy)-26,28-dihydroxycalixarene (8). Yield 40%. Mp 281-284 °C (decomposed). ¹H-NMR (400 MHz, CDCl₃): δ = 8.39 (s, 2H, ArOH), 7.10 (d, *J* = 7 Hz, 4H, *m*-HArOH), 6.98 (d, *J* = 8 Hz, 4H, *m*-HArOCH₂), 6.83 (t, *J* = 8 Hz, 2H, *p*-HArOH), 6.73 (t, *J* = 8 Hz, 2H, *p*-HArOCH₂), 4.26 (d, *J* = 13 Hz, 4H_A, ArCH₂Ar), 4.14 (t, *J* = 5 Hz, 4H, CH₂OAr), 4.06 (q, *J* = 5 Hz, 4H, CH₂NH), 3.46 (d, *J* = 13 Hz, 4H_B, ArCH₂Ar), 3.40 (s, 4H, CH₂CN). ¹³C-NMR (100 MHz, CDCl₃): δ = 162.17, 151.86, 150.81, 133.01, 128.61, 128.34, 127.32, 125.32, 119.57, 116.36, 74.62, 39.24, 30.27, 25.55. MALDI-TOF MS [M + Na]⁺ (*m/z*) = 667.68. (Calcd. 667.25). Anal. Calcd. C₃₈H₃₆N₄O₆: C, 70.79; H, 5.63; N, 8.69. Found: C, 70.13; H, 5.33; N, 8.28.

General procedures for preparation of compounds 9-12. In a 100 mL one-necked round bottom flask equipped with a magnetic bar, a cyanoacetamidocalix[4]arene was mixed with 2-aminothiophenol at 1:10 mol ratio and heated at 120 °C under N₂ atmosphere for 3 h. After cooling, the product was dissolved in CH₂Cl₂ and loaded on a silica column. The column was first washed with CH₂Cl₂ to remove excess 2-aminothiophenol after then gradient eluted with a mixture of CH₂Cl₂ and ethyl acetate. The fraction containing benzothiazolylacetamidocalix[4]arene was evaporated to dryness under reduced pressure to give a white solid of the desired product.

5,11,17,23-Tetra-*p*-*tert*-butyl-25,27-bis(benzothiazolylacetamidobutoxy)-26,28-dihydroxycalix[4]arene (9). Yield 59%. Mp 109-111 °C. ¹H-NMR (400 MHz, CDCl₃): δ = 7.93 (d, 2H, *J* = 8 Hz, BTArH), 7.84 (br, 2H, NH), 7.77 (d, *J* = 8 Hz, 2H, BTArH), 7.40 (t, *J* = 7 Hz, 2H, BTArH), 7.39 (t, *J* = 8 Hz, 2H, BTArH), 7.38 (s, 2H, ArOH), 7.04 (s, 4H, *m*-

HArOH), 6.76 (s, 4H, *m-HArOCH*₂), 4.19 (d, *J* = 13 Hz, 4H_A, *ArCH*₂*Ar*), 4.14 (s, 4H, *CH*₂*BT*), 3.94 (t, 4H, *J* = 6.0 Hz, *CH*₂*OAr*), 3.50 (q, *J* = 6 Hz, 4H, *CH*₂*NH*), 3.28 (d, *J* = 13 Hz, 4H_B, *ArCH*₂*Ar*), 1.97 (q, *J* = 7 Hz, 4H, *CH*₂*CH*₂*OAr*), 1.88 (q, *J* = 7 Hz, 4H, *CH*₂*CH*₂*NH*), 1.29 (s, 18 H, *t*-C₄H₉), 0.93 (s, 18 H, *t*-C₄H₉). ¹³C NMR (100 MHz, CDCl₃) δ 167.5, 165.0, 152.7, 150.3, 149.7, 147.0, 141.8, 135.4, 132.4, 127.8, 126.0, 125.5, 125.13, 125.08, 122.7, 121.6, 76.5, 41.3, 39.6, 33.91, 33.85, 31.7, 31.6, 31.0, 27.1, 26.1; ESI-MS 1175.3. ESI-MS 1175.3 [M + Cl]⁻ (calcd 1177.1). Anal. calcd. for C₇₀H₈₄N₄O₆S₂: C, 73.65; H, 7.42; N, 4.91. Found: C, 73.68; H, 7.45; N, 4.94.

25,27-Bis(benzothiazolylacetamidobutoxy)-26,28-dihydroxycalix[4]arene (10). Yield 64%. Mp 107-109 °C. ¹H-NMR (400 MHz, CDCl₃): δ = 8.05 (br, 2H, *NH*), 8.00 (s, 2H, *ArOH*), 7.99 (d, *J* = 8 Hz, 2H, *BTArH*), 7.82 (d, *J* = 7 Hz, 2H, *BTArH*), 7.46 (t, *J* = 7 Hz, 2H, *BTArH*), 7.42 (t, *J* = 8, 2H, *BTArH*), 7.07 (d, *J* = 8 Hz, 4H, *m-HArOH*), 6.91 (d, *J* = 8 Hz, 4H, *m-HArOCH*₂), 6.75 (t, *J* = 7 Hz, 2H, *p-HArOH*), 6.69 (t, *J* = 7 Hz, 2H, *p-HArOCH*₂), 4.26 (s, 4H, *CH*₂*BT*), 4.25 (d, *J* = 14 Hz, 4H_A, *ArCH*₂*Ar*), 4.02 (t, *J* = 6 Hz, 4H, *CH*₂*OAr*), 3.54 (q, *J* = 6 Hz, 4H, *CH*₂*NH*), 3.38 (d, *J* = 13 Hz, 4H, *ArCH*₂*Ar*), 2.08-2.05 (m, 4H, *CH*₂*CH*₂*OAr*), 1.99 (q, *J* = 7 Hz, 4H, *CH*₂*CH*₂*NH*). ¹³C NMR (100 MHz, CDCl₃) δ 167.3, 165.4, 153.0, 151.8, 135.1, 133.1, 129.0, 128.5, 128.1, 126.3, 125.4, 125.3, 122.4, 121.7, 119.3, 76.4, 41.0, 39.6, 31.3, 27.3, 25.9. ESI-MS 951.1 [M + Cl]⁻ (calcd 952.7). Anal. calcd. for C₅₄H₅₂N₄O₆S₂: C, 70.72; H, 5.71; N, 6.11. Found: C, 70.73; H, 5.69; N, 6.11.

5,11,17,23-Tetra-*p*-tert-butyl-25,27-bis(benzothiazolylacetamidoethoxy)-26,28-dihydroxycalix[4] arene (11). Yield 64% (0.16 g). Mp 249-251 °C. ¹H-NMR (400 MHz, CDCl₃): δ = 8.85 (br, 2H, *NH*), 8.37 (s, 2H, *ArOH*), 7.94 (d, *J* = 8 Hz, 2H, *BTArH*), 7.80 (d, *J* = 8 Hz, 2H, *BTArH*), 7.45 (t, *J* = 8 Hz, 2H, *BTArH*), 7.37 (t, *J* = 8 Hz, 2H, *BTArH*), 7.00 (s, 4H, *m-HArOH*), 6.97 (s, 4H, *m-HArOCH*₂), 4.24 (s, 4H, *CH*₂*BT*), 4.18 (d, *J* = 13 Hz, 4H_A, *ArCH*₂*Ar*), 4.08 (t, *J* = 5 Hz, 4H, *CH*₂*OAr*), 3.82 (q, *J* = 5 Hz, 4H, *CH*₂*NH*), 3.33 (d, *J* = 13 Hz, 4H, *ArCH*₂*Ar*), 1.28 (s, 18H, *t*-C₄H₉), 1.19 (s, 18H, *t*-C₄H₉). ¹³C NMR (100 MHz, CDCl₃) δ 167.6, 164.5, 152.4, 149.2, 148.6, 148.0, 142.7, 135.7, 133.0, 127.6, 126.02, 125.98, 125.6, 125.1, 122.5, 121.6, 75.5, 41.7, 39.6, 34.1, 33.8, 32.1, 31.6, 31.0. ESI-MS 1120.5 [M + Cl]⁻ (calcd 1120.94). Anal. calcd. for C₆₆H₇₆N₄O₆S₂: C, 73.03; H, 7.06; N, 5.16. Found: C, 73.03; H, 7.08; N, 5.12.

25,27-Bis(benzothiazolylacetamidobutoxy)-26,28-dihydroxycalix[4]arene (12). Yield 20% (0.054 g). Mp 232-235 °C. ¹H-NMR (400 MHz, CDCl₃): 8.70 (br, 2H, *NH*), 8.13 (s, 2H, *ArOH*), 7.95 (d, *J* = 8 Hz, 2H, *BTArH*), 7.78 (d, *J* = 8 Hz, 2H, *BTArH*), 7.47 (t, *J* = 7 Hz, 2H, *BTArH*), 7.38 (t, *J* = 8 Hz, 2H, *BTArH*), 6.95 (d, *J* = 7 Hz, 4H, *m-HArOH*), 6.91 (d, *J* = 8 Hz, 4H, *m-HArOCH*₂), 6.78 (t, *J* = 8 Hz, 2H, *p-HArOH*), 6.61 (t, *J* = 8 Hz, 2H, *p-HArOCH*₂), 4.27 (s, 4H, *COCH*₂), 4.17 (d, *J* = 14 Hz, 4H_A, *ArCH*₂*Ar*), 4.14 (t, *J* = 8

Hz, 4H, *CH*₂*OAr*), 3.89 (q, *J* = 4 Hz, 4H, *CH*₂*NH*), 3.32 (d, *J* = 13 Hz, 4H, *ArCH*₂*Ar*). ¹³C NMR (100 MHz, CDCl₃) δ 167.7, 164.4, 152.6, 151.9, 150.5, 135.6, 133.3, 129.2, 128.7, 128.0, 126.2, 126.0, 125.1, 122.5, 121.6, 120.2, 75.5, 60.4, 41.7, 39.7, 31.3. ESI-MS 895.4 [M + Cl]⁻ (calcd 896.5). Anal. calcd. for C₅₄H₄₄N₄O₆S₂·H₂O: C, 68.32; H, 5.27; N, 6.37. Found: C, 67.70; H, 5.16; N, 6.06.

Ion-selective electrode preparation and measurements.

The ion-selective membrane was prepared using the procedure described by Craggs and colleague.¹⁵ The weighed amount of ligands, plasticizer (*o*-nitrophenyloctylether, *o*-NPOE), cation exchanger (potassium tetrakis(*p*-chlorophenyl)borate, KTpClPB) and PVC were mixed in a vial with 6 mL THF. The weight percent composition of the membrane was 1.0:65.5:33.0:0.5 (ligand: *o*-NPOE:PVC:KTpClPB). Four to five PVC-tubes (5 mm i.d., 3 mm-wall thickness, 30 mm long) were glued at one end with PVC-THF solution and put on the membrane. After the solvent was evaporated, the membrane around each tube was cut to obtain a PVC-tube with membrane sealed at one end. The open-end of the PVC-tube was then fitted into a glass tube after which made into a ISE by filling with 0.10 M AgNO₃ and putting in a Ag/AgCl electrode. The ISE was pre-conditioned by immersing in a 0.010 M AgNO₃ solution for 12 h before used.

Acknowledgments. The author thanks the Thailand Research Fund for financial support (grant no. RTA5080006). NM is a Ph.D. student under supports of Mahasarakham University.

References

- Asfari, Z.; Bhmer, V.; Harrowfield, J.; Vicens, J. *Calixarenes 2001*; Kluwer Academic: Dordrecht, 2001.
- Diamond, D.; Nolan, K. *Anal. Chem.* **2001**, *73*, 23A-29A.
- Kim, Y. D.; Jeong, H. S.; Kang, S. O.; Nam, K. C.; Jeon, S. W. *Bull. Kor. Chem. Soc.* **2001**, *22*, 405-408.
- Cobben, P. H. L. M.; Egberink, R. J. M.; Bomer, J. G.; Bergvett, P.; Verboom, U.; Reinhoudt, D. N. *J. Am. Chem. Soc.* **1992**, *114*, 10573-10582.
- Park, S. J.; Shon, O. J.; Rim, J. A.; Lee, J. K.; Kim, J. S.; Nam, H.; Kim, H. *Talanta* **2001**, *55*, 297-304.
- Kimura, K.; Yajima, S.; Tatsumi, K.; Yokoyama, M.; Oue, M. *Anal. Chem.* **2000**, *72*, 5290-5294.
- Zeng, X.; Weng, L.; Chen, L.; Xu, F.; Li, Q.; Leng, X.; He, X.; Zang, Z. *Tetrahedron* **2002**, *58*, 2647-2658.
- Allen, C. F. H.; van Allen, J. *Organic Syntheses* **1946**, *26*, 92-93.
- Skoog, D. A.; West, D. M.; Holler, F. J. *Fundamentals of Analytical Chemistry* 7th Ed.; Saunders College Publishing: 1996.
- Badr, I. H. A. *Microchim. Acta* **2005**, *149*, 87-94.
- Chung, S.; Kim, W.; Park, S. B.; Kim, D. Y.; Lee, S. S. *Talanta* **1997**, *44*, 1291-1298.
- Lee, S. S.; Ahn, M. K.; Park, S. B. *Analyst* **1998**, *123*, 383-386.
- Zhang, W.-C.; Huang, Z.-T. *Synthesis* **1997**, 1073-1076.
- Aeungmaitrepirom, W.; Hagège, A.; Asfari, Z.; Bennouna, L.; Vicens, J.; Leroy, M. *Tetrahedron Lett.* **1999**, *40*, 6389-6392.
- Craggs, A.; Moody, G. J.; Thomas, J. D. R. *J. Chem. Ed.* **1974**, *51*, 541-544.

Synthesis and Characterization of Monomeric and Dimeric Structures of Calix[4]arenes Containing Amidoferrocene

Chomchai Suksai · Pannee Leeladee ·
Colin Jennings · Thawatchai Tuntulani ·
Palangpon Kongsaree

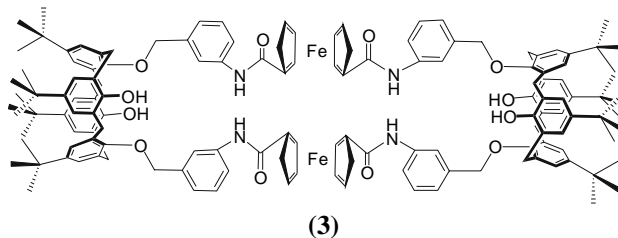
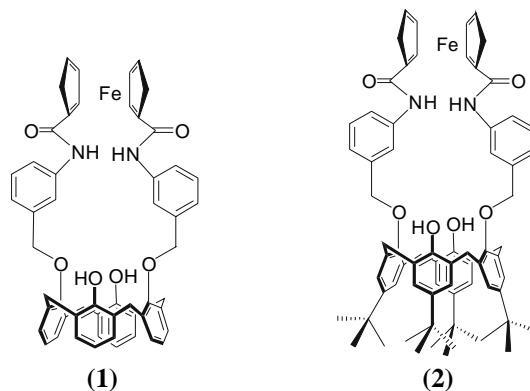
Received: 4 July 2007 / Accepted: 5 November 2007 / Published online: 17 November 2007
© Springer Science+Business Media, LLC 2007

Abstract The reaction of 1,1'-bis(chlorocarbonyl)ferrocene with bis-aminobenzylcalix[4]arene gave amidoferrocene calix[4]arene monomer **1**. Compound **1** crystallized in the monoclinic system P21/c with $a = 11.196(6)$ Å, $b = 14.971(11)$ Å, $c = 32.007(2)$ Å, $\beta = 96.413(4)^\circ$ and $V = 5330.9(6)$ Å³. X-ray diffraction analyses of **1** showed that the calix[4]arene scaffold was in cone conformation in which the intramolecular hydrogen bonding were formed through OH groups at the lower rim to stabilize the structure. Moreover, the intramolecular hydrogen bond between the amide groups of the amidoferrocene unit also presented in the crystal structure. On the other hand, the condensation of 1,1'-bis(chlorocarbonyl)ferrocene with *p-tert*-bis-aminobenzylcalix[4]arene resulted in the monomeric **2** and [2 + 2] dimeric compounds **3**. ¹H-NMR studies signified that the calix[4]arene building block in compounds **2** and **3** adopted the cone conformation.

Keywords Metallocene · Amidoferrocene · Calix[4]arene

Introduction

Calixarenes are synthetic macrocycles used as building blocks in nanotechnology and supramolecular chemistry [1]. They were also used as molecular scaffolds for the preparation of novel selective receptors for ions and neutral molecules [2]. Moreover, calix[4]arene bearing a sensory unit have been attracted much chemist's attention in recent years owing to possible applications as chemical sensors [3–5]. For example, calixarenes functionalized with the amidoferrocene group have been shown to be very effective electrochemical sensors for cations [6–8] anions [9–12] and neutral molecules [13–14]. Herein, we report the synthesis and characterization of calix[4]arenes containing amidoferrocene units **1–3** including the crystal structure of **1** determined by X-ray diffraction analysis.



C. Suksai (✉)
Department of Chemistry, Faculty of Science, Burapha
University, Chonburi 20131, Thailand
e-mail: jomjai@buu.ac.th

P. Leeladee · C. Jennings · T. Tuntulani (✉)
Department of Chemistry, Faculty of Science, Chulalongkorn
University, Bangkok 10330, Thailand
e-mail: tthawac@chula.ac.th

P. Kongsaree
Department of Chemistry, Faculty of Science, Mahidol
University, Bangkok 10400, Thailand

Experimental

All reagents were of reagent grade and were used without further purification unless stated otherwise. ^1H -NMR, ^{13}C -NMR and 2D-NMR spectra were recorded in $\text{DMSO}-d_6$ on a BRUKER AVANCE 400 NMR spectrometer. Elemental analyses were performed on a Perkin-Elmer 2400 CHN elemental analyzer.

Synthesis of compound **1**

bis-Nitrobenzylcalix[4]arene (**a**)

Calix[4]arene (0.50 g, 1.20 mmol), K_2CO_3 (0.162 g, 1.20 mmol) and a catalytic amount of KI in 50 mL of dry acetonitrile were stirred at room temperature for 30 min under N_2 . The solution of 3-nitrobenzylchloride (0.50 g, 2.90 mmol) in 30 mL of dried acetonitrile was then added dropwise and the solution mixture was refluxed for 24 h. After cooling to room temperature, the solvent was evaporated in vacuo and the residue was dissolved in CH_2Cl_2 (100 mL). The organic layer was washed with 3 M HCl (2×100 mL) and water (2×100 mL). The organic layer was dried with anhydrous MgSO_4 and filtered. The solvent was removed under a reduced pressure to obtain a residue. Purification by SiO_2 column chromatography using a mixture of CH_2Cl_2 /hexane (1:1) as eluent gave bis-nitrobenzylcalix[4]arene (**a**) as a white powder (0.52 g, 63%).

bis-Aminobenzylcalix[4]arene (**b**)

Reduction of the bis-nitrobenzylcalix[4]arene (**a**) to bis-aminobenzylcalix[4]arene was carried out using Raney Nickel and hydrazine. Hydrazine (2.28 mL, 46 mmol) was added to the solution mixture of bis-nitrobenzylcalix[4]arene (0.50 g, 0.72 mmol) and Raney Nickel (0.376 g, 6.5 mmol) in the mixture of ethyl acetate:methanol (15:11 mL) under N_2 atmosphere. The solution was heated at 60 °C for 1 h. After cooling to room temperature, the solution was filtered and the solvent was evaporated. The residue was dissolved in 50 mL of CH_2Cl_2 and washed with water (2×50 mL). The organic layer was then dried with anhydrous MgSO_4 , filtered and the solvent was evaporated to give bis-aminobenzylcalix[4]arene (**b**) in a quantitative yield.

Compound (**1**)

Compound **b** (0.40 g, 0.60 mmol) was reacted with 1,1'-bis(chlorocarbonyl)ferrocene (0.19 g, 0.60 mmol) in the

presence of triethylamine (0.26 mL, 1.50 mol) in dried CH_2Cl_2 and the solution was stirred at room temperature for 4 h under N_2 . The organic layer was washed with water (3×100 mL), dried with anhydrous MgSO_4 and filtered. The solvent was removed under reduced pressure. The residue was purified by SiO_2 column chromatography using CH_2Cl_2 :EtOAc (2:1) as eluant to obtain compound **1** as an orange powder in 0.135 g (25% yield). Orange crystals of **1** suitable for X-ray structural investigations were obtained by slow evaporation of the solution of **1** in CHCl_3 . ^1H -NMR (400 MHz, CDCl_3 , ppm): δ 8.49 (s, 2H, NH), 8.19 (s, 2H, OH), 8.10 (s, 2H, ArH), 7.75 (d, 2H, ArH), 7.32 (t, 2H, ArH), 7.18 (d, 2H, ArH), 7.08 (d, 4H, ArH), 6.95 (d, 4H, ArH), 6.82 (t, 2H, ArH), 6.65 (t, 2H, ArH), 5.01 (s, 4H, $-\text{OCH}_2-$), 4.86 (s, 4H, CpH), 4.55 (s, 4H, CpH), 4.32 (d, $J = 12$ Hz, AB system, Ar- CH_2 -Ar), 3.95 (d, $J = 12$ Hz, AB system, Ar- CH_2 -Ar). ESI-MS (positive mode) m/z : 873.34 $[\text{M} + \text{H}]^+$. Analysis calculated for $\text{C}_{54}\text{H}_{44}\text{FeN}_2\text{O}_6$: C 74.31, H 5.08, N 3.21%; found: C 74.35, H 5.10, N 3.25%.

Synthesis of Compounds **2** and **3**

p-tert-Butyl-bis-nitrobenzylcalix[4]arene (**c**)

A mixture of p-tert-butyl-calix[4]arene (2.00 g, 3.13 mmol), K_2CO_3 (0.435 g, 3.13 mmol) and a catalytic amount of KI in 50 mL of dried acetonitrile was stirred at room temperature under N_2 for 30 min. The solution of 3-nitrobenzylchloride (1.31 g, 7.63 mmol) in 30 mL of dried acetonitrile was added dropwise and the solution mixture was refluxed for 24 h. The solvent was evaporated in vacuo and CH_2Cl_2 (100 mL) was added. The organic phase was washed with 3 M HCl (2×100 mL) and water (2×100 mL). The organic layer was dried with anhydrous MgSO_4 and filtered. The solvent was removed to give crude **c**. The crude product was placed on a silica gel column using 30% Hexane: CH_2Cl_2 as eluant to obtain compound **c** as a white powder (1.982 g, 69%).

p-tert-Butyl-bis-aminobenzylcalix[4]arene (**d**)

Compound **c** (0.67 g, 0.73 mmol) and Raney Ni (0.42 g, 7.30 mmol) were suspended in a mixture of ethylacetate 15 mL and MeOH 11 mL under N_2 . Subsequently, hydrazine (2.3 mL, 47 mmol) was added and the mixture was heated at reflux for 2 h. The unreacted Raney Ni was removed while the solution was still warm and the filtrate was removed under reduce pressure. The crude product was then dissolved in CH_2Cl_2 50 mL and washed with water (3×50 mL). The organic layer was separated and

dried over anhydrous MgSO_4 . The solvent was removed in vacuo to obtain compound **d** as a white solid in a quantitative yield.

Compounds (2) and (3)

To a stirred solution of compound **d** (0.67 g, 0.73 mmol) and triethylamine (0.26 mL, 1.83 mmol) in 150 mL of CH_2Cl_2 was added a solution of 1,1'-bis(chlorocarbonyl)ferrocene (0.23 g, 0.73 mmol) in dichloromethane (20 mL). The solution was stirred at room temperature for 4 h. The solution was subsequently washed with water (2×100 mL) and the organic layer was dried over anhydrous Na_2SO_4 . The solvent was removed by a rotary evaporator to give a red oily residue which was purified by column chromatography (SiO_2) using 20% $\text{EtOAc}:\text{CH}_2\text{Cl}_2$ as eluent. The orange solid of monomeric compound **2** ($R_f = 0.65$) (0.16 g, 22%) and dimeric compound **3** ($R_f = 0.78$) (0.24 g, 5%) were obtained.

Compound (2)

^1H -NMR (400 MHz, CDCl_3 , ppm): δ 8.60 (s, 2H, NH), 8.08 (s, 2H, OH), 7.76 (s, 2H, ArH), 7.67 (d, 2H, $J = 6.4$ Hz, ArH), 7.28 (t, 2H, $J = 7.2$ Hz, ArH), 7.17 (d, 2H, $J = 7.6$ Hz, ArH), 7.03 (s, 4H, ArH), 6.90 (s, 4H, ArH), 4.95 (s, 4H, $-\text{OCH}_2-$), 4.87 (s, 4H, CpH), 4.50 (s, 4H, CpH), 4.27 (d, $J = 13.2$ Hz, AB system, Ar- CH_2 -Ar), 3.31 (d, $J = 12.8$ Hz, AB system, Ar- CH_2 -Ar), 1.26 (s, 18H, Ar- CH_3), 1.05 (s, 18H, Ar- CCH_3). ESI-MS (positive mode) m/z : 1154.24 $[\text{M} + \text{H}_2\text{O} + \text{K}]^+$. Analysis calculated for $\text{C}_{70}\text{H}_{76}\text{FeN}_2\text{O}_6$: C 76.63, H 6.98, N 2.55%; found: C 76.65, H 7.01, N 2.53%.

Compound (3)

^1H -NMR (400 MHz, CDCl_3 , ppm): δ 8.85 (br, s, 2H, NH), 8.16 (br, s, 2H, ArH), 8.03 (br, s, 2H, ArH), 7.70 (br, s, 2H, OH), 7.43 (br, s, 2H, ArH), 7.28 (br, s, 2H, ArH), 7.13 (s, 4H, ArH), 6.88 (s, 4H, ArH), 5.05 (s, 4H, $-\text{OCH}_2-$), 4.56 (s, 4H, CpH), 4.40 (s, 4H, CpH), 4.39 (d, $J = 12.0$ Hz, AB system, Ar- CH_2 -Ar), 3.39 (d, $J = 11.6$ Hz, AB system, Ar- CH_2 -Ar). ^{13}C -NMR (400 MHz, CDCl_3 , ppm): δ 168.98, 150.64, 149.52, 147.33, 141.87, 139.08, 137.89, 132.62, 129.89, 127.83, 125.66, 125.19, 121.71, 118.98, 117.34, 71.39, 71.03, 31.73, 31.01. ESI-MS (positive mode) m/z : 2212.03 $[\text{M} + \text{H}_2\text{O} + \text{H}]^+$. Analysis calculated for $\text{C}_{140}\text{H}_{152}\text{Fe}_2\text{N}_4\text{O}_{12}$: C 76.63, H 6.98, N 2.55%; found: C 76.66, H 6.96, N 2.57%.

X-ray Crystal Structure Determination

X-ray diffraction measurement for **1** was performed on a Bruker–Nonius Kappa CCD diffractometer with graphite-monochromated Mo- $\text{K}\alpha$ radiation ($\lambda = 0.7107$ Å). The data collection was performed on COLLECT program [15]. Crystal cell refinement and data reduction were carried out using HKL DENZO and SCALEPACK [16]. The structures were solved by direct method and were refined on F^2 by full-matrix least-squares technique using the SHELXL-97 [17] program on WinGX package [18]. Crystal data, data collection parameters and structure refinement details are given in Table 1. During the last stage of the refinement, disorder on chlorine atoms of chloroform in the structure of **1** was found. The disorder was modeled with two equally weighted sets of chlorine atoms. The non-H atoms were refined with anisotropic displacement thermal

Table 1 Crystallographic data and final refinement parameters for (**1**)

(1)	
Chemical formula	$\text{C}_{56}\text{H}_{46}\text{Cl}_6\text{N}_2\text{FeO}_6$
Molecular weight	1111.49
Color	Orange
Size (mm^3)	$0.284 \times 0.203 \times 0.113$
Temperature (K)	293(2) K
Crystal system	Monoclinic
Space group	$P2_1/c$
a (Å)	11.1960 (6)
b (Å)	14.9700 (11)
c (Å)	32.007 (2)
α (°)	90
β (°)	96.413 (4)
γ (°)	90
V (Å 3)	5330.9 (6)
Z	4
$F(000)$	2284
D_{calc} (g cm^{-3})	1.384
μ (mm^{-1})	0.635
θ range for data collection	$2.11\text{--}21.92^\circ$
Index ranges	$-10 \leq h \leq 11$ $-15 \leq k \leq 14$ $-33 \leq l \leq 31$
Reflections collected/observed	15388/5976 [$R(\text{int}) = 0.0783$]
Data/restraints/parameters	5976/0/704
Goodness-of-fit on F^2	1.006
Final R indices [$I > 2 \sigma(I)$]	$R1 = 0.0740$, $wR2 = 0.1711$
R indices (all data)	$R1 = 0.1326$, $wR2 = 0.2084$
Largest diff. peak and hole ($e - \text{\AA}^{-3}$)	0.358, -0.234

parameters at the latter stages of refinement. All hydrogen atoms (except H22, H27 and H45) are placed in geometrically idealized positions and refined using general isotropic temperature factors. The H atom bonded to C56 of the CHCl_3 solvent molecule in (**1**) is not found in the Fourier maps, but is accounted for in the formula sum and formula weight calculations.

Results and Discussion

Synthesis and Characterization

The synthetic methods of calix[4]arenes containing amidoferrocene **1**, **2** and **3** are summarized in Scheme 1. The structures of all compounds were characterized by ESI-MS, NMR and elemental analyses.

The cone conformation of the synthesized compounds was confirmed by ^1H -NMR spectrum. A typical AB pattern of the methylene bridge (ArCH_2Ar) protons was observed at 4.37 and 3.13 ppm ($J = 12.0$ Hz), 4.37 and 3.13 ppm ($J = 12.0$ Hz), 4.37 and 3.13 ppm ($J = 12.0$ Hz) for compounds **1**, **2** and **3**, respectively. The NH amide protons were found at downfield positions around 8.50–8.85 ppm due to the formation of an intramolecular hydrogen bonding of the amidoferrocene unit, in agreement with the crystal structure, *vide infra*. The positive ion electrospray mass spectrometry of **1** and **2** show the peak corresponding to the monomer species at $m/z = 1321.63$ $[\text{M} + \text{Na}]^+$ and 1154.24 $[\text{M} + \text{H}_2\text{O} + \text{K}]^+$, respectively.

Interestingly, the ^1H -NMR spectra of compounds **2** and **3** (Fig. 1) show that the integration of all peaks in the spectrum of **3** is equal to that of **2**. However, the feature of the peaks of compounds **2** and **3** are totally different. The dimeric molecule **3** shows broader peaks in the ^1H -NMR spectrum. Moreover, the two singlet protons of the Cp ring

of **3** are closer to each other than that of compound **2**. The dimeric structure of compound **3** was substantiated by ESI-MS revealing the $[\text{M} + \text{H}_2\text{O} + \text{H}]^+$ at $m/z = 2212.03$. The transannular 1,3-hydroxyl groups distance of *p*-*tert*-butyl-calix[4]arene is probably small to allow only 1 + 1 or 2 + 2 bridged ferrocene-calixarene species to occur whereas the 3 + 3 oligomers can be produced from the wider transannular of unsubstituent *para*-calix[4]arene [19]. However, in our system the 2 + 2 and 3 + 3 bridge ferrocene-calix[4]arenes of compound **1** were not observed.

Molecular Structure of Compound 1

Molecular structure of compound **1** is shown in Fig. 2. The conformation of **1** exists as a cone conformation. The two strong intramolecular O–H...O hydrogen bonding between the phenolic oxygens and the proximal etheral oxygens,

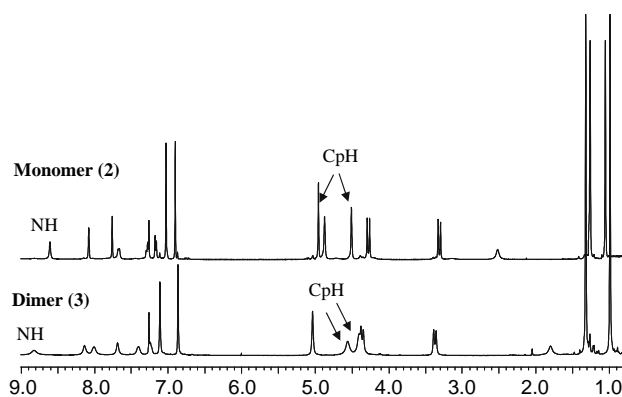
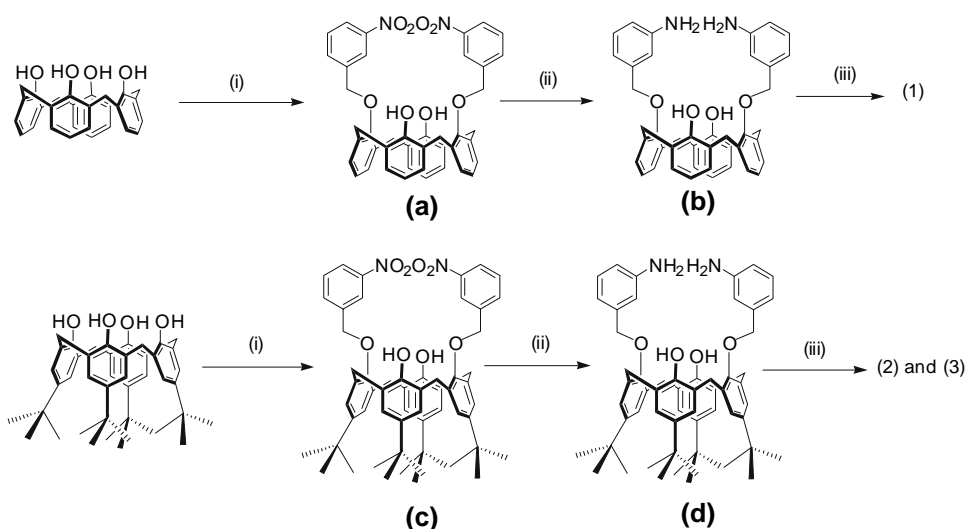


Fig. 1 ^1H -NMR spectra of monomer **2** and dimer **3** in CDCl_3

Scheme 1 Strategy for the synthesis of calix[4]arene amidoferrocene derivatives (**1**)–(**3**); (i) CH_3CN , KI, reflux 24 h, (ii) Raney/Ni, hydrazine, EtOAc:MeOH 15:11, reflux 60 °C 1 h and (iii) 1,1'-bis(chlorocarbonyl)ferrocene, CH_2Cl_2 , rt, 3 h



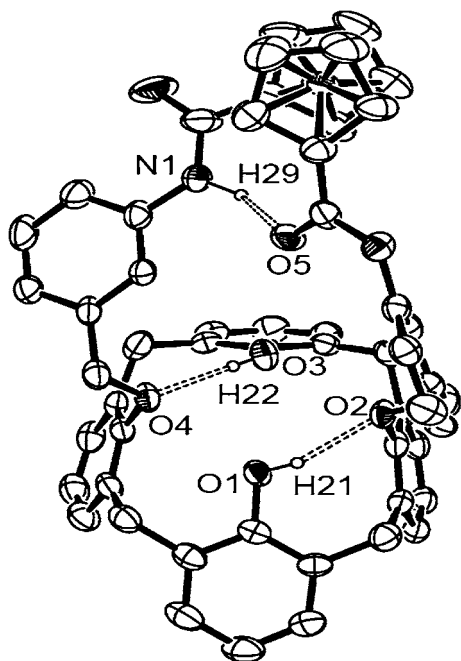


Fig. 2 A view of the asymmetric unit of **1**, displacement ellipsoids are drawn at 30% probability level and intramolecular hydrogen bonds are shown as dashed lines. H atoms have been omitted for clarity, except for those involved in hydrogen bonding

O(1)–O(2) 2.815 Å and O(3)–O(4) 2.754(6) Å, are jointly responsible for such a cone conformation. This result is in agreement with the reports by Brunink [20] and Böhmer [21] which presented that the presence of two vicinal or two opposite phenolic groups is sufficient to stabilize the cone conformation, with a preference for OH-depleted or substituted calix[4]arenes to adopt the 1,3-alternate formation. It should be mentioned that the distance of separation of the transannular 1,3-hydroxyl groups 3.169 Å which is larger than the distance of the original calix[4]arene (ca. 2 Å) [22]. However, this distance is less than the cyclopentadienyl–cyclopentadienyl distance of 3.25 Å [23]. The average Fe–Cp(centroid) distance is 1.620 Å which is identical to other ferrocenyl derivatives [24–25], and the angle of Cp–Fe–Cp is 178.81°.

The more intriguing feature of this molecule is the intramolecular hydrogen bonding between amide groups of amidoferrocene, N(1)–O(5) 2.925(7) Å, was also observed and affected to the cyclopentadiene rings within the ferrocene unit are not perfectly eclipsed (Table 2).

Supplementary Material

CCDC-650164 contains the supplementary crystallographic data for this paper. Copies of available can be obtained free of charge on application to the Director,

Table 2 (a) Selected bond lengths (Å) and angles (°) of compound **1**. (b) Hydrogen-bonding geometry (Å, °) for compound **1**

(a)				
Bond lengths				
C(20)–O(3)	1.370(7)	C(54)–O(4)	1.457(7)	
C(26)–O(2)	1.409(7)	C(36)–O(5)	1.231(7)	
C(29)–O(2)	1.452(6)	C(47)–N(1)	1.344(10)	
C(47)–O(6)	1.212(10)	C(48)–N(1)	1.434(8)	
C(4)–O(1)	1.368(8)	C(35)–N(2)	1.423(9)	
C(13)–O(4)	1.403(7)	C(36)–N(2)	1.352(9)	
Bond angles				
O(1)–C(4)–C(5)	116.9(7)	N(2)–C(36)–C(37)	115.8(6)	
O(1)–C(4)–C(3)	121.4(6)	N(1)–C(47)–C(46)	116.0(8)	
C(8)–C(13)–O(4)	118.8(6)	C(53)–C(48)–N(1)	118.7(6)	
C(12)–C(13)–O(4)	117.6(7)	C(49)–C(48)–N(1)	121.9(8)	
O(3)–C(20)–C(15)	121.8(6)	O(4)–C(54)–C(52)	109.6(6)	
O(3)–C(20)–C(19)	116.0(6)	C(26)–O(2)–C(29)	111.6(4)	
O(2)–C(29)–C(30)	110.1(5)	C(13)–O(4)–C(54)	117.0(4)	
C(33)–C(35)–N(2)	119.2(6)	O(6)–C(47)–N(1)	124.4(8)	
C(34)–C(35)–N(2)	121.7(6)	O(6)–C(47)–C(46)	119.7(9)	
O(5)–C(36)–N(2)	121.7(7)	C(47)–N(1)–C(48)	129.0(7)	
O(5)–C(36)–C(37)	122.6(7)	C(36)–N(2)–C(35)	125.5(6)	
(b)				
D–H...A	D–H	H...A	D...A	D–H...A
O1–H21...O2	0.82	2.05	2.815(5)	155.9
O3–H22...O4	0.81(7)	1.95(8)	2.754(6)	173(8)
N1–H29...O5	0.96	2.16	2.925(7)	135.6

CCDC, 12 Union Road, Cambridge CB2 1EZ, UK (Fax: +44-1233-336033; e-mail: deposit@ccdc.cam.ac.uk).

Acknowledgements The financial support from The Thailand Research Fund and the Center of Innovation in Chemistry: Postgraduate Education and Research Program in Chemistry (PERCH-CIC) are gratefully acknowledged. CJ is supported by the NSF-REU Thailand program.

References

- Vicens J, Harrowfield J (2007) Calixarenes in the nanoworld. Springer, Dordrecht
- Asfari Z, Böhmer V, Harrowfield J, Vicens J (2001) Calixarenes 2001. Kluwer Academic, Dordrecht
- Oueslati F, Dumazet-Bonnamour I, Lamartine R (2003) New J Chem 3:644
- Banthia S, Samanta A (2005) Org Biomol Chem 18:1428
- Chen C-F, Chen Q-Y (2006) New J Chem 2:143
- Plenio H, Diodone R (1995) Inorg Chem 34:3964
- Medina JC, Goodnow TT, Bott S, Atwood JL, Kaifer AE, Gokel GW (1991) J Chem Soc Chem Commun 290
- Chen Z, Pilgrim AJ, Beer PD (1998) J Electroanal Chem 444:209

9. Beer PD, Cadman J (2000) *Coord Chem Rev* 205:131
10. Beer PD, Hayes EJ (2003) *Coord Chem Rev* 240:167
11. Tomapatanaget B, Tuntulani T, Chailapakul O (2003) *Org Lett* 5:1539
12. Suksai C, Leeladee P, Jainuknan D, Tuntulani T, Muangsin N, Chailapakul O, Kongsaree P, Pakavatchai C (2005) *Tetrahedron Lett* 46:765
13. Doorn ARV, Bos M, Harkema S, Eerden JV, Verboom W, Reinhoudt DN (1991) *J Org Chem* 56:2371
14. Carr JD, Lambert L, Hibbs DE, Hursthouse MB, Malik KMA, Tucker JHR (1997) *Chem Commun* 1649
15. Enraf-Nonius COLLECT. Nonius BV, Delft, The Netherlands, 1997–2000
16. Otwinowski Z, Minor W (1997) In: Carter CW, Sweet RM (eds) *Methods in enzymology, macromolecular crystallography, part A*, vol 276. Academic Press, London, pp 307–326
17. Sheldrick GM (1997) SHELXL-97. University of Gottingen, Gottingen, Germany
18. Farrugia LJ (1999) *J Appl Crystal* 32:837
19. Beer PD, Keefe AD (1990) *J Chem Soc Dalton Trans* 3675
20. Brunink JAJ, Verboom W, Engbersen JFJ, Harkema S, Reinhoudt DN (1992) *Recl Trav Chim Pays-Bas* 111:511
21. Böhmer V (1995) *Angew Chem Int Ed Engl* 34:713
22. Gutsche CD, Alam I (1988) *Tetrahedron* 44:4689
23. Greenwood NN, Earnshaw A (eds) (1984) *Chemistry of the elements*. Pergamon, Oxford, p 369
24. Beer PD, Bernhardt PV (2001) *J Chem Soc Dalton Trans* 1428
25. Barišić L, Rapić V, Pritzkow H, Pavlović G, Nemet I (2003) *J Organomet Chem* 682:131



This article appeared in a journal published by Elsevier. The attached copy is furnished to the author for internal non-commercial research and education use, including for instruction at the authors institution and sharing with colleagues.

Other uses, including reproduction and distribution, or selling or licensing copies, or posting to personal, institutional or third party websites are prohibited.

In most cases authors are permitted to post their version of the article (e.g. in Word or Tex form) to their personal website or institutional repository. Authors requiring further information regarding Elsevier's archiving and manuscript policies are encouraged to visit:

<http://www.elsevier.com/copyright>



Contents lists available at ScienceDirect

Sensors and Actuators B: Chemical

journal homepage: www.elsevier.com/locate/snb

New silver selective electrode fabricated from benzothiazole calix[4]arene: Speciation analysis of silver nanoparticles

Wittaya Ngeontae^a, Wanwisa Janrungroatsakul^a, Neramit Morakot^b,
Wanlapa Aeungmaitrepirom^a, Thawatchai Tuntulani^{a,*}

^a Department of Chemistry, Faculty of Science, Chulalongkorn University, Bangkok 10330, Thailand

^b Department of Chemistry, Faculty of Science, Mahasarakham University, Mahasarakham 44150, Thailand

ARTICLE INFO

Article history:

Received 26 March 2008

Received in revised form 2 May 2008

Accepted 7 May 2008

Available online 18 May 2008

Keywords:

Ion selective electrode

Ag⁺ ionophore

Calix[4]arene

Silver nanoparticles

ABSTRACT

A new calix[4]arene containing benzothiazolyl pendants was synthesized and used as an ionophore to fabricate macro- and micro-Ag⁺ selective membrane electrodes. PVC membranes plasticized with NPOE provided better selectivity coefficient towards Ag⁺ than those plasticized with DOS. The selectivity coefficients ($\log K_{Ag,j}^{pot}$) for macro- and microelectrode were, respectively, -2.8 and -2.5 for Hg(II) and lower than -4.0 and -3.5 for other cations tested. The fabricated electrodes can be used in a wide pH range (pH 2–8) with a response time less than 5 s. The electrodes exhibit near theoretical Nernstian slope (59.7 ± 0.8 mV decade⁻¹ for macroelectrode and 59.8 ± 1.0 mV decade⁻¹ for microelectrode) with low detection limits (ca. 5.0×10^{-7} M) and wide linear working range (10^{-6} to 10^{-2} M). The electrodes were used as an indicator electrode for the argentometric titration of the mixture of Cl⁻ and Br⁻. The fabricated electrodes were also used for the first time in speciation analysis of Ag nanoparticles with good accuracy and precision. This Ag-ISE should be beneficial to researches regarding Ag nanoparticles.

© 2008 Elsevier B.V. All rights reserved.

1. Introduction

It is well known that Ag ions and Ag-based compounds have strong antimicrobial effects [1]. Silver nanoparticles (AgNPs) are now received much interest in various applications including antibacterial clothes [2]. However, antimicrobial mechanisms of Ag ions and Ag nanoparticles are not well understood. Microbiologists have used a number of techniques to study the effects of Ag nanoparticles on microbial growth inhibition such as SEM, TEM [3] and ESR [4]. Ag⁺ selective electrode may be a valuable tool for measuring concentration of Ag⁺ to find a suitable condition for synthesizing desired silver nanoparticles and may be used to study antimicrobial properties of AgNPs.

Ion selective electrode (ISE) is an ion analysis technique that provides many unique characteristics. ISE may have response to ion activity change in the aqueous phase [5] based on the measurement of the phase boundary potential at the sample/membrane interface. Recently, backside calibration potentiometry has been demonstrated [6] as a new concept in the field of ISE, and further exploration to prove the validity of this technique has also been

reported [7]. The principle of ISE, thus, still continues to develop to valuable applications.

The ionophore is one of the important compositions in a polymeric membrane ion selective electrode. The ionophore selectivity over the interfering ion is the concerning issue in ionophore discovery. Good selectivity resulted from a stronger complex between an ionophore and a detecting ion rather than a weaker complex of the ionophore and interfering ions. A number of Ag-ISE's have been reported during the past 10 years. PVC membranes based on macrocyclic compounds such as pyridine tetramide [8], calix[2]furano[2]pyrrole [9] and tris(pentafluorophenyl)corrole [10] were reported to give high selectivity towards Ag⁺.

It is well known that sulfur containing ligands preferred to bind heavy metal ions such as Ag⁺ and Hg²⁺. Non-macrocyclic ionophores containing thiocarbamates [11,12], phosphorothiolates [13] and carboxythiophenoxy groups [14] have been reported to be selective ionophore for Ag⁺. In addition, cyclic thioethers were also employed as ionophore in Ag-ISE's [15,16].

Calixarene is the most frequently employed building block for ionophores. Kimura and co-workers reported Ag⁺ selective electrodes using π -coordinate calix[4]arene derivatives as soft neutral carriers in the membrane phase [17]. Bitter and co-workers have synthesized a variety of calix[4]arene derivatives containing sulfur donors and π -coordinate groups and studied their binding properties towards Ag⁺ [18]. Pretsch and colleague,

* Corresponding author. Tel.: +66 2 2187643; fax: +66 2 2187598.

E-mail address: thawattc@chula.ac.th (T. Tuntulani).

then, showed that selectivity coefficients of membranes containing π -coordinating calix[4]arene ionophores were worse than those containing calix[4]arene incorporating sulfur donors [19]. Demirel et al., reported that the Ag^+ selective PVC membrane using thiocrown-4 as an ionophore exhibited high selectivity towards Ag^+ over other ions [20]. Heterocyclic ionophores containing sulphur as donor sites were synthesized by Zhang's and He's groups [21–23]. They used two groups of thiobenzothiazole (four sulphur atoms in one molecule). This molecule exhibited good characteristics of Ag^+ ionophores. Recently, we have synthesized benzothiazole-derivatized calix[4]arenes by varying chain lengths of the benzothiazole tethers and *p*-tertbutyl substituents on the calix[4]arene. It was found that calix[4]arene with shortest chain length and no substituents possessed the best characteristic of the Ag^+ -ionophore [24]. In the light of this study, we synthesized a new calix[4]arene derivative containing two benzothiazole groups with a methylene tether and used the compound as an ionophore to make a Ag-ISE.

The principle of potentiometry states that potentiometry is less dependent on scaling laws. Recently, Bakker and co-workers have showed that they can successfully made solid-contact silver microelectrodes [25]. Therefore, a simple-to-make micropipette tip electrode (microelectrode) and a conventional standard size electrode (macroelectrode) have been constructed using the synthesized calix[4]arene ionophore. We also demonstrated the use of our Ag-ISE's in the argentometric titration of the mixture of Cl^- and Br^- . According to aforementioned literatures, there is no report in uses of Ag-ISE's in analysis of Ag nanoparticles. Therefore, in this article we have shown that our Ag-ISE's can be used in speciation analysis of Ag nanoparticles.

2. Experimental

2.1. Reagents and general method

Nuclear magnetic resonance (NMR) spectra were recorded on a Varian Mercury Plus 400 MHz nuclear magnetic resonance spectrometer. In all cases, samples were dissolved in deuterated chloroform. Chemical shifts were recorded in part per million (ppm) using a residue proton as internal reference. MALDI-TOF mass spectra were recorded on a Micromass Platform II. Calix[4]arene [26] as well as silver nanoparticles [27] were prepared by the previously published procedure.

High molecular weight polyvinyl chloride (PVC), *o*-nitrophenyl octyl ether (*o*-NPOE), bis (2-ethylhexyl)sebacate (DOS), potassium tetrakis(4-chlorophenyl)borate (KTPClPB) and tetrahydrofuran (THF) were purchased from Fluka with Selectophore® grade. Nitrate salts of cations were of analytical grade obtained from Merck, Fluka, Sigma–Aldrich, Reidel and Carlo Erba. The solution pH was adjusted by HNO_3 or NaOH. All solutions were prepared with ultrapure water from Milli-Q (Bedford, MA, USA) water purification system (Millipore).

2.2. Synthesis of the ionophore

2.2.1. Synthesis of

25,27-di(cyanomethoxy)-26,28-dihydroxycalix[4]arene (**1**)

In a 250 mL two-necked round bottom flask equipped with a magnetic bar, 25,26,27,28-tetrahydroxycalix[4]arene (5.00 g, 11.8 mmol), potassium carbonate (4.60 g, 33.2 mmol) and acetonitrile (120 mL) were stirred under nitrogen at room temperature for 1 h. Bromoacetonitrile (6.20 g, 51.6 mmol) was then added and the mixture was heated at reflux for 7 h. The mixture was cooled to room temperature and filtered. The filtrate was evaporated to

reduce the volume of the solution. Methanol was then added to precipitate 25,27-di(cyanomethoxy)-26,28-dihydroxycalix[4]arene, **1**, as a white solid (3.60 g, 60%).

^1H NMR spectrum (400 MHz, CDCl_3): δ (in ppm) 7.13 (d, $J = 7.2$ Hz, 4H, *m*-HArOH) 6.83 (d, $J = 7.6$ Hz, 4H, *m*-HArOCH₂) 6.79–6.73 (m, 4H, *p*-HArOH and *p*-HArOCH₂) 6.02 (s, 2H, ArOH) 4.85 (s, 4H, CH₂CN) 4.26 (d, $J = 13.6$ Hz, 4H, Ar-CH₂-Ar) 3.52 (d, $J = 13.6$ Hz, 4H, Ar-CH₂-Ar).

2.2.2. 25,27-Di(benzothiazolyl)-26,28-hydroxycalix[4]arene (**CU1**)

Compound **1** (0.50 g, 1.0 mmol) was mixed with 2-aminothiophenol (0.34 mL, 2.3 mmol). The reaction mixture was heated at reflux and stirred for 3 h under nitrogen. The reaction mixture was then cooled to room temperature. Dichloromethane (50 mL) was added into the mixture, and methanol was subsequently added to precipitate 25,27-di(benzothiazolyl)-26,28-hydroxycalix[4]arene, **CU1**, as a white solid (0.58 g, 81%).

^1H NMR spectrum (400 MHz, CDCl_3): δ (in ppm) 8.05 (d, $J = 8.4$ Hz, 2H, BTArH), 7.51 (t, $J = 7.6$ Hz, 2H, BTArH), 7.43 (d, $J = 8.4$ Hz, 2H, BTArH), 7.29 (t, $J = 7.6$ Hz, 2H, BTArH), 7.25 (s, 2H, OH), 7.11 (d, $J = 7.6$ Hz, 4H, *m*-HArOH), 6.89 (d, $J = 7.6$ Hz, 4H, *m*-HArCH₂), 6.78 (t, $J = 7.2$ Hz, 2H, *p*-HArOH), 6.72 (t, $J = 7.4$ Hz, 2H, *p*-HArCH₂), 5.45 (s, 4H, ArOCH₂), 4.42 (d, $J = 13.6$ Hz, 4H, Ar-CH₂-Ar), 3.47 (d, $J = 13.6$ Hz, 4H, Ar-CH₂-Ar). ^{13}C NMR spectrum (100 MHz, CDCl_3): δ (in ppm) 167.6, 153.2, 152.8, 151.4, 135.1, 132.7, 129.3, 128.7, 127.7, 126.2, 126.0, 125.2, 123.0, 122.0, 119.2, 75.5, 31.2 MALDI-TOF for $[\text{C}_{44}\text{H}_{34}\text{N}_2\text{O}_4\text{S}_2 + \text{K}]^+$, Anal calc: $m/z = 757.1$, Found: $m/z = 756.9$.

2.3. Membrane preparation

The membrane cocktail consisting of ionophore **CU1** (10 mmol kg⁻¹), KTPClPB, 33 wt.% PVC and 66 wt.% plasticizer were dissolved in 2.5 mL of THF (total mass of 220 mg). The cocktail solution was then poured into a glass ring (30 mm i.d.) fixed on a glass plate. The solvent was allowed to evaporate overnight at room temperature to give a transparent membrane (thickness ~0.2 mm). The membrane was punched into small sizes (7.5 mm i.d.) and glued with a PVC/THF slurry on the top of PVC tube and connected to a micropipette tip as an electrode body. For microelectrodes, the tip of 1 mL micropipette (0.5 mm i.d.) was dipped into membrane cocktail for 3 s. It was left to stand in vertical position to allow the solvent to evaporate. The membrane thickness is around 0.5 mm. Membrane compositions and electrode response properties are collected in Table 1.

2.4. EMF measurements

The polymeric membrane electrodes were conditioned overnight in 0.01 M solution possessing identical composition as inner filling solution. Membrane potentials were measured in stirring solution at ambient temperature in the galvanic cell:

Ag, AgCl/3 M KCl//1 M LiOAc/sample solution/membrane/IFS/AgCl, Ag.

The reference electrode Ag/AgCl with double junction was used (type 6.0726.100, Metrohm AG, CH-9010 Herisau, Switzerland) with 1 M LiOAc as salt bridge electrolyte. Continuous EMF measurements were carried out with a 16-channel electrode monitor (Lawson Labs Inc., Malvern, PA 19355, USA) while discrete EMF measurements were monitored by a pH meter (Orion Research Inc., Boston, MA 02129, USA). Activity coefficients of cations in aqueous solutions were calculated according to the Debye–Hückel approximation [28].

Table 1
Membrane compositions and electrode response properties

Electrode number	Membrane composition (wt.%)				Slope (mV decade ⁻¹)	Linear range (M)	Detection limit (M)
	Ionophore (mmol kg ⁻¹)	KTpClPB (mmol kg ⁻¹)	PVC	Plasticizer			
I	0.72 (10.00)	0.11 (2.23)	32.42	DOS, 66.74	40.8 ± 1.0	10 ⁻³ to 10 ⁻²	7.9 × 10 ⁻⁵
II	0.73 (10.17)	0.25 (5.03)	33.02	DOS, 66.00	51.5 ± 0.5	10 ⁻⁶ to 10 ⁻²	3.9 × 10 ⁻⁷
III	0.78 (10.94)	0.37 (7.47)	33.02	DOS, 65.82	56.2 ± 1.2	10 ⁻⁶ to 10 ⁻²	3.9 × 10 ⁻⁷
IV	0.69 (9.67)	0.11 (2.23)	32.22	<i>o</i> -NPOE, 66.97	59.4 ± 0.3	10 ⁻⁶ to 10 ⁻²	4.0 × 10 ⁻⁷
V-Macro	0.72 (10.05)	0.25 (5.04)	32.42	<i>o</i> -NPOE, 66.60	59.7 ± 0.8	10 ⁻⁶ to 10 ⁻²	4.4 × 10 ⁻⁷
V-Micro	0.73 (10.12)	0.25 (5.06)	32.87	<i>o</i> -NPOE, 66.14	59.8 ± 1.0	10 ⁻⁶ to 10 ⁻²	5.0 × 10 ⁻⁷
VI	0.76 (10.50)	0.36 (7.30)	32.72	<i>o</i> -NPOE, 66.16	58.5 ± 0.3	10 ⁻⁶ to 10 ⁻²	4.2 × 10 ⁻⁷

2.5. Selectivity measurements

An electrode with 0.01 M interfering cations (chloride salt) as an inner filling solution was conditioned in a metal nitrate solution overnight. The response of the electrode was first measured against the same interfering metal ions (10⁻⁷ to 10⁻² M). The electrode was then used to measure the response of silver nitrate solutions. The measurement was done in triplicate (using new membrane for one replicate). The interfering ions studied were H⁺, Na⁺, K⁺, Ca²⁺, Mg²⁺, Ni²⁺, Cu²⁺, Zn²⁺, Cd²⁺, Pb²⁺ and Hg²⁺. For determination of the selectivity coefficient of Hg²⁺, the solution pH was adjusted to pH 2 using 0.1 M HNO₃.

2.6. Reversibility of the membrane potential

The membrane reversibility was examined by measuring the EMF of Ag-ISE in a 10⁻⁴ M Ag⁺ solutions. Subsequently, the electrode was rinsed and dipped into a 10⁻³ M Ag⁺ solution. The cycle was repeated three times.

2.7. Effects of the solution pH

The reference electrode and pH electrode were immersed in 0.1 M KNO₃ solution and the solution was adjusted to pH 8 with 1% KOH. Subsequently, 500 μL of 0.01 M AgNO₃ was added into the solution to obtain 10⁻⁴ M Ag⁺ sample solution. The pH of the solution was varied from 8 to 1.6 by gradually adding 0.01 M HNO₃. Both pH and EMF values were read simultaneously. These measurements were carried out using the same electrode, but concentrations of the sample solution were varied from 10⁻⁴ to 10⁻² M.

2.8. Long-term measurements

After conditioning a membrane overnight in 0.01 M AgNO₃, Ag-ISE's response were recorded over the concentration range of 10⁻⁸ to 10⁻² M Ag⁺. This procedure was repeated several times. The slopes and response potentials during a period of 30 days were recorded. The electrodes were kept in the dark after use.

2.9. Applications of fabricated electrodes

2.9.1. Application as the indicator electrodes for argentometric titration

The Ag-ISE was used as an indicator electrode in potentiometric titrations to determine the concentration of mixed Cl⁻ and Br⁻. Sample solutions were prepared by adding 25 μL of 1 M KCl and 1 M KBr into 50 mL ultra pure water. The mixed solution was stirred and titrated with 0.01 M AgNO₃.

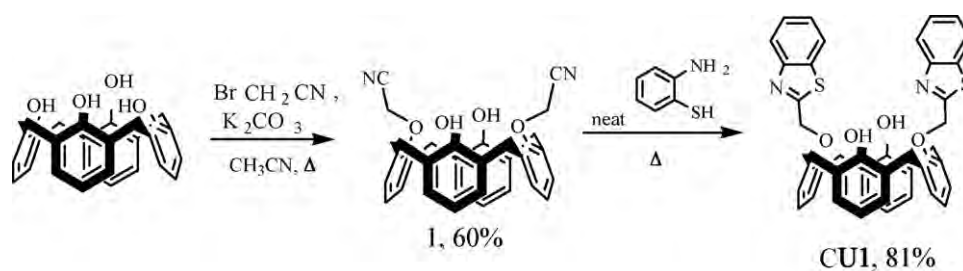
2.10. Application for determination of silver nanoparticles

The speciation analysis of Ag nanoparticles (AgNPs) was started by determination of free Ag⁺. The AgNPs, 1 mL, was diluted to 10 mL by water. The Ag⁺-ISE can be directly immersed to the dilute solution. The response signal was corresponding to the concentration of free Ag⁺. Total amount of Ag⁺ in AgNPs was then determined by adding 40 μL of AgNPs into 10 mL of water. Subsequently, 4% (v/v) H₂O₂ (5 μL) was added into the solution and the EMF of the solution was measured. The procedure was repeated several times. The calibration curve was always evaluated before and after each experiment.

3. Results and discussion

The new benzothiazole calix[4]arene was synthesized by the method shown in Scheme 1. The reaction between calix[4]arene and bromoacetonitrile in the presence of K₂CO₃ yielded 25,27-di(cyanomethoxy)-26,28-dihydroxycalix[4]arene, compound **1**, in 60% yield. Subsequently, **1** reacted with neat 2-aminothiophenol to give 25,27-di(benzothiazolyl)-26,28-dihydroxycalix[4]arene, **CU1**, as a product in 81% yield.

The synthesized ionophore, **CU1**, was incorporated into the plasticized PVC membrane in the presence of a cationic ion exchanger. Compositions of the membrane were optimized by keeping a constant ratio of PVC and plasticizer to 1:2 by weight. Two types of plasticizers, DOS and NPOE, were used, and the responses of their corresponding ISE's were compared as shown in Fig. 1. Fig. 1a showed that the response characteristic of DOS membrane was highly dependent on the amount of the ion exchanger. In the pres-



Scheme 1. Synthesis of **CU1**.

ence of 25 mol% of KTpCIPB (relative to ionophore) the membrane did not give the expected EMF changed while the concentrations of Ag^+ were increased. However, when the ion exchanger was increased to 50 and 75 mol%, the membrane response was found with a slope of 51.5 ± 0.5 and $56.2 \pm 1.2 \text{ mV decade}^{-1}$, respectively. For the membrane plasticized with NPOE the response characteristic shown in Fig. 1b seemed to be independent from the amount of the ion exchanger added. Moreover, the slopes obtained from NPOE membranes were close to the theoretical Nernstian slope as summarized in Table 1. This behavior may stem from the better complexation of the ionophore **CU1** towards Ag^+ in a more polar matrix.

The lower detection limits were found to be relatively low. In the membrane plasticized with DOS the lower detection limits (IUPAC definition) were found to be 7.9×10^{-5} , 3.9×10^{-7} and $3.9 \times 10^{-7} \text{ M}$ for the membrane containing 25%, 50% and 75% KTpCIPB, respectively. The lower detection limit in membrane plasticized with NPOE was found to be around $4.0 \times 10^{-7} \text{ M}$ or about 47 ppb which is comparable to the detection limit in FAAS method.

According to phase-boundary model, the EMF of a polymeric membrane electrode is directly proportional to the logarithmic activity of analyte ions. This means the electrode area or electrode size does not affect the ISE response. From this principle we have fabricated a microelectrode from **CU1** using NPOE as plasticizer. A smaller electrode has an advantage that very low concentration of an analyte can be measured or the electrode can be used in a limited space. The response characteristics of the microelectrode have also been evaluated in the same manner as macroelectrode (NPOE as plasticizer). The electrode behaviors were similar to the macroelectrode. Theoretical Nernstian slope ($59.8 \pm 1.0 \text{ mV decade}^{-1}$) was

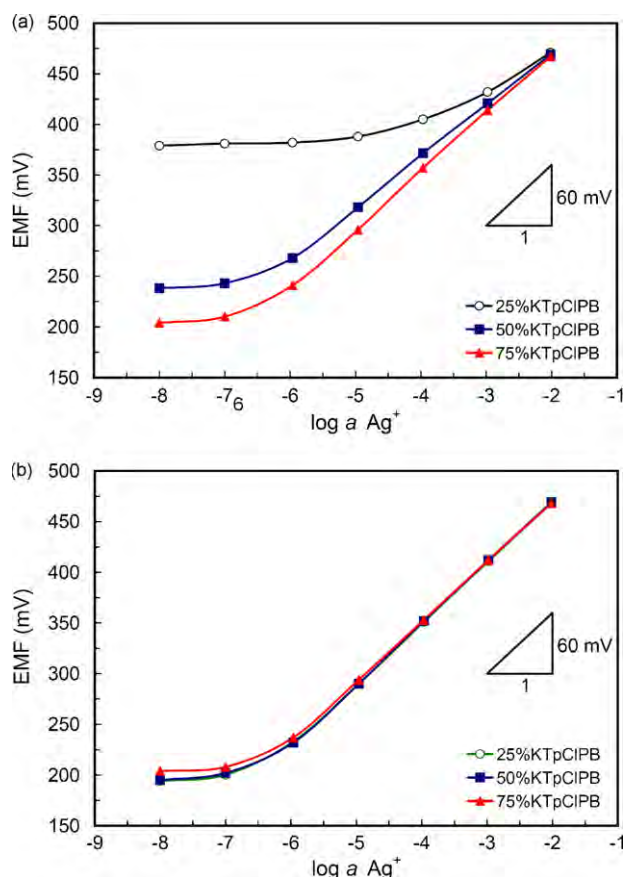


Fig. 1. Effect of % ion exchanger (relative to the ionophore) to the membrane response in different plasticizer (a) DOS and (b) NPOE.

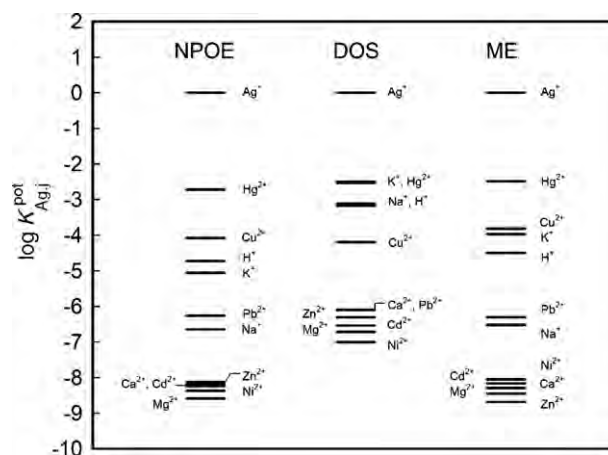


Fig. 2. Comparison of selectivity coefficients ($\log K_{\text{Ag},j}^{\text{Pot}}$) in membrane plasticized with NPOE and DOS (in macroelectrode) and NPOE (in microelectrode, ME). The membrane compositions are 10 mmol kg^{-1} ionophore and 5 mmol kg^{-1} KTpCIPB in NPOE membrane and 10 mmol kg^{-1} ionophore and 7.5 mmol kg^{-1} KTpCIPB in DOS membrane.

observed and the lower detection limit was $5.0 \times 10^{-7} \text{ M}$ (54 ppb). The performance characteristics of the micro-size electrode are thus comparable with the regular size electrode.

Selectivity of an ionophore is the most crucial characteristic of an ISE. The ionophore should have good selectivity over interfering ions in order to avoid the bias response from such interfering ions. The selectivity of the ionophore results from the complex formation between the ionophore and an analyte ion. The selectivity of ISE's was explored based on the so-called "unbiased selectivity coefficient" proposed by Bakker and co-workers [19]. The calibration curve of the interfering ion was performed by membranes that did not expose to the Ag^+ solution. Most studied ions showed near Nernstian slope in which such behavior was not seen when the membrane was conditioned in 0.01 M AgNO_3 . Subsequently, the same membrane was used again to record a calibration curve for Ag^+ . The super Nernstian slopes were always observed at concentration of Ag^+ below 10^{-4} M due to the effect of the strong inward ion flux to the inner side of the membrane [29]. However, when the concentration of Ag^+ increased from 10^{-4} to 10^{-2} M , the expected Nernstian slopes were observed. The selectivity order of standard-size membrane plasticized with NPOE and

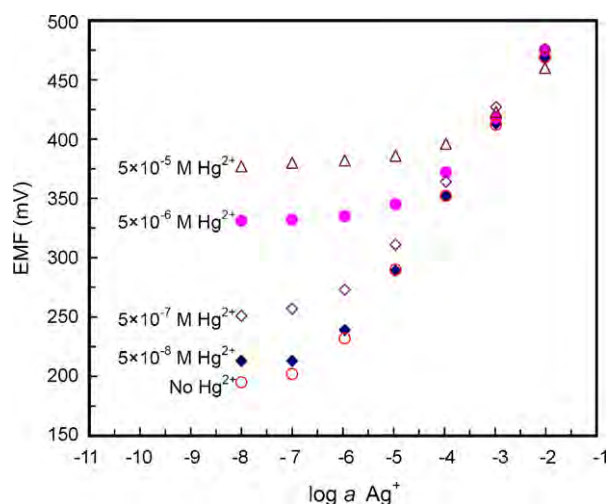


Fig. 3. Potential response of Ag-ISE using NPOE as plasticizer in the presence of different concentrations of Hg^{2+} at pH 2.0.

DOS and microelectrode using NPOE as plasticizer are shown in Fig. 2.

From Fig. 2, it can be seen that the synthesized ionophore, **CU1**, exhibited the selectivity over transition metals up to $\log K_{Ag^+,j}^{pot} = -8$. The synthesized ionophore, **CU1**, can thus be used in the presence of several metal ions in high concentration levels. The most common interfering ion for Ag-ISE's is Hg^{2+} due to its mercaptophilic property [30]. The synthesized ionophore, **CU1**, shows clearly that it can be used in the system contained Hg^{2+} ion with the logarithmic selectivity coefficient around -2.5 . In order to evaluate the usable range of the electrode in the presence of Hg^{2+} , the electrode responses of Ag^+ in different concentrations of Hg^{2+} have been measured. The results are shown in Fig. 3. It can be seen that the linear working range decreases while the concentration of Hg^{2+} increases. Nevertheless, it can be deduced that the electrode can be used with Nernst's slope up to 5×10^{-6} M Hg^{2+} with working concentration ranging of 10^{-4} to 10^{-2} M. The selectivity pattern of the microelectrode-based NPOE is similar to the macroelectrode using NPOE. This can be concluded that the size of the electrode does not affect the selectivity of the ionophore when the membrane composition was identical. Due to the better selectivity coefficients found in the NPOE membrane, we decide to use the membrane plasticized with NPOE for further explorations.

Acidity and alkalinity of aqueous solution always play an important role in the metal ion measurement. This may

stem from the formation of hydroxo complexes of metal or protonation–deprotonation of the ionophore. The effect of solution pH towards the membrane potential was then evaluated by adding HNO_3 to Ag^+ solution at pH 8 until the significant EMF change was observed. The pH was measured concurrently with the EMF change. Three kinds of solutions contained 0.1 M KNO_3 and Ag^+ at 10^{-4} , 10^{-3} and 10^{-2} M were studied. The results are shown in Fig. 4a. It can be seen that the ISE can be used in a wide range of solution pH from pH 8 to 2.5 with no significant change in the EMF value. The electrode was affected when $pH < 2.5$ probably due to the interference from H^+ and $pH > 8$ due to the precipitation of silver hydroxide. However, the effective pH range found in this study was wide enough to use in the sample without critical pH adjustment needed.

The same procedure was also carried out for the microelectrode measurement. The results are shown in Fig. 4b, it was found that the behavior of the microelectrode was similar to the macroelectrode with the same pH range for all concentration levels. This supported the fact that reducing the electrode size will not affect the electrode responses.

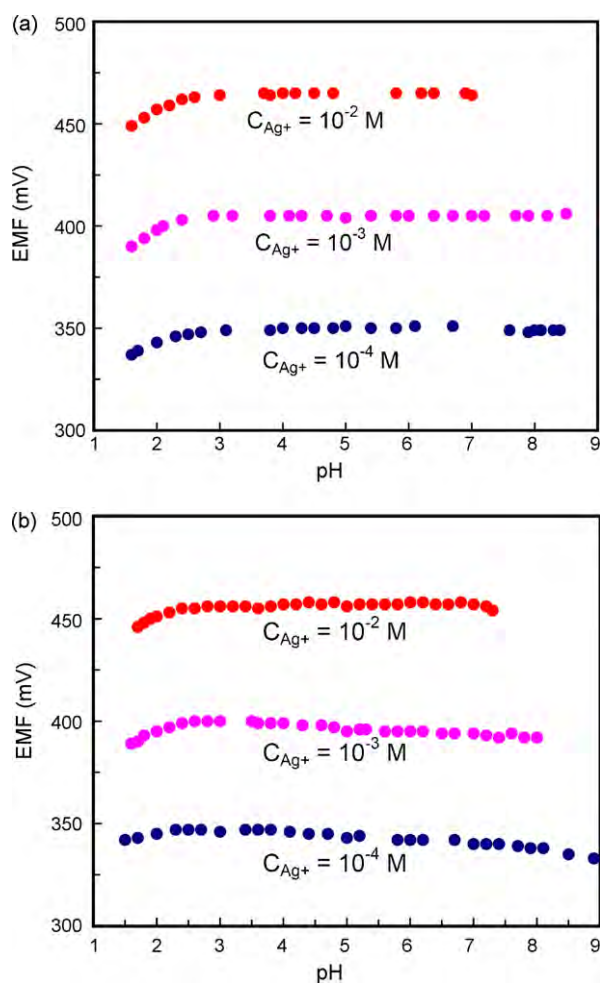


Fig. 4. Potential response of NPOE plasticized Ag-ISE (a) macroelectrode and (b) microelectrode at variation of solution pH observed in three different Ag^+ concentrations in the presence of 0.01 M KNO_3 .

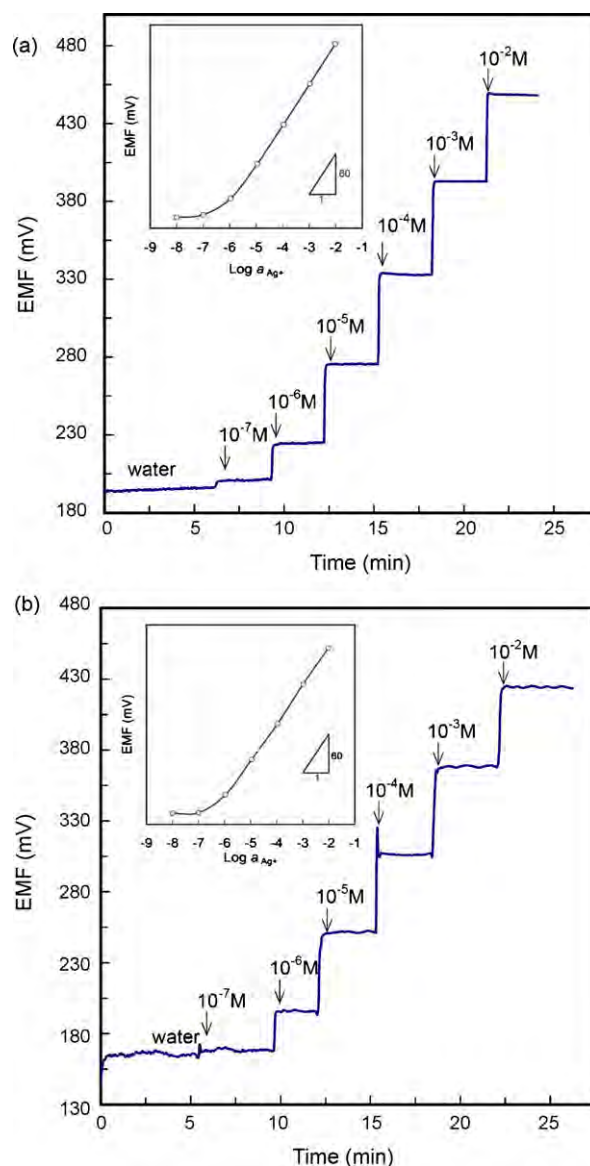


Fig. 5. Time trace line observation of Ag-ISE electrode after adding Ag^+ to the solution (a) macroelectrode and (b) microelectrode.

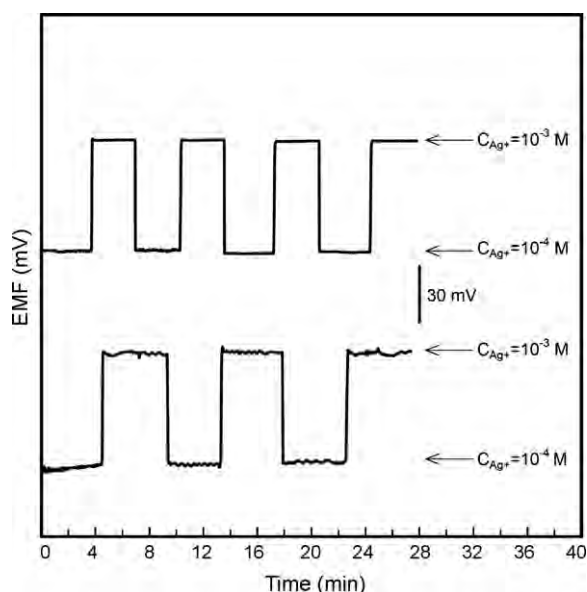


Fig. 6. Reversibility of Ag-ISE electrode at the concentration between 10^{-4} and 10^{-3} M in the presence of 0.01 M KNO_3 . Top: macro-Ag-ISE. Down: micro-Ag-ISE.

The response time and reversibility of an electrode are also important characteristic of a ISE. Fig. 5a illustrates a time trace line of the electrode response using macroelectrode. The macro-electrode shows very fast response time (less than 5 s) to reach a stable EMF value. After the EMF signals reach the plateau at a given concentration level, the traces shows very slight signal fluctuation. The microelectrode, however, shows slower response time (10 s) and more fluctuated signals as depicted in Fig. 5b. A faraday cage is essentially needed in the case of the microelectrode to decrease noise. However it is not required in the case of macroelectrodes. The potentials were very stable after changing the concentration. The reversibility of the electrode was evaluated by alternatively measured EMF's of two different concentrations, 10^{-4} and 10^{-3} M Ag^+ . The results are shown in Fig. 6. The EMF signals were found

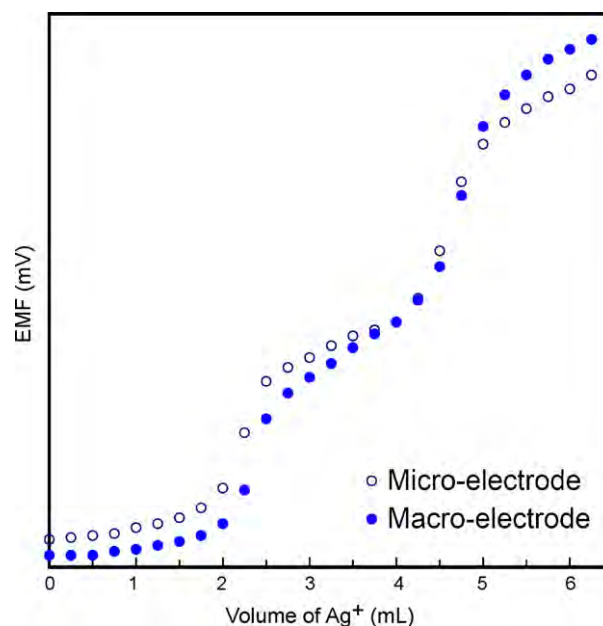


Fig. 8. Potentiometric titration curves of the mixture of 1.0 M (25 μL) of KBr and KCl with 0.01 M AgNO_3 using macro- and microelectrodes.

to be restored at the same concentration of Ag^+ in every cycle. The electrode can, therefore, be used to measure the Ag^+ concentration with excellent reversibility.

Long-term stability of the proposed electrodes was evaluated in order to find the life time of the electrode membrane. The life time of a membrane was evaluated by frequent calibration over 1 month. The EMF responses showed no significant drift for 18 days with the concentration range 10^{-5} to 10^{-2} M as shown in Fig. 7. However, after 18 days the potential changed significantly from the freshly conditioned membrane. The electrode membrane also turned black, and silver metal-like color appeared on the membrane surface.

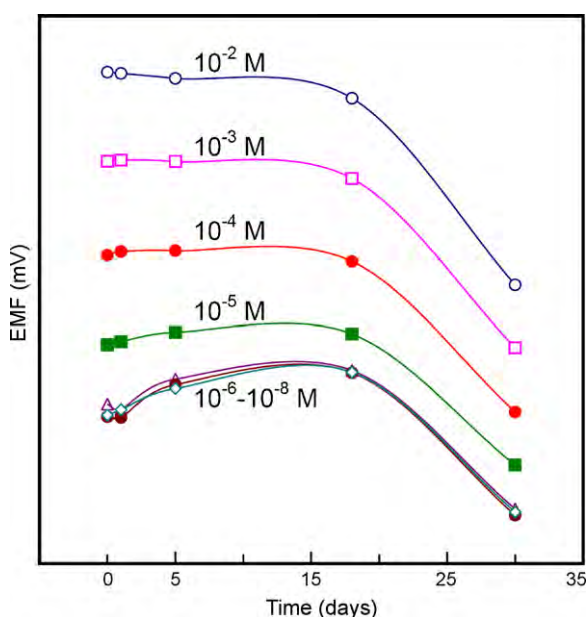


Fig. 7. Long-term response of the macro-Ag-ISE measured by using the same electrode.

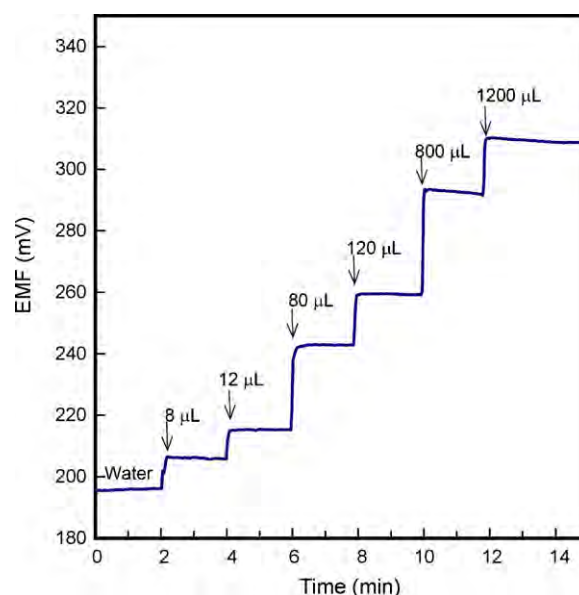


Fig. 9. Ag-ISE response after adding appropriate volumes of concentrated AgNPs into 10.0 mL of water. The response is corresponding to the residual silver ion presented in the AgNPs solution.

The life time of microelectrode is shorter. It can be used for only 1 day after condition. This disadvantage stems from the fact that sensing ingredients in the membrane are very low, and leaching of the sensing ingredients makes the membrane response changed negatively. Nevertheless a microelectrode needs very small amount of membrane ingredients. It can thus be produced at a very low cost and can be disposed after use.

The fabricated electrodes were applied in potentiometric titrations of the mixture of chloride and bromide ions. Because K_{sp} of AgBr is 1000 times lower than that of AgCl. Therefore, it is theoretically possible to potentiometrically titrate the mixture of chloride and bromide in one experiment. Titration curves of 25 μ L of 1.0 M KBr and 1.0 M KCl with 0.01 M AgNO₃ are illustrated in Fig. 8. Two end points are clearly established for both types of electrodes. The first end point is corresponding to the quantity of Br[−] and the second end point is pertinent to the amount of Cl[−].

Nowadays, nanoparticles are a subject of high interest because the nanometer-sized materials provide special characteristics that are not seen in the macro-sized materials of the same element.

AgNPs are one of the most interested nanoparticles developed for industrial and medical uses [1–4]. Actually, AgNPs can be synthesized by several procedures with different size and particle size distribution [31,32]. Our Ag-ISEs were also explored their applications in speciation analysis of the AgNPs. The rationale was from the preparative procedure of AgNPs which were reduced from salts of Ag(I). Usually, Ag ions were left after reduction of a Ag(I) salt to AgNPs. The presence of residual Ag⁺ would degrade the reactivity and property of AgNPs. Hence, determination of residual Ag⁺ and total Ag⁺ concentration is needed in order to control the nanoparticle quality. From the principle of basic atomic spectroscopy, commercial spectroscopic instruments such as FAAS cannot determine differences between Ag⁺ and Ag nanoparticles. This problem can be solved by an ISE because the ISE senses only Ag⁺ presented in the solution.

Here, we demonstrate a simple procedure to determine Ag⁺ in AgNPs solution using our fabricated Ag⁺-ISEs. Both macro- and microelectrodes can be used directly to the AgNPs solution to determine residual Ag⁺. Effects of the sample matrix to the electrode response are shown in Fig. 9. Calibration curves in the presence and absence of the AgNPs show insignificant differences. Therefore, the AgNPs solution matrix does not interfere the electrode membrane.

Upon adding AgNPs solution to the sample vial, residual Ag⁺ in the solution was observed from the potential jump as shown in Fig. 9. In order to check the amount of free silver and the matrix interference in the AgNPs solution, different amounts of AgNPs were added to the solution. The pattern of potential jumps was similar to a calibration curve generated with the Ag⁺ standard solution. This result showed that the response of the membrane towards the residual Ag⁺ presented in the AgNPs solution could be measured without bias from the sample matrix.

AgNPs (1.00 mL) was diluted to 10.00 mL for determination of residual Ag⁺ presented in the AgNPs solution. The comparison time trace lines between the system in the presence and absence of AgNPs are shown in Figs. 10a and b for macro- and microelectrode, respectively. The residual Ag⁺ concentration that presented in the original AgNPs solution was calculated by direct calibration curve and found to be 3.77 ± 0.2 and 3.61 ± 0.2 ppm for macro- and microelectrode, respectively. Therefore, the residual Ag⁺ measured from both electrodes is not statistically different.

The total concentrations of the silver content in the AgNPs solution were determined by oxidizing with H₂O₂ to yield Ag⁺.

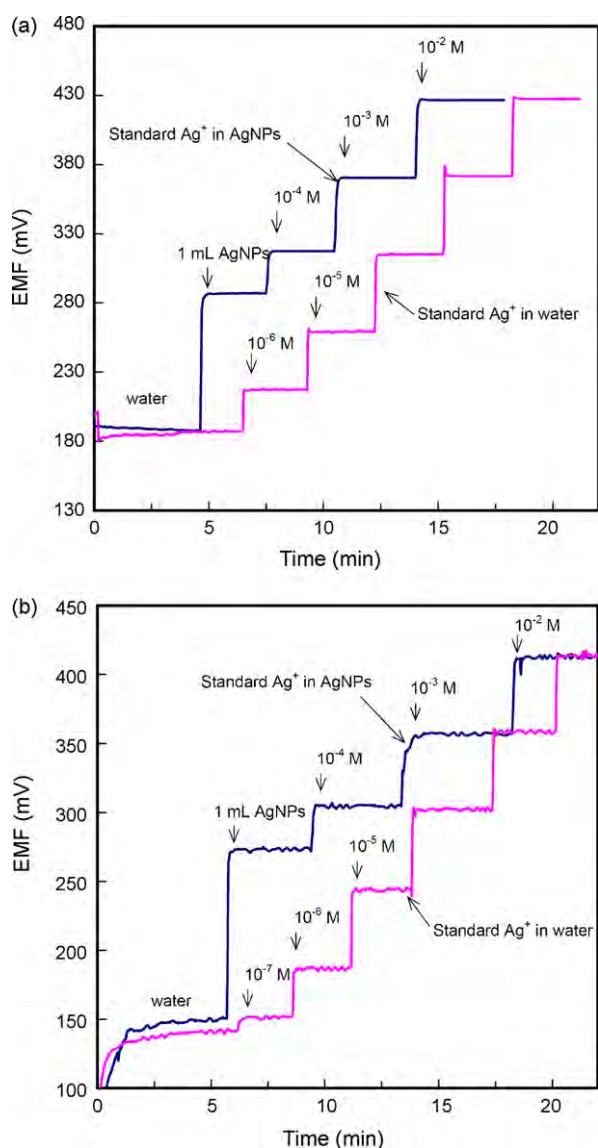


Fig. 10. Comparison of time trace lines in the absence and presence of 1.0 mL of concentrated AgNPs solution diluted to 10 mL in water for (a) macro- and (b) microelectrode.

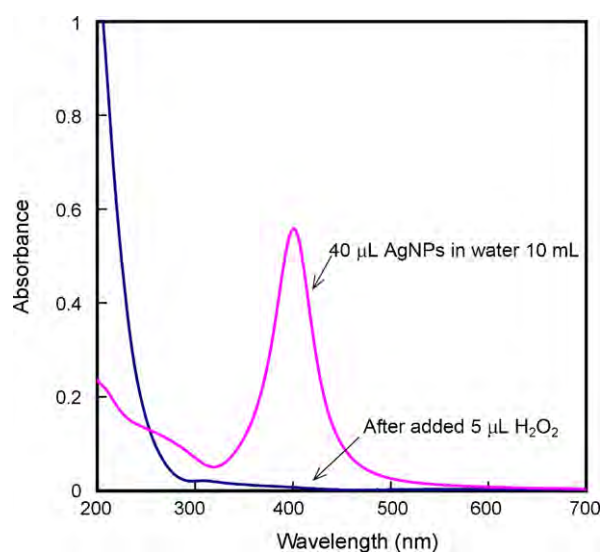


Fig. 11. UV-visible spectrum of AgNPs solution before and after adding 5 μ L of H₂O₂.

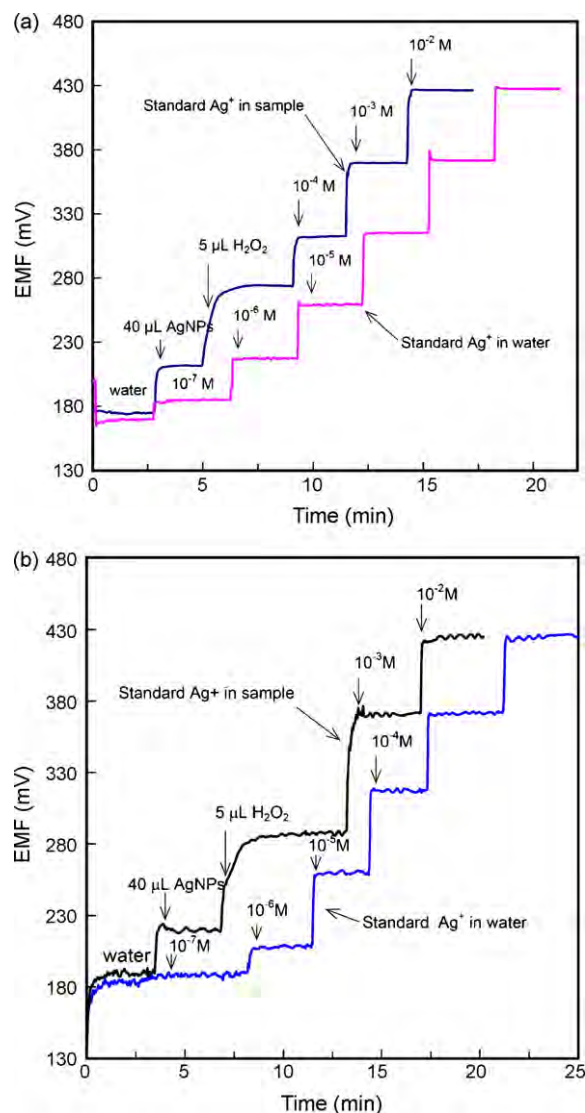


Fig. 12. Time trace line of the Ag-ISE electrode, comparison between calibration curve time trace line and the system containing AgNPs. In the lower line, 40 µL of concentrated AgNPs was added to 10 mL of water following by adding 5 µL of H₂O₂ for (a) macro- and (b) microelectrode.

The complete conversion of AgNPs was confirmed by UV–visible spectrophotometry as shown in Fig. 11. The characteristic sharp absorption peak at 401 nm disappears when 5 µL of 4% (v/v) H₂O₂ was added. The potential jumps while the H₂O₂ was added suggests the increment of Ag⁺ in the solution as showed in Fig. 12a. The microelectrode could be used to measure total Ag⁺ content in the AgNPs solution in the same manner as the macroelectrode as illustrated in Fig. 12b. After the residual Ag⁺ in the mixture solution was measured, 100 µL of 4% (v/v) H₂O₂ were added. It was found that H₂O₂ was able to harm the sensing membrane. The potential of the standard Ag⁺ added to the solution (after added H₂O₂) were lower than the calibration curve (before total Ag⁺ measurement) indicating the loss of the sensor materials. Therefore, the amount of H₂O₂ was reduced to the smallest volume (5 µL) that was enough to provide complete oxidation (confirmed by UV–visible spectrophotometer). The membrane responses of both macro- and microelectrodes after contacting H₂O₂ did not changed significantly.

The EMF values can be used to calculate the total concentration of Ag⁺ by direct calibration curve. The concentration of total Ag content in the AgNPs (dilution by adding 40 µL of AgNPs to 10 mL solution) determined using macro- and microelectrode by direct calibration was 3.57 ± 0.17 and 3.43 ± 0.15 ppm, respectively. In addition, the concentration of total silver content in the same AgNPs solution determined by FAAS method was 3.62 ± 0.05 ppm. By using a pair *t*-test, the concentration of Ag⁺ from ISE method was insignificantly different from the FAAS result at 95% confidence level. Therefore, the performance of our fabricated ISE is comparable with such an expensive instrument. Moreover, the FAAS method cannot differentiate silver species in the AgNPs sample.

After determination of total concentration of AgNPs had done, the calibration curve was always rechecked again in order to confirm that the measuring value was not bias. The calibration curve after adding H₂O₂ showed insignificant difference with the original membrane observed. However, this problem did not observe in the macroelectrode because of more sensor ingredients.

4. Conclusions

A novel calix[4]arene containing benzothiazole groups, **CU1**, has been synthesized and exhibits a good characteristic for Ag⁺-ISE. The membrane plasticized with NPOE shows better selectivity coefficients than DOS membrane. Nernstian's slope can be observed with the detection limit in micro-molar range. The working linear ranges are found to be 4 orders of magnitude. The response time is very fast and the measured potentials are very stable. We have demonstrated that the microelectrode can be used in a similar manner as regular-size electrode. The application in the determination of the mixture of chloride and bromide ion was successful by the presence of two distinguishable end points. We have also shown that our fabricated electrodes can remarkably be employed in speciation analysis of the AgNPs solution in which both residual Ag⁺ and the total Ag content can be determined by a simple procedure.

Acknowledgements

This research was financially supported by The Thailand Research Fund (RTA5080006). Professor Dr. Sanong Ekgsatit and Mr. Pattwat Maneewattanapinyo are gratefully acknowledged for providing AgNPs.

References

- [1] F. Furno, K.S. Morley, B. Wong, B.L. Sharp, P.L. Arnold, S.M. Howdle, R. Bayson, P.D. Brown, P.D. Winship, H.J. Reid, Silver nanoparticles and polymeric medical devices: a new approach to prevention of infection? *J. Antimicrob. Chemother.* 54 (2004) 1019.
- [2] N. Durán, P.D. Marcato, G.I.H. De Souza, O.L. Alves, E. Esposito, Antibacterial effect of silver nanoparticles produced by fungal process on textile fabrics and their effluent treatment, *J. Biomed. Nanotech.* 3 (2007) 203.
- [3] I. Sondi, B. Salopek-Sondi, Silver nanoparticles as antimicrobial agent: a case study on *E. coli* as a model for Gram-negative bacteria, *J. Colloid Interface Sci.* 275 (2004) 177.
- [4] J.S. Kim, E. Kuk, K.N. Yu, J.-H. Kim, S.J. Park, H.J. Lee, S.H. Kim, Y.K. Park, C.-Y. Wang, Y.-W. Kim, Y.-S. Lee, D.H. Jeong, M.-H. Cho, Antimicrobial effects of silver nanoparticles, *Nanomedicine* 3 (2007) 95.
- [5] E. Bakker, P. Bühlmann, E. Pretsch, Carrier-based ion-selective electrodes and bulk optodes. 1. General characteristics, *Chem. Rev.* 97 (1997) 3083.
- [6] A. Malon, E. Bakker, E. Pretsch, Backside calibration potentiometry: ion activity measurements with selective supported liquid membranes by calibrating from the inner side of the membrane, *Anal. Chem.* 79 (2007) 632.
- [7] W. Ngeontae, Y. Xu, C. Xu, W. Aeungmaitrepirom, T. Tuntulani, E. Pretsch, E. Bakker, Sensitivity and working range of backside calibration potentiometry, *Anal. Chem.* 79 (2007) 8705.
- [8] R.K. Mahajan, O. Parkash, Silver(I) ion selective PVC membrane based on bis-pyridine tetramide macrocycle, *Talanta* 52 (2000) 691.
- [9] S.M. Kim, H.J. Chung, K.-J. Paeng, C.-H. Lee, H.N. Choi, W.-Y. Lee, Calix[2]furan[2]pyrrole and related compounds as the neutral carrier in silver ion-selective electrode, *Anal. Chim. Acta* 453 (2002) 81.

- [10] X.-B. Zhang, Z.-X. Han, Z.-H. Fang, G.-L. Shen, R.-Q. Yu, 5,10,15-Tris(pentafluorophenyl)corrole as highly selective neutral carrier for a silver ion-sensitive electrode, *Anal. Chim. Acta* 562 (2006) 210.
- [11] B.Y. Kim, H.P. Hong, K.T. Cho, J.H. On, Y.M. Jun, I.S. Jeong, G.S. Cha, H. Nam, Silver (I) ion selective ionophores containing dithiocarbamoyl moieties on steroid backbone, *Talanta* 66 (2005) 794.
- [12] Z. Yan, Y. Lu, X. Li, Silver ion-selective electrodes based on bis(dialkylthiocarbamates) as neutral ionophores, *Sens. Actuators B* 122 (2007) 174.
- [13] D. Xu, T. Katsu, O,O,O-Trialkyl phosphorothioates as simple and effective ionophores for silver ion-selective membrane electrodes, *Anal. Chim. Acta* 443 (2001) 235.
- [14] M.K. Amini, M. Ghaedi, A. Rafi, I. Mohamadpoor-Baltork, K. Niknam, Silver selective electrodes based on methyl-2-pyridyl ketone oxime, phenyl-2-pyridyl ketone oxime and bis[2-(o-carboxythiophenoxy)methyl]-4-bromo-1-methoxybenzene carriers, *Sens. Actuators B* 96 (2003) 669.
- [15] W. Wróblewski, Z. Brzózka, Ag⁺-selective electrodes based on lipophilic thioethers, *Sens. Actuators B* 24 (1995) 183.
- [16] M. Shamsipur, M. Javanbakht, V. Lippolis, A. Garau, G.D. Filippo, M.R. Ganjali, A. Yari, Novel Ag⁺ ion-selective electrodes based on two new mixed azathioether crowns containing a 1,10-phenanthroline sub-unit, *Anal. Chim. Acta* 462 (2002) 225.
- [17] K. Kimura, S. Yajima, K. Tatsumi, M. Yokoyama, M. Oue, Silver ion-selective electrodes using π -coordinate calix[4]arene derivatives as soft neutral carriers, *Anal. Chem.* 72 (2000) 5290.
- [18] V. Csokai, A. Grün, B. Balázs, A. Simon, G. Tóth, I. Bitter, Functionalized thiocalix- and calix[4]arene-based Ag⁺ ionophores: synthesis and comparative NMR study, *Tetrahedron* 62 (2006) 10215.
- [19] Z. Szigeti, A. Malon, T. Vigassy, V. Csokai, A. Grün, K. Wygladacz, N. Ye, C. Xu, V.J. Chebny, I. Bitter, R. Rathore, E. Bakker, E. Pretsch, Novel potentiometric and optical silver ion-selective sensors with subnanomolar detection limits, *Anal. Chim. Acta* 572 (2006) 1.
- [20] A. Demirel, A. Doğan, G. Akkuş, M. Yilmaz, E. Kiliç, Silver(I)-selective PVC membrane potentiometric sensor based on a recently synthesized calix[4]arene, *Electroanalysis* 18 (2006) 1019.
- [21] X. Zeng, L. Weng, L. Chen, X. Leng, Z. Zhang, X. He, Improved silver ion-selective electrodes using novel 1, 3-bis(2-benzothiazolyl)thioalkoxy-*p*-tert-butylcalix[4]arenes, *Tetrahedron Lett.* 41 (2000) 4917.
- [22] L. Chen, H. Ju, X. Zeng, X. He, Z. Zhang, Silver ion-selective electrodes based on novel containing benzothiazolyl calix[4]arene, *Anal. Chim. Acta* 437 (2001) 191.
- [23] X. Zeng, L. Weng, L. Chen, F. Xu, Q. Li, X. Leng, X. He, Z.-Z. Zhang, The syntheses and Ag⁺-selective electrode properties of benzothiazolylthioalkoxy functionalized calix[4]arenes: an investigation of the structure-selectivity relationship in the ionophore-based ISEs, *Tetrahedron* 58 (2002) 2647.
- [24] N. Morakot, W. Ngeontae, W. Aeungmaitrepirom, T. Tuntulani, Synthesis of novel calix[4]arene having benzothiazolylacetamidoalkoxy pendants and their potential application as Ag⁺-selective electrodes, *Bull. Korean Chem. Soc.* 21 (2008) 221.
- [25] N. Rubinova, K. Chumbimuni-Torres, E. Bakker, Solid-contact potentiometric polymer membrane microelectrodes for the detection of silver ions at the femtomole level, *Sens. Actuators B* 121 (2007) 135.
- [26] C.D. Gutsche, M. Iqbal, *p*-tert-Butylcalix[4]arene, *Org. Synth.* 68 (1990) 234.
- [27] H. Wang, X. Qiao, J. Chen, S. Ding, Preparation of silver nanoparticles by chemical reduction method, *Colloids Surf. A* 256 (2005) 111.
- [28] P.C. Meier, Two-parameter debye-hückel approximation for the evaluation of mean activity coefficients of 109 electrolytes, *Anal. Chim. Acta* 136 (1982) 363.
- [29] E. Bakker, E. Pretsch, The new wave of ion-selective electrodes, *Anal. Chem.* 74 (2002) 420A.
- [30] W.E. Morf, G. Kahr, W. Simon, Theoretical treatment of the selectivity and detection limit of silver compound membrane electrodes, *Anal. Chem.* 46 (1974) 1538.
- [31] C.J. Murphy, Nanocubes and nanoboxes, *Science* 298 (2002) 2139.
- [32] Y. Sun, Y. Xia, Shape-controlled synthesis of gold and silver nanoparticles, *Science* 298 (2002) 2176.

Biographies



Wittaya Ngeontae is currently a lecturer in the Department of Chemistry, Khon Kaen University, Khon Kaen, Thailand. He earned his PhD in analytical chemistry with assistant prof. Wanlapa Aeungmaitrepirom and associate prof. Thawatchai Tuntulani at Chulalongkorn University under the Development and Promotion of Science and Technology Talent project (DPST). In 2006, he was a visiting scholar with professor Eric Bakker. His research interests include synthesis of new ionophores based on the calixarene platform. Moreover, he is interested in the applications of ISEs and optical sensors for bio-molecules and environments.



Wanwisa Janrungratsakul received her MS degree in chemistry from Chulalongkorn University under the supervision of associate prof. Thawatchai Tuntulani. She is currently a PhD student in chemistry supported by the Commission on Higher Education. Her research interest is concerning ISEs and their applications in sensing bio-molecules.



Neramit Morakot is currently a lecturer in the Department of Chemistry, Mahasarakham University, Mahasarakham, Thailand. He obtained his PhD in chemistry under the supervision of assistant prof. Wanlapa Aeungmaitrepirom and associate prof. Thawatchai Tuntulani at Chulalongkorn University with funding from Mahasarakham University. He is interested in design, synthesis and application of receptors for metal ion analysis.



Wanlapa Aeungmaitrepirom is currently an assistant professor in the Department of Chemistry at Chulalongkorn University, Thailand. She earned her PhD in analytical chemistry at Université Louis Pasteur, France after obtaining BSc in chemistry and MSc in polymers and petrochemistry from Chulalongkorn University. Her research interests include fabrications of new ion selective electrodes and development of new extractants for environmental concerns.



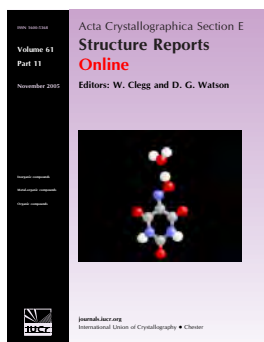
Thawatchai Tuntulani is currently an associate professor in the Department of Chemistry at Chulalongkorn University, Thailand. He earned his PhD in Chemistry with Prof. Marcetta Y. Darensbourg at Texas A&M University, U.S.A. after obtaining a Bachelor Degree of Engineering from Chiang Mai University, Thailand. He did his postdoctoral studies with Prof. Jean-Marie Lehn before joining Chulalongkorn University in 1995. His research interests include syntheses of derivatives of calix[4]arene and other macrocyclic compounds and development of electrochemical and optical sensing materials for ions and bio-molecules.

Diaqua{2,6-bis[*N*-(2-pyridinylmethyl)carbamoyl]phenolato- $\kappa^2 O^1, O^2$ }zinc(II)

Chomchai Suksai, Sarayut Watchasit, Thawatchai Tuntulani and Chaveng Pakawatchai

Acta Cryst. (2008). **E64**, m884–m885

This article is distributed under the terms of the Creative Commons Attribution Licence <http://creativecommons.org/licenses/by/2.0/uk/legalcode>, which permits unrestricted use, distribution, and reproduction in any medium, provided the original authors and source are cited.



Acta Crystallographica Section E: Structure Reports Online is the IUCr's highly popular open-access structural journal. It provides a simple and easily accessible publication mechanism for the growing number of inorganic, metal-organic and organic crystal structure determinations. The electronic submission, validation, refereeing and publication facilities of the journal ensure very rapid and high-quality publication, whilst key indicators and validation reports provide measures of structural reliability. In 2007, the journal published over 5000 structures. The average publication time is less than one month.

Crystallography Journals **Online** is available from journals.iucr.org

Diaqua{2,6-bis[*N*-(2-pyridinylmethyl)-carbamoyl]phenolato- $\kappa^2\text{O}^1,\text{O}^2$ }zinc(II)

Chomchai Suksai,^{a*} Sarayut Watchasit,^a Thawatchai Tuntulani^b and Chaveng Pakawatchai^c

^aDepartment of Chemistry, Faculty of Science, Burapha University, Chonburi 20131, Thailand, ^bDepartment of Chemistry, Faculty of Science, Chulalongkorn University, Bangkok 10330, Thailand, and ^cDepartment of Chemistry, Faculty of Science, Prince of Songkla University, Songkhla 90112, Thailand

Correspondence e-mail: jomjai@buu.ac.th, tthawac@chula.ac.th

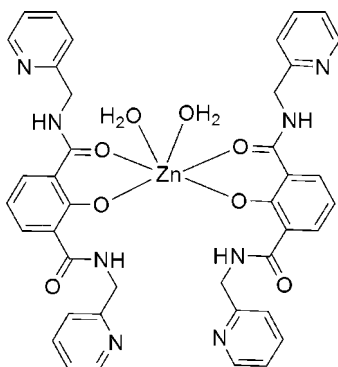
Received 14 May 2008; accepted 1 June 2008

Key indicators: single-crystal X-ray study; $T = 293\text{ K}$; mean $\sigma(\text{C}-\text{C}) = 0.005\text{ \AA}$; R factor = 0.060; wR factor = 0.131; data-to-parameter ratio = 16.9.

In the title compound, $[\text{Zn}(\text{C}_{20}\text{H}_{17}\text{N}_4\text{O}_3)_2(\text{H}_2\text{O})_2]$, the Zn^{II} atom, lying on a twofold rotation axis, is six-coordinated in a distorted octahedral geometry by two phenolate O atoms and two carbonyl O atoms from two 2,6-bis[(pyridin-2-ylmethyl)-carbamoyl]phenolate ligands and by two water molecules. A three-dimensional network is built up from an extensive array of hydrogen bonds and π - π interactions between the pyridyl rings, with a centroid-centroid distance of $3.666(3)\text{ \AA}$.

Related literature

For related literature, see: Chaudhuri *et al.* (2007); Goldsmith *et al.* (2002); Gumbley & Stewart (1984); Ingle *et al.* (2007); Kimura (1994); Lipscomb & Sträter (1996); Szajna-Fuller *et al.* (2007).



Experimental

Crystal data

$[\text{Zn}(\text{C}_{20}\text{H}_{17}\text{N}_4\text{O}_3)_2(\text{H}_2\text{O})_2]$
 $M_r = 824.18$

Monoclinic, $C2/c$
 $a = 16.357(4)\text{ \AA}$

$b = 14.723(4)\text{ \AA}$
 $c = 15.135(4)\text{ \AA}$
 $\beta = 91.938(7)^\circ$
 $V = 3642.9(16)\text{ \AA}^3$
 $Z = 4$

Mo $K\alpha$ radiation
 $\mu = 0.74\text{ mm}^{-1}$
 $T = 293(2)\text{ K}$
 $0.35 \times 0.3 \times 0.2\text{ mm}$

Data collection

Bruker SMART APEX CCD area-detector diffractometer
Absorption correction: multi-scan (*SADABS*; Sheldrick, 1996)
 $T_{\text{min}} = 0.757$, $T_{\text{max}} = 0.854$

21455 measured reflections
4398 independent reflections
3575 reflections with $I > 2\sigma(I)$
 $R_{\text{int}} = 0.061$

Refinement

$R[F^2 > 2\sigma(F^2)] = 0.060$
 $wR(F^2) = 0.130$
 $S = 1.11$
4398 reflections

260 parameters
H-atom parameters constrained
 $\Delta\rho_{\text{max}} = 0.52\text{ e \AA}^{-3}$
 $\Delta\rho_{\text{min}} = -0.42\text{ e \AA}^{-3}$

Table 1

Selected geometric parameters (\AA , $^\circ$).

O1—Zn1	1.9772 (18)	O4—Zn1	2.149 (2)
O2—Zn1	2.1572 (19)		
O1—Zn1—O1 ⁱ	175.44 (11)	O4—Zn1—O2	91.26 (8)
O1—Zn1—O4 ⁱ	85.97 (8)	O1—Zn1—O2 ⁱ	92.61 (8)
O1—Zn1—O4	97.42 (8)	O4—Zn1—O2 ⁱ	168.82 (8)
O4 ⁱ —Zn1—O4	84.55 (12)	O2—Zn1—O2 ⁱ	94.67 (12)
O1—Zn1—O2	84.29 (7)		

Symmetry code: (i) $-x, y, -z + \frac{1}{2}$.

Table 2

Hydrogen-bond geometry (\AA , $^\circ$).

$D-H\cdots A$	$D-H$	$H\cdots A$	$D\cdots A$	$D-H\cdots A$
N3—H3A \cdots O1	0.86	1.93	2.623 (3)	136
N1—H1 \cdots N4 ⁱⁱ	0.86	2.20	3.007 (4)	155
O4—H24 \cdots O3 ⁱⁱⁱ	0.85	1.87	2.712 (3)	174
O4—H23 \cdots N2 ^{iv}	0.87	2.03	2.879 (3)	163

Symmetry codes: (ii) $x + \frac{1}{2}, y + \frac{1}{2}, z$; (iii) $-x, -y, -z$; (iv) $-x + \frac{1}{2}, y - \frac{1}{2}, -z + \frac{1}{2}$.

Data collection: *SMART* (Bruker, 2007); cell refinement: *SAINT* (Bruker, 2007); data reduction: *SAINT*; program(s) used to solve structure: *SHELXS97* (Sheldrick, 2008); program(s) used to refine structure: *SHELXL97* (Sheldrick, 2008); molecular graphics: *ORTEP-3* (Farrugia, 1997) and *Mercury* (Macrae *et al.*, 2006); software used to prepare material for publication: *SHELXL97*.

Financial support from the Thailand Research Fund (MRG5080149 and RTA5080006) and the Centre of Innovation in Chemistry: Postgraduate Education and Research Program in Chemistry (PERCH-CIC) are gratefully acknowledged.

Supplementary data and figures for this paper are available from the IUCr electronic archives (Reference: HY2136).

References

- Bruker (2007). *SMART* and *SAINT*. Bruker AXS Inc., Madison, Wisconsin, USA.
- Chaudhuri, U. P., Yang, L., Whiteaker, L. R., Mondal, A., Fultz, M. R., Powell, D. R. & Houser, R. P. (2007). *Polyhedron*, **26**, 5420–5431.
- Farrugia, L. J. (1997). *J. Appl. Cryst.* **30**, 565.
- Goldsmith, C. R., Jonas, R. T. & Stack, T. D. P. (2002). *J. Am. Chem. Soc.* **124**, 83–96.
- Gumbley, S. J. & Stewart, R. (1984). *J. Chem. Soc. Perkin Trans. 2*, pp. 529–531.
- Ingle, G. K., Makowska-Grzyska, M. M., Szajna-Fuller, E., Sen, I., Price, J. C., Arif, A. M. & Berreau, L. M. (2007). *Inorg. Chem.* **46**, 1471–1480.
- Kimura, E. (1994). *Prog. Inorg. Chem.* **41**, 443–450.
- Lipscomb, W. N. & Sträter, N. (1996). *Chem. Rev.* **96**, 2375–2434.
- Macrae, C. F., Edgington, P. R., McCabe, P., Pidcock, E., Shields, G. P., Taylor, R., Towler, M. & van de Streek, J. (2006). *J. Appl. Cryst.* **39**, 453–457.
- Sheldrick, G. M. (1996). *SADABS*. University of Göttingen, Germany.
- Sheldrick, G. M. (2008). *Acta Cryst.* **A64**, 112–122.
- Szajna-Fuller, E., Ingle, G. K., Watkins, R. W., Arif, A. M. & Berreau, L. M. (2007). *Inorg. Chem.* **46**, 2353–2355.

supplementary materials

Acta Cryst. (2008). E64, m884-m885 [doi:10.1107/S1600536808016693]

Diaqua{2,6-bis[*N*-(2-pyridinylmethyl)carbamoyl]phenolato- $\kappa^2 O^1, O^2$ }zinc(II)

C. Suksai, S. Watchasit, T. Tuntulani and C. Pakawatchai

Comment

Zinc complexes of common amide-containing ligands have been widely explored and have received much attention in biomimetic research (Ingle *et al.*, 2007). For example, the zinc complex with 6-(pivaloylamido-2-pyridylmethyl)amine ligand has been synthesized to serve as models for amide hydrolysis activity (Szajna-Fuller *et al.*, 2007). Recently, zinc and copper complexes with a family of pyridylmethanamide ligands have been synthesized and showed that these ligands coordinate to metal ions with different coordination modes (Chaudhuri *et al.*, 2007). It should be mentioned that zinc complexes containing aqua ligands have been used as model studies for zinc-hydrolase enzyme because of the functional unit at the active site of zinc-hydrolase enzyme is a zinc-bound water molecule, which is deprotonated at near neutral pH to generate a strongly nucleophilic Zn—OH group (Lipscomb & Sträter, 1996). Moreover, the aqua ligand bound to zinc ion is further stabilized *via* the formation of a hydrogen bond with a carboxylate or phenolic group from amino acid residues (Kimura, 1994). This hydrogen bond has been postulated to play a role in the activation of the coordinated aqua ligand in the catalytic pathway.

In an ongoing effort to study the interaction of zinc ion with aqua ligand, we report here the synthesis and characterization of the title compound, a new zinc complex with 2,6-bis[(pyridin-2-ylmethyl)carbamoyl]phenolate and aqua ligands. The electrospray mass spectrometry (ESI-MS) of the title compound confirmed the presence of the molecular species in solution. The compound has fragmentation patterns with peaks at $m/z = 823.17$ and 787.19 ; the former corresponds to the $[M+2H_2O+H^+]$ ion and the latter is consistent with the loss of two coordinated water molecules $[M-2H_2O+H^+]$. The evidence for the presence of water in the complex is also given by IR absorption at 3568 cm^{-1} . The elemental analysis agrees well with the proposed structure.

In the title compound, the Zn^{II} atom is situated on a twofold rotation axis in a distorted octahedral coordination geometry, which is defined by two phenolate O atoms, two carbonyl O atoms and two *cis* water molecules (Fig. 1). The $O1—Zn1—O1^i$ and $O4—Zn1—O2^i$ [symmetry code: (i) $-x, y, 1/2 - z$] angles deviate from linearity (Table 1). These results are in accordance with the distorted octahedral geometry. It is noteworthy that each ligand behaves in a bidentate coordination fashion involving one phenolate O atom and one carbonyl O atom, while the two amide N atoms and pyridyl N atoms are free of coordination with the Zn atom. The two phenyl rings of coordinated molecules are tilted to one another with a dihedral angle of $72.3(3)^\circ$. Remarkably, the intramolecular $N3—H3A\cdots O1$ hydrogen bond forms a pseudo-six-membered ring (Fig. 1).

The water molecule is involved in an extensive intermolecular hydrogen-bonding network, as shown in Fig. 2. Atom O4 of aqua ligand acts as a hydrogen-bond donor to the uncoordinated carbonyl O3 atom and uncoordinated pyridyl N2 atom of adjacent complex molecules, respectively (Table 2). Additionally, the molecules are held together by intermolecular hydrogen bond between the uncoordinated amide N1 atom and uncoordinated pyridyl N4 atom. Not only the intermolecular hydrogen bonds, but also there are intermolecular $\pi-\pi$ interactions in the crystal structure, which occur between the pyridyl rings containing atoms N2 and N4 of adjacent molecules, with a centroid-centroid distance of $3.666(3)\text{ \AA}$.

Experimental

Intermediate products (I), (II) (Gumbley & Stewart, 1984) and (III) (Goldsmith *et al.*, 2002) have been synthesized in accordance with the published procedures. The methods to synthesize compounds (IV) and (V) are shown in Fig. 3.

A methanol solution (5 ml) of $\text{Zn}(\text{ClO}_4)_2 \cdot 6\text{H}_2\text{O}$ (2.22 g, 5.96 mmol) was added dropwise to a stirred solution of compound (V) (1.00 g, 2.98 mmol) in methanol (10 ml) at room temperature and the solution was stirred for 3 h. Water (10 ml) was added to the solution to precipitate a white solid. The precipitate was filtered off and washed with water to obtain the white powder of the title compound (yield 28%, 0.66 g). m.p. 170–173 °C. Recrystallization of this powder in methanol yielded colourless block crystals of the title compound, suitable for X-ray diffraction study. Analysis, calculated for $\text{C}_{40}\text{H}_{38}\text{N}_8\text{O}_8\text{Zn}$: C 58.29, H 4.65, N 13.60%; found: C 58.20, H 4.67, N 13.61%. ^1H -NMR (400 MHz, $\text{DMSO}-d_6$): δ 10.95 (bs, 2H, $-\text{NH}$), 8.50 (d, J = 4.0 Hz, 2H, ArH), 7.95 (s, 2H, ArH), 7.74 (t, J = 7.6 Hz, 2H, ArH), 7.33 (t, J = 8.0 Hz, 2H, ArH), 7.26 (t, J = 5.6 Hz, 2H, ArH), 6.60 (bs, 1H, ArH), 4.60 (s, 2H, $-\text{CH}_2-$), 4.59 (s, 2H, $-\text{CH}_2-$). ^{13}C -NMR (100 MHz, $\text{DMSO}-d_6$): δ 168.97, 159.20, 149.25, 137.39, 133.99, 122.61, 121.66, 111.55, 44.73. ESI-MS: m/z 787.19 [$\text{M}-2\text{H}_2\text{O}+\text{H}^+$], 823.17 [$\text{M}+2\text{H}_2\text{O}+\text{H}^+$].

Refinement

H atoms on C and N atoms were positioned geometrically and refined as riding atoms, with $\text{C}-\text{H}$ = 0.93 (aromatic CH), 0.97 (CH_2) Å and $\text{N}-\text{H}$ = 0.86 Å and $U_{\text{iso}}(\text{H}) = 1.2U_{\text{eq}}(\text{C}, \text{N})$. H atoms attached to the water molecule were found in difference Fourier map and refined isotropically with atomic coordinates fixed.

Figures

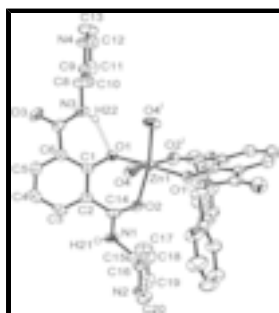


Fig. 1. The molecular structure of the title compound. Displacement ellipsoids are drawn at the 50% probability level. H atoms have been omitted except those involved in hydrogen bonds. Hydrogen bonds are shown as dashed lines. [Symmetry code: (i) $-x, y, 0.5 - z$.]

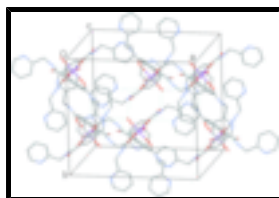


Fig. 2. The three-dimensional hydrogen bonding network in the title compound. H atoms have been omitted for clarity. Hydrogen bonds are shown as dashed lines.



Fig. 3. The synthesis of compounds (IV) and (V).

Diaqua{2,6-bis[N-(2-pyridylmethyl)carbamoyl]phenolato- $\kappa^2 O^1, O^2$ }zinc(II)}

Crystal data

[Zn(C₂₀H₁₇N₄O₃)₂(H₂O)₂]

$M_r = 824.18$

Monoclinic, $C2/c$

Hall symbol: $-C\ 2yc$

$a = 16.357\ (4)\ \text{\AA}$

$b = 14.723\ (4)\ \text{\AA}$

$c = 15.135\ (4)\ \text{\AA}$

$\beta = 91.938\ (7)^\circ$

$V = 3642.9\ (16)\ \text{\AA}^3$

$Z = 4$

$F_{000} = 1712$

$D_x = 1.503\ \text{Mg m}^{-3}$

Mo $K\alpha$ radiation

$\lambda = 0.71073\ \text{\AA}$

Cell parameters from 4398 reflections

$\theta = 1.9\text{--}28.0^\circ$

$\mu = 0.74\ \text{mm}^{-1}$

$T = 293\ (2)\ \text{K}$

Prism, colourless

$0.35 \times 0.3 \times 0.2\ \text{mm}$

Data collection

Bruker SMART APEX CCD area-detector diffractometer

Monochromator: graphite

$T = 293\ (2)\ \text{K}$

ϕ and ω scans

Absorption correction: multi-scan (SADABS; Sheldrick, 1996)

$T_{\min} = 0.757$, $T_{\max} = 0.854$

21455 measured reflections

4398 independent reflections

3575 reflections with $I > 2\sigma(I)$

$R_{\text{int}} = 0.061$

$\theta_{\max} = 28.0^\circ$

$\theta_{\min} = 1.9^\circ$

$h = -21 \rightarrow 21$

$k = -19 \rightarrow 19$

$l = -19 \rightarrow 19$

Refinement

Refinement on F^2

Least-squares matrix: full

$R[F^2 > 2\sigma(F^2)] = 0.060$

$wR(F^2) = 0.130$

$S = 1.11$

4398 reflections

260 parameters

Primary atom site location: structure-invariant direct methods

Secondary atom site location: difference Fourier map

Hydrogen site location: inferred from neighbouring sites

H-atom parameters constrained

$w = 1/[\sigma^2(F_o^2) + (0.0553P)^2 + 3.7977P]$

where $P = (F_o^2 + 2F_c^2)/3$

$(\Delta/\sigma)_{\max} < 0.001$

$\Delta\rho_{\max} = 0.52\ \text{e \AA}^{-3}$

$\Delta\rho_{\min} = -0.42\ \text{e \AA}^{-3}$

Extinction correction: none

Special details

Experimental. Compound (IV): To a solution of (III) (2.38 g, 10.2 mmol) in dry CH_2Cl_2 (5 ml) was added to a well stirred mixture of 2-(aminomethyl)-pyridine (2.60 ml, 25.5 mmol) and NEt_3 (5.33 ml, 38.3 mmol) in dried CH_2Cl_2 (5 ml) under nitrogen atmosphere and the reaction was then left stirring overnight. Next, the solvent was removed under vacuum and the residue was purified by column chromatography on Al_2O_3 with 50% EtOAc: CH_2Cl_2 as eluent. The resulting pale yellow solid was recrystallized in diethyl ether to give a pure white solid (IV) (yield 68%, 2.68 g). m.p. 120–125 °C. ^1H -NMR (400 MHz, CDCl_3): δ 8.70 (s, 2H, –NH), 8.61 (d, J = 4.4 Hz, 2H, ArH), 8.20 (d, J = 8.0 Hz, 2H, ArH), 7.71 (m, 2H, PyH), 7.38 (m, 3H, ArH), 7.25 (m, 2H, ArH), 4.85 (s, 2H, – CH_2 –), 4.83 (s, 2H, – CH_2 –), 3.88 (s, 3H, – CH_3). ^{13}C -NMR (100 MHz, $\text{DMSO}-d_6$): δ 164.90, 156.69, 156.53, 149.18, 136.81, 134.82, 127.60, 125.11, 122.45, 122.24, 63.83, 45.16.

Compound (V): Anhydrous LiI (3.89 g, 28.9 mmol) was added to a well stirred solution of (IV) (0.78 g, 2.89 mmol) in anhydrous pyridine (20 ml) at room temperature. The reaction was allowed to proceed for 7 d with constant stirring. Then pyridine was removed in *vacuum* and the residue was dissolved in 1 M HCl (20 ml) and extracted with ethyl acetate (3 x 20 ml). The combined organic phase was dried over anhydrous Na_2SO_4 , filtered and brought to dryness by rotary evaporation. The crude product was recrystallized in a solution of methanol and diethyl ether, giving (V) as a white solid (yield 92%, 0.95 g). m.p 100–103 °C. Analysis, calculated for $\text{C}_{20}\text{H}_{18}\text{N}_4\text{O}_3$: C 66.29, H 5.01, N 15.46%; found: C 66.31, H 4.99, N 15.45%. ^1H -NMR (400 MHz, CDCl_3): δ 8.77 (s, 2H, –NH), 8.61 (d, J = 4.8 Hz, 2H, ArH), 8.11 (d, J = 7.6 Hz, 2H, ArH), 7.71 (m, 2H, ArH), 7.39 (d, J = 7.6 Hz, 2H, ArH), 7.26 (m, 2H, ArH), 7.03 (t, J = 8.0 Hz, 1H, ArH), 4.82 (s, 2H, – CH_2 –), 4.81 (s, 2H, – CH_2 –). ^{13}C -NMR (100 MHz, CDCl_3): δ 167.66, 160.59, 156.26, 149.06, 137.01, 133.28, 122.52, 122.08, 118.61, 117.94, 44.73. ESI: m/z 348.1458 [$\text{M}+\text{H}^+$].

Fractional atomic coordinates and isotropic or equivalent isotropic displacement parameters (\AA^2)

	<i>x</i>	<i>y</i>	<i>z</i>	$U_{\text{iso}}^*/U_{\text{eq}}$
C1	0.02286 (15)	0.19100 (17)	0.05522 (17)	0.0236 (5)
C2	0.09384 (16)	0.24793 (18)	0.06360 (17)	0.0269 (6)
C3	0.14191 (17)	0.26133 (19)	−0.0097 (2)	0.0343 (6)
H3	0.1885	0.2972	−0.0036	0.041*
C4	0.12260 (19)	0.2232 (2)	−0.0905 (2)	0.0403 (7)
H4	0.156	0.2329	−0.1382	0.048*
C5	0.05325 (18)	0.1705 (2)	−0.10030 (19)	0.0368 (7)
H5	0.0395	0.1457	−0.1553	0.044*
C6	0.00339 (16)	0.15366 (17)	−0.02945 (17)	0.0264 (6)
C7	−0.06868 (17)	0.09354 (18)	−0.04851 (19)	0.0312 (6)
C8	−0.17697 (17)	0.0002 (2)	0.0089 (2)	0.0389 (7)
H8A	−0.183	−0.0314	0.0645	0.047*
H8B	−0.1619	−0.0445	−0.0347	0.047*
C9	−0.25903 (17)	0.04027 (19)	−0.01925 (18)	0.0299 (6)
C10	−0.27189 (18)	0.1306 (2)	−0.0387 (2)	0.0377 (7)
H10	−0.2288	0.1718	−0.0348	0.045*
C11	−0.3496 (2)	0.1594 (2)	−0.0642 (2)	0.0461 (8)
H11	−0.3598	0.2203	−0.0764	0.055*
C12	−0.4113 (2)	0.0968 (3)	−0.0711 (2)	0.0539 (9)
H12	−0.4638	0.1139	−0.0897	0.065*
C13	−0.3936 (2)	0.0081 (3)	−0.0498 (3)	0.0578 (10)
H13	−0.4358	−0.0343	−0.0539	0.069*

C14	0.11584 (15)	0.29456 (18)	0.14819 (19)	0.0291 (6)
C15	0.1960 (2)	0.4212 (2)	0.2162 (2)	0.0428 (8)
H15A	0.2548	0.4131	0.2219	0.051*
H15B	0.1723	0.3991	0.2701	0.051*
C16	0.17668 (18)	0.5211 (2)	0.20506 (19)	0.0352 (6)
N2	0.23880 (15)	0.57968 (17)	0.21397 (17)	0.0372 (6)
C20	0.2219 (2)	0.6684 (2)	0.2034 (2)	0.0478 (8)
H20	0.2647	0.7097	0.2104	0.057*
C19	0.1456 (3)	0.7013 (3)	0.1829 (2)	0.0544 (9)
H19	0.137	0.7633	0.1753	0.065*
C18	0.0825 (2)	0.6416 (3)	0.1738 (3)	0.0615 (10)
H18	0.0298	0.6619	0.1599	0.074*
N1	0.16417 (16)	0.36823 (17)	0.14154 (17)	0.0383 (6)
H1	0.1771	0.3851	0.0894	0.046*
C17	0.0979 (2)	0.5508 (3)	0.1857 (3)	0.0553 (9)
H17	0.0553	0.5091	0.1806	0.066*
N3	−0.11105 (14)	0.06472 (16)	0.01965 (16)	0.0339 (5)
H3A	−0.0987	0.0852	0.0716	0.041*
N4	−0.31909 (16)	−0.02078 (19)	−0.02365 (19)	0.0458 (7)
O1	−0.02465 (11)	0.17550 (13)	0.12131 (12)	0.0297 (4)
O2	0.09257 (12)	0.26946 (14)	0.22198 (13)	0.0363 (5)
O3	−0.08908 (14)	0.07239 (16)	−0.12543 (15)	0.0473 (6)
O4	0.08829 (13)	0.06216 (15)	0.24782 (15)	0.0431 (5)
Zn1	0	0.17016 (3)	0.25	0.02664 (14)
H24	0.0847	0.0211	0.2086	0.052 (11)*
H23	0.1415	0.067	0.2476	0.078 (14)*

Atomic displacement parameters (\AA^2)

	U^{11}	U^{22}	U^{33}	U^{12}	U^{13}	U^{23}
C1	0.0218 (12)	0.0203 (12)	0.0284 (13)	0.0028 (10)	−0.0027 (10)	0.0033 (10)
C2	0.0270 (13)	0.0237 (13)	0.0299 (14)	0.0008 (11)	0.0002 (11)	0.0035 (11)
C3	0.0272 (14)	0.0312 (15)	0.0447 (17)	−0.0039 (12)	0.0047 (12)	0.0051 (13)
C4	0.0400 (17)	0.0441 (18)	0.0376 (17)	0.0014 (14)	0.0120 (13)	0.0059 (14)
C5	0.0395 (16)	0.0410 (17)	0.0299 (15)	0.0054 (14)	0.0015 (12)	−0.0021 (13)
C6	0.0261 (13)	0.0243 (14)	0.0286 (13)	0.0041 (10)	−0.0012 (10)	0.0015 (10)
C7	0.0315 (14)	0.0255 (14)	0.0362 (16)	0.0068 (11)	−0.0054 (12)	−0.0068 (12)
C8	0.0300 (15)	0.0307 (16)	0.055 (2)	−0.0043 (12)	−0.0110 (13)	0.0031 (14)
C9	0.0305 (14)	0.0292 (14)	0.0296 (14)	−0.0046 (11)	−0.0042 (11)	0.0031 (11)
C10	0.0344 (16)	0.0315 (15)	0.0472 (18)	−0.0007 (13)	−0.0008 (13)	0.0027 (13)
C11	0.0454 (19)	0.0428 (19)	0.050 (2)	0.0122 (15)	−0.0002 (15)	0.0050 (15)
C12	0.0333 (17)	0.068 (2)	0.060 (2)	0.0082 (17)	−0.0099 (15)	0.0120 (19)
C13	0.0321 (17)	0.062 (2)	0.078 (3)	−0.0144 (17)	−0.0142 (17)	0.019 (2)
C14	0.0208 (13)	0.0247 (13)	0.0412 (16)	0.0002 (10)	−0.0071 (11)	0.0041 (12)
C15	0.0442 (18)	0.0369 (17)	0.0462 (19)	−0.0125 (14)	−0.0135 (14)	0.0017 (14)
C16	0.0353 (16)	0.0353 (16)	0.0346 (16)	−0.0068 (13)	−0.0049 (12)	0.0002 (12)
N2	0.0360 (13)	0.0322 (13)	0.0427 (14)	−0.0078 (11)	−0.0071 (11)	−0.0002 (11)
C20	0.059 (2)	0.0314 (16)	0.052 (2)	−0.0095 (16)	−0.0073 (16)	−0.0007 (15)

supplementary materials

C19	0.078 (3)	0.0413 (19)	0.043 (2)	0.0131 (19)	−0.0050 (18)	−0.0011 (15)
C18	0.046 (2)	0.067 (3)	0.071 (3)	0.0168 (19)	−0.0048 (18)	−0.002 (2)
N1	0.0448 (15)	0.0336 (13)	0.0361 (14)	−0.0177 (11)	−0.0047 (11)	0.0052 (11)
C17	0.0342 (18)	0.060 (2)	0.071 (3)	−0.0095 (16)	−0.0053 (17)	−0.0001 (19)
N3	0.0292 (12)	0.0327 (13)	0.0393 (14)	−0.0066 (10)	−0.0069 (10)	−0.0016 (10)
N4	0.0349 (14)	0.0403 (15)	0.0615 (18)	−0.0121 (12)	−0.0109 (12)	0.0156 (13)
O1	0.0258 (9)	0.0377 (11)	0.0256 (9)	−0.0075 (8)	0.0001 (7)	0.0014 (8)
O2	0.0420 (12)	0.0356 (11)	0.0309 (11)	−0.0135 (9)	−0.0033 (9)	0.0007 (9)
O3	0.0514 (13)	0.0489 (14)	0.0410 (13)	−0.0034 (11)	−0.0087 (10)	−0.0180 (11)
O4	0.0323 (12)	0.0397 (12)	0.0567 (14)	0.0075 (9)	−0.0049 (10)	−0.0215 (11)
Zn1	0.0272 (2)	0.0271 (2)	0.0254 (2)	0	−0.00199 (16)	0

Geometric parameters (\AA , $^\circ$)

C1—O1	1.307 (3)	C13—H13	0.93
C1—C6	1.421 (4)	C14—O2	1.248 (3)
C1—C2	1.434 (4)	C14—N1	1.348 (3)
C2—C3	1.395 (4)	C15—N1	1.455 (4)
C2—C14	1.486 (4)	C15—C16	1.514 (4)
C3—C4	1.373 (4)	C15—H15A	0.97
C3—H3	0.93	C15—H15B	0.97
C4—C5	1.378 (4)	C16—N2	1.336 (4)
C4—H4	0.93	C16—C17	1.383 (4)
C5—C6	1.391 (4)	N2—C20	1.344 (4)
C5—H5	0.93	C20—C19	1.365 (5)
C6—C7	1.495 (4)	C20—H20	0.93
C7—O3	1.240 (3)	C19—C18	1.361 (6)
C7—N3	1.332 (4)	C19—H19	0.93
C8—N3	1.442 (4)	C18—C17	1.371 (5)
C8—C9	1.514 (4)	C18—H18	0.93
C8—H8A	0.97	N1—H1	0.86
C8—H8B	0.97	C17—H17	0.93
C9—N4	1.332 (4)	N3—H3A	0.86
C9—C10	1.377 (4)	O1—Zn1	1.9772 (18)
C10—C11	1.382 (4)	O2—Zn1	2.1572 (19)
C10—H10	0.93	O4—Zn1	2.149 (2)
C11—C12	1.368 (5)	O4—H24	0.85
C11—H11	0.93	O4—H23	0.87
C12—C13	1.374 (5)	Zn1—O1 ⁱ	1.9772 (18)
C12—H12	0.93	Zn1—O4 ⁱ	2.149 (2)
C13—N4	1.338 (4)	Zn1—O2 ⁱ	2.1572 (19)
O1—C1—C6	120.1 (2)	C16—C15—H15A	109.3
O1—C1—C2	122.3 (2)	N1—C15—H15B	109.3
C6—C1—C2	117.5 (2)	C16—C15—H15B	109.3
C3—C2—C1	119.3 (2)	H15A—C15—H15B	108
C3—C2—C14	119.5 (2)	N2—C16—C17	121.2 (3)
C1—C2—C14	121.2 (2)	N2—C16—C15	117.5 (3)
C4—C3—C2	122.1 (3)	C17—C16—C15	121.3 (3)

C4—C3—H3	118.9	C16—N2—C20	117.6 (3)
C2—C3—H3	118.9	N2—C20—C19	123.7 (3)
C3—C4—C5	119.3 (3)	N2—C20—H20	118.2
C3—C4—H4	120.4	C19—C20—H20	118.2
C5—C4—H4	120.4	C18—C19—C20	118.6 (3)
C4—C5—C6	121.3 (3)	C18—C19—H19	120.7
C4—C5—H5	119.3	C20—C19—H19	120.7
C6—C5—H5	119.3	C19—C18—C17	118.8 (4)
C5—C6—C1	120.4 (2)	C19—C18—H18	120.6
C5—C6—C7	115.9 (2)	C17—C18—H18	120.6
C1—C6—C7	123.7 (2)	C14—N1—C15	124.6 (3)
O3—C7—N3	121.1 (3)	C14—N1—H1	117.7
O3—C7—C6	121.0 (3)	C15—N1—H1	117.7
N3—C7—C6	117.8 (2)	C18—C17—C16	120.1 (3)
N3—C8—C9	115.3 (2)	C18—C17—H17	119.9
N3—C8—H8A	108.4	C16—C17—H17	119.9
C9—C8—H8A	108.4	C7—N3—C8	122.0 (3)
N3—C8—H8B	108.4	C7—N3—H3A	119
C9—C8—H8B	108.4	C8—N3—H3A	119
H8A—C8—H8B	107.5	C9—N4—C13	117.6 (3)
N4—C9—C10	122.3 (3)	C1—O1—Zn1	130.85 (16)
N4—C9—C8	113.4 (2)	C14—O2—Zn1	127.87 (18)
C10—C9—C8	124.3 (3)	Zn1—O4—H24	121
C9—C10—C11	119.2 (3)	Zn1—O4—H23	128
C9—C10—H10	120.4	H24—O4—H23	96
C11—C10—H10	120.4	O1—Zn1—O1 ⁱ	175.44 (11)
C12—C11—C10	118.9 (3)	O1—Zn1—O4 ⁱ	85.97 (8)
C12—C11—H11	120.5	O1 ⁱ —Zn1—O4 ⁱ	97.42 (8)
C10—C11—H11	120.5	O1—Zn1—O4	97.42 (8)
C11—C12—C13	118.3 (3)	O1 ⁱ —Zn1—O4	85.97 (8)
C11—C12—H12	120.8	O4 ⁱ —Zn1—O4	84.55 (12)
C13—C12—H12	120.8	O1—Zn1—O2	84.29 (7)
N4—C13—C12	123.6 (3)	O1 ⁱ —Zn1—O2	92.61 (8)
N4—C13—H13	118.2	O4 ⁱ —Zn1—O2	168.82 (8)
C12—C13—H13	118.2	O4—Zn1—O2	91.26 (8)
O2—C14—N1	120.2 (3)	O1—Zn1—O2 ⁱ	92.61 (8)
O2—C14—C2	124.2 (2)	O1 ⁱ —Zn1—O2 ⁱ	84.29 (7)
N1—C14—C2	115.7 (2)	O4 ⁱ —Zn1—O2 ⁱ	91.26 (8)
N1—C15—C16	111.5 (3)	O4—Zn1—O2 ⁱ	168.82 (8)
N1—C15—H15A	109.3	O2—Zn1—O2 ⁱ	94.67 (12)
O1—C1—C2—C3	179.9 (2)	C17—C16—N2—C20	0.0 (5)
C6—C1—C2—C3	−2.4 (4)	C15—C16—N2—C20	179.5 (3)
O1—C1—C2—C14	−1.7 (4)	C16—N2—C20—C19	−1.0 (5)
C6—C1—C2—C14	176.1 (2)	N2—C20—C19—C18	1.0 (6)
C1—C2—C3—C4	1.4 (4)	C20—C19—C18—C17	0.0 (6)
C14—C2—C3—C4	−177.1 (3)	O2—C14—N1—C15	2.9 (4)

supplementary materials

C2—C3—C4—C5	0.5 (5)	C2—C14—N1—C15	−177.0 (3)
C3—C4—C5—C6	−1.3 (5)	C16—C15—N1—C14	−127.1 (3)
C4—C5—C6—C1	0.2 (4)	C19—C18—C17—C16	−1.0 (6)
C4—C5—C6—C7	−178.5 (3)	N2—C16—C17—C18	1.0 (5)
O1—C1—C6—C5	179.4 (2)	C15—C16—C17—C18	−178.5 (3)
C2—C1—C6—C5	1.6 (4)	O3—C7—N3—C8	6.7 (4)
O1—C1—C6—C7	−1.9 (4)	C6—C7—N3—C8	−174.4 (2)
C2—C1—C6—C7	−179.8 (2)	C9—C8—N3—C7	−83.3 (4)
C5—C6—C7—O3	−10.8 (4)	C10—C9—N4—C13	1.4 (5)
C1—C6—C7—O3	170.5 (3)	C8—C9—N4—C13	−178.6 (3)
C5—C6—C7—N3	170.3 (2)	C12—C13—N4—C9	−0.8 (6)
C1—C6—C7—N3	−8.4 (4)	C6—C1—O1—Zn1	151.87 (19)
N3—C8—C9—N4	−176.5 (3)	C2—C1—O1—Zn1	−30.4 (4)
N3—C8—C9—C10	3.5 (5)	N1—C14—O2—Zn1	168.55 (19)
N4—C9—C10—C11	−0.3 (5)	C2—C14—O2—Zn1	−11.5 (4)
C8—C9—C10—C11	179.7 (3)	C1—O1—Zn1—O4 ⁱ	−143.2 (2)
C9—C10—C11—C12	−1.4 (5)	C1—O1—Zn1—O4	−59.2 (2)
C10—C11—C12—C13	1.9 (5)	C1—O1—Zn1—O2	31.3 (2)
C11—C12—C13—N4	−0.8 (6)	C1—O1—Zn1—O2 ⁱ	125.8 (2)
C3—C2—C14—O2	−159.3 (3)	C14—O2—Zn1—O1	−9.8 (2)
C1—C2—C14—O2	22.2 (4)	C14—O2—Zn1—O1 ⁱ	173.6 (2)
C3—C2—C14—N1	20.6 (4)	C14—O2—Zn1—O4 ⁱ	19.8 (6)
C1—C2—C14—N1	−157.9 (2)	C14—O2—Zn1—O4	87.6 (2)
N1—C15—C16—N2	−127.8 (3)	C14—O2—Zn1—O2 ⁱ	−101.9 (2)
N1—C15—C16—C17	51.7 (4)		

Symmetry codes: (i) $-x, y, -z+1/2$.

Hydrogen-bond geometry (\AA , $^\circ$)

$D-H\cdots A$	$D-H$	$H\cdots A$	$D\cdots A$	$D-H\cdots A$
N3—H3A \cdots O1	0.86	1.93	2.623 (3)	136
N1—H1 \cdots N4 ⁱⁱ	0.86	2.20	3.007 (4)	155
O4—H24 \cdots O3 ⁱⁱⁱ	0.85	1.87	2.712 (3)	174
O4—H23 \cdots N2 ^{iv}	0.87	2.03	2.879 (3)	163

Symmetry codes: (ii) $x+1/2, y+1/2, z$; (iii) $-x, -y, -z$; (iv) $-x+1/2, y-1/2, -z+1/2$.

Fig. 1

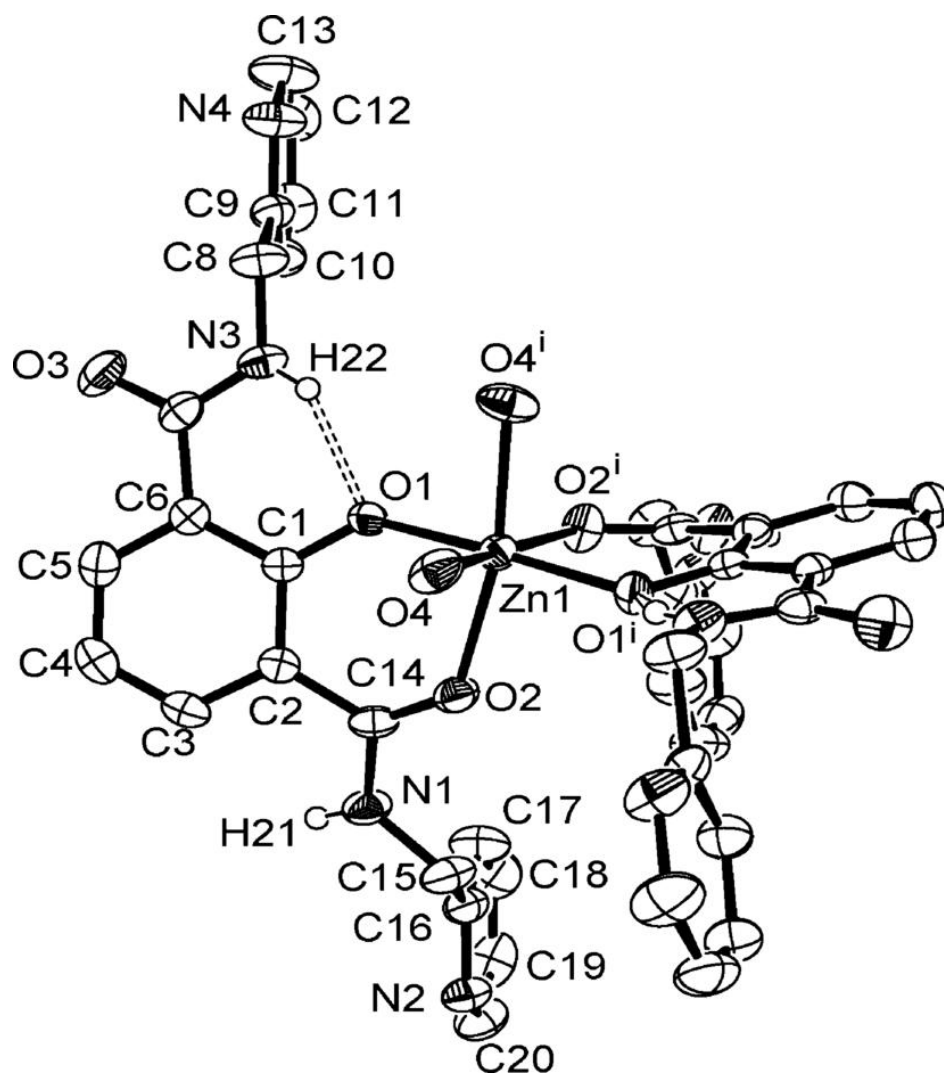


Fig. 2

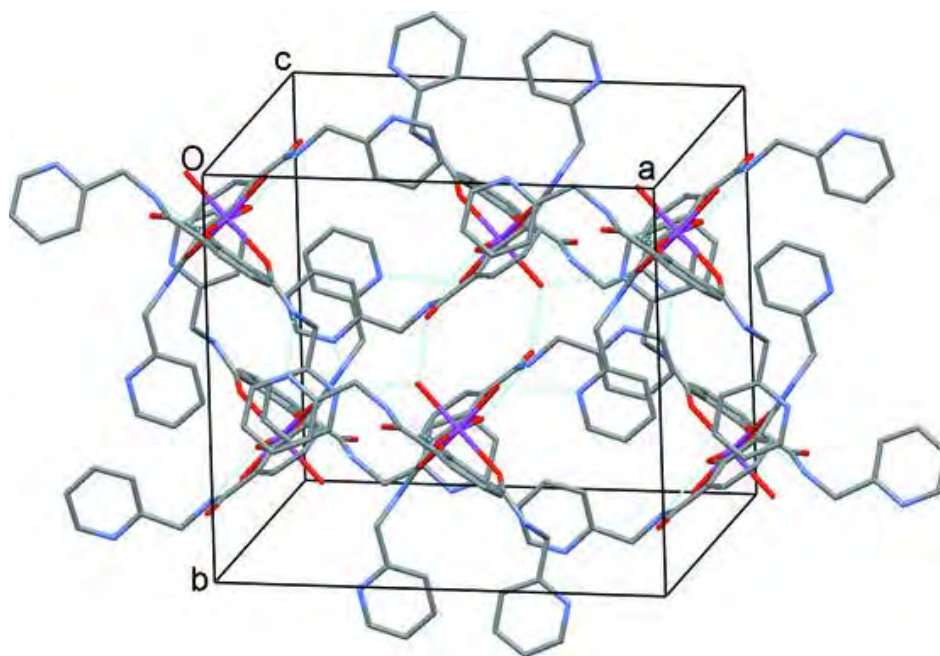
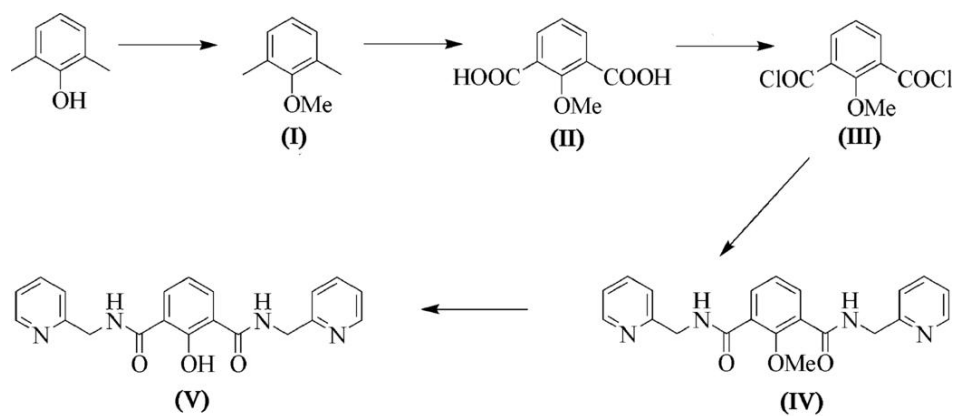


Fig. 3





Synthesis, optical and electrochemical properties of new receptors and sensors containing anthraquinone and benzimidazole units

Boontana Wannalerse, Thawatchai Tuntulani, Boosayarat Tomapatanaget*

Supramolecular Chemistry Research Unit, Department of Chemistry, Faculty of Science, Chulalongkorn University, Bangkok 10330, Thailand

ARTICLE INFO

Article history:

Received 13 May 2008

Received in revised form 5 August 2008

Accepted 21 August 2008

Available online 30 August 2008

ABSTRACT

Novel anion receptors and sensors, **HBIMANQ** and **BIMANQ** fabricated from the imidazolole unit and anthraquinone moieties were synthesized. ^1H NMR spectroscopy and UV–vis titrations in DMSO- d_6 and DMSO, respectively, showed that both receptors underwent deprotonation at the NH- moiety of the amide–anthraquinone unit in the presence of basic anions such as F^- and AcO^- . These phenomena gave a dramatic color change due to charge transfer transition corresponding to the shift of λ_{max} from 371 nm to 489 nm. Redox chemistry of **HBIMANQ** and **BIMANQ** in the presence of anions (F^- , Cl^- , AcO^- , BzO^- , and H_2PO_4^-) using cyclic voltammetry showed the different CV responses upon addition of various anions. In the case of **HBIMANQ** with various anions, the CV changes are dependent on the basic strength of anions in order of $\text{F}^- > \text{AcO}^-$, $\text{BzO}^- > \text{H}_2\text{PO}_4^- > \text{Cl}^-$, Br^- . Interestingly, the CV responses of **BIMANQ** with H_2PO_4^- exhibited the most significant changes. **BIMANQ**, thus, has an excellent electrochemical selectivity toward H_2PO_4^- .

© 2008 Elsevier Ltd. All rights reserved.

1. Introduction

In recent years, a number of research groups have used anthraquinone derivatives to function as potential naked-eye anion sensors.¹ Das and co-workers² reported a novel colorimetric receptor based on disubstituted-1,2-diaminoanthraquinone as a chromogenic signaling unit for detecting fluoride ion. Miyaji and Sessler³ evaluated the visual properties of the complexes of anthraquinone derivatives with various anions, and found that the significant color change depends on the basicity and the appropriate orientation of anions to undergo hydrogen bonding interactions with the NH_2 -site of anthraquinone. Brooks and co-workers⁴ investigated an anthraquinone-based anion receptor to study hydrogen bonding through intra- or intermolecular interactions using the cyclic voltammetry, in the presence of F^- . Two one-electron quasi-reversible electrochemical properties were observed. Carneiro and coworkers⁵ used anthraquinone-based chlorotriazine reactive dyes as dyeing agents removed from aqueous solution using electrochemical reduction.

Imidazolium cations have been widely used in ionic liquids^{6–11} and for generation of carbenes in organometallic processes and catalysts.^{12–16} Moreover, imidazolium derivatives are employed as a complementary binding enhancement for anions. Particularly, $(\text{C-H})^+ \cdots \text{X}^-$ interaction at the C(2) H position is a powerful tool to encourage strong hydrogen bonding interaction with concomitant

electrostatic forces toward anions.¹⁷ Beer and co-workers synthesized and studied interlock molecules, known as pseudorotaxanes and rotaxanes employing the $(\text{C-H})^+ \cdots \text{X}^-$ hydrogen bonding interaction.^{18–22} Such fascinating behaviors prompted to synthesize novel molecular sensors, **HBIMANQ** and **BIMANQ**, based on imidazolium as a binding site, and anthraquinone as a visual and electrochemical sensory unit. Herein, we studied the binding and sensing behaviors of **HBIMANQ** and **BIMANQ** toward F^- , Cl^- , Br^- , H_2PO_4^- , AcO^- , and BzO^- . We would like to compare binding properties between receptors with and without the positive charge on the benzimidazole unit, which was expected to enhance the binding affinity toward anions. Binding and sensing properties of **HBIMANQ** and **BIMANQ** were studied by ^1H NMR spectroscopy, UV–vis spectrophotometry, and cyclic voltammetry.

2. Results and discussion

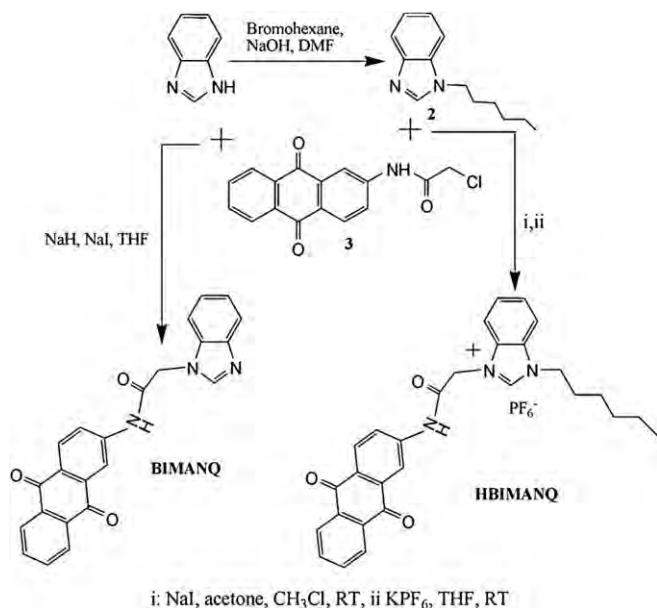
2.1. Synthesis

Compounds **HBIMANQ** and **BIMANQ** were synthesized as outlined in Scheme 1. The synthesis of **HBIMANQ** was started by a reaction between benzimidazole and 1-bromohexane using NaOH as base in dimethylformamide at reflux to give compound **2** in 80% yield. A coupling reaction of **2** with compound **3** in a mixture of acetone and chloroform in the presence of NaI followed by conversion of counter anions using KPF_6 in THF yielded **HBIMANQ** in 85% yield. **BIMANQ** was synthesized in 80% yield by coupling benzimidazole with compound **3** using NaH as base in THF. The

* Corresponding author. Tel.: +662 2187642; fax: +662 2541309.

E-mail address: tboosayarat@gmail.com (B. Tomapatanaget).

structures of **HBIMANQ** and **BIMANQ** were characterized by NMR spectroscopy, ESI MS spectroscopy, and elemental analysis. However, the elemental analysis result of **HBIMANQ** obtained from the experiment is not in good agreement with those from calculation since this ligand is very hygroscopic.



Scheme 1. Synthesis of **HBIMANQ** and **BIMANQ**.

2.2. Binding studies using ^1H NMR spectroscopy and UV–vis spectrophotometry

From the ^1H NMR spectra, the characteristic peaks namely, the NH_{amide} on anthraquinone, $\text{C}(2)\text{H}$, and $-\text{N}_{\text{imid}}\text{CH}_2\text{N}_{\text{amide}}-$ of **HBIMANQ** and **BIMANQ** displayed at 11.30 and 11.13 ppm, 9.78 and 8.45 ppm as well as 5.60 and 5.28 ppm, respectively. Binding studies of **HBIMANQ** toward F^- , Cl^- , Br^- , H_2PO_4^- , AcO^- , and BzO^- were carried out by NMR spectroscopy in $\text{DMSO}-d_6$. Figure 1 shows the ^1H NMR spectra of the complexation of **HBIMANQ** and all guests at 4 equiv.

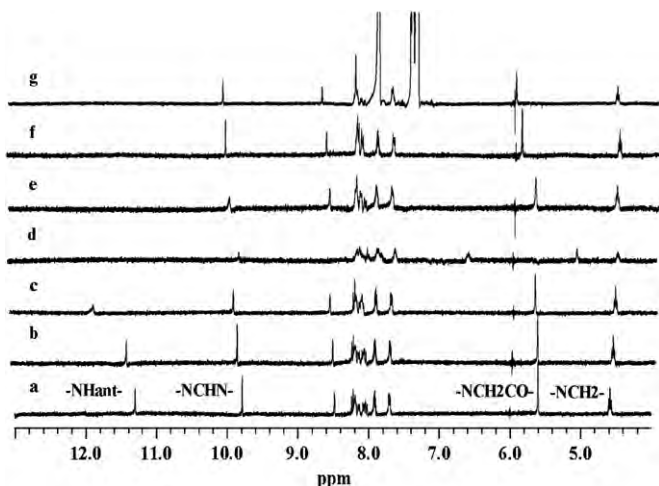


Figure 1. ^1H NMR spectrum in $\text{DMSO}-d_6$ at 298 K of (a) **HBIMANQ** (5×10^{-3} M), (b) **HBIMANQ**+4 equiv Bu_4NBr , (c) **HBIMANQ**+4 equiv Bu_4NCl , (d) **HBIMANQ**+4 equiv Bu_4NF , (e) **HBIMANQ**+4 equiv $\text{Bu}_4\text{NH}_2\text{PO}_4$, (f) **HBIMANQ**+4 equiv Bu_4NAcO , and (g) **HBIMANQ**+4 equiv Bu_4NBzO .

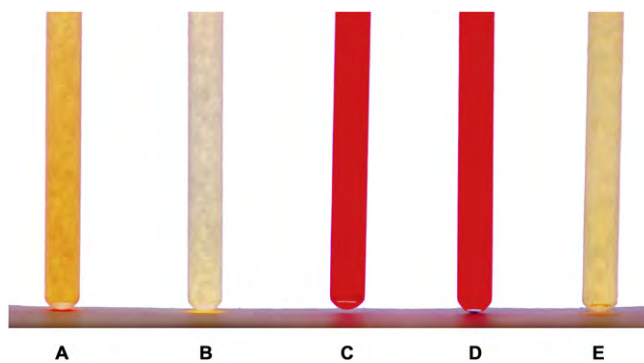


Figure 2. The color change of (A) **HBIMANQ**+4 equiv CH_3COO^- , (B) **HBIMANQ**, (C) **HBIMANQ**+4 equiv F^- , (D) **HBIMANQ**+10 equiv F^- , and (E) **HBIMANQ**+4 equiv $\text{F}^- + \text{H}_2\text{O}$ under each condition in DMSO .

The NH_{ant} signals of **HBIMANQ** vanished upon addition of 0.1, 0.1, 0.1, and 2.5 equiv of F^- , AcO^- , BzO^- , and H_2PO_4^- , respectively. The features of the spectra for the bound ligand differ from the spectral pattern for the unbound ligand indicating that **HBIMANQ** can bind with all guests with the different binding abilities independent of size or geometry of the anions, only on the basicity. From ^1H NMR titrations for ligand and F^- , it should be noted that NH_{ant} resonances shifted downfield and were then followed by the disappearance of a proton and the upfield-shift of aromatic protons on further addition of F^- . Moreover, an appearance of new triplet signals of bifluoride (HF_2^-) protons was found ca. 16.05 ppm (Supplementary data). These evidences showed that H-bond interactions occurred between NH_{ant} with F^- prior to deprotonation.

Upon addition of 5 equiv of H_2PO_4^- , AcO^- , BzO^- , and F^- into **BIMANQ** solutions, it was found that the NH_{ant} signal disappeared signifying deprotonation. However, the $-\text{C}(2)\text{H}-$ signal of **BIMANQ** slightly shifted downfield due to hydrogen bonding interactions. We attempted to find the association constants of **BIMANQ** toward anions, but they could not be obtained due to the deprotonation process.

Concomitant with deprotonation, dramatically color changes were observed upon addition of F^- and AcO^- to **HBIMANQ** and **BIMANQ**. In the presence of 4 equiv F^- , the color of the solution was changed from yellow to orange, and further addition of F^- shifted the color to deep red (Fig. 2). However, the color change is less intense in the case of AcO^- . This is probably due to the stronger basic character of F^- . Upon addition of H_2O , the red color of **HBIMANQ}· F^- turned to the initial color (Fig. 2). This signified that the deprotonation of **HBIMANQ** is reversible. In the case of BzO^- and H_2PO_4^- , the color of the solutions of **HBIMANQ** changed slightly upon addition of such anions. For Br^- and Cl^- , there was no color change at all. This agrees with the ^1H NMR spectra, which showed that the NH_{ant} was still present. The behavior of **BIMANQ** has a similar fashion to **HBIMANQ**. The UV–vis spectra of **HBIMANQ** and **BIMANQ** with 4 equiv F^- are illustrated in Figure 3. The new peak at 489 nm developed in the spectrum (as shown in Fig. 3d) is concomitant with color changes from colorless to yellow. Presumably, F^- is able to deprotonate NH_{ant} and to induce charge transfer from the negative charge of NH_{ant} to anthraquinone.³ Upon addition of NH_4OH to the solution of **HBIMANQ**, a new absorption band displayed at 489 nm (green line in Fig. 3c) and the color of the solution turned deep red similar to the case of F^- . This band was undoubtedly corresponding to the deprotonated **HBIMANQ** species. This result agrees with Gunnlaugsson's report on the deprotonation process of a urea-based anion receptor.^{23–25} For other anions, UV–vis spectra of **HBIMANQ** exhibit a gradual decrease of the initial absorption band without the appearance of a new peak. Interestingly, the color change and a new absorption band were not**

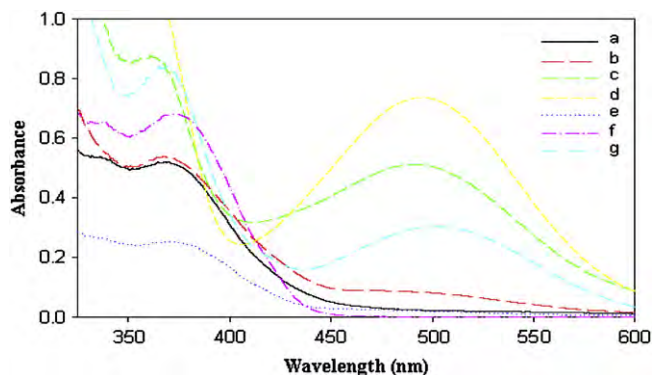


Figure 3. UV spectrum of (a) **HBIMANQ** (7.5×10^{-4} M), (b) **HBIMANQ** + 4 equiv Bu_4NF , (c) **HBIMANQ** + 4 equiv Bu_4NOH , (d) **HBIMANQ** + 4 equiv $\text{Bu}_4\text{CH}_3\text{COO}$, (e) **HBIMANQ** + 4 equiv Bu_4NF + ex. H_2O , (f) **BIMANQ**, and (g) **BIMANQ** + 4 equiv Bu_4NF in DMSO at 298 K.

observed upon the addition of AcO^- to **HBIMANQ**, possibly caused by the low concentration of **HBIMANQ**. The naked-eye detectability of **HBIMANQ** and **BIMANQ** with F^- is independent of its concentration. Deprotonation was found to be completely reversible because **HBIMANQ**· F^- showed the original color and spectrum of **HBIMANQ** in the presence of H_2O (blue line in Fig. 3e).

Anion binding constants of receptors **HBIMANQ** and **BIMANQ** were measured by UV–vis titrations in DMSO. The titration graph of **HBIMANQ** with F^- is shown in Figure 4. Job's plot measured by UV spectrophotometry indicated that ligands bind anions in a 1:1 fashion. Results of titrations of **BIMANQ** toward anion guests are similar to those of **HBIMANQ**. All log K values were calculated by Spectfit 32 program in the model of 1:1 complexation. The log K values of **HBIMANQ** with various anions are of 3.71 for Cl^- , 3.63 for Br^- , 4.22 for $\text{H}_2\text{PO}_4^{2-}$, and 5.63 for BzO^- . Unfortunately, we could not obtain the binding constants between **HBIMANQ** with F^- and AcO^- because of the occurrence of two processes toward ligands including binding and deprotonation. The log K values of **HBIMANQ** with anions are in order of $\text{Br}^- < \text{Cl}^- < \text{H}_2\text{PO}_4^{2-} < \text{C}_6\text{H}_5\text{COO}^-$. The results showed that **HBIMANQ** appreciated Y-shape anions over spherical anions. In the case of **BIMANQ**, its binding constants could not be refined because this receptor contained one NH amide and no positive charge on benzimidazole. Therefore, the binding site may not have enough binding affinity.

2.3. Electrochemical properties of HBIMANQ and BIMANQ

HBIMANQ and **BIMANQ** have anthraquinone moiety, which typically exhibits two redox couples. The reversible first wave represents an electron transfer of the quinone moiety (AQ) to form

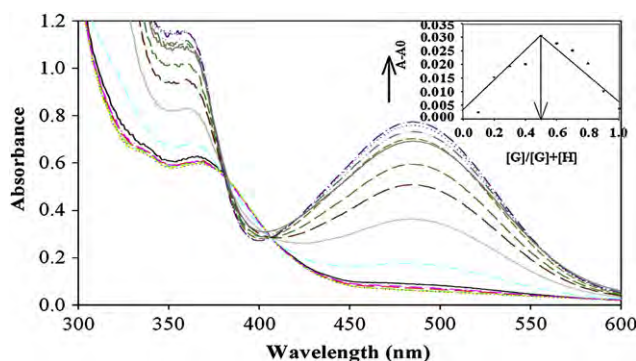


Figure 4. UV–vis titrations of **HBIMANQ** with Bu_4NF in DMSO. $[\text{HBIMANQ}] = 7.5 \times 10^{-4} \text{ mol L}^{-1}$ and $[\text{Bu}_4\text{NF}] = 0\text{--}0.004 \text{ mol L}^{-1}$.

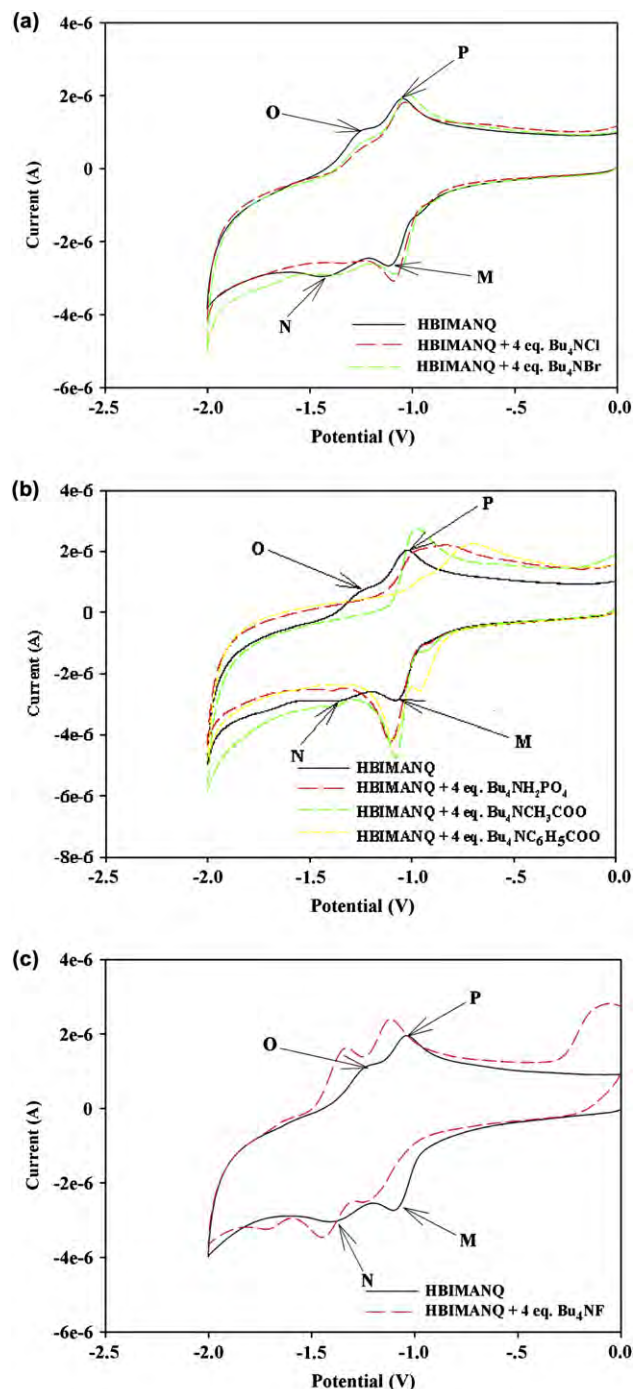


Figure 5. Cyclic voltammograms of ligand **HBIMANQ** upon addition of 4 equiv of (a) Bu_4NBr and Bu_4NCl , (b) $\text{Bu}_4\text{NH}_2\text{PO}_4$, $\text{Bu}_4\text{NCH}_3\text{COO}$, and $\text{Bu}_4\text{NC}_6\text{H}_5\text{COO}$, and (c) Bu_4NF .

a semiquinone anion radical ($\text{AQ}^{\cdot-}$). The second irreversible reduction wave corresponds to the subsequent addition of a second electron to the semiquinone anion radical, producing a hydroquinone dianion (AQ^{2-}).^{26,27} To explore the electrochemical behaviors of **HBIMANQ** and **BIMANQ** with anions, both ligands were examined by cyclic voltammetry.

The electrochemical studies of **HBIMANQ** upon adding 4 equiv of various anions. The cyclic voltammograms are shown in Figure 5 and the potential values are collected in Table 1. In the case of Br^- and Cl^- , the CVs showed slight shifts from the initial electrochemical potential because both anions can bind to the ligand with a weak interaction.

Table 1
The potential values of compound **HBIMANQ** with 4 equiv of various anions

	E_{pc} (V)	E_{pc} (V)	E_{pa} (V)	E_{pa2} (V)	ΔE_{pc} (V)	ΔE_{pc} (V)	ΔE_{pa} (V)	ΔE_{pa} (V)
	M	N	O	P	M	N	O	P
HBIMANQ	−1.083	−1.392	−1.257	−1.041	—	—	—	—
+Cl [−]	−1.083	—	−1.038	−1.251	0	—	−0.219	0.200
+F [−]	−1.193	−1.443	−1.352	−1.120	0.110	0.051	0.095	0.079
+H ₂ PO ₄ [−]	−1.099	—	−0.967	—	0.0160	—	−0.290	—
+CH ₃ COO [−]	−1.077	—	−0.983	—	−0.006	—	−0.274	—
+C ₆ H ₅ COO [−]	−0.970	−1.047	−0.784	—	−0.113	−0.345	−0.473	—

In the presence of Cl[−], Br[−], CH₃COO[−], C₆H₅COO[−], and H₂PO₄[−], CVs of these anions with **HBIMANQ** showed a similar shape but gave different shifts of reduction and oxidation waves, which depend on the basicity of the anions. As with NMR and UV–vis results mentioned above CH₃COO[−], C₆H₅COO[−], and H₂PO₄[−] could bind to **HBIMANQ** by electrostatic forces and hydrogen bonding interaction, which occurred from the intermolecular proton transfer of the NH_{ant} amide and anions. These complexes might inhibit further reduction process of the semiquinone species to dianion species resulting in the high current intensity of semiquinone peak with concomitant low current intensity or disappearance of dianion peak.

In the case of F[−], both redox couples of **HBIMANQ** show the cathodic shifts because of the enhancement of negative charge by the deprotonation of the NH amide moiety.^{4,28,29} Therefore, it is difficult to reduce the anthraquinone of **HBIMANQ**. Since the F[−] anion is a strong base, it prefers to deprotonate the NH amide without the hydrogen bonding formation. Possibly, this anion could not obstruct the further reduction process to the dianion species. Therefore, this receptor has the ability to detect the F[−] anion selectively, correlating to the significant change of CV response.

The complexation behaviors of **BIMANQ** with anions were investigated by cyclic voltammetry. Unlike the typical cyclic voltammogram of anthraquinone, **BIMANQ** showed two redox couples, which were not the reversible processes. The first redox couple was a one-electron irreversible process, corresponding to the semiquinone species and the second one was attributed to the dianionic species as shown in Figure 6. The CV responses of **BIMANQ** with 4 equiv of Cl[−], CH₃COO[−], C₆H₅COO[−], and F[−] changed slightly with the intensities of the oxidation peaks but **BIMANQ** with F[−] and AcO[−] displayed the largest changes of intensities of the semiquinone species (see in Supplementary data).

Interestingly, H₂PO₄[−] induced the significant change in cyclic voltammogram most depicted in Figure 6. CV response exhibits three reduction and oxidation peaks. The appearances of the new reduction and oxidation peaks were observed at −1.624 V and −1.470 V, respectively. The semiquinone peak of **BIMANQ** and H₂PO₄[−] showed the shift to a more negative potential and the enhancement of the current.

In addition, **BIMANQ** has no charge on benzimidazole to encourage the electrostatic interactions toward anions. The significant changes of CV responses possibly stemmed from multiple hydrogen bonding interactions between the reduced form of **BIMANQ** and H₂PO₄[−] leading to the strong binding affinity compared to other anions.

3. Conclusions

We have developed novel colorimetric anion sensors for F[−] and AcO[−]. Interestingly, **HBIMANQ** in the presence of F[−], AcO[−], BzO[−], and H₂PO₄[−] underwent deprotonation on NH_{ant}. From complexation studied by UV–vis and NMR techniques, **HBIMANQ** prefers Y-shape anions over spherical anions due to the complementary π – π stacking interactions. Meanwhile, **BIMANQ** could bind with anions with a weak interaction. Cyclic voltammograms of **HBIMANQ** in the presence of various anions showed changes of redox signals. It means that this receptor has responded to all anions electrochemically. However, it was found that CVs showed the most significant changes by shifting to more negative potentials in the presence of F[−]. Interestingly, CVs of **BIMANQ** with all anions except H₂PO₄[−] exhibited only small changes. The electrochemical study of **BIMANQ** with H₂PO₄[−] showed a larger change than other anions probably due to multiple hydrogen bonding interactions between two hydrogens of H₂PO₄[−] and the oxygen of anthraquinone. Therefore, **BIMANQ** was a powerful electrochemical sensor for H₂PO₄[−].

4. Experimental

4.1. Materials and methods

Nuclear magnetic resonance (NMR) spectra were recorded in DMSO-*d*₆, CDCl₃, and CD₃CN on a Varian 400 MHz spectrometer. Electrospray mass spectra were determined on a Micromass Platform quadrupole mass analyser with an electrospray ion source using acetonitrile as solvent. All melting points were obtained on an Electrothermal 9100 apparatus. Infrared spectra were carried out on a Nicolet Impact 410 FTIR spectrometer at room temperature with potassium bromide (KBr) disks. Elemental analyses were carried out on a Perkin–Elmer CHON/S analyzer (PE 2400 series II). Absorption spectra were measured by a Varian Cary 50 UV–vis spectrophotometer. Cyclic voltammetry was performed using a μ Autolab Type III potentiostat. Unless otherwise specified, the solvents and all materials were reagent grade without further purification prior to use. Commercial grade solvents such as acetone, dichloromethane, hexane, methanol, and ethylacetate were purified by distillation before use. Acetonitrile, dimethylformamide, and dichloromethane were dried over calcium hydride and THF was dried over benzoquinone and sodium and freshly distilled under nitrogen atmosphere prior to use. All anion salts and ligands were dried in vacuo prior to use.

4.2. Synthesis

4.2.1. 1-*n*-Hexylbenzimidazole (2)

To a stirred solution of benzimidazole (0.50 g, 4.2 mmol) and sodium hydroxide (0.17 g, 4.2 mmol), a solution of hexylbromide (0.60 mL, 2.3 mmol) in 65 mL dimethylformamide was slowly

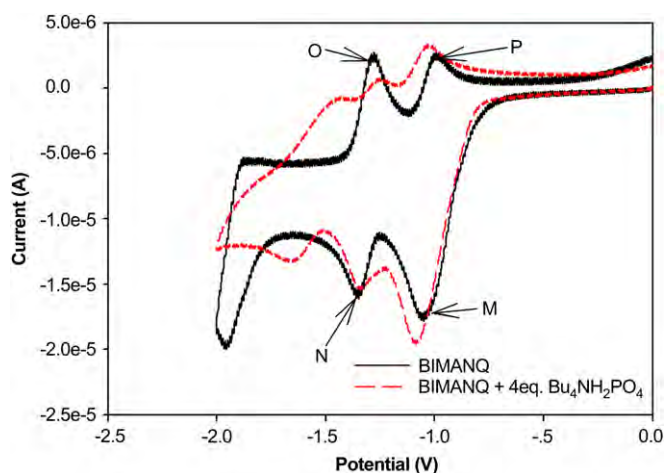


Figure 6. Cyclic voltammograms of ligand **BIMANQ** upon the addition of 4 equiv of Bu₄NH₂PO₄.

added and heated at reflux for 24 h under nitrogen atmosphere. The mixture was evaporated in vacuo. The residue was purified by column chromatography (SiO₂) using 50% ethylacetate/dichloromethane as eluent to afford compound **2** as colorless liquid (80% yield). ¹H NMR (400 MHz, CDCl₃) δ 8.20 (s, 1H, –NCHN–), 7.58 (m, 2H, –ArH–), 7.22 (m, 2H, –ArH–), 4.21 (m, 2H, –NCH₂–), 1.75 (m, 2H, –CH₂–), 1.22 (m, 6H, –CH₂–), 0.80 (m, 3H, –CH₃); FTIR (KBr disk) ν [cm^{–1}] 2928 (m), 1496 (s), 1457 (s), 1368 (s), 743 (s).

4.2.2. Chloroethyleneamidoanthraquinone (**3**)³⁰

A solution of aminoanthraquinone (1.00 g, 4.5 mmol) and pyridine (0.86 mL, 5.4 mmol) was stirred in 50 mL dichloromethane and cooled to 0 °C. After slowly adding a solution of chloroacetylchloride (0.61 g, 5.4 mmol) in (15 mL) dichloromethane, a brown precipitate appeared. HCl (3 M) was added to the mixture and the organic layer was extracted with water (3×50 mL). The organic layer was dried with anhydrous sodium sulfate and evaporated in vacuo to obtain a brown solid and further crystallized with dichloromethane/hexane. The purified compound **3** yielded as the brown crystalline solid in 70%. Mp 250 °C. ¹H NMR (400 MHz, CDCl₃) δ 8.64 (s, 1H, –NH–), 8.36 (m, 4H, –ArH–), 8.26 (s, 1H, –ArH–), 7.85 (m, 2H, –ArH–), 4.30 (s, 2H, –CH₂–); FTIR (KBr disk) ν [cm^{–1}] 3344 (m), 1720 (s), 1669 (s), 1420 (m); ESI MS: *m/z* = 299.03.

4.2.3. 2-(1H-Benzo[d]imidazol-1-yl)-N-(9,10-dioxo-9,10-dihydroanthracen-2-yl) hexyl actamide, **HBIMANQ**

To a solution of **2** (0.20 g, 1.0 mmol) and a catalytic amount of sodium iodide in (15 mL) acetone/chloroform, **3** (0.29 g, 1.00×10^{–3} mol) was added and the mixture was stirred. The precipitate was separated and recrystallized in a mixture of dichloromethane/hexane to obtain the product **HBIMANQCI** (10% yield). Anion exchange of **HBIMANQCI** was carried out using KPF₆ in THF for 24 h to afford **HBIMANQ** (85% yield); mp 355–357 °C. ¹H NMR (400 MHz, DMSO-*d*₆) δ 11.30 (s, 1H, –NH–), 9.78 (s, 1H, –NCHN–), 8.48 (s, 1H, –ArH–), 8.22 (m, 2H, –ArH–), 8.15 (m, 2H, –ArH–), 8.08 (m, 2H, –ArH–), 7.90 (m, 2H, –ArH–), 7.70 (m, 2H, –ArH–), 5.60 (s, 2H, –CH₂CON–), 4.58 (m, 2H, –NCH₂–), 1.91 (m, 2H, –CH₂–), 1.30 (m, 6H, –CH₂–), 0.83 (m, 3H, –CH₃). ¹³C NMR (400 MHz, DMSO-*d*₆) δ 183.4, 182.6, 165.2, 144.5, 143.8, 135.3, 135.3, 134.9, 134.1, 134.1, 132.8, 131.7, 129.7, 129.4, 127.8, 127.6, 127.5, 127.5, 125.0, 117.1, 114.5, 114.3, 50.1, 48.0, 31.4, 29.3, 26.2, 22.8, 14.2; FTIR (KBr disk) ν [cm^{–1}] 3384 (m), 2925 (s), 1724 (s), 1672 (s), 841 (s); HRMS (positive ESI) *m/z* calcd for C₂₉H₂₈N₃O₃ (M⁺) 466.213, found 466.223; UV–vis (DMSO) λ_{max} = 368 nm.

4.2.4. 2-(1H-Benzo[d]imidazol-1-yl)-N-(9,10-dioxo-9,10-dihydroanthracen-2-yl) actamide, **BIMANQ**

To a solution of benzimidazole (0.123 g, 0.5 mmol) and a catalytic amount of sodium iodide in (60 mL) DMF, **3** (0.179 g, 0.6 mmol) and NaH (0.012 g, 0.5 mmol) were added and the reaction mixture was stirred for 24 h under nitrogen atmosphere. Then, the mixture was evaporated in vacuo. The residue was purified by column chromatography (SiO₂) using ethylacetate as eluent to afford compound **BIMANQ** as brown solid (80% yield). Mp 300–301 °C. ¹H NMR (400 MHz, DMSO-*d*₆) δ 11.13 (s, 1H, –CONH–), 8.45 (s, 1H, –NCH=N), 8.27 (s, 1H, –ArH–), 8.20 (m, 3H, –ArH–), 8.07 (d, 1H, –ArH–), 7.89 (m, 2H, –ArH–), 7.59 (d, 1H, –ArH–(benzimidazole)), 7.56 (d, 1H, –ArH–(benzimidazole)), 7.23 (m, 2H, –ArH–(benzimidazole)), 5.28 (s, 2H, –COCH₂–); ¹³C NMR (400 MHz, DMSO-*d*₆) δ 31.2, 36.2, 47.9, 110.9, 116.4, 119.7, 122.2, 123.0, 124.4, 127.1, 127.2, 128.7, 129.0, 133.5, 134.7, 135.1, 144.4, 145.4, 162.7, 181.8, 182.8; FTIR (KBr disk) ν [cm^{–1}] 3366 (w), 3058 (m), 1712 (s), 1663 (s), 1423 (s); ESI MS (ES⁺): *m/z*(%) = 381.764 (100) [M+H⁺]. Anal. Calcd for C₂₃H₁₅N₃O₃: C, 72.43; H, 3.96; N, 11.02. Found: C, 72.15; H, 3.97; N, 11.02.

4.3. NMR studied on host and guests

The NMR experiments were measured in DMSO-*d*₆. The solution of ligand in DMSO, which was added with 4 equiv of solid tetrabutylammonium salts (F[–], Cl[–], Br[–], AcO[–], BzO[–], and H₂PO₄[–]) was recorded.

4.4. UV–vis titrations for binding constants of host–guests

All UV–vis experiments were carried out in DMSO with tetrabutylammoniumhexafluorophosphate as supporting electrolyte. The solutions of **HBIMANQ** (7.5×10^{–4} M) and **BIMANQ** (1.5×10^{–4} M) were prepared and gradually added with the solution of guests (0.02 M) until the system reached the equilibrium point observed by a small change in UV–vis spectrum. Each addition was recorded and all data were used for the calculation of the stability constants with Spectfit 32 program.

4.5. CV studies on host and guests

Typically, a 0.001 mol dm^{–3} solution of a ligand (5×10^{–6} mol) in 0.1 mol dm^{–3} supporting electrolyte (5 mL of NBu₄PF₆ in freshly distilled DMSO) was prepared. A stock solution of an anionic 0.5 mmol in supporting electrolyte (0.1 mol dm³) was prepared. All electrochemical experiments were carried out in a three-electrode cell designed in-house comprising of a working electrode, a counter electrode, and a reference electrode. The working electrode was a glassy carbon disk with a diameter of 3 mm embedded in Teflon and the counter electrode was a platinum coil. Ag/AgNO₃ electrode was used as a reference electrode in DMSO solution.

Acknowledgements

We thank the Thailand Research Fund (MRG4780187 and RTA5080006) and National Center of Excellence for Petroleum, Petrochemical, and Advanced Materials (NCE-PPAM) for financial supports. B.W. is a Ph.D. student supported by the Commission on Higher Education.

Supplementary data

The analysis of the synthesized compounds including NMR spectra, mass spectrometry, and cyclic voltammograms are provided. Supplementary data associated with this article can be found in the online version, at doi:10.1016/j.tet.2008.08.073.

References and notes

- (a) Gale, P. A.; Quesada, R. *Coord. Chem. Rev.* **2006**, *250*, 3219–3244; (b) Gunlaugsson, T.; Glynn, M.; Tocci, M. G.; Kruger, P. E.; Pfeffer, F. M. *Coord. Chem. Rev.* **2006**, *250*, 3094–3117; (c) Sukai, C.; Tuntulani, T. *Top. Curr. Chem.* **2005**, *255*, 163–198.
- Jose, A. A.; Kumar, K. D.; Ganguly, B.; Das, A. *Org. Lett.* **2004**, *6*, 3445–3448.
- Miyaji, H.; Sessler, J. L. *Angew. Chem., Int. Ed.* **2001**, *40*, 154–157.
- Brooks, S. J.; Birkin, P. R.; Gale, P. A. *Electrochem. Commun.* **2005**, *7*, 1351–1356.
- Carneiro, P. A.; Boralle, N.; Stradiotto, N. R.; Furlan, M.; Zanoni, M. V. B. *J. Braz. Chem. Soc.* **2004**, *15*, 587–594.
- Welton, T. *Chem. Rev.* **1999**, *99*, 2071–2083.
- Liu, Z.; Chen, Z.-C.; Zheng, Q.-G. *Org. Lett.* **2003**, *5*, 3321–3323.
- Dupont, J.; Fonseca, G. S.; Umpierre, A. P.; Fichtner, P. F. P.; Teixeira, S. R. *J. Am. Chem. Soc.* **2002**, *124*, 4228–4229.
- Itoh, H.; Naka, K.; Chujo, Y. *J. Am. Chem. Soc.* **2004**, *126*, 3026–3027.
- Forbes, D. C.; Patrawala, S. A.; Tran, K. L. T. *Organometallics* **2006**, *25*, 2693–2695.
- Fei, Z.; Kuang, D.; Zhao, D.; Klein, C.; Ang, W. H.; Zakeeruddin, S. M.; Gratzel, M.; Dyson, P. J. *Inorg. Chem.* **2006**, *45*, 10407–10409.
- Voutchkova, A. M.; Appelhaus, L. N.; Chianese, A. R.; Crabtree, R. H. *J. Am. Chem. Soc.* **2005**, *127*, 17624–17625.
- Fei, Z.; Zhao, D.; Scopelliti, R.; Dyson, P. J. *Organometallics* **2004**, *23*, 1622–1628.
- Boydston, A. J.; Rice, J. D.; Sanderson, M. D.; Dykhno, O. L.; Bielawski, C. W. *Organometallics* **2006**, *25*, 6087–6098.

15. Dupont, J.; de Souza, R. F.; Suarez, P. A. Z. *Chem. Rev.* **2002**, *102*, 3667–3692.
16. Scheeren, C. W.; Machado, G.; Dupont, J.; Fichtner, P. F. P.; Teixeira, S. R. *Inorg. Chem.* **2003**, *42*, 4738–4742.
17. Kim, H.; Kang, J. *Tetrahedron Lett.* **2005**, *46*, 5443–5445.
18. (a) Wisner, J. A.; Beer, P. D.; Drew, M. G. B. *Angew. Chem., Int. Ed.* **2001**, *40*, 3606–3609; (b) Wisner, J. A.; Beer, P. D.; Berry, N. G.; Tomapatanaget, B. *Proc. Natl. Acad. Sci. U.S.A.* **2002**, *99*, 4983–4986.
19. (a) Tomapatanaget, B.; Tuntulani, T.; Wisner, J. A.; Beer, P. D. *Tetrahedron Lett.* **2004**, *45*, 663–666; (b) Wong, W. W. H.; Vickers, M. S.; Cowley, A. R.; Paul, R. L.; Beer, P. D. *Org. Biomol. Chem.* **2005**, *3*, 4201–4208.
20. Kim, S. K.; Kang, B.-G.; Koh, H. S.; Yoon, Y. J.; Jung, S. J.; Jeong, B.; Lee, K.-D.; Yoon, J. *Org. Lett.* **2004**, *6*, 4655–4658.
21. Ihm, H.; Yun, S.; Kim, H. G.; Kim, J. K.; Kim, K. S. *Org. Lett.* **2002**, *4*, 2897–2900.
22. Yun, S.; Ihm, H.; Kim, H. G.; Lee, C.-W.; Indrajit, B.; Oh, K. S.; Gong, Y. J.; Lee, J. W.; Yoon, J.; Lee, H. C.; Kim, K. S. *J. Org. Chem.* **2003**, *68*, 2467–2470.
23. (a) Camiolo, S.; Gale, P. A.; Hursthouse, M. B.; Light, M. E. *Org. Biomol. Chem.* **2003**, *1*, 741–744; (b) Gunnlaugsson, T.; Kruger, P. E.; Pfeffer, F. M.; Hussey, G. M. *Tetrahedron Lett.* **2003**, *44*, 8909–8913; (c) Herrmann, W. A.; Köcher, C. *Angew. Chem., Int. Ed.* **1997**, *36*, 2162–2187; (d) Pfeffer, F. M.; Gunnlaugsson, T.; Jensen, P.; Kruger, P. E. *Org. Lett.* **2005**, *7*, 5357–5360.
24. Vázquez, M.; Fabbrizzi, L.; Taglietti, A.; Pedrido, R. M.; González-Noya, A. M.; Bermejo, M. R. *Angew. Chem., Int. Ed.* **2004**, *43*, 1962–1965.
25. Boiocchi, M.; Boca, L. D.; Gómez, D. E.; Fabbri, L.; Licchelli, M.; Monzani, E. *J. Am. Chem. Soc.* **2004**, *126*, 16507–16514.
26. Gupta, N.; Linschitz, H. *J. Am. Chem. Soc.* **1997**, *119*, 6384–6391.
27. Pletcher, D.; Thompson, H. *J. Chem. Soc., Faraday Trans.* **1998**, *94*, 3445–3450.
28. Gomez, M.; Gonzalez, F. J.; Gonealez, I. *J. Electroanal. Chem.* **2005**, *578*, 193–202.
29. Gomez, M.; Gomez-Castro, C. Z.; Padilla-Martínez, I. I.; Martínez-Martínez, F. J.; González, F. J. *J. Electroanal. Chem.* **2004**, *567*, 269–276.
30. Ngeontae, W.; Aeunmaitrepirom, W.; Tuntulani, T. *Talanta* **2007**, *71*, 1075–1082.



This article appeared in a journal published by Elsevier. The attached copy is furnished to the author for internal non-commercial research and education use, including for instruction at the authors institution and sharing with colleagues.

Other uses, including reproduction and distribution, or selling or licensing copies, or posting to personal, institutional or third party websites are prohibited.

In most cases authors are permitted to post their version of the article (e.g. in Word or Tex form) to their personal website or institutional repository. Authors requiring further information regarding Elsevier's archiving and manuscript policies are encouraged to visit:

<http://www.elsevier.com/copyright>



Contents lists available at ScienceDirect

Sensors and Actuators B: Chemical

journal homepage: www.elsevier.com/locate/snb

Novel potentiometric approach in glucose biosensor using silver nanoparticles as redox marker

Wittaya Ngeontae^{a,b}, Wanwisa Janrungroatsakul^a, Pattwat Maneewattanapinyo^a, Sanong Ekgasit^a, Wanlapa Aeungmaitrepirom^a, Thawatchai Tuntulani^{a,*}^a Department of Chemistry, Faculty of Science, Chulalongkorn University, Bangkok 10330, Thailand^b Department of Chemistry and Center of Excellence for Innovation in Chemistry, Faculty of Science, Khon Kaen University, Khon Kaen 40002, Thailand

ARTICLE INFO

Article history:

Received 14 September 2008

Received in revised form 4 November 2008

Accepted 4 November 2008

Available online 13 November 2008

Keywords:

Silver selective electrode

Silver nanoparticles

Glucose biosensor

Potentiometric redox marker

ABSTRACT

A new approach in glucose biosensor based on polymeric membrane Ag-ISE fabricated from benzothiazole calix[4]arene was investigated. Silver nanoparticles (AgNPs) were synthesized and demonstrated for the first time to be used as a potentiometric redox marker in a glucose biosensor. The linear relationship between logarithmic of H_2O_2 concentration and activity of free Ag^+ releasing from silver nanoparticles was observed by direct potentiometry. Basically, the enzyme–substrate reaction between β -D-glucose and glucose oxidase (GOx) produced H_2O_2 as a product. The generated H_2O_2 was able to oxidize AgNPs to free Ag^+ ions. The amount of Ag^+ ions corresponded to the concentration of glucose could be directly monitored using the Ag-ISE. The working linear range was 0.1–3 mM in 10 mM magnesium acetate buffer pH 6.0. Parameters affected the reaction rate such as pH and the amount of GOx and AgNPs were explored. The lower detection limit was 1.0×10^{-5} M. The sensors exhibited very good repeatability with %R.S.D. < 7 and high sensor-to-sensor reproducibility. The proposed sensor provided a double selective function and could be used to determine glucose in beverages with good accuracy and precision.

© 2008 Elsevier B.V. All rights reserved.

1. Introduction

Glucose biosensors have long been developed. Up until now, three generations of glucose biosensors using (i) natural oxygen co-substrate and generation and detection of hydrogen peroxide, (ii) synthetic electron mediators, and (iii) direct electron transfer between GOx and the electrode, have been reported [1]. Amperometry is the main detection technique used in glucose biosensors due to good sensitivity and low detection limit. To improve the performance of glucose biosensors, various nanomaterials such as carbon nanotube (CNT) and metal nanoparticles have been incorporated into the biosensor platform.

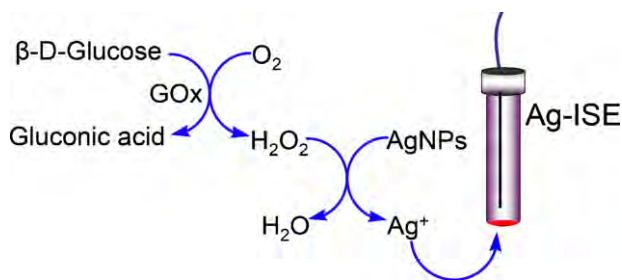
Wang and Musameh have shown that a CNT-modified sensor strip facilitates low potential amperometric measurements of H_2O_2 and NADH [2]. Luong and colleagues demonstrated that coupling of CNT with Pt nanoparticles could improve the detection limit and response time of GOx-based glucose biosensors (0.5 mM and 3 s, respectively) [3]. Willner and co-workers showed that the gold nanoparticle, immobilized onto the gold electrode by means of a thiol linker acted as an electrical nanoplug for the electrical wiring of the redox center of GOx [4,5]. Later, the same group used platinum nanoparticles as catalytic labels for detecting biorecognition

events through the electrocatalyzed reduction of H_2O_2 [6]. Another efficient probe for GOx employed aligned single walled CNT modified gold electrode has been reported by Gooding and colleagues [7]. This approach allowed more efficient electron transfer to the FAD with a rate constant of 9 s^{-1} . Recently, detection of glucose by a CdS-nanoparticles modified electrode has been demonstrated by Huang et al. to give significantly enhanced electron transfer activity [8].

Despite its numerous uses, the amperometric technique seems to exhibit some disadvantages such as selectivity due to the interference of other reducible species in blood. Potentiometry such as ion selective electrode (ISE) has an advantage over amperometry in selectivity. However, a quite important drawback of ISEs is that only charge molecules can be directly detected using the ISEs. To overcome this obstacle, an analyte must undergo a reaction that produces an ion in an amount proportional to the concentration of the analyte in the sample. The ion generated or “the marker” is then detected using an appropriate ISE. Górski et al. used F^- selective electrodes based on zirconium(IV) 5,10,15,20-tetraphenylporphyrin as a detector for glucose in a FIA system [9]. Meyerhoff has demonstrated the determination of glucose using a coupled-enzymatic reaction with fluoride selective optical sensing polymeric film coated in microliter plate wells [10]. Iodide selective electrode has also been used as a new glucose sensor detecting the decreasing amount of I^- upon the release of H_2O_2 [11].

* Corresponding author. Tel.: +66 2 2187643; fax: +66 2 2187598.

E-mail address: tthawattc@chula.ac.th (T. Tuntulani).



Scheme 1. Use of AgNPs as a new potentiometric redox marker in a glucose biosensor.

Thus far, no reports regarding the use of cation as marker have been found. This reason stems from the lack of cation markers available. Recently, metal nanoparticles such as gold and silver nanoparticles have been used as nanomaterial labels or “markers” in electrochemical biosensors and immunosensors [12–14]. Our group has fabricated a silver ion selective electrode or Ag-ISE using benzothiazole calix[4]arene as ionophore [15]. This Ag-ISE can be used in speciation analysis of silver nanoparticles (AgNPs). The key idea of this paper is to use AgNPs as cation marker in glucose biosensors as shown in Scheme 1. The enzyme–substrate reaction between glucose oxidase and glucose is well known to yield H_2O_2 . The oxidizing power of H_2O_2 is sufficient to convert Ag^0 of AgNPs to free Ag^+ . The activity of Ag^+ is immediately measured by a Ag-ISE.

2. Materials and methods

2.1. Materials

Glucose oxidase from *Aspergillus niger* (GOx, EC 1.1.3.4, 208.17 U mg^{-1}), magnesium acetate tetrahydrate, fructose, sucrose, high molecular weight polyvinyl chloride (PVC), *o*-nitrophenyl octyl ether (*o*-NPOE), potassium tetrakis (4-chlorophenyl) borate (KTPCIPB) and tetrahydrofuran (THF) were obtained from Fluka. Urea and glycine were purchased from Merck. β -D-Glucose was obtained from Sigma–Aldrich. The ionophore **CU1** [15] was prepared according to previously published procedures. The aqueous solutions were prepared from Milli-Q (Bedford, MA, USA) water purification system (Millipore).

Water colloids of high concentration silver nanoparticles (10,000 ppm) were synthesized via the chemical reduction process adapted from previous reports [16–18]. An aqueous solution of silver nitrate, 0.094 M (Merck) was prepared with methyl cellulose (Shin-Etsu) as a stabilizer. An aqueous solution of 0.07 M sodium borohydride reducing agent (Merck) with the methyl cellulose solution as a solvent was sequentially prepared. The silver solution was then added dropwise to the sodium borohydride solution under a vigorous stirring. A dark cloud appeared and turned to yellowish brown within a few seconds. When all reactants were completely added, the solution turned dark brown. The solution appeared golden yellow when diluted with distilled water under the concentration lower than 10 ppm.

2.2. Membrane preparation and EMF measurements

The Ag-ISE was prepared according to the procedure developed by us [15]. For this purpose, the ionophore **CU1** (10 mmol kg^{-1}), KTPCIPB (5 mmol kg^{-1}), 33 wt.% PVC and 66 wt.% *o*-NPOE were dissolved in 2.5 mL of THF. The cocktail solution was then poured into a glass ring (30 mm i.d.) fixed on a glass plate. The solvent was allowed to evaporate overnight at room temperature to give a transparent membrane (thickness $\sim 0.2 \text{ mm}$). The membrane was punched into small sizes (7.5 mm i.d.) and glued with a PVC/THF

slurry on the top of PVC tube and connected to a micro-pipette tip as an electrode body. The polymeric membrane electrodes were conditioned overnight in 0.01 M AgNO_3 identical to the filling solution. Potentiometric measurements were carried out with a 16-channel electrode monitor (Lawson Labs Inc., Malvern, PA 19355, USA). A Ag/AgCl was used as reference electrode with 1 M LiOAc as salt bridge electrolyte. Membrane potentials were measured in a stirring solution at ambient temperature in a galvanic cell:

Ag, AgCl/3 M KCl//1 M LiOAc//sample solution/membrane/0.01 M AgNO_3 /AgCl, Ag.

2.3. Determination of the releasing Ag^+ from oxidized AgNPs using H_2O_2

AgNPs (1000 ppm, 100 μL) were added into 10 mL of a buffer solution. Then, 0, 10, 30 and 100 μL of 0.092 M H_2O_2 was added separately in each solution. After stirring for 30 min, solutions were directly measured by the Ag-ISE to determine the activity of free silver ions. The experiment was repeated by increasing H_2O_2 concentration from 0.092 to 9.2 M and 10,000 ppm AgNPs was employed.

2.4. General EMF measurements

A buffer solution (10 mL) of 10 mM magnesium acetate was used as enzyme assay solution. The solution was adjusted to an appropriate pH by dilute acetic acid. Glucose was first diluted in a buffered solution, and the EMF was then measured. Subsequently, AgNPs was added into the solution of glucose. After the EMF was stable GOx (308 U mL^{-1}) was added and the EMF increased consecutively. The experiments were repeated three times for each point. The initial slope method described by Hassan et al. [19–22] was used in all measurements. The EMF was continuously monitored every 3 s (defined as an interval time). Plots of reaction rate were obtained from the differentiation of the change of EMF per interval time under assumption that the rate of potential change (dEMF/dt) is directly related to the change in $[\text{H}_2\text{O}_2]$. The maximum rate of potential change (dEMF/dt) was graphically determined by using the rate portion of the curve.

2.5. Studies of interferences

The Ag-ISE was immersed in the buffer solution (25 mL) containing glucose oxidase, and the base line EMF was then recorded. Subsequently, 50 μL of AgNPs (1000 ppm) was added. The EMF immediately jumped to higher base line because of the residual Ag^+ in AgNPs. After the EMF was stable, urea (8.5 mM), glycine (0.5 mM), fructose (10 mM) and sucrose (10 mM) were added after one another. The EMF was recorded after each addition.

2.6. Real sample measurements

A carbonated beverage was diluted by 10 mM magnesium acetate buffer, and pH was adjusted to pH 6. AgNPs (1000 ppm, 20 μL) and GOx (308 U mL^{-1}) were added into the sample solution. The EMF was then recorded. For a glucose-spiked sample, a known amount of glucose was added into the carbonated beverage. AgNPs and GOx were then added in the same manner as described previously. The experiment was carried out in triplicate. The amount of glucose in the sample and the glucose-spiked sample were determined from the maximum rate of the enzyme–substrate reaction.

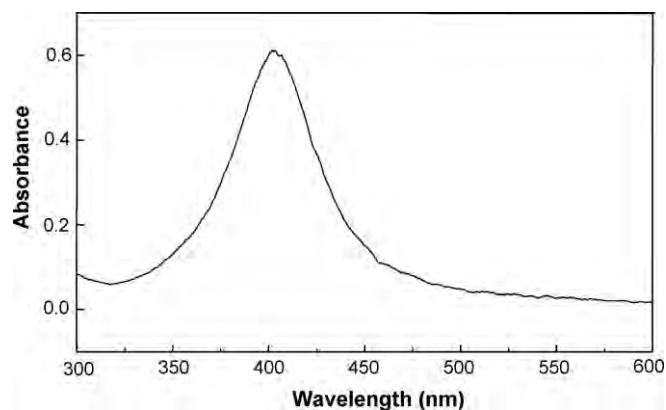


Fig. 1. The plasmon absorption band of diluted 100–1000 from high concentration of the synthesized AgNPs (10,000 ppm) ($\lambda_{\text{max}} = 403$ nm).

3. Results and discussion

3.1. Preparation of AgNPs

AgNPs were synthesized via the chemical reduction process of AgNO_3 using NaBH_4 as adapted from previous reports [15–17]. The plasmon extinction of the synthesized silver nanoparticles measured by a portable UV/vis spectrophotometer (Ocean Optics USB 4000 UV/Vis spectrophotometer) shown in Fig. 1 has a maxima at 403 nm with a narrow full width at half height (FWHH ~ 50 nm). This indicates that the synthesized nanoparticles have a narrow size distribution. The size and shape of the synthesized silver nanoparticles have been further observed by transmission electron microscope (JEOL JEM-2010). The TEM images indicate that AgNPs are spherical and have an average particle size of 14 nm as shown in Fig. 2.

3.2. The fabricated Ag-ISE

The Ag-ISE employed in this article was fabricated using the methodology reported previously [15]. The calix[4]arene containing benzothiazole groups, **CU1**, was used as a neutral ionophore and mixed in PVC plasticized with NPOE. Nernstian's slope can be

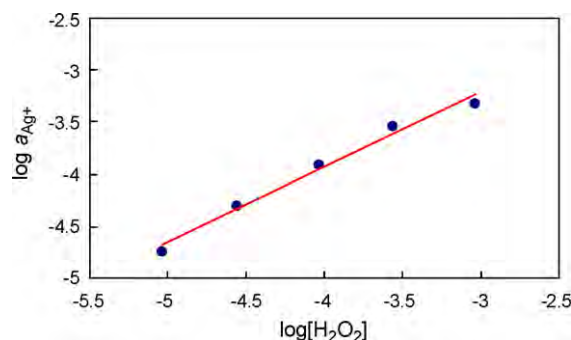


Fig. 3. The relationship between the concentration of H_2O_2 and the activity of free Ag^+ releasing from AgNPs.

observed with the detection limit in micro-molar range and with 4 orders of magnitude working linear range from the non-optimized inner filling solution (10^{-2} M AgNO_3). However, in optimized inner filling solution using the procedure described by Pretsch and co-workers [23], the Ag-ISE fabricated from the synthesized **CU1** exhibits the lower detection limit around 10^{-8} M. The response time of the fabricated Ag-ISE is very fast and the measured potentials are very stable. Principally, a Ag-ISE responds to Ag^+ exclusively; this, therefore, allows us to use the Ag-ISE in the speciation analysis of AgNPs. Both residual Ag^+ and the total Ag content in AgNPs (after oxidizing with H_2O_2) can be determined with good accuracy and precision.

3.3. Relationship between the concentration of H_2O_2 and the releasing of Ag^+ from AgNPs

The relationship between the concentration of H_2O_2 and the concentration of the free Ag^+ generated from AgNPs is investigated by using the different concentration of the mixture of H_2O_2 and AgNPs solution. The concentrations of Ag^+ in each H_2O_2 concentration are determined by direct potentiometry using our fabricated Ag-ISE. According to our previous report [15], AgNPs always contain residual free Ag^+ in the solution. Therefore, the free Ag^+ from AgNPs is first measured and then it is subtracted from the concentration of the mixture. The response EMF is then converted to activity of Ag^+ . It is found that the logarithmic of the concentration

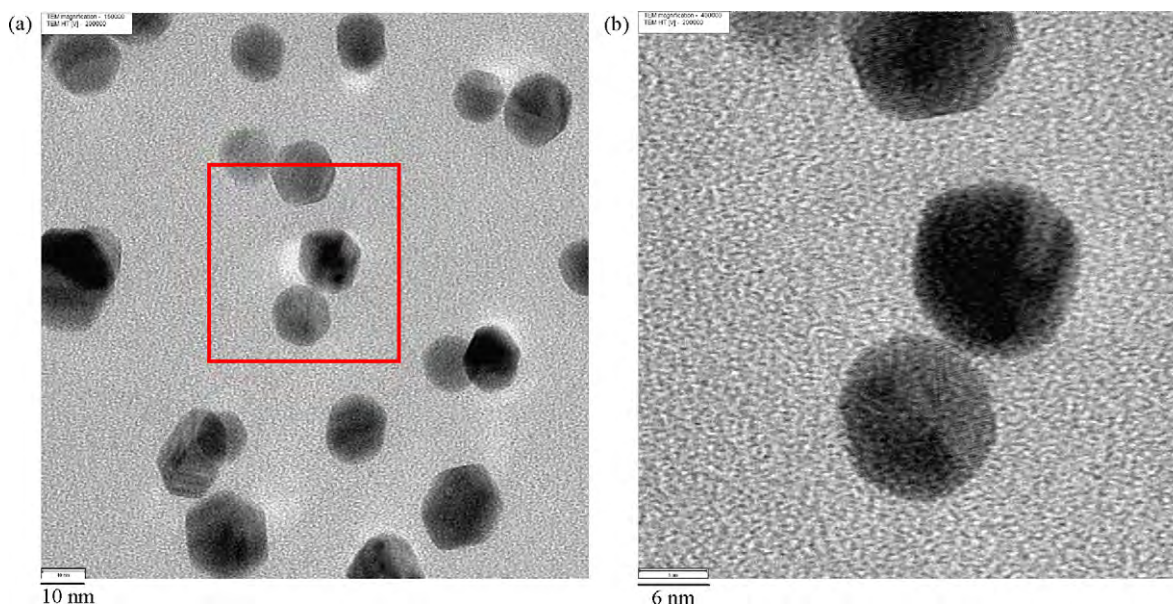


Fig. 2. TEM images of the synthesized AgNPs (a) TEM magnification, 150,000. (b) TEM magnification, 400,000.

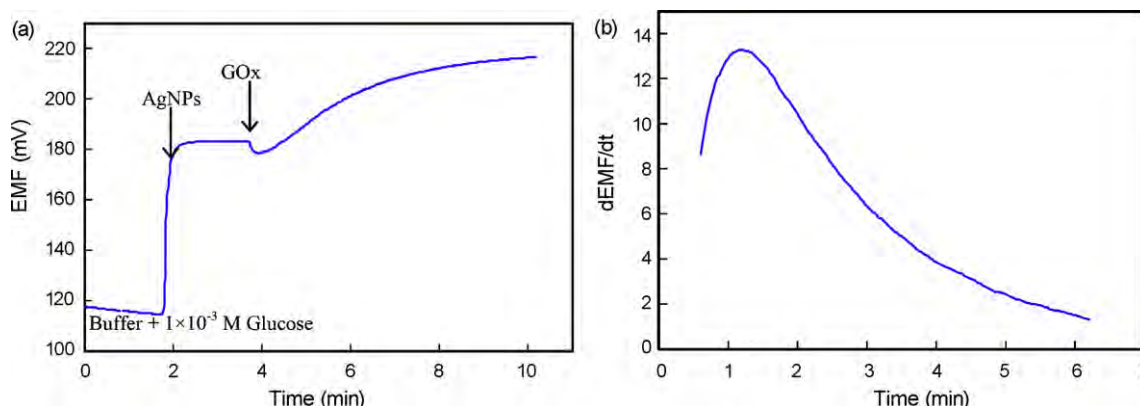


Fig. 4. (a) Continuous time trace line of the EMF change with time. (b) Change of the reaction rate with time after adding GOx.

of H_2O_2 and activity of Ag^+ possesses a linear relationship as illustrated in Fig. 3. This experiment signifies that the change of H_2O_2 concentration corresponds very well to the generation of Ag^+ from oxidized AgNPs. Therefore, free Ag^+ released from AgNPs can be used to determine glucose concentration.

3.4. Measurement of Ag^+ releasing from oxidized AgNPs in reactions of glucose and GOx

Fig. 4a illustrates the resulting EMF versus time of the general experimental procedure. The Ag-ISE is first immersed in the buffer solution of glucose. After the addition of AgNPs, the EMF increases due to the present of residual Ag^+ in AgNPs. GOx is added after the potential stabilizes. The addition of GOx dilutes the sample solution, which causes the sudden drop in EMF. As time proceeds, the GOx converts glucose to gluconic acid and H_2O_2 . The generated H_2O_2 oxidizes AgNPs to free Ag^+ resulting in the gradual increase of the EMF. The increasing EMF is continuously monitored and recorded with respect to an interval sampling time. The derivative of EMF with respect to time is considered as the reaction rate of the enzyme–substrate reaction as presented in Fig. 4b. This value corresponds very well to the glucose concentration, and the maximum rate is used here as a monitoring signal. This approach is quite remarkable because the absolute EMF is not required; only the differences in EMF are needed. Therefore, the accuracy of the reference electrode is rather unimportant.

3.5. Effect of the solution pH

Our Ag-ISE fabricated from **CU1** works well at wide pH range (pH 2–8) without significant EMF change [15]. This characteristic provides many advantages because it does not require a crucial pH adjustment. However, enzyme activity is always affected by several parameters. Solution pH is one of the important factors to the enzyme activity. Therefore, pH of the working assay must be adjusted to a suitable value. To avoid precipitation of Ag^+ , 10 mM magnesium acetate is chosen as a working buffer. The solution pH is varied in the range of 4.5–7 by adjusting with acetic acid as shown in Fig. 5. It is found that at the pH range 6–7, there is a slight change in the reaction rate. Therefore, pH 6 is chosen as a working pH.

3.6. Effect of glucose oxidase (GOx) concentration

The effect of enzyme concentration is studied by fixing glucose concentration at 1.0 mM. The concentration of GOx is varied from 0.38 to 15.4 $U\ mL^{-1}$. The results in Fig. 6 show that where the concentration of the enzyme is less than 7.6 $U\ mL^{-1}$, the reaction rate is depended on the enzyme concentration. This phenomenon always

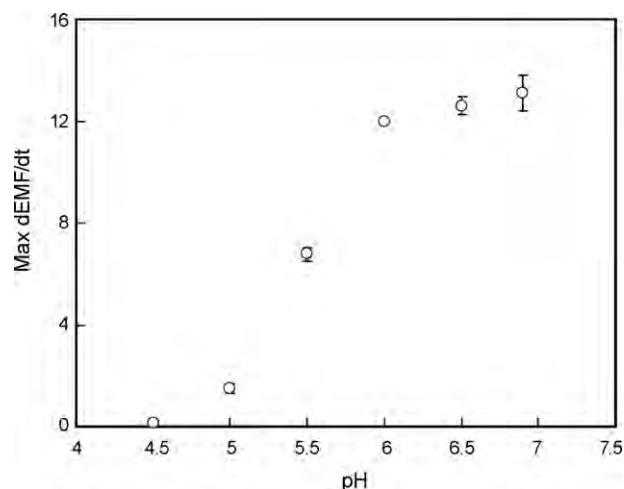


Fig. 5. Effect of the solution pH to the maximum reaction rate.

occurs when the concentration of the enzyme is lower than the substrate. In addition, when the concentration of enzyme is increased from 7.6 to 11.5 $U\ mL^{-1}$ the reaction rate shows insignificant difference. This signifies that the reaction rate depends on the substrate concentration. However, when the concentration of GOx is higher than 7.6 $U\ mL^{-1}$, the precision of the reaction rate is aggravated. Therefore, 7.6 $U\ mL^{-1}$ is chosen as the working enzyme concentration for the given concentration range (mM range).

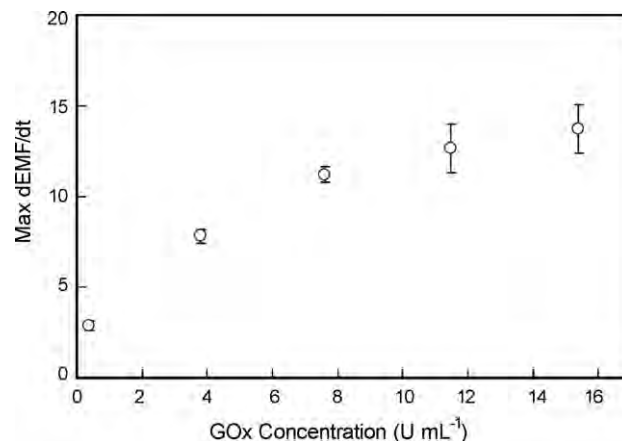


Fig. 6. Effect of the GOx concentration to the maximum reaction rate of 1 mM glucose at pH 6 in 10 mM magnesium acetate buffer.

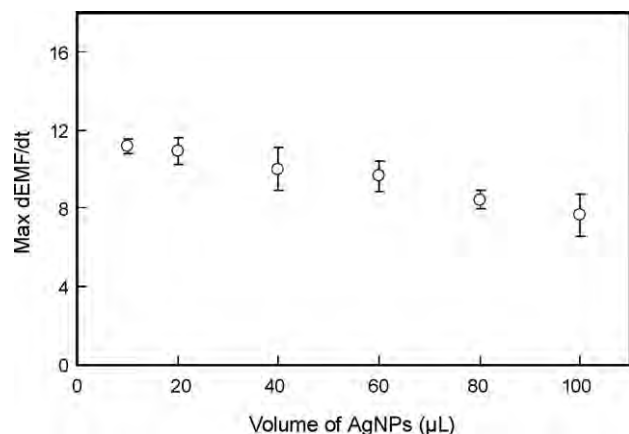


Fig. 7. Effect of the volume of AgNPs solution used in the assay.

3.7. Effect of the quantity of AgNPs

Volumes of AgNPs used in the assay can affect the reaction rate. If the increasing amount of AgNPs causes of the increasing of the reaction rate, it implies that AgNPs involves in a rate-determining step. The relation between the amount of AgNPs and the reaction rate is illustrated in Fig. 7. The results show that the reaction between AgNPs and H_2O_2 is faster than the reaction between the enzyme and the substrate. Therefore, AgNPs do not involve in the rate-determining step. However, when the amount of AgNPs is increased, the reaction rates seem to decrease slightly. Higher volume of AgNPs added results in higher concentration of free Ag^+ that can inhibit enzyme activity. However, residual Ag^+ in 10–20 μL of AgNPs shows no significant inhibition to the enzyme. Therefore, 20 μL of 1000 ppm AgNPs were used in further experiments.

3.8. Glucose calibration curve

All optimized parameters mentioned previously are applied in order to make a glucose calibration curve. Glucose concentrations are varied from 3×10^{-5} to 3×10^{-2} M and the reaction rate is monitored at different concentration change. Fig. 8a shows that the rate of the EMF change (reaction rate) depends on the glucose concentration. The glucose calibration curve is illustrated in Fig. 8b. When the concentration of glucose changes, the reaction rate also changes significantly; a linear correlation between the reaction rate and logarithmic concentration of glucose is obtained (maximum $[dEMF/dt] = 8.62 \times \log[\text{glucose}] + 38.19$). The working linear range is found to be 1×10^{-4} to 3×10^{-3} M and can cover the glucose

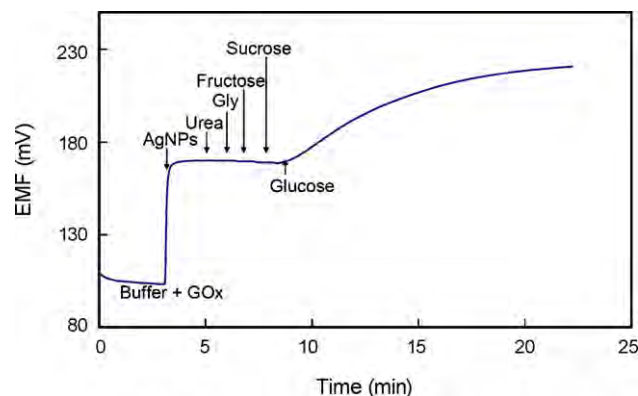


Fig. 9. The time trace line of the EMF change with time after adding interferences.

concentration in many detecting environments especially in diabetic serum. In addition, the lower detection limit of this sensor, obtained from the lowest glucose concentration that can give the EMF change after reacting with GOx, is 1.0×10^{-5} M.

3.9. Study of interferences

The selectivity of a glucose biosensor depends on two major factors: the enzyme–substrate reaction and selective measurements. The enzyme–substrate reaction is very specific due to the nature of enzyme functionality. Glucose oxidase can only react with β -D-glucose without interfering from other types of sugars. Possible interferences in glucose determination such as urea (a protein metabolite), glycine, fructose and sucrose are tested in our measuring system. The results are shown in Fig. 9. The EMF does not significantly change upon addition of interferences. Therefore, the tested chemicals cannot meddle the measuring system. Furthermore after glucose is added, the EMF increases with the same behavior when compared to the system with no interferences.

However, our new method may have some drawback in the presence of possible interferences such as a reducing agent, for example ascorbic acid that can convert Ag^+ to Ag^0 . Moreover, chelating agents that possibly present in the real sample can also reduce the activity of free Ag^+ .

3.10. Repeatability, sensor-to-sensor reproducibility and analysis of real samples

Our approach deals with the enzyme–substrate reaction of GOx and glucose which the rate of reaction depends on oxygen. Therefore, the fluctuation of oxygen in the sample will definitely affect

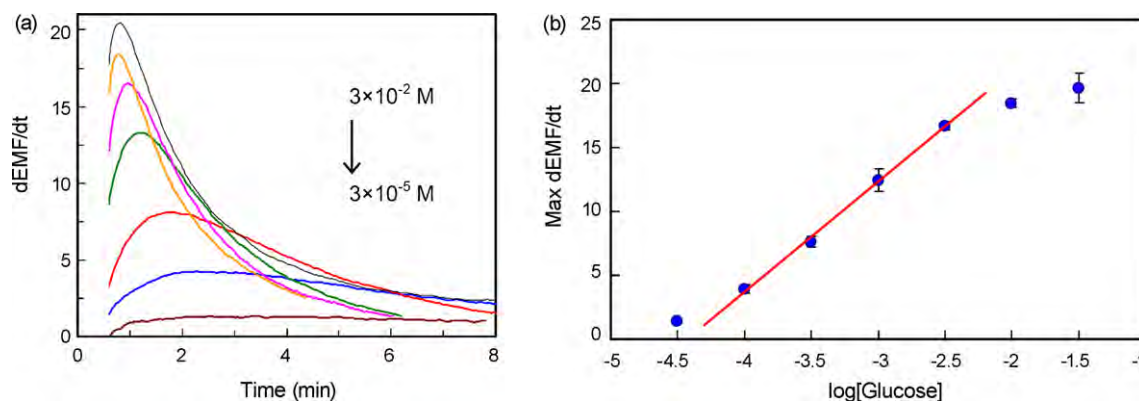


Fig. 8. (a) The derivative of the EMF change with time at different glucose concentration. (b) Calibration curve of the glucose, plotting the maximum reaction rate against logarithmic of glucose concentration.

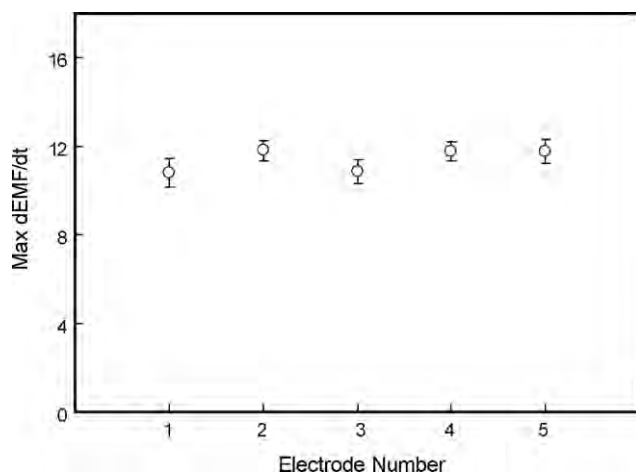


Fig. 10. The sensor-to-sensor reproducibility of 5 Ag-ISEs (1 mM of glucose).

Table 1

Analysis of glucose concentration in beverages.

Sample no.	Glucose added (μmol)	Glucose found (μmol^a)	Recovery (%)	R.S.D. (%)
1	0	1.05 ± 0.09	–	–
	3	4.01 ± 0.19	98	6
2	0	1.56 ± 0.17	–	–
	3	4.46 ± 0.26	97	9
3	0	2.99 ± 0.14	–	–
	10	12.5 ± 0.80	96	8

^a in 10 mL solution.

the reproducibility of the method. The repeatability of our proposed method can be evaluated by measuring the reaction rate of 1 mM glucose repeatedly with the same electrode. Reaction rates of each measuring experiments have showed that the Ag-ISE can be used several times with the relative standard deviation (R.S.D.) less than 7%. Moreover, we also evaluate sensor-to-sensor reproducibility by measuring three replicates of 1 mM glucose by using five different electrodes. The results in Fig. 10 show that the maximum of reaction rates obtained from different electrodes are not significantly different. Therefore, the proposed method in detecting glucose is reliable.

Glucose concentration in beverages is then measured by the proposed method, and results are shown in Table 1. The recovery of the spike samples is higher than 96% with good precision (R.S.D. < 10%). Our concept thus gives good analytical characteristics of glucose detection and can be used for development of future glucose biosensors.

4. Concluding remarks

We have demonstrated the use of silver nanoparticles as metal marker in our Ag-ISE glucose biosensor. The fabricated Ag-ISE remarkably combines two specificities in glucose detection: the enzyme–substrate reaction of GOx and glucose and the selective detection of Ag^+ . The optimum solution pH was 6.0 in 10 mM magnesium acetate buffer. The suitable enzyme concentration used was 7.6 U mL^{-1} and the appropriate volume of Ag nanoparticle redox marker was $20 \mu\text{L}$. The lower detection limit was $1.0 \times 10^{-5} \text{ M}$. The proposed method can be used for determination of glucose concentration range of 0.1–3 mM with good selectivity, accuracy, repeatability and reproducibility. We optimistically think that this method can be further applied for other oxidase enzyme system.

Acknowledgments

This research was financially supported by the Thailand Research Fund (RTA5080006 and IUG5080025). W.J. is a

Ph.D. student supported by Commission on Higher Education.

References

- [1] J. Wang, Electrochemical glucose biosensors, *Chem. Rev.* 108 (2008) 814.
- [2] J. Wang, M. Musameh, Carbon nanotube screen-printed electrochemical sensors, *Analyst* 129 (2004) 1.
- [3] S. Hrapovic, Y.L. Liu, K.B. Male, J.H.T. Luong, Electrochemical biosensing platforms using platinum nanoparticles and carbon nanotubes, *Anal. Chem.* 76 (2004) 1083.
- [4] Y. Xiao, F. Patolsky, E. Katz, J.F. Hainfeld, I. Willner, "Plugging into enzymes": nanowiring of redox enzymes by a gold nanoparticle, *Science* 299 (2003) 1877.
- [5] F. Patolsky, Y. Weizmann, I. Willner, Long-range electrical contacting of redox enzymes by SWCNT connectors, *Angew. Chem. Int. Ed.* 43 (2004) 2113.
- [6] R. Polsky, R. Gill, L. Kaganovsky, I. Willner, Nucleic acid-functionalized Pt nanoparticles: catalytic labels for the amplified electrochemical detection of biomolecules, *Anal. Chem.* 78 (2006) 2268.
- [7] J.Q. Liu, A. Chou, W. Rahmat, M.N. Paddon-Row, J.J. Gooding, Achieving direct electrical connection to glucose oxidase using aligned single walled carbon nanotube arrays, *Electroanalysis* 17 (2004) 38.
- [8] Y. Huang, W. Zhang, H. Xiao, G. Li, An electrochemical investigation of glucose oxidase at a CdS nanoparticles modified electrode, *Biosens. Bioelectron.* 21 (2005) 817.
- [9] Ł. Górski, D. Klimaszewska, M. Pietrzak, E. Malinowska, Enzymatic detection of glucose using fluoride-selective electrodes with polymeric membranes, *Anal. Bioanal. Chem.* 289 (2007) 533.
- [10] H.S.M. Abd-Rabboh, M.E. Meyerhoff, Determination of glucose using a coupled-enzymatic reaction with new fluoride selective optical sensing polymeric film coated in microtiter plate wells, *Talanta* 72 (2007) 1129.
- [11] Ş. Kalayci, G. Somer, G. Ekmekci, Preparation and application of a new glucose sensor based on iodide ion selective electrode, *Talanta* 65 (2005) 87.
- [12] G.D. Liu, Y.H. Lin, Nanomaterial labels in electrochemical immunosensors and immunoassays, *Talanta* 74 (2007) 308.
- [13] R. Koncki, Recent developments in potentiometric biosensors for biomedical analysis, *Anal. Chim. Acta* 599 (2007) 7.
- [14] J. Wang, Nanoparticle-based electrochemical bioassays of proteins, *Electroanalysis* 19 (2007) 769.
- [15] W. Ngeontae, W. Janrungsakul, N. Morakot, W. Aeungmaitrepirom, T. Tuntulani, New silver selective electrode fabricated from benzothiazole calix[4]arene: speciation analysis of silver nanoparticles, *Sens. Actuators B: Chem.* 134 (2008) 377.
- [16] D.L.V. Hyning, C.F. Zukoski, Formation mechanisms and aggregation behavior of borohydride reduced silver particles, *Langmuir* 14 (1998) 7034.
- [17] N. Shirtcliffe, U. Nickel, S. Schneider, Reproducible preparation of silver sols with small particle size using borohydride reduction: for use as nuclei for preparation of larger particles, *J. Colloid Interf. Sci.* 211 (1999) 122.
- [18] Z.Q. Zhang, R.C. Patel, R. Kothari, C.P. Johnson, S.E. Friberg, Stable silver clusters and nanoparticles prepared in polyacrylate and inverse micellar solutions, *J. Phys. Chem. B* 104 (2000) 1176.
- [19] S.S.M. Hassan, A.F. El-Baz, H.S.M. Abd-Rabboh, A novel potentiometric biosensor for selective L-cysteine determination using L-cysteine-desulfhydrase producing *Trichosporon jirovecii* yeast cells coupled with sulfide electrode, *Anal. Chim. Acta* 602 (2007) 108.
- [20] S.S.M. Hassan, G.A. Rechnitz, Determination of glutathione and glutathione reductase with a silver sulfide membrane electrode, *Anal. Chem.* 54 (1982) 1972.
- [21] S.S.M. Hassan, S.A.M. Marzouk, M.M. Abdel Fattah, G.M.S.M. Shoukry, Potentiometric determination of arylsulfatase activity using a novel nitrocathecol sulfate PVC membrane sensor, *Anal. Chem.* 67 (1995) 1887.
- [22] S.S.M. Hassan, R.M. El-Bahnasawy, N.M. Risk, Potentiometric determination of salicylhydroxamic acid (urinary struvite stone inhibitor) based on the inhibition of urease activity, *Anal. Chim. Acta* 351 (1997) 91.
- [23] A. Ceresa, A. Radu, S. Peper, E. Bakker, E. Pretsch, Rational design of potentiometric trace level ion sensors. A Ag^+ -selective electrode with a 100 ppt detection limit, *Anal. Chem.* 74 (2002) 4027.

Biographies



Wittaya Ngeontae is currently a lecturer in the Department of Chemistry, Khon Kaen University, Khon Kaen, Thailand. He earned his Ph.D. in analytical chemistry with Assistant Prof. Wanlapa Aeungmaitrepirom and Associate Prof. Thawatchai Tuntulani at Chulalongkorn University under the Development and Promotion of Science and Technology Talent project (DPST). In 2006, he was a visiting scholar with Professor Eric Bakker. His research interests include synthesis of new ionophores based on the calixarene platform. Moreover, he is interested in the applications of ISEs and optical sensors for bio-molecules and environments.



Wanwisa Janrungroatsakul received her MS degree in chemistry from Chulalongkorn University under the supervision of Associate Prof. Thawatchai Tuntulani. She is currently a Ph.D. student in chemistry supported by the Commission on Higher Education. Her research interest is concerning ISEs and their applications in sensing biomolecules.



Pattwat Maneewattanapinyo is currently a Ph.D. student in physical chemistry, Faculty of Science, Chulalongkorn University, Thailand. He got his Bachelor Degree in Chemistry in 1998 and Master Degree in Petrochemistry and Polymer Science in 2002 from Faculty of Science, Chulalongkorn University, Thailand. His research interests include synthesis of highly concentrated silver nanoparticles for industrial applications.



Sanong Ekgsat is currently an associate professor at the Department of chemistry, Faculty of Science, Chulalongkorn University, Thailand. He got his Bachelor Degree in Chemistry in 1989, Master Degree in Polymer Technology in 1992 from Chulalongkorn University, and Ph.D. in Polymer Science and Engineering in 1996 from Case Western Reserve University, USA. His research interests include molecular-spectroscopy, surface plasmon resonance spectroscopy, and synthesis and applications of metal nanoparticles for optical sensors.



Wanlapa Aeungmaitrepirom is currently an assistant professor in the Department of Chemistry at Chulalongkorn University, Thailand. She earned her Ph.D. in Analytical Chemistry at Université Louis Pasteur, France after obtaining B.Sc. and M.Sc. in Chemistry from Chulalongkorn University. Her research interests include fabrications of new ion selective electrodes and development of new extractants for environmental concerns.



Thawatchai Tuntulani is currently an associate professor in the Department of Chemistry at Chulalongkorn University, Thailand. He earned his PhD in Chemistry with Prof. Marcetta Y. Darensbourg at Texas A&M University, USA after obtaining a Bachelor Degree of Engineering from Chiang Mai University, Thailand. He did his post-doctoral studies with Prof. Jean-Marie Lehn before joining Chulalongkorn University in 1995. His research interests include syntheses of derivatives of calix[4]arene and other macrocyclic compounds and development of electrochemical and optical sensing materials for ions and biomolecules.

Synthesis and Crystal Structure Analysis of Thiourea-Pendant Pyridines

Chomchai Suksai · Chaveng Pakawatchai ·
Thawatchai Tuntulani

Received: 30 October 2007 / Accepted: 3 October 2008 / Published online: 21 October 2008
© Springer Science+Business Media, LLC 2008

Abstract The crystal structures of pyridine containing thiourea moieties as substituents, (**1**) and (**2**), have been determined. The *ortho*-substituted pyridine (**1**) crystallized in monoclinic space group $P2_1/c$ with $a = 16.091(3)$ Å, $b = 11.368(2)$ Å, $c = 7.4364(14)$ Å, $\beta = 100.489(4)^\circ$, $V = 1337.5(4)$ Å³, $z = 4$. In this structure an intramolecular N–H...N hydrogen bond forms a pseudo-seven-membered ring. The *meta*-substituted pyridine (**2**) crystallized in monoclinic space group $P2_1/c$ with $a = 14.5408(15)$ Å, $b = 8.8508(9)$ Å, $c = 10.7959(11)$ Å, $\beta = 106.435(2)^\circ$, $V = 1332.6(2)$ Å³, $z = 4$. Crystal packing revealed that compounds (**1**) and (**2**) can form dimeric structures via intermolecular H-bonding using N–H...S and N–H...N interactions, respectively.

Keywords Pseudo-seven-membered ring ·
Heterocyclic thiourea

Introduction

Thioureas are of importance in medicinal chemistry due to their biological activity [1] as anti-bacteria and antimicrobial infection [2], as fungicides, herbicides, and

rodenticides [3, 4] and in connection with biomimetic models [5]. Thiourea is well known as a good hydrogen bond donor and has been used as anion recognition sites for anion sensing using hydrogen bonding interactions [6, 7]. Furthermore, thiourea functionalities can form diverse hydrogen-bonded networks, making them a powerful building block for crystal engineering [8, 9].

In this work we present the synthesis and structural X-ray analysis of two thiourea-*pendant* pyridines. The influence of the position of the substituents on the pyridine ring regarding intra- and intermolecular hydrogen bonding interactions between molecules in crystals has been discussed.

Experimental

General

All reagents were of reagent grade and were used without further purification unless stated otherwise. ¹H-NMR, ¹³C-NMR spectra were recorded in DMSO-*d*₆ on a BRUKER AVANCE 400 NMR spectrometer. Elemental analyses for C, H and N were performed on a Perkin-Elmer 2400 CHN elemental analyzer.

Synthesis

Scheme 1

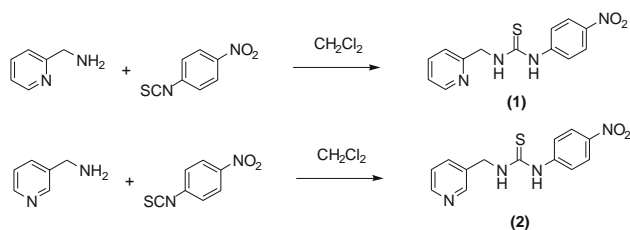
1-(4-Nitrophenyl)-2-pyridin-2-ylmethylthiourea (**1**)

To a well stirred solution of 2-picolyamine (0.16 mL, 1.64 mmole) in dry CH₂Cl₂ (10 mL) was slowly added a solution of 4-nitrophenylisothiocyanate (0.44 g, 2.46 mmole)

C. Suksai (✉)
Department of Chemistry, Faculty of Science, Burapha
University, Chonburi 20131, Thailand
e-mail: jomjai@bua.ac.th

C. Pakawatchai
Department of Chemistry, Faculty of Science, Prince of Songkla
University, Songkhla 90112, Thailand

T. Tuntulani
Department of Chemistry, Faculty of Science, Chulalongkorn
University, Bangkok 10330, Thailand



Scheme 1 Preparation of 1-(4-Nitrophenyl)-2-pyridin-2-ylmethylthiourea (1) and 1-(4-Nitrophenyl)-3-pyridin-3-ylmethylthiourea (2)

in dry CH₂Cl₂ (10 mL). The mixture was stirred for 3 days under N₂ leading to formation of a precipitate. The pale yellow product was isolated by filtration, washed with dichloromethane and dried in vacuo (0.31 g, 66%). m.p.: 159–160°C. ¹H NMR (400 MHz, DMSO-*d*₆) δ: 10.537 (s, 1H, -NH-), 8.790 (s, 1H, -NH-), 8.570 (s, 1H, ArH), 8.202 (d, *J* = 7.2 Hz, 2H, ArH), 7.940 (d, *J* = 7.6 Hz, 2H, ArH), 7.805 (m, 1H, ArH), 7.410 (m, 1H, ArH), 7.318 (m, 1H, ArH), 4.860 (s, 2H, -CH₂-). ¹³C NMR (100 MHz, DMSO-*d*₆) δ: 180.76, 157.22, 149.30, 146.83, 142.41, 137.30, 124.97, 122.89, 122.15, 120.99, 49.29. Anal. Calcd. for C₁₃H₁₂N₄O₂S C, 54.15; H, 4.20; N, 19.43. Found: C, 54.17; H, 4.18; N, 19.48.

1-(4-Nitrophenyl)-3-pyridin-3-ylmethylthiourea (2)

To a well stirred solution of 3-picolylamine (0.16 mL, 1.64 mmol) in dry CH₂Cl₂ (10 mL) was slowly added a solution of 4-nitrophenylisothiocyanate (0.44 g, 2.46 mmol) in dry CH₂Cl₂ (10 mL). The mixture was stirred for 3 days under N₂ leading to formation of a precipitate. The pale yellow product was isolated by filtration, washed with dichloromethane and dried in vacuo (0.33 g, 70%). m.p.: 184–185°C. ¹H NMR (400 MHz, DMSO-*d*₆) δ: 10.356 (s, 1H, -NH-), 8.790 (s, 1H, -NH-), 8.674 (s, 1H, ArH), 8.597 (m, 1H, ArH), 8.188, (d, *J* = 8.4 Hz, 2H, ArH), 7.859 (d, *J* = 8.4 Hz, 2H, ArH), 7.786 (d, *J* = 7.2 Hz, 1H, ArH), 7.380 (m, 1H, ArH), 3.488 (s, 2H, -CH₂-). ¹³C NMR (100 MHz, DMSO-*d*₆) δ: 181.09, 149.40, 148.67, 146.67, 142.49, 135.89, 134.46, 124.93, 123.94, 121.29, 45.22. Anal. Calcd. for C₁₃H₁₂N₄O₂S C, 54.15; H, 4.20; N, 19.43. Found: C, 54.10; H, 4.24; N, 19.45.

Crystal Structure Determination of (1) and (2)

X-ray quality crystals were obtained by slow evaporation of acetonitrile solutions of (1) and (2). Crystallographic data was collected on a BRUKER APEX CCD diffractometer (graphite-monochromated Mo-K α radiation with λ = 0.71073 Å). The structures were solved by direct methods using the program SHELXS-97 and refined by full-matrix least squares techniques against F² using the

SHELXL-97 [10] on WinGX package [11]. All non-hydrogen atoms were refined with anisotropic thermal parameters in the latter stage of refinement. All hydrogen atoms (except H14 and H15) placed in geometrically idealized positions and refined as riding atoms. Packing diagrams were produced using Mercury [12]. The detailed crystallographic data and structure refinement parameters of (1) and (2) are summarized in Table 1.

Table 1 Crystallographic data and final refinement of (1) and (2)

	(1)	(2)
CCDC Number	665445	665446
Formula	C ₁₃ H ₁₂ N ₄ O ₂ S	C ₁₃ H ₁₂ N ₄ O ₂ S
Formula weight	288.33	288.33
Temperature	293(2) K	293(2) K
Crystal system	Monoclinic	Monoclinic
Space group	<i>P</i> 2 ₁ / <i>c</i>	<i>P</i> 2 ₁ / <i>c</i>
<i>a</i> (Å)	16.091(3)	14.5408(15)
<i>b</i> (Å)	11.368(2)	8.8508(9)
<i>c</i> (Å)	7.4364(14)	10.7959(11)
β (°)	100.489(4)	106.435(2)
Color	Colourless	Colourless
Size (mm)	0.222 × 0.18 × 0.088	0.254 × 0.13 × 0.111
Volume (Å ³)	1337.5(4)	1332.6(2)
<i>Z</i>	4	4
ρ_{calc} (g cm ⁻³)	1.432	1.437
Absorption coefficient (mm ⁻¹)	0.249	0.250
<i>T</i> _{min} , <i>T</i> _{max}	0.962, 0.973	0.947, 0.978
<i>F</i> (000)	600	600
Theta range for data collection	1.29 to 28.06°	1.46 to 28.05°
Index ranges	-21 ≤ <i>h</i> ≤ 21 -14 ≤ <i>k</i> ≤ 15 -9 ≤ <i>l</i> ≤ 9	-18 ≤ <i>h</i> ≤ 19 -11 ≤ <i>k</i> ≤ 11 -14 ≤ <i>l</i> ≤ 14
Reflections collected	15,600	15,544
Independent reflections	3,212 [<i>R</i> (int) = 0.0335]	3,237 [<i>R</i> (int) = 0.0394]
Absorption correction	None	None
Data/restraints/parameters	3,212/0/189	3,237/0/189
Goodness-of-fit on <i>F</i> ²	1.095	1.129
Final <i>R</i> indices [<i>I</i> > 2σ(<i>I</i>)]	<i>R</i> 1 = 0.0481 <i>wR</i> 2 = 0.1118	<i>R</i> 1 = 0.0523 <i>wR</i> 2 = 0.1142
<i>R</i> indices (all data)	<i>R</i> 1 = 0.0618 <i>wR</i> 2 = 0.118/8	<i>R</i> 1 = 0.0689 <i>wR</i> 2 = 0.1216
Largest diff. peak and hole (e. Å ⁻³)	0.232 and -0.231	0.286 and -0.157

Results and Discussion

The reactions of 2- and 3-picolyamine with phenylisothiocyanate gave the corresponding heterocyclic thiourea derivatives **(1)** and **(2)**, respectively. Bond distances and angles of compounds **(1)** and **(2)** are given in Table 2.

Table 2 Selected bond distances (Å) and angles (°) of **(1)** and **(2)**

Bond distances

(1)

C(1)–C(2)	1.374(2)	C(8)–C(9)	1.508(3)
C(1)–C(6)	1.382(2)	C(9)–N(4)	1.339(2)
C(1)–N(1)	1.461(2)	C(9)–C(10)	1.380(3)
C(2)–C(3)	1.378(2)	C(10)–C(11)	1.381(3)
C(4)–N(2)	1.411(2)	C(11)–C(12)	1.367(3)
C(5)–C(6)	1.375(2)	C(12)–C(13)	1.371(3)
C(7)–N(3)	1.336(2)	C(13)–N(4)	1.335(2)
C(7)–N(2)	1.352(2)	N(1)–O(2)	1.215(2)
C(7)–S(1)	1.6917(17)	N(1)–O(1)	1.216(2)
C(8)–N(3)	1.463(2)		

(2)

C(1)–C(6)	1.370(3)	C(8)–N(3)	1.452(2)
C(1)–C(2)	1.379(3)	C(8)–C(9)	1.507(3)
C(1)–N(1)	1.458(3)	C(9)–C(10)	1.382(3)
C(2)–C(3)	1.372(3)	C(9)–C(13)	1.383(3)
C(3)–C(4)	1.389(3)	C(10)–C(11)	1.374(3)
C(4)–C(5)	1.396(3)	C(11)–C(12)	1.374(3)
C(4)–N(2)	1.401(2)	C(12)–N(4)	1.333(3)
C(5)–C(6)	1.374(3)	C(13)–N(4)	1.330(3)
C(7)–N(3)	1.340(2)	N(1)–O(1)	1.218(3)
C(7)–N(2)	1.360(2)	N(1)–O(2)	1.222(3)
C(7)–S(1)	1.6758(18)		

Bond angles

(1)

C(2)–C(1)–C(6)	122.22(15)	N(4)–C(9)–C(10)	121.70(18)
C(2)–C(1)–N(1)	119.42(15)	N(4)–C(9)–C(8)	115.30(16)
C(6)–C(1)–N(1)	118.36(16)	C(10)–C(9)–C(8)	122.99(17)
C(1)–C(2)–C(3)	118.50(15)	C(9)–C(10)–C(11)	118.81(19)
C(2)–C(3)–C(4)	120.32(16)	C(12)–C(11)–C(10)	119.60(19)
C(3)–C(4)–C(5)	120.22(15)	C(11)–C(12)–C(13)	118.3(2)
C(3)–C(4)–N(2)	117.67(15)	N(4)–C(13)–C(12)	123.10(19)
C(5)–C(4)–N(2)	121.95(14)	O(2)–N(1)–O(1)	123.01(18)
C(6)–C(5)–C(4)	119.75(15)	O(2)–N(1)–C(1)	118.26(17)
C(5)–C(6)–C(1)	118.98(16)	O(1)–N(1)–C(1)	118.73(18)
N(3)–C(7)–N(2)	115.50(15)	C(7)–N(2)–C(4)	127.21(15)
N(3)–C(7)–S(1)	120.54(12)	C(7)–N(3)–C(8)	127.16(15)
N(2)–C(7)–S(1)	123.89(13)	C(13)–N(4)–C(9)	118.44(16)
N(3)–C(8)–C(9)	115.27(16)		

(2)

C(6)–C(1)–C(2)	121.38(19)	C(10)–C(9)–C(13)	116.44(18)
C(6)–C(1)–N(1)	119.4(2)	C(10)–C(9)–C(8)	123.17(17)

Table 2 continued

C(2)–C(1)–N(1)	119.2(2)	C(13)–C(9)–C(8)	120.39(17)
C(3)–C(2)–C(1)	118.8(2)	C(11)–C(10)–C(9)	119.89(18)
C(2)–C(3)–C(4)	120.91(19)	C(12)–C(11)–C(10)	118.97(19)
C(3)–C(4)–C(5)	119.19(18)	N(4)–C(12)–C(11)	122.8(2)
C(3)–C(4)–N(2)	117.21(17)	N(4)–C(13)–C(9)	124.79(19)
C(5)–C(4)–N(2)	123.48(18)	O(1)–N(1)–O(2)	123.1(2)
C(6)–C(5)–C(4)	119.68(19)	O(1)–N(1)–C(1)	118.2(2)
C(1)–C(6)–C(5)	120.03(19)	O(2)–N(1)–C(1)	118.7(2)
N(3)–C(7)–N(2)	112.55(16)	C(7)–N(2)–C(4)	129.43(16)
N(3)–C(7)–S(1)	122.46(14)	C(7)–N(3)–C(8)	125.52(16)
N(2)–C(7)–S(1)	124.93(14)	C(13)–N(4)–C(12)	117.13(18)
N(3)–C(8)–C(9)	112.67(16)		

Table 3 Hydrogen bonds distances (Å) and angles (°) for **(1)** and **(2)**

D–H...A	D–H	H...A	D...A	D–H...A
(1)				
N(2)–H(14)...N(4)	0.85(2)	1.98(2)	2.793(2)	162.2(19)
N(3)–H(15)...S(1) ⁱ	0.80(2)	2.58(2)	3.3459(17)	160.3(19)
(2)				
N(2)–H(14)...N(4) ⁱⁱ	0.89(2)	2.02(2)	2.902(2)	171(2)
N(3)–H(15)...N(4) ⁱⁱ	0.80(2)	2.69(2)	3.309(3)	135(2)
N(3)–H(15)...S(1) ⁱⁱⁱ	0.80(2)	2.84(2)	3.4429(17)	134(2)

Symmetry transformations used to generate equivalent atoms: (i) $-x, -y, -z$, (ii) $-x, -y + 2, -z$, (iii) $x, -y + 5/2, z - 1/2$

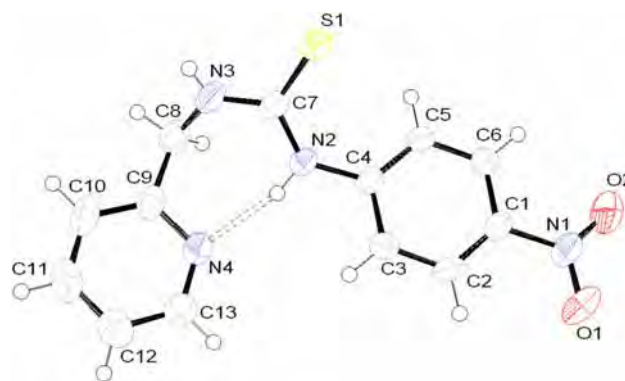


Fig. 1 Molecular structure of **(1)**. Thermal ellipsoids shown at 50% possibility

Hydrogen bond distances and angles of those two compounds are presented in Table 3. Compound **(1)** crystallized in the monoclinic space group $P2_1/c$. A molecular diagram of the H-bonded dimeric structure is shown in Fig. 2. It should be noted that the compound **(1)** possesses an intramolecular N–H...N hydrogen bond (H(14)...N(4) = 1.98(2) Å and N(2)–H(14)...N(4) = 162.2(19)°) forming a pseudo-seven-membered ring, thus locking the molecular

conformation and eliminating conformational flexibility (Fig. 1). The crystal structure of (1) also shows intermolecular interactions of the N–H⋯S bonds ($H(15) \cdots S(1)^i = 2.58(2) \text{ \AA}$ and $N(3) \cdots H(15) \cdots S(1)^i = 160.3(19)^\circ$) generating a dimeric structure along the crystallographic 'a'-axis (Fig. 2).

Compound (2) also crystallized in monoclinic space group $P2_1/c$, Fig. 3. However, there is no intramolecular hydrogen bonding in the structure. The structure of (2) had a different intermolecular hydrogen bonding pattern when compared to (1). There are pairs of intramolecular hydrogen bond between the nitrogen pyridine and NH thioureas ($H(14) \cdots N(4)^{ii} = 2.02(2) \text{ \AA}$ and $N(2) \cdots H(14) \cdots N(4)^{ii} = 171(2)^\circ$ and $H(15) \cdots N(4)^{ii} = 2.69 \text{ \AA}$ and $N(3) \cdots H(15) \cdots N(4)^{ii} = 135(2)^\circ$), Fig. 4.

The packing is not only stabilized by hydrogen bonding, but also by π – π packing interactions in the distance of 3.683 \AA (Phenyl⋯Phenyl) and 3.718 \AA (Pyridine⋯Pyridine) responsible for the crystal packing of (1). It should be mentioned that the relatively long N⋯S distances encountered for both compounds are facilitated by resonance lengthening of C=S [13] and are similar to those of previously determined thiourea dimers [14–16]. Moreover, the torsion angles of N2–C7–N3–C8 are $-11.8(3)^\circ$ and

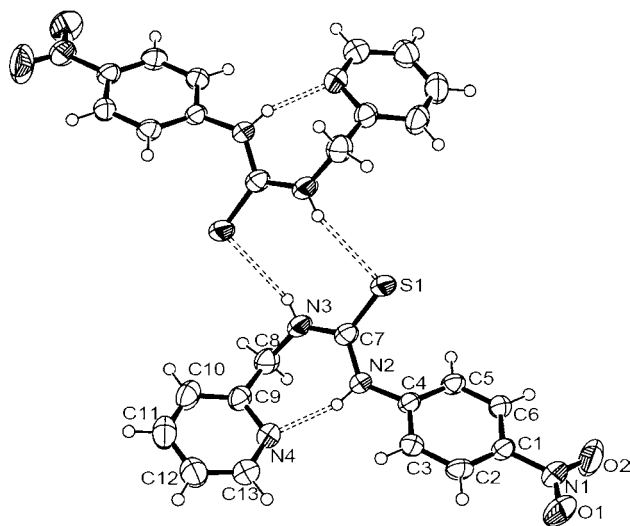


Fig. 2 The N–H⋯S intramolecular hydrogen bonding in the dimeric structure of (1)

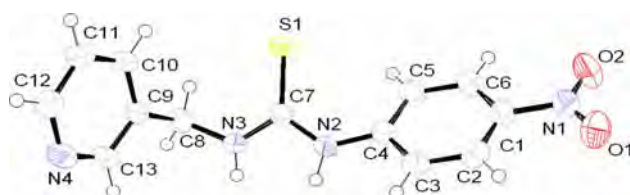


Fig. 3 Molecular structure of (2). Thermal ellipsoids shown at 50% possibility

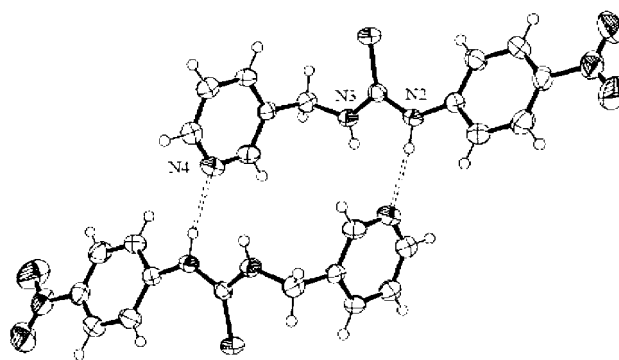


Fig. 4 The N–H⋯N intramolecular hydrogen bonding in the dimeric structure of (2)

$175.51(18)^\circ$ for (1) and (2), respectively. This is due to the formation of a pseudo-seven-membered ring in compound (1).

From the structural features described above it is clear that the intramolecular hydrogen bonding has been found in the *ortho*-pyridine substituted thiourea derivatives. In addition, the supramolecular aggregation in both structures are due to N–H⋯N, N–H⋯S and π ⋯ π intermolecular interactions.

Supplementary Material

Supplementary crystal data are available from the CCDC, 12 Union Road, Cambridge, CB2 1EZ, UK (fax: +44-1223-336033; e-mail: deposit@ccdc.cam.ac.uk or [www: http://www.ccdc.cam.ac.uk](http://www.ccdc.cam.ac.uk)) on request, quoting the deposition numbers: CCDC 665445 and 665446 for compounds (1) and (2), respectively.

Acknowledgements Financial support from the Thailand Research Fund (MRG5080149 and RTA5080006) and the Center of Excellence for Innovation in Chemistry (PERCH-CIC), Commission on Higher Education, Ministry of Education are gratefully acknowledged.

References

- Walpole C, Ko SY, Brown M, Beattie D, Campbell E, Dickerson F, Ewan S, Hughes GA, Lemaire M, Lerpiniere J, Partel S, Urban L (1998) *J Med Chem* 41:3159. doi:10.1021/jm970499g
- Mallams AK, Moron JB, Reichert P (1981) *J Chem Soc, Perkin Trans 1*:2186. doi:10.1039/p19810002186
- Schroeder DC (1955) *Chem Rev* 55:181. doi:10.1021/cr50001a005
- Sarkis GY, Faisal ED (1985) *J Heterocycl Chem* 22:137
- Tobe Y, Sasaki S, Hirose K, Naemura K (1997) *Tetrahedron Lett* 38:4791. doi:10.1016/S0040-4039(97)01034-4
- Nie L, Li Z, Han J, Zhang X, Yang R, Liu W-X, Wu F-Y, Xie J-W, Zhao Y-F, Jiang Y-B (2004) *J Org Chem* 69:6449. doi:10.1021/jo049088f
- Pfeffer FM, Gunnlaugsson T, Jensen P, Kruger PE (2005) *Org Lett* 7:5357. doi:10.1021/ol051497q

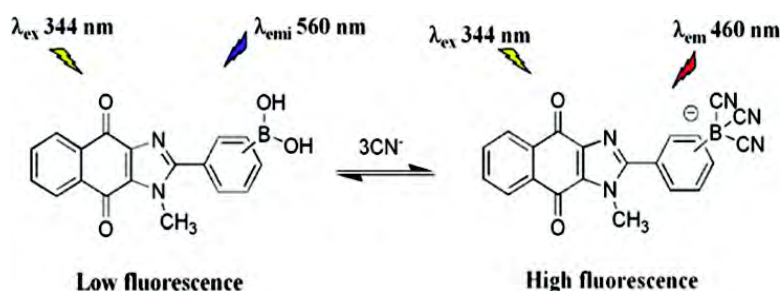
8. McBride MT, Luo T-JM, Palmore GTR (2001) *Cryst Growth Des* 1:39. doi:[10.1021/cg0000060](https://doi.org/10.1021/cg0000060)
9. Succaw GL, Weakley TJR, Han F, Doxsee KM (2005) *Cryst Growth Des* 5:2288. doi:[10.1021/cg050162c](https://doi.org/10.1021/cg050162c)
10. Sheldrick GM (1997) *Shelxl97*, Program for crystal structure determination. University of Göttingen, Germany
11. Farrugia LJ (1999) *J Appl Cryst* 32:837. doi:[10.1107/S0021889899006020](https://doi.org/10.1107/S0021889899006020)
12. Mercury 1.4.2 (2007) Cambridge Crystallographic Data Centre. Cambridge, UK
13. Allen FH, Bird CM, Rowland RS, Raithby PR (1997) *Acta Crystallogr B* 53:680. doi:[10.1107/S0108768197002656](https://doi.org/10.1107/S0108768197002656)
14. Valdes-Martines J, Hernandez-Ortega S, West DX, Ackerman LJ, Swearingen JK, Hermetet AK (1999) *J Mol Struct* 478:219. doi:[10.1016/S0022-2860\(98\)00746-7](https://doi.org/10.1016/S0022-2860(98)00746-7)
15. Kaminsky W, Goldberg KI, Wesr DX (2002) *J Mol Struct* 605:9. doi:[10.1016/S0022-2860\(01\)00655-X](https://doi.org/10.1016/S0022-2860(01)00655-X)
16. Venkatachalam TK, Sudbeck E, Uckun FM (2004) *J Mol Struct* 687:45. doi:[10.1016/j.molstruc.2003.08.022](https://doi.org/10.1016/j.molstruc.2003.08.022)

A-D-A Sensors Based on Naphthoimidazoledione and Boronic Acid as Turn-On Cyanide Probes in Water

Matinee Jamkratoke, Vithaya Ruangpornvisuti, Gamolwan Tumcharern, Thawatchai Tuntulani, and Boosayarat Tomapatanaget

J. Org. Chem., **2009**, 74 (10), 3919-3922 • DOI: 10.1021/jo900170r • Publication Date (Web): 16 April 2009

Downloaded from <http://pubs.acs.org> on May 10, 2009



More About This Article

Additional resources and features associated with this article are available within the HTML version:

- Supporting Information
- Access to high resolution figures
- Links to articles and content related to this article
- Copyright permission to reproduce figures and/or text from this article

[View the Full Text HTML](#)

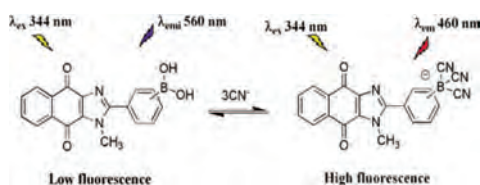
A-D-A Sensors Based on Naphthoimidazoledione and Boronic Acid as Turn-On Cyanide Probes in Water

Matinee Jamkratoke,[†] Vithaya Ruangpornvisuti,[†]
Gamolwan Tumchareon,[‡] Thawatchai Tuntulani,[†] and
Boosayarat Tomapatanaget^{†,*}

Supramolecular Chemistry Research Unit, Department of
Chemistry, Faculty of Science, Chulalongkorn University,
Bangkok 10330, Thailand, and National Nanotechnology
Center, National Science and Technology Development
Agency, Patumthanee 12120, Thailand

tboosayarat@gmail.com

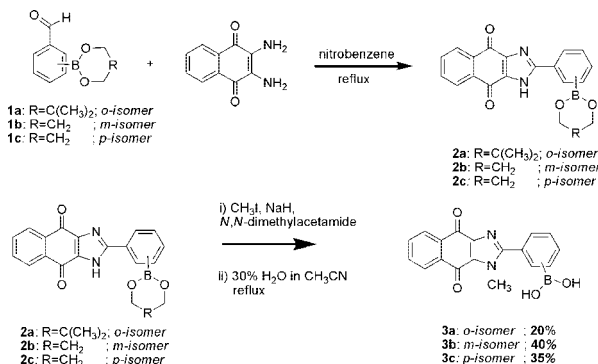
Received January 26, 2009



Three fluorescence sensors based on naphthoquinoneimidazole and boronic acid (A-D-A system) have been developed with high selectivity for cyanide in water. The fluorescence band at 460 nm was switched on upon substitution of cyanide on sensors in the CTAB micelle.

Cyanide ion is one of the analytes of most concern in environments due to its toxicity. The toxicity of the cyanide ion is attributed to its ability to effectively bind with the active site of cytochrome *c* oxidase resulting in the disruption of the electron transport chain. Tissues that mainly depend on aerobic respiration, such as the central nervous system and the heart, are acutely affected.¹ Fluorescent detection of CN⁻ is one of the best tools because of its excellent sensitivity. Several organic and inorganic compounds such as boronic acid,² cationic boran,³

SCHEME 1. Synthesis Pathway of 3a, 3b, and 3c



oxazine,⁴ squarine,⁵ dipyrrole carboxamide,⁶ acridinium salt,⁷ acyltriazenes,⁸ and coumarin⁹ derivatives were used as sensors for detecting cyanide employing the nucleophilic substitution reaction.

From a variety of signal transductions, many researchers are interested in taking the profit of the internal charge transfer (ICT) process, which is well-known to be extremely sensitive to small perturbations.¹⁰ Usually, common ICT organic dyes consist of electron acceptor and electron donor sites.¹¹ To be a chemosensor, the interaction of a guest molecule (cation or anion) with an electron donor or an acceptor site must induce the fluorescence or absorption changes. Recently, chemists have paid attention to boronic acid based sensors for detecting the cyanide ion. Although there were many reports regarding highly sensitive chemosensors for the cyanide ion, a few sensors gave a large wavelength shift and high intensity change in their emission spectra.² It is a challenging task to design turn-on cyanide probes which can perform a fluorescence intensified signal with a large shift. Therefore, we have developed high response fluorescence probes using an acceptor–donor–acceptor (A-D-A) system. The A-D-A sensors are composed of naphthoquinone connecting to boronic acid with imidazole as a conjugative spacer. Naphthoquinone and imidazole groups are a main A-D system that is expected to have a large dipole moment change when excited

(3) Hudnall, T. W.; Gabbai, F. P. *J. Am. Chem. Soc.* **2007**, *129*, 11978–11986.

(4) (a) Tomosulo, M.; Raymo, F. M. *Org. Lett.* **2005**, *7*, 4633–4636. (b) Tomosulo, M.; Sortino, S.; White, A. J. P.; Raymo, F. M. *J. Org. Chem.* **2006**, *71*, 744–753. (c) Ren, J.; Zhu, W.; Tian, H. *Talanta* **2008**, *75*, 760–764.

(5) Ros-Lis, J. V.; Martines-Manes, R.; Soto, J. *Chem. Commun.* **2002**, 2248–2249.

(6) Chen, C.-L.; Chen, Y.-H.; Chen, C.-Y.; Sun, S.-S. *Org. Lett.* **2006**, *8*, 5053–5056.

(7) Yang, Y.-K.; Tae, J. *Org. Lett.* **2006**, *8*, 5721–5723.

(8) Chung, Y.; Lee, H.; Ahn, K. H. *J. Org. Chem.* **2006**, *71*, 9470–9474.

(9) Lee, K.-S.; Kim, H.-J.; Shin, I.; Hong, J.-I. *Org. Lett.* **2008**, *10*, 49–51.

(10) Valure, B. *Topic in Fluorescence Spectroscopy*; Lakowicz, J. R., Ed.; Plenum: New York, 1994.

(11) (a) Fery-Forgues, S.; Le Bris, M.-T.; Guette, J.-P.; Valuer, B. *J. Phys. Chem. A* **1988**, *92*, 6233–6237. (b) Fery-Forgues, S.; Le Bris, M.-T.; Mialocq, J.-C.; Pouget, J.; Rittig, W.; Valuer, B. *J. Phys. Chem. A* **1992**, *96*, 701–710. (c) Marcotte, N.; Plaza, P.; Lavabre, D.; Fery-Forgues, S.; Martin, M. M. *J. Phys. Chem. A* **2003**, *107*, 2394–2402.

[†] Chulalongkorn University.

[‡] National Science and Technology Development Agency.

(1) (a) Hathaway, G. J.; Proctor, N. H. *Chemical Hazards of the Workplace*, 5th ed.; John Wiley & Sons, Inc: Hoboken, NJ, 2004; pp 190–191. (b) Patnaik, P. *A Comprehensive Guide to the Hazardous Properties of Chemical Substances*; van Nostrand Reinhold: New York, 1992; pp 229–244. (c) Ishii, A.; Seno, H.; Watanabe-Suzuki, K.; Suzuki, O.; Kumazawa, T. *Anal. Chem.* **1998**, *70*, 4873–4876.

(2) (a) Badugu, R.; Lakowicz, J. R.; Geddes, C. D. *Curr. Anal. Chem.* **2005**, *1*, 157–170. (b) Badugu, R.; Lakowicz, J. R.; Geddes, C. D. *Dyes Pigments* **2005**, *64*, 49–55. (c) Badugu, R.; Lakowicz, J. R.; Geddes, C. D. *Anal. Biochem.* **2004**, *327*, 82–90. (d) Badugu, R.; Lakowicz, J. R.; Geddes, C. D. *J. Am. Chem. Soc.* **2005**, *127*, 3635–3641. (e) Badugu, R.; Lakowicz, J. R.; Geddes, C. D. *Anal. Chem. Acta* **2004**, *522*, 9–17.

by light.^{11,12} These sensors utilize an alternation of electron deficiency to electron rich of the boron center to give a distinct change in their spectra. This process is stimulated by cyanide substitution on the boron atom.

The synthetic pathway of new fluorescent sensors **3a**, **3b**, and **3c** is shown in Scheme 1. The oxidative condensation¹³ of 2,3-diamino-1,4-naphthoquinone¹⁴ and the protected corresponding formylphenylboronate in nitrobenzene yielded the precipitate of heterocyclic compounds **2a**, **2b**, or **2c** in 29%, 45%, and 71% yield, respectively. These products were indicated by the appearance of the NH proton at ca. 14.3 ppm and the new series of aromatic protons at around 8.09 and 7.84 ppm in the ¹H NMR spectra. Methylation on the N-atom of the heterocyclic ring was achieved by the reaction of the protected derivative with CH₃I in the presence of NaH in *N,N*-dimethylacetamide at room temperature. Finally, the ester protecting group was removed by refluxing in 30% H₂O:CH₃CN to give **3a**, **3b**, and **3c** as yellow solids in 20%, 40%, and 45% yields, respectively.

In the mixture of DMSO:H₂O (50 μ M of receptor in 0.1 mol/L of NaCl in 50% HEPES pH 7.4:DMSO), sensors **3a**, **3b**, and **3c** gave yellow solutions with absorption maxima at 338 and 387 nm. Moreover, all sensors showed the characteristic luminescence with different emission maxima at 562, 565, and 572 nm for ortho, meta, and para isomers, respectively. Figure 1a shows fluorescence spectra of compound **3b** with and without 500 equiv of anions. A high-intensity fluorescence band at 460 nm was observed upon addition of cyanide into solutions of sensor **3b**. The high response was also observed in sensor **3c**, whereas the ortho isomer, **3a**, showed a slight response in the presence of CN[−] (Figure 1b). Furthermore, upon exposure to UV irradiation at 365 nm, the solution of **3b** + CN[−] gave a brighter luminescence than that of **3b** + F[−] as shown in Figure 2.

In the presence of a very high concentration of cyanide ion (500 equiv), pH 7.4 HEPES solution was changed to pH 11. It is possible that at high pH, OH[−] could be generated and substituted on the boron center to form RB(OH)₃[−]. This weak point was averted by incorporating compounds **3b** and **3c** to a CTAB micellar system to allow the detection of CN[−] at very low concentration (50 μ M). In this system, the pH of the solution remained pH 7.0 and the emission band at 460 nm appeared intensely upon the addition of 50 μ M CN[−] as shown in Figure 3 as well as Figure S9 in the Supporting Information.

Moreover, the probe **3b** in the CTAB micellar system exhibited promising selective binding with cyanide ion similar to that in 50% HEPES pH 7.4:DMSO. This suggested that the boron center was substituted with the cyanide anion. The hybridization of the boron center changed from the electron deficiency sp² boron, R-B(OH)₂, to the electron rich sp³ boron, R-B(CN)₃,^{15,16} resulting in the emission band at 460 nm.

Fluorescence responses of sensors **3b** and **3c** in the presence of 50 μ M of CN[−] showed a large response giving a high

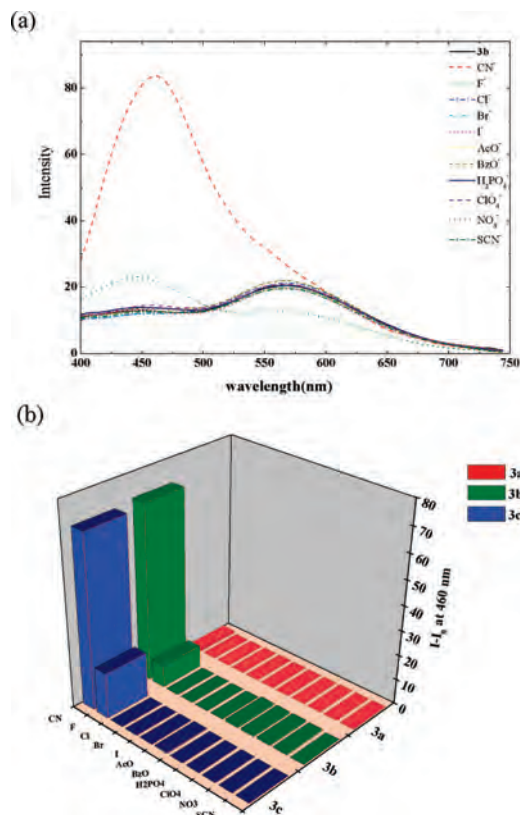


FIGURE 1. (a) Fluorescence spectral changes of **3b** after the addition of 500 equiv of various anions (potassium salts). (b) Fluorescence responses of **3a**, **3b**, and **3c** with 500 equiv of various anions (50 μ M of receptor in 0.1 mol/L of NaCl in 50% HEPES pH 7.4:DMSO).

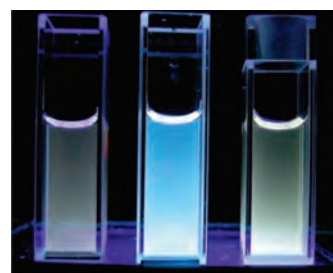


FIGURE 2. Fluorescence responses of 50% HEPES pH 7.4:DMSO solutions of **3b** (left), **3b** + CN[−] (middle), and **3b** + F[−] (right).

intensity change (18-fold enhancement) and a large stoke shift ($\Delta\lambda_{\text{ex-em}} = 120$ nm) as well as a large blue shift of ca. 100 nm. The fluorescence band at 460 nm possibly assigned to the ICT state was switched on by the cyanide ion. This ICT state was predominant with a poor acceptability on the boron center after cyanide addition. A large fluorescence response toward CN[−] recognition of these receptors occurred since the boronic center behaved as a complementary acceptor of a standard electron donor–acceptor system (D-A or A-D).¹¹ The presence of the electron donor (imidazole group) and the electron acceptor (naphthoquinone group) as a main A-D site caused a prerequisite dipole moment change resulting in a large change in spectral properties.¹¹

For better understanding of the fluorescence behaviors, structures of the sensors **3a–c** and their cyanide-substituted products have been calculated by using density function theory (DFT) at the B3LYP/6-31+G(d) level. Natural bond orbital (NBO) charges of donor–acceptor segments of sensors

(12) de Silva, A. P.; Gunaratne, H. Q. N.; Habib-Jiwan, J. L.; McCoy, C. P.; Rice, T. E.; Soumilion, J. P. *Angew. Chem., Int. Ed. Engl.* **1995**, *34*, 1728–1731.

(13) Kim, S. J.; Kool, E. T. *J. Am. Chem. Soc.* **2006**, *128*, 6164–6171.

(14) Wunkelmann, E. *Tetrahedron* **1969**, *25*, 2427–2454.

(15) (a) Lorand, J. P.; Edward, J. O. *J. Org. Chem.* **1959**, *24*, 769–774. (b) Katz, H. E. *J. Am. Chem. Soc.* **1986**, *108*, 7640–7645.

(16) (a) Cooper, C. R.; Spencer, N.; James, T. D. *Chem. Commun.* **1998**, 1365–1366. (b) DiCesare, N.; Lakowicz, J. R. *Anal. Biochem.* **2002**, *301*, 111–116. (c) Kubo, Y.; Kobayashi, A.; Ishida, T.; Misawa, Y.; James, T. D. *Chem. Commun.* **1998**, 1365–1366. (d) Badugu, R.; Lakowicz, J. R.; Geddes, C. D. *Sens. Actuators.* **2005**, *104*, 103–110.

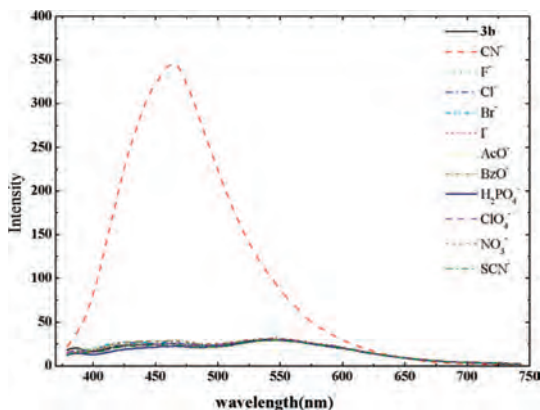
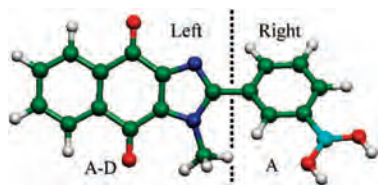


FIGURE 3. Fluorescence spectra of **3b** (50 μM) with 50 μM of various anions in the CTAB micellar system (5 mM of CTAB in 10% ethanol: water).

TABLE 1. NBO Charges of Segments of **3a**, **3b**, and **3c** and of **3a(CN)₃[−]**, **3b(CN)₃[−]**, and **3c(CN)₃[−]** Derived from the B3LYP/6-31+G(d) Computations

			
species	charge ^a		total charge ^a
	left segment	right segment	
free hosts			
3a	−0.02685	0.02685	0.00
3b	−0.03985	0.03985	0.00
3c	−0.02358	0.02358	0.00
full CN-substituted hosts			
3a(CN)₃[−]	−0.04235	−0.95762	−1.00
3b(CN)₃[−]	−0.08330	−0.91670	−1.00
3c(CN)₃[−]	−0.01968	−0.97892	−1.00

^a The elementary charge unit = 1.602×10^{-19} coulombs.

3a–c suggested that naphthoquinoneimidazole possessing negative charges acted as a donor site and boronic acid possessing positive charges acted as an acceptor site (Table 1). Upon the addition of CN^- , the right segment charge became negative corresponding to the reduction in acceptability of boronic acid and subsequent appearance of a fluorescence band at 460 nm.

Considering the sensitivity of each isomer, calculated structures (Figure S10, Supporting Information) showed that the dihedral angles of the donor and acceptor planes of **3a**, **3b**, and **3c** were 56.5° , 37.5° , and 37.7° , respectively. After cyanide substitution, the dihedral angles of CN-substituted **3b** and **3c** changed slightly ($\sim 2^\circ$) while that of substituted **3a** changed significantly (nearly 12°). This probably inhibited the substitution of cyanide in the boronic center of **3a**. The calculated structures thus agreed very well with the experimental results, which showed that the emission spectra of **3a** before and after cyanide substitution were insignificantly different.

In summary, we have successfully synthesized A-D-A fluorescence sensors containing naphthoquinoneimidazole and boronic acid, **3a**, **3b**, and **3c**, as turn-on cyanide probes in the CTAB micellar system. In this approach, CTAB can incorporate

3b and **3c** to provide powerful probes for detecting a very low concentration of CN^- in water. These A-D-A probes offer considerable promises as cyanide selective fluorescence probes with a large response emission band at 460 nm and a large blue shift (ca. 100 nm).

Experimental Section

Compounds 2a, 2b, and 2c. The protected formylphenylboronate was synthesized according to literature procedure.¹⁷ To a solution of 2,3-diamino-1,4-naphthoquinone (0.940 g, 5 mmol) in nitrobenzene (75 mL) was added the protected corresponding formylphenylboronate (5 mmol) in nitrobenzene (25 mL) dropwise. The reaction mixture was heated at 150°C and stirred for 12 h under nitrogen. The solution was then cooled to room temperature and the precipitate was slowly formed. The precipitate was filtered and washed with diethyl ether to give a yellow solid of the protecting products (**2a** 29%, **2b** 45%, and **2c** 71%).

Compound 2a: ^1H NMR (400 MHz, $\text{DMSO}-d_6$) δ 14.40 (broad, 1H), 8.12 (m, 3H), 7.84 (m, 2H), 7.47 (m, 3H), 3.74 (s, 4H), 1.06 (s, 6H). Anal. Calcd for $\text{C}_{22}\text{H}_{19}\text{BN}_2\text{O}_4$: C, 68.42; H, 4.96; N, 7.25. Found: C, 67.99; H, 4.82; N, 7.55. EI-MS m/z 387.15 ($\text{M} + 2\text{H}$)⁺.

Compound 2b: ^1H NMR (400 MHz, $\text{DMSO}-d_6$) δ 14.42 (s, 1H), 8.57 (s, 1H), 8.26 (d, $J = 7.6$ Hz, 1H), 8.083 (m, 2H), 7.83 (m, 2H), 7.77 (d, $J = 7.6$ Hz, 1H), 7.50 (t, $J = 7.2$ Hz, 1H), 4.14 (t, $J = 4.8$ Hz, 4H), 2.02 (t, $J = 5.2$ Hz, 2H). Anal. Calcd for $\text{C}_{22}\text{H}_{19}\text{BN}_2\text{O}_4$: C, 67.07; H, 4.22; N, 7.82. Found: C, 66.96; H, 4.23; N, 7.88. MALDI-TOF m/z 359.64 ($\text{M} + 2\text{H}$)⁺.

Compound 2c: ^1H NMR (400 MHz, $\text{DMSO}-d_6$) δ 14.39 (s, 1H), 8.19 (d, $J = 8.5$ Hz, 2H), 8.09 (m, 2H), 7.49 (m, 2H), 7.78 (d, $J = 8.0$ Hz, 2H), 4.12 (t, $J = 4.1$ Hz, 4H), 2.01 (t, $J = 5.2$ Hz, 2H). Anal. Calcd for $\text{C}_{20}\text{H}_{15}\text{BN}_3\text{O}_4$: C, 67.07; H, 4.22; B, 3.02; N, 7.82. Found: C, 67.06; H, 4.59; N, 7.76. MALDI-TOF m/z 358.63 ($\text{M} + \text{H}$)⁺.

Compounds 3a, 3b, and 3c. Compounds **2a**, **2b**, or **2c** (5 mmol) and NaH (0.132 g, 5.5 mmol) were charged with 25 mL of *N,N*-dimethylacetamide under nitrogen. Methyl iodide (343 μL , 5.5 mmol) was added to the reaction mixture. The reaction mixture was stirred at room temperature for 2 days. The solvent was removed under vacuum to give the solid of methylated products. The protecting group was removed by refluxing in 30% H_2O : CH_3CN . The solution was filtered and washed with diethyl ether to provide a yellow solid of compound **3** (**3a** 20%, **3b** 40%, and **3c** 35%).

Compound 3a: ^1H NMR (400 MHz, $\text{DMSO}-d_6$) δ 8.11 (m, 2H), 8.01 (s, 2H), 7.87 (m, 2H), 7.77 (m, 1H), 7.54 (m, 3H), 3.84 (s, 3H). ^{13}C NMR (100.6 MHz, $\text{DMSO}-d_6$) δ 178.9, 174.4, 157.0, 142.6, 134.6, 134.5, 134.4, 133.1, 132.7, 129.8, 129.6, 126.8, 126.6, 34.3. Anal. Calcd for $\text{C}_{18}\text{H}_{23}\text{BN}_2\text{O}_4$: 65.10; H, 3.95; N, 8.43. Found: C, 65.27; H, 3.98; N, 8.48. MALDI-TOF m/z 334.66 ($\text{M} + 3\text{H}$)⁺.

Compound 3b: ^1H NMR (400 MHz, $\text{DMSO}-d_6$) δ 8.29 (s, 2H), 8.21 (s, 1H), 8.09 (t, $J = 8.1$ Hz, 2H), 7.99 (d, $J = 8.0$ Hz, 1H), 7.85 (d, $J = 7.8$ Hz, 1H), 7.56 (t, $J = 7.5$ Hz, 1H), 4.06 (s, 3H). ^{13}C NMR (100.6 MHz, $\text{DMSO}-d_6$) δ 178.9, 176.4, 154.9, 143.0, 136.5, 135.5, 134.5, 134.3, 133.8, 133.3, 132.9, 131.3, 128.3, 127.8, 126.8, 126.6, 34.8. Anal. Calcd for $\text{C}_{18}\text{H}_{23}\text{BN}_2\text{O}_4$: 65.10; H, 3.95; N, 8.43. Found: C, 65.28; H, 3.90; N, 8.48. MALDI-TOF m/z 331.60 (M)⁺.

Compound 3c: ^1H NMR (400 MHz, $\text{DMSO}-d_6$) δ 8.26 (s, 2H), 8.09 (t, $J = 8.0$ Hz, 2H), 7.98 (d, $J = 8.0$ Hz, 2H), 7.86 (t, $J = 7.8$ Hz, 2H), 7.78 (d, $J = 7.8$ Hz, 2H), 4.08 (s, 3H). ^{13}C NMR (100.6 MHz, $\text{DMSO}-d_6$) δ 178.8, 176.4, 154.5, 143.0, 134.7, 134.5, 134.3, 133.8, 133.3, 132.8, 129.9, 128.7, 126.8, 126.6, 34.8. Anal. Calcd for $\text{C}_{18}\text{H}_{23}\text{BN}_2\text{O}_4$: 65.10; H, 3.95; N, 8.43. Found: C, 65.07; H, 3.90; N, 8.56. MALDI-TOF m/z 332.39 ($\text{M} + \text{H}$)⁺.

(17) James, T. D.; Sandanayake, K. R. S.; Iguchi, R.; Shinkai, S. *J. Am. Chem. Soc.* **1995**, *117*, 8982–8987.

Fluorescence Measurement Procedure of Sensors 3a–3c with Excess Anions in 50% HEPES pH 7.4:DMSO. Receptors **3a**, **3b**, and **3c** were prepared as stock solution in spectroscopic grade DMSO at concentrations of 0.1 mM. Stock solutions of sensors (1.5 mL) and 500 equiv of anions (KCN, KF, KAcO, KBzO, KH₂PO₄, KNO₃, KClO₄, KCl, KBr, KSCN, and KI) which were dissolved in 1.5 mL of 0.2 mol/L of NaCl in HEPES buffer pH 7.4 were mixed to give a final concentration of sensors (50 μ M) with 500 equiv of anions added in 0.1 mol/L of NaCl in 50% HEPES pH 7.4:DMSO. Fluorescence spectra were recorded with the excitation wavelength of 344 nm. In the case of the addition of KF, stock solution sensors and KF were mixed to give a final concentration of sensors (50 μ M) with 500 equiv of anions added in 0.1 mol/L of NaCl in 60% HEPES pH 7.4:DMSO because of KF solubility.

Fluorescence Measurement Procedure of Sensors 3b with Excess Anion in the CTAB Micellar System. In a 5 mL volumetric flask, 1.0 mL of an ethanol solution of fluorescence probes (0.025 mM) was mixed with 2.0 mL of 12.5 mM CTAB in water. Then, 10 μ L of 2.5 mM potassium salt solution (KCN, KF,

KAcO, KBzO, KH₂PO₄, KNO₃, KClO₄, KCl, KBr, KSCN, and KI) was added to the probe. Fluorescence spectra were recorded with the excitation wavelength of 344 nm.

Acknowledgment. M.J. is a Ph.D student supported by the Royal Golden Jubilee Program (PHD/0049/2550). We thank the National Nanotechnology Center (NN-B-22-b15-94-49-55), the Thailand Research Fund (RTA5080006), and the National Center of Excellence for Petroleum, Petrochemical, and Advanced Materials (NCE-PPAM) for financial support.

Supporting Information Available: Details of the procedure for the synthesis of protected formylphenylboronate; ¹H and ¹³C NMR spectra of **3a**, **3b**, and **3c**; fluorescence spectra changes of **3a**, **3b**, and **3c** after addition of various anions (potassium salts); and other data. This material is available free of charge via the Internet at <http://pubs.acs.org>.

JO900170R

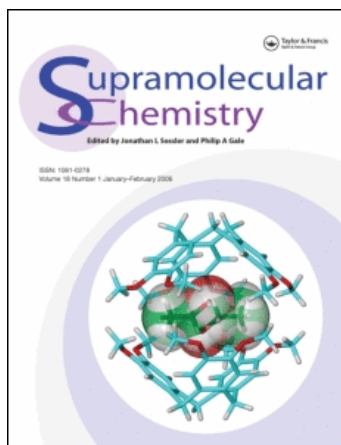
This article was downloaded by: [Tuntulani, Thawatchai]

On: 19 August 2009

Access details: Access Details: [subscription number 914044514]

Publisher Taylor & Francis

Informa Ltd Registered in England and Wales Registered Number: 1072954 Registered office: Mortimer House, 37-41 Mortimer Street, London W1T 3JH, UK



Supramolecular Chemistry

Publication details, including instructions for authors and subscription information:

<http://www.informaworld.com/smpp/title~content=t713649759>

Tryptophan receptors containing acridine-based thiourea

Anchalee Sirikulajorn ^a; Preeyanut Duanglaor ^a; Vithaya Ruangpornvisuti ^a; Boosayarat Tomapatnaget ^a; Thawatchai Tuntulani ^a

^a Supramolecular Chemistry Research Unit, Department of Chemistry, Faculty of Science, Chulalongkorn University, Bangkok, Thailand

First Published: September 2009

To cite this Article Sirikulajorn, Anchalee, Duanglaor, Preeyanut, Ruangpornvisuti, Vithaya, Tomapatnaget, Boosayarat and Tuntulani, Thawatchai (2009) 'Tryptophan receptors containing acridine-based thiourea', *Supramolecular Chemistry*, 21:6, 486 — 494

To link to this Article: DOI: 10.1080/10610270802348235

URL: <http://dx.doi.org/10.1080/10610270802348235>

PLEASE SCROLL DOWN FOR ARTICLE

Full terms and conditions of use: <http://www.informaworld.com/terms-and-conditions-of-access.pdf>

This article may be used for research, teaching and private study purposes. Any substantial or systematic reproduction, re-distribution, re-selling, loan or sub-licensing, systematic supply or distribution in any form to anyone is expressly forbidden.

The publisher does not give any warranty express or implied or make any representation that the contents will be complete or accurate or up to date. The accuracy of any instructions, formulae and drug doses should be independently verified with primary sources. The publisher shall not be liable for any loss, actions, claims, proceedings, demand or costs or damages whatsoever or howsoever caused arising directly or indirectly in connection with or arising out of the use of this material.

Tryptophan receptors containing acridine-based thiourea

Anchalee Sirikulkajorn, Preeyanut Duanglaor, Vithaya Ruangpornvisuti, Boosayarat Tomapatanaget*
and Thawatchai Tuntulani*

Supramolecular Chemistry Research Unit, Department of Chemistry, Faculty of Science, Chulalongkorn University, Bangkok, Thailand

(Received 3 April 2008; final version received 14 July 2008)

Four derivatives of acridine and acridinium compounds (**L1**, **L2**, **L1H** and **L2H**) comprised thiourea-binding sites were synthesised. The binding abilities of receptors **L1**, **L2**, **L1H** and **L2H** towards amino acids (L-Trp, L-Phe, L-Leu, L-Ala and L-Gly) were studied by ¹H NMR spectroscopy, UV-vis and fluorescence spectrophotometry. Hydrogen bonding interactions between thiourea-binding site of the ligand and the carboxylate groups in zwitterionic amino acids were found to be the main interactions driving complexation to take place. The stoichiometry of 1:1 ligand to amino acid was observed in all cases. Neutral ligands **L1** and **L2** showed weak binding towards all studied amino acids. The cyclic ligand **L1** showed better binding ability towards tryptophan (Trp) than the acyclic ligand **L2** did (*K* for Trp is 307 and 266 M⁻¹ for **L1** and **L2**, respectively). Interestingly, binding abilities of the protonated ligands, **L1H** and **L2H**, towards studied amino acids, especially Trp (*K* for Trp is 3157 and 2873 M⁻¹ for **L1H** and **L2H**, respectively), were increased due to R-COO⁻...H...N⁺-acridinium interactions. Calculated structures of **L1H**·Trp and **L2H**·Trp showed that the polyglycol moiety in **L1H** provided a hydrophobic cavity for binding Trp resulting in a stronger binding affinity of **L1H** over **L2H**.

Keywords: acridine; acridinium; amino acid receptor; fluorescence sensor

Introduction

Molecular recognition of amino acids and their derivatives has been one of the most attractive objects in host-guest chemistry (1–4). It is partly due to the importance of amino acids as major components of proteins in natural living systems and partly due to their potential characteristics that make amino acids suitable for guest molecules in artificial recognition systems. Amino acids have versatile abilities to form complexes with other molecules via various kinds of intermolecular interactions (5–7). Ammonium and carboxylate groups in amino acids are expected to bind host molecules via hydrogen bonding and electrostatic interactions. Side chain of amino acids on the α-carbon can also form complexes with receptors using electrostatic interactions, van der Waals forces, hydrophobic interactions and π–π stacking interactions.

High sensitivity and abundance of fluorophores makes fluorescence spectrophotometry an ideal tool in developing biosensors (8–11). However, fluorescence sensors for amino acids are still rare. The binding of fluorophores with an aromatic amino acid such as tryptophan (Trp) causes quenching of the emission (12, 13). Recently, many fluorescent supramolecular systems have been constructed and their abilities for amino acids recognition using non-covalent interactions have been investigated (14–17). A system of metal complexes and fluorescent indicators was used successfully in sensing amino acids (18, 19).

The changing in colour or switching on/off in fluorescence occurred from the displacement of the indicator by amino acids. Transformation of the ligand structure from a closed ring to an opened form after the binding of amino acids was also employed to obtain significant changes in fluorescence intensity (20, 21).

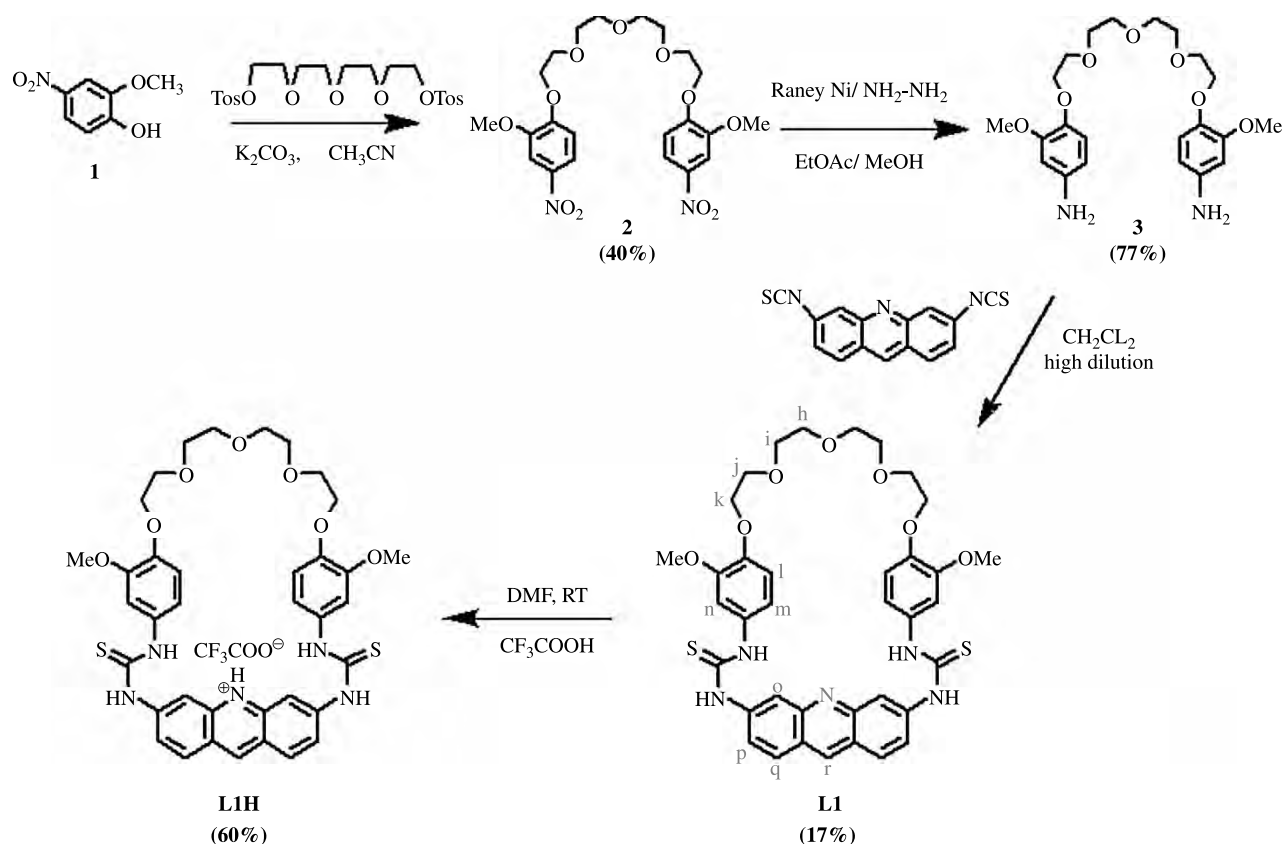
We reported herein the syntheses of thiourea-containing acridine groups that are classified into two types: cyclic (**L1** and **L1H**) and acyclic receptors (**L2** and **L2H**). **L1H** and **L2H** are the protonated forms of **L1** and **L2**, respectively. We then examine the effects of cyclic or acyclic structure on the binding ability towards amino acids (L-Trp, L-Phe, L-Leu, L-Ala and L-Gly). **L1H** and **L2H** were expected to improve the binding properties with amino acids under the complementary interactions including electrostatic force and hydrogen bonding interactions.

Results and discussion

Design and synthesis

Acridine derivatives such as acridinium salt (18), acridinone (19, 20) and acridinedione (21, 22) have been used quite successfully in sensing strong basic anions. Our design is to use acridine as a signalling unit connecting to a thiourea receptor. König (23) and de Mendoza (24)

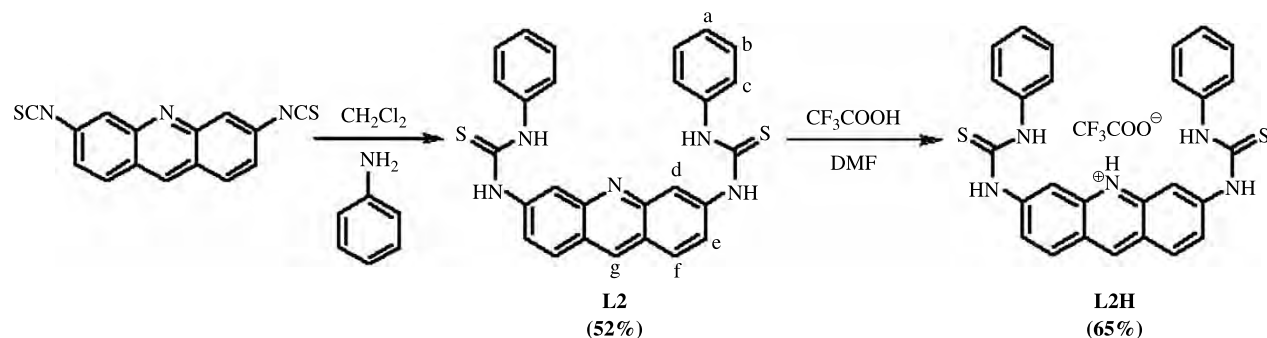
*Corresponding authors. Email: tboosayarat@gmail.com; tthawatc@chula.ac.th

Scheme 1. Syntheses of receptors **L1** and **L1H**.

reported selective amino acid receptors containing crown ether moieties. We, therefore, incorporate a polyglycol unit into our desired ligand **L1**. A controlled ligand having no crown unit, **L2**, has also been synthesised to compare with **L1**. Both **L1** and **L2** were then protonated to produce **L1H** and **L2H**, respectively.

Syntheses of all receptors are summarised in Schemes 1 and 2. The synthesis of **L1** was started by a coupling reaction of compound **1** with tetraethylene glycol ditosylate in the presence of K_2CO_3 in CH_3CN

giving the crown-like ether compound **2** in 40% yield. Diamino compound **3** was obtained in 77% yield by the reduction of compound **2** with Raney nickel and hydrazine. A coupling reaction of diamino **3** and proflavinedithioisocyanate produced the desired product (**L1**) as a red solid in 17% yield. The receptor **L2** was prepared in one step by a reaction of proflavinedithioisocyanate and aniline to yield a pale orange powder in 52%. 1H NMR spectra of **L1** and **L2** showed that the NH thiourea resonanced at downfield positions, 10.19

Scheme 2. Synthesis of receptors **L2** and **L2H**.

and 10.09 ppm for **L1** as well as 10.28 and 10.14 ppm for **L2**. The receptor **L1H** and **L2H** were obtained as a dark red powder and as a bright orange powder from reactions of **L1** and **L2**, respectively, with trifluoroacetic acid. ^1H NMR spectra of **L1H** and **L2H** showed that the NH thiourea and acridine protons appeared at farther downfield positions around 10.50–11.40 and 7.60–9.60 ppm for the aromatic region resulting from the protonation of *N*-acridine (25, 26).

Complexation studies using ^1H NMR spectroscopy and UV-vis spectrophotometry

Binding properties of **L1** and **L2** with hydrophobic aliphatic amino acids (L-Leu, L-Ala and L-Gly) and hydrophobic aromatic amino acids (L-Trp and L-Phe) were first studied using ^1H NMR spectroscopy. Addition of excess amount of the amino acids to **L1** and **L2** in $\text{DMSO}-d_6$ resulted in remarkable downfield shifts of the NH thiourea resonances, particularly Trp and Phe (Figure 1).

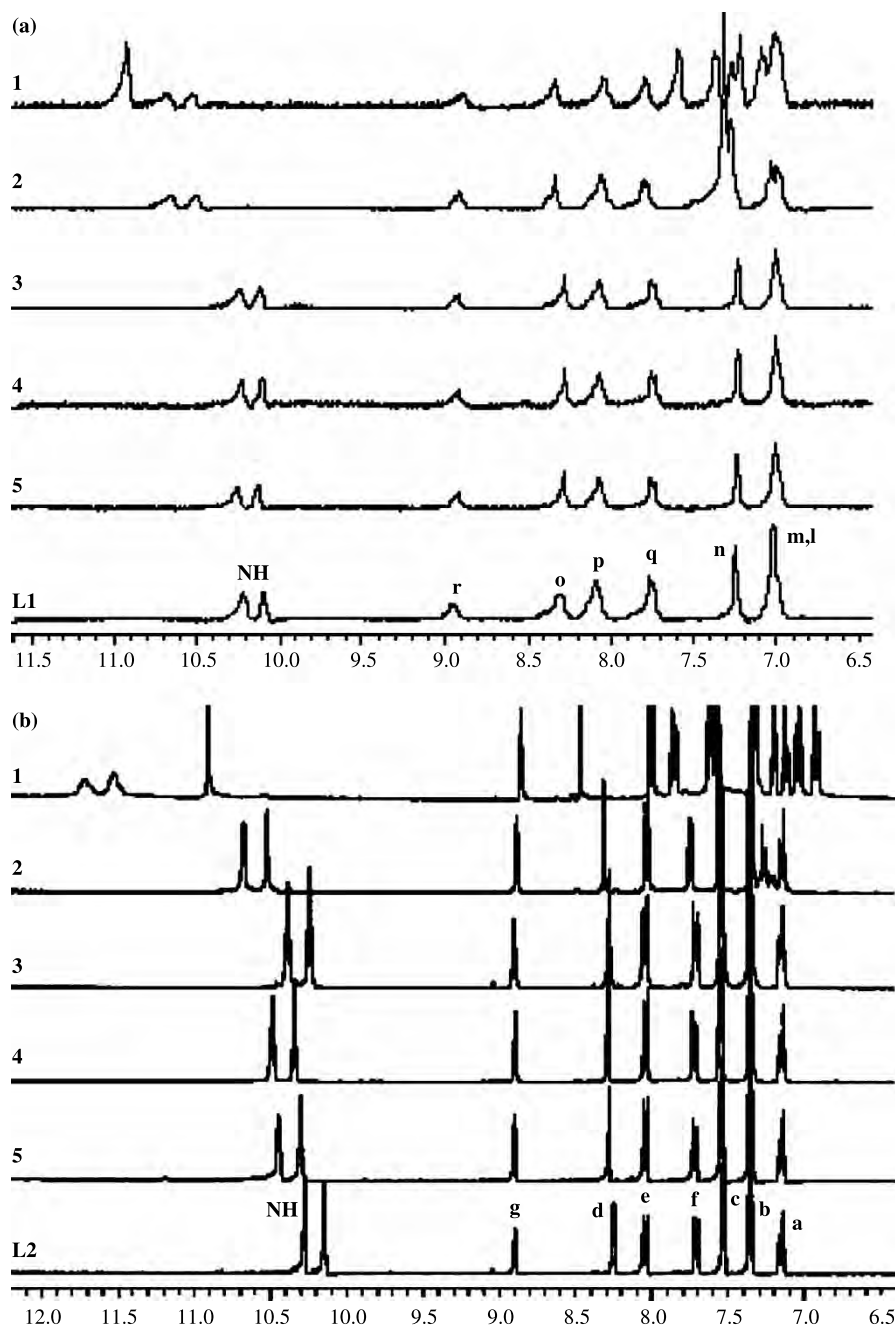


Figure 1. ^1H NMR (400 MHz) of (a) **L1** and (b) **L2** in $\text{DMSO}-d_6$ upon addition of excess amount of (1) Trp, (2) Phe, (3) Leu, (4) Ala and (5) Gly.

The complexes of both receptors and guests occurred via hydrogen bonding interactions between thiourea units on receptor and the carboxylate moiety of zwitterionic amino acids. The stoichiometry of the complexes of **L1** and **L2** with Trp and Phe was evaluated by the Job plot analysis monitoring the NH thiourea signals indicating a 1:1 ratio for the ligand and the guest.

Considering ^1H NMR spectra shown in Figure 2, the NH thiourea and acridinium protons of **L1H** exhibited upfield shifts upon addition of Trp. Phe and aliphatic amino acids caused slight shifts of the NH thiourea and acridinium protons. This is probably due to the higher pK ($\alpha\text{-COOH}$) of Trp which enhances the interactions between the carboxylate group and NH^+ -acridinium. Addition of Trp beyond 1 equivalent induced the downfield shift of the NH thiourea protons of **L1H** in a manner similar to that found in **L1**. This indicated that amino acids bound to the thiourea-binding site via H-bonding interactions. **L2H** also displayed changes in ^1H NMR spectra similar to those of **L1H** upon addition of the studied amino acids.

UV-vis spectra of **L1** and **L2** in the presence of amino acids in DMSO were recorded. The absorption or emission of acridine was derived from an inversion of two excited states: $n\text{-}\pi^*$ and $\pi\text{-}\pi^*$. In aprotic solvents such as DMSO, the $n\text{-}\pi^*$ state is presumably the lowest state (27) resulting in the appearance of the maximum absorption band of both receptors at 400 nm. As shown in Figure 3(a), the band at 400 nm of **L1** shifted to 460 nm in the presence of amino acids. The similar result was found in the case of **L2** upon adding Trp. Other amino acids displayed a slight decrease in the absorption band at 400 nm without the

appearance of a new band. Presumably, the new absorption band at 460 nm corresponded to the acridinium ion produced from the protonation at *N*-acridine by amino acids. This protonation stabilised $\pi\text{-}\pi^*$ excited state, caused the level inversion and resulted in the bathochromic shift of the absorption band.

The acridinium receptors **L1H** and **L2H** showed a maximum absorption band at 460 nm. The absorption band of **L1H** and **L2H** at 460 nm progressively decreased while a new band at 400 nm appeared with an isosbestic point at 415 nm upon amino acids. It was found that ligands **L1H** and **L2H** showed significant changes in UV-vis spectra upon addition of Trp. Addition of 10 equivalent of Trp induced the complete disappearance of the absorption band at 460 nm of **L1H** (Figure 3(b)), while the other amino acids needed more than 20 equivalent to suppress this band completely. However, **L2H** exhibited complete disappearance of the absorption band at 460 nm with 5 equivalent Trp and more than 10 equivalent of other amino acids.

^1H NMR and UV-vis studies showed that **L1** and **L2** formed complexes with amino acids, especially Trp due to H-bonding interactions only. The acridinium forms, **L1H** and **L2H**, employed both $\text{R-COO}^- \cdots \text{H} \cdots \text{N}^+$ -acridinium interactions and H-bonding interactions. Therefore, **L1H** and **L2H** were expected to give higher binding affinity towards amino acids.

2D-NMR studies of **L1**·Trp and **L2**·Trp

In the light of ^1H NMR and UV-vis titrations, the structure of the complex **L1**·Trp was deduced from

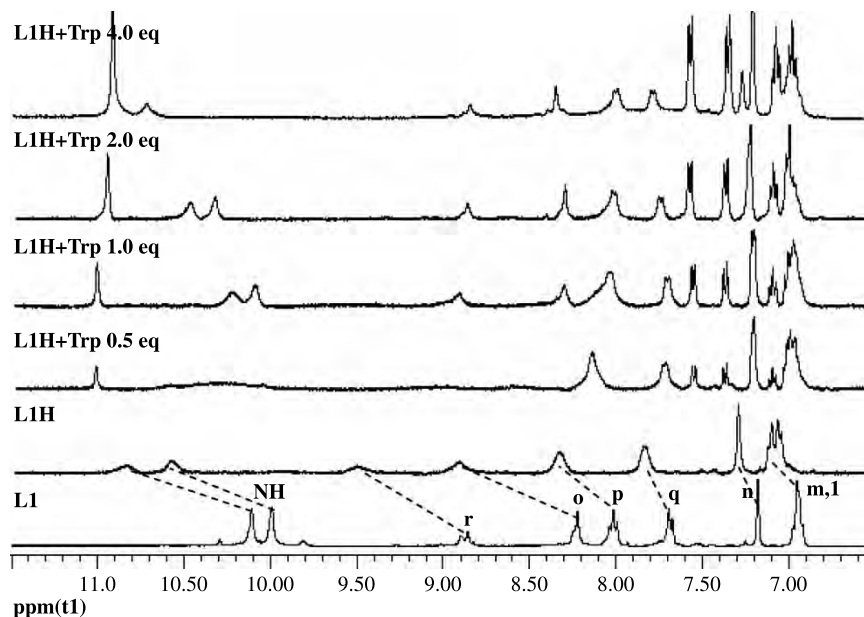


Figure 2. A comparison of ^1H NMR (400 MHz) spectra of **L1** (3×10^{-3} M) and **L1H** (3×10^{-3} M) in $\text{DMSO-}d_6$ upon addition of Trp 0.5, 1, 2 and 4 equivalent.

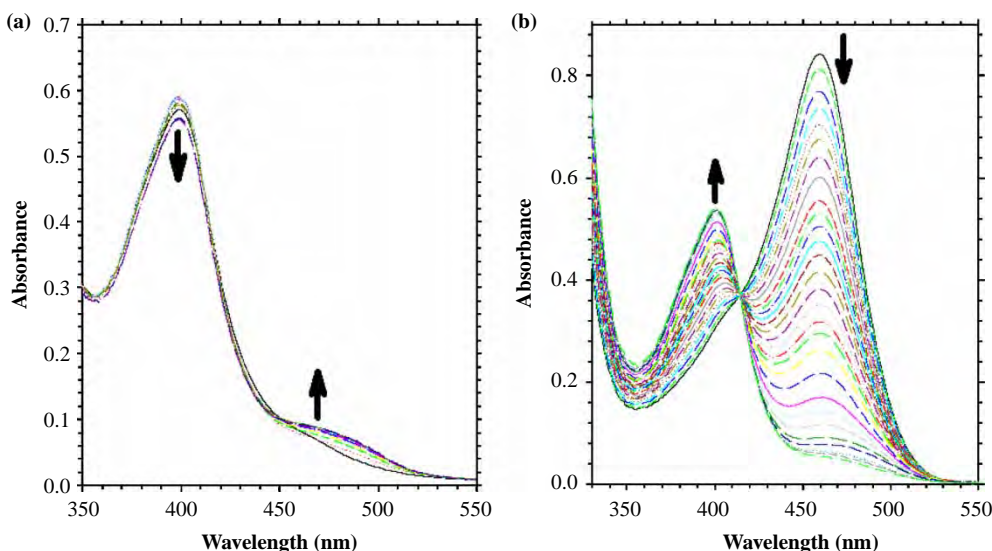


Figure 3. Changes in absorption spectra of (a) **L1** (2.5×10^{-5} M) upon addition of Trp 40 equivalent and (b) **L1H** (2.5×10^{-5} M) upon addition of Trp 30 equivalent.

NOESY. Correlation peaks between glycolic protons H_h , H_i and H_j of **L1** and aromatic protons H_s , H_u and H_t of Trp were observed. However, cross-relation peaks of acridine protons and Trp aromatic side-chain protons were not found. The proposed structure of the complex **L1**·Trp is shown in Figure 4.

In the case of **L2**, acridine protons H_d and H_f shifted downfield, while protons H_e and H_g shifted slightly upfield upon adding Trp. However, there are almost no changes in the protons of Trp. In addition, a NOESY spectrum of the complex **L2**·Trp did not show cross relationship of **L2** and Trp. The results implied that the existence of the polyethylene glycol unit in **L1** increased the interactions between **L1** and Trp.

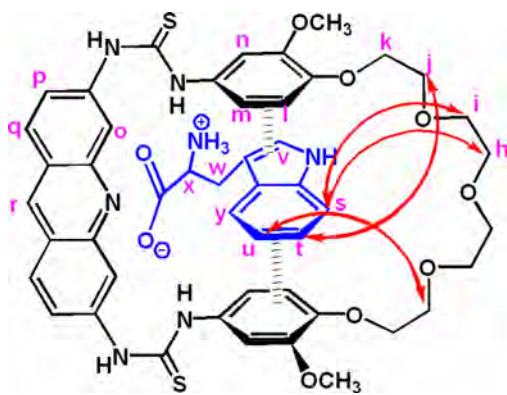


Figure 4. The proposed structure of **L1**·Trp deduced from NOESY cross relationship of **L1** and Trp.

Molecular modelling for **L1H**·Trp and **L2H**·Trp complexes

Figure 5 shows optimised structures of **L1H**·Trp and **L2H**·Trp. The calculated structures are consistent with the structures of **L1**·Trp and **L2**·Trp deduced from NOESY. Besides H-bonding interactions between the carboxylate unit and acridine protons, the macrocycle **L1H** provided a hydrophobic cavity for accommodating Trp. Weak interactions of an aryl ring proton of Trp and *O*-glycol of **L1H**, as well as $\text{RNH}_3^+ - \pi$ interactions were also observed. Moreover, the methoxy proton (H_{MeO}) of the host **L1H** showed weak interactions with the imidazole ring of Trp.

In contrast to **L1H**, **L2H** does not possess the polyethylene glycol unit. The supramolecular interactions with Trp guest relied on weak $\text{RNH}_3^+ - \pi$ interactions. Therefore, the binding affinity of **L2H** towards Trp is not as strong as that of **L1H**.

Complexation studies using fluorescence spectrophotometry

Fluorescence spectrometry was used to determine binding affinities of the synthesised hosts towards amino acid guests. The mechanism for sensing can operate via photoinduced electron transfer (PET) (28–30) and intramolecular charge transfer (31–34). Fluorescence emission change of **L1** (Figure 6(a)) and **L2** showed a small enhancement of emission bands at 528 and 520 nm, respectively, upon adding aromatic and aliphatic amino acids, but a large enhancement was observed for aromatic amino acid (Trp and Phe). The non-emissive via PET

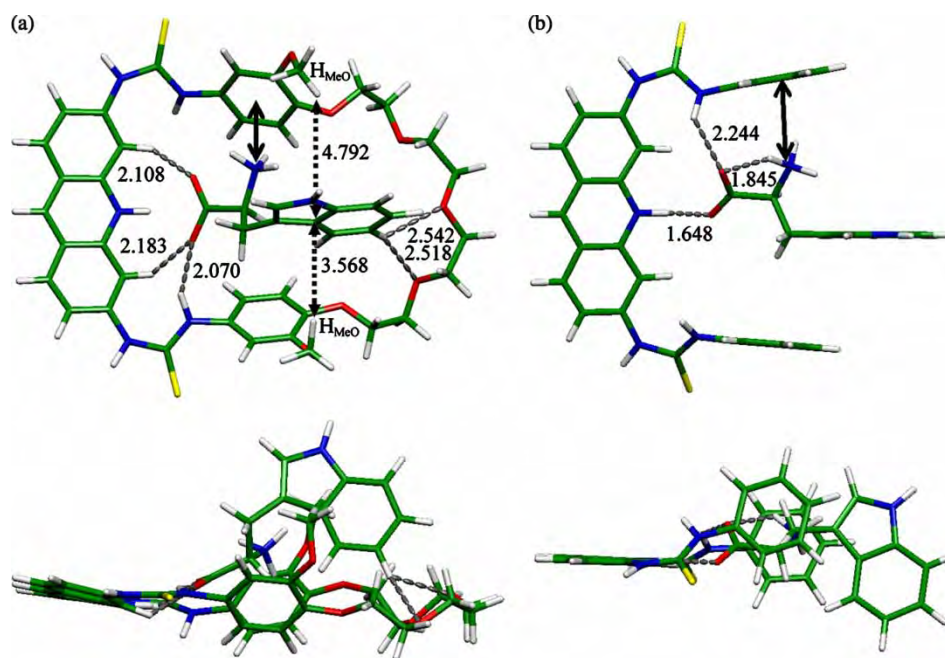


Figure 5. Top and side view optimised structures of the complexes of (a) **L1H** and (b) **L2H** and Trp. Bond distances shown are in Å.

mechanism of the unbound **L1** and **L2** may be ascribed to the electron-donating ability of the heteroatom in acridine leading to the electron transfer quenching pathway. For complexes of **L1** and **L2** with amino acids, this quenching pathway was eliminated possibly due to the protonation on N-atom of acridine by amino acids. Tables 1 and 2

summarise the binding constants (K) and the fluorescence enhancement (FE) factor, respectively, of all receptors in the presence of various amino acids. Data in both tables showed that the FEs of **L1** with aromatic amino acids are higher than those of **L1** with aliphatic amino acids. Therefore, the rigidified **L1** containing the glycolic ether

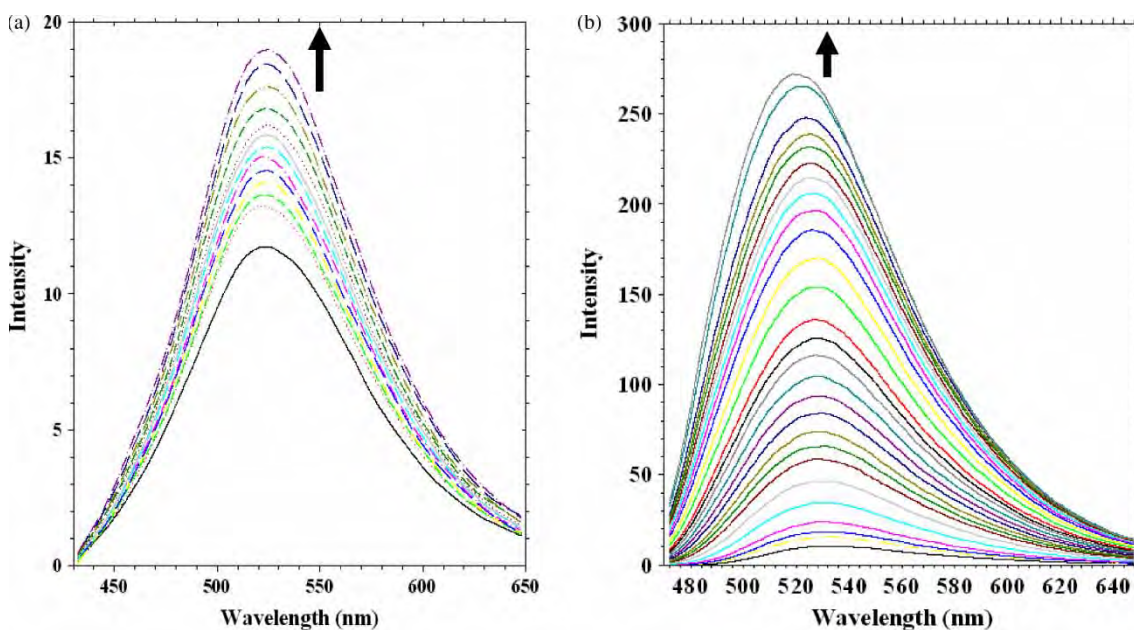


Figure 6. Changes in emission spectra of (a) **L1** (2×10^{-4} M, excitation at 400 nm) upon addition of Trp 30 equivalent in DMSO using $[\text{Bu}_4\text{N}]\text{PF}_6$ as a supporting electrolyte and (b) **L1H** (2×10^{-4} M, excitation at 460 nm) upon addition of Phe 25 equivalent in DMSO using $[\text{Bu}_4\text{N}]\text{PF}_6$ as a supporting electrolyte.

Table 1. The binding constants of interaction between **L1**, **L1H**, **L2** and **L2H** amino acids calculated from fluorescence titration using Benesi–Hildebrand equation (38).

	K				
	Trp	Phe	Leu	Ala	Gly
L1	307	578	<i>a</i>	219	<i>a</i>
L1H	3157	2748	855	900	957
L2	266	<i>a</i>	<i>a</i>	<i>a</i>	<i>a</i>
L2H	2873	2365	1418	1483	1367

a, values cannot be calculated.

bound more tightly with aromatic amino acids. On the contrary, there is no significant difference in FE values of **L2** with all amino acids.

The emission band of **L1H** was observed at 545 nm. This band undergoes a small bathochromic shift (17 nm in comparison with emission band of **L1**). This red shift is presumably due to the inversion from $n-\pi^*$ to $\pi-\pi^*$ excited state (27, 35, 36). The fluorescence intensity of **L1H** at 545 nm was gradually enhanced upon addition of Trp (Figure 6(b)). There was also a shift of emission band from 545 to 528 nm. Similar emission spectral changes were obtained for other amino acids. Upon addition of amino acids to **L2H**, the enhancement of emission band at 535 nm and the blue shift from 535 to 520 nm were observed. All amino acids gave the same results, except for Trp, which induced a higher fluorescent enhancement in both receptors. From Tables 1 and 2, **L1H** and **L2H** showed higher binding constants and FE values than **L1** and **L2**. This suggested that protonated hosts improved the binding abilities towards amino acids. The pK (α -COOH) values of Trp, Phe, Leu, Ala and Gly are 2.83, 1.83, 2.36, 2.34 and 2.34, respectively (37). These pK values are not significantly different. However, binding constants obtained from fluorescence titrations varied significantly among aromatic and aliphatic amino acids. Therefore, binding enhancement of **L1H** and **L2H** can be attributed to cooperation between $R-COO^- \cdots H \cdots N^+$ -acridinium interactions and H-bonding interactions. Besides, other supramolecular interactions suggested by 2D NMR and modelling studies also contributed to the binding abilities of **L1H** and **L2H** towards studied amino acids, especially Trp.

Table 2. FE of receptors **L1**, **L1H**, **L2** and **L2H** with several guests^a.

	FE				
	Trp	Phe	Leu	Ala	Gly
L1	3.12	2.42	1.22	1.77	1.73
L1H	34.42	31.43	27.42	26.13	22.52
L2	1.53	1.42	1.29	1.35	1.28
L2H	24.17	20.98	18.86	17.55	17.99

^aFE values were calculated as the ratio of fluorescence intensity in the presence and in the absence of guests.

Conclusion

We have synthesised four derivatives of acridine and acridinium compounds (**L1**, **L2**, **L1H** and **L2H**) containing thiourea-binding sites. Binding abilities of receptors **L1**, **L2**, **L1H** and **L2H** towards amino acids (Trp, Phe, Leu, Ala and Gly) were studied by 1H NMR spectroscopy, UV–vis and fluorescence spectrophotometry, and showed that the preorganised host **L1** could bind selectively to aromatic amino acid such as Trp. Hydrogen bonding interactions between thiourea-binding sites of the ligands and carboxylate groups in zwitterionic amino acids were found to be the main interactions driving complexation to take place. Protonated hosts **L1H** and **L2H** showed the interactions of carboxylate group of Trp and NH^+ -acridinium, which improved the binding ability of both ligands towards amino acids. Calculated structures of **L1H**·Trp and **L2H**·Trp showed that the glycolic unit in **L1H** provided the hydrophobic cavity for binding Trp (with additional supramolecular interactions) resulting in a stronger binding affinity of **L1H** over **L2H**.

Experimental

Materials and spectroscopic measurements

All materials were of standard analytical grade, purchased from Fluka, Aldrich or Merck and used without further purification. UV absorption spectra were obtained at 25°C on a Varian Cary 50 Probe UV–vis spectrophotometer. Fluorescence emission spectra were obtained on a Varian Cary Eclipse Fluorescence spectrophotometer. The solvent (DMSO) was of spectroscopic grade and used without further purification. Samples were contained in 10 mm path length quartz cuvettes (3.5 ml volume). Tetrabutylammonium hexafluorophosphate was used as a supporting electrolyte. NMR spectra were recorded in DMSO- d_6 on Varian 400 MHz spectrometer using tetramethylsilane as an internal standard.

Synthesis of **L1**, **L2**, **L1H** and **L2H**

Synthesis of 2-methoxy-1-(2-(2-(2-(2-(2-methoxy-4-nitrophenoxy)ethoxy)ethoxy)ethoxy) ethoxy)-4-nitrobenzene (2)

A mixture of **1** (0.2011 g, 0.0012 mol), catalytic amount of tetrabutylammonium bromide and potassium carbonate (1.6530 g, 0.012 mol) in 80 ml acetonitrile, was stirred at room temperature for 30 min. Then, a solution of tetraethylene glycol ditosylate (0.3010 g, 0.006 mol) in acetonitrile was added and the reaction mixture was heated under nitrogen atmosphere for 5 days. After the mixture cooled down to room temperature, the solvent was removed to dryness *in vacuo*. The residue was dissolved in dichloromethane and then washed with 3 M hydrochloric acid (50 ml) and extracted with dichloromethane

(3 × 50 ml). The organic phase was dried over anhydrous sodium sulphate and the solvent was removed. The desired product (**2**) was obtained as a bright yellow crystalline solid (40% yield) after recrystallisation in dichloromethane/methanol. ¹H NMR (400 MHz, CDCl₃): δ 7.916 (2H, dd, *J* = 2.8, 2.4 Hz), 7.765 (2H, d, *J* = 2.4 Hz), 6.985 (2H, d, *J* = 8.8 Hz), 4.308 (4H, t, *J* = 4.8 Hz), 3.966 (10H, s), 3.766 (4H, m, *J* = 2.8 Hz), 3.710 (4H, m, *J* = 2.8 Hz). IR (KBr, cm⁻¹): 3443, 3093, 2898, 1590, 1520, 1334, 1275, 1139, 1092. Anal. calcd for C₃₂H₂₈N₂O₁₁: C, 53.22; H, 5.68; N, 5.64; found: C, 53.22; H, 5.63; N, 5.74.

Synthesis of 4-(2-(2-(2-(2-(4-amino-2-methoxyphenoxy)-ethoxy)ethoxy)ethoxy)ethoxy)-3-methoxybenzenamine (**3**)

Hydrazine (0.4876 g, 0.021 mol) and Raney nickel (0.3073 g) was added to a vigorously stirred solution of **2** (0.2095 g, 0.004 mol) in 60 ml of 1:1 ethyl acetate:methanol. After 2 h, the mixture was filtered to remove Raney nickel and the filtrate was freed of solvent. The residue was dissolved in dichloromethane and dried over sodium sulphate anhydrous. Evaporation of the solvent gave the product **3**, as a yellow liquid in 70% yield. ¹H NMR (400 MHz, CDCl₃): δ 6.76 (2H, dd, *J* = 6.4, 2.4 Hz), 6.25 (2H, s), 6.14 (2H, dd, *J* = 6.2, 2.4), 4.04 (4H, m), 3.90 (4H, s), 3.80 (4H, m), 3.74 (3H, s), 3.69 (4H, m), 3.63 (4H, m).

Synthesis of **L1**

A solution of proflavinedithioisocyanate (1.1677 g, 0.004 mol) in dichloromethane was slowly added to the solution of **3** with the controlled temperature at 0°C and the reaction was stirred at room temperature overnight. The reaction mixture was filtered to remove dimer product as a dark red powder and then the organic solvent was evaporated under reduced pressure. The residue was dissolved in DMF and then methanol was added to precipitate the desired product **L1** as an orange powder (16% yield). ¹H NMR (400 MHz, DMSO-*d*₆): δ 10.092 (2H, d, *J* = 7.6 Hz), 9.975 (2H, d, *J* = 6.0 Hz), 8.855 (1H, d, *J* = 12.0 Hz), 8.234 (2H, s), 8.001 (2H, d, *J* = 8.0 Hz), 7.680 (2H, d, *J* = 9.6 Hz), 7.181 (2H, s), 6.954 (4H, s), 4.041 (4H, s), 3.727 (10H, s), 3.571 (8H, d, *J* = 7.6 Hz). ¹³C{¹H} NMR (400 MHz, DMSO-*d*₆): δ 179.4, 149.2, 148.6, 145.4, 141.6, 135.1, 132.5, 128.3, 123.3, 123.0, 117.6, 116.3, 113.2, 109.3, 69.9, 69.8, 68.9, 68.1, 55.6. IR (KBr, cm⁻¹): 3338, 2921, 2867, 1602, 1513, 1458, 1225, 1131. MS (ESI): *m/z* for C₃₇H₃₉N₅O₇S₂ 729.23 [M⁺ - H]. Anal. calcd for C₃₇H₃₉N₅O₇S₂·0.6 CH₂Cl₂·0.4 DMF: C, 57.47; H, 5.31; N, 9.33; found: C, 57.14; H, 5.32; N, 9.60.

Synthesis **L1H**

To a solution of **L1** (0.0031 g, 0.0405 mmol) in DMF, an excess amount of trifluoroacetic acid (0.1000 ml) was

added and then stirred at room temperature for 2 days. The desired product (**L1H**) was obtained as an orange solid in 60% yield after an addition of methanol to the reaction mixture. The final product (**L1H**) was obtained as a dark red solid in 60% yield. ¹H NMR (400 MHz, DMSO-*d*₆): δ 11.532 (2H, s), 10.821 (2H, s), 10.547 (2H, s), 9.413 (1H, s), 8.848 (2H, s), 8.230 (2H, s), 7.738 (2H, s), 7.199 (2H, s), 7.003 (2H, s), 6.966 (2H, s), 4.055 (4H, s), 3.731 (10H, s), 3.563 (8H, d, *J* = 8.4 Hz). IR (KBr, cm⁻¹): 3529, 2918, 2867, 1676, 1509, 1458, 1201, 1123. MS (ESI): *m/z* for C₃₉H₄₀F₃N₅O₉S₂ 844.864 [M + H⁺].

Synthesis of **L2**

To a solution of aniline (0.1026 ml, 0.0011 mol) in 30 ml dichloromethane was cooled to 0°C and slowly added with a solution of proflavinedithioisocyanate (0.1500 g, 0.0005 mol) in dichloromethane. After the reaction mixture was stirred at room temperature overnight, a yellow solid was precipitated and the solid was filtered under vacuum and washed with dichloromethane to yield a pale orange powder as the final product (**L2**; 52% yield). ¹H NMR (400 MHz, DMSO-*d*₆): δ 10.284 (2H, s), 10.144 (2H, s), 8.894 (1H, s), 8.251 (2H, s), 8.037 (2H, d, *J* = 8.8 Hz), 7.697 (2H, dd, *J* = 8.8, 3 Hz), 7.526 (4H, d, *J* = 7.2 Hz), 7.350 (4H, m, *J* = 7.6 Hz), 7.142 (2H, m). ¹³C{¹H} NMR (400 MHz, DMSO-*d*₆): δ 179.6, 149.3, 142.1, 139.8, 135.4, 129.2, 124.8, 124.0, 123.8, 123.5, 118.0. IR (KBr, cm⁻¹): 3217, 3027, 1618, 1544, 1446, 1252, 1147. Anal. calcd for C₂₇H₂₁N₅S₂: C, 67.61; H, 4.41; N, 14.60; found: C, 67.59; H, 4.42; N, 14.61.

Synthesis of **L2H**

To a solution of **L2** (0.0031 g, 0.0405 mmol) in DMF, an excess amount of trifluoroacetic acid (0.1000 ml) was added and then stirred at room temperature for 2 days. The desired product (**L2H**) was obtained as an orange solid in 65% yield after an addition of methanol to the reaction mixture. The final product (**L2H**) was obtained as a dark red solid in 65% yield. ¹H NMR (400 MHz, DMSO-*d*₆): δ 11.085 (2H, s), 10.804 (2H, s), 9.453 (1H, s), 8.885 (2H, s), 8.274 (2H, m), 7.784 (2H, d, *J* = 9.2 Hz), 7.545 (4H, d, *J* = 7.6 Hz), 7.364 (4H, t, *J* = 8.0 Hz), 7.171 (4H, t, *J* = 7.2 Hz). ¹³C{¹H} NMR (400 MHz, DMSO-*d*₆): δ 179.3, 159.7, 159.4, 159.0, 139.3, 130.8, 129.0, 125.6, 124.4, 123.3, 122.1, 118.9. IR (KBr, cm⁻¹): 3478, 3050, 2781, 1696, 1536, 1458, 1193. MS (ESI): *m/z* for C₃₂H₂₉F₃N₆O₃S₂ 665.752 [M⁺ + DMF].

UV-vis titrations

UV-vis titration of all receptors (in a range of 2 × 10⁻⁵ – 3 × 10⁻⁵ M) in the presence of amino acids were recorded in DMSO (using [Bu₄N][PF₆] as a supporting

electrolyte). A solution of amino acids was prepared in spectroscopic grade DMSO and then it was introduced in portions (total volume 1.5 ml) into a solution of receptor (2 ml). Absorption spectra of solution were recorded after each addition until absorbance of a new peak (at 460 and 400 nm for neutral and protonated receptors, respectively) was constant.

Fluorescence titrations

Fluorescence titration of all receptors (2×10^{-4} M) in the presence of amino acids were recorded in DMSO (using $[\text{Bu}_4\text{N}][\text{PF}_6]$ as a supporting electrolyte). A solution of amino acids was prepared in spectroscopic grade DMSO and then it was introduced in portions (total volume 1.5 ml) into a solution of receptor (2 ml). Fluorescence intensity changes were recorded for all titrations. The neutral receptors (**L1** and **L2**) and the protonated receptors (**L1H** and **L2H**) were excited at 400 and 460 nm, respectively. Binding constants were calculated from fluorimetric data using Benesi–Hildebrand equation (38). The quantity $I_F^0/(I_F - I_F^0)$ is plotted versus $[\text{M}]^{-1}$, and the binding constants is given by the ratio intercept/slope.

Computation methods

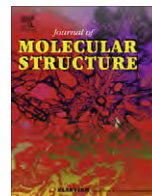
Full geometry optimisation of complexes of **L1H** and **L2H** and Trp were computed by density functional theory using the Becke's three-parameter hybrid density function and the Lee, Yang, and Parr correlation function (B3LYP) (39, 40) with the 6-31+G(d,p) basis set. All calculations were performed using GAUSSIAN 03 program (41).

Acknowledgements

The authors wish to thank the support provided by the Development and Promotion of Science and Technology Talent (DPST) project, Ratchadaphiseksomphot Endowment Fund and the Thailand Research Fund (MRG4780187 and RTA5080006).

References

- (1) Cram, D.J. *Angew. Chem., Int. Ed. Engl.* **1988**, 27, 1009–1020.
- (2) Tecilla, P.; Jubian, V.; Hamilton, A. D. *Tetrahedron* **1995**, 51, 435–448.
- (3) Dobashi, A.; Hara, S. *Tetrahedron Lett.* **1983**, 24, 1509–1510.
- (4) Liu, R.; Sanderson, P. E. J.; Still, W. C. *J. Org. Chem.* **1990**, 55, 5184–5186.
- (5) Tsukube, H. *Tetrahedron Lett.* **1981**, 22, 3981–3984.
- (6) Echavarren, A.; Galan, A.; Lehn, J.-M.; de Mendoza, J. *J. Am. Chem. Soc.* **1989**, 111, 4994–4995.
- (7) Sunamoto, J.; Iwamoto, K.; Mohri, Y.; Kominato, T. *J. Am. Chem. Soc.* **1982**, 104, 5502–5504.
- (8) dos Santos, C.M.G.; McCabe, T.; Gunnlaugsson, T. *Tetrahedron Lett.* **2007**, 48, 3135–3139.
- (9) Quinlan, E.; Matthews, S.E.; Gunnlaugsson, T. *J. Org. Chem.* **2007**, 72, 7497–7503.
- (10) Brooks, S.J.; Caltagirone, C.; Corrins, A.J.; Gale, P.A.; Light, M. *Supramol. Chem.* **2008**, 20, 349–355.
- (11) Caltagirone, C.; Bates, G.W.; Gale, P.A.; Light, M.E. *Chem. Commun.* **2008**, 61–63.
- (12) Estévez, C.M.; Bach, R.D.; Hass, K.C.; Schneider, W.F. *J. Am. Chem. Soc.* **1997**, 119, 5445–5446.
- (13) Blancafort, L.; González, D.; Olivucci, M.; Robb, M.A. *J. Am. Chem. Soc.* **2002**, 124, 6398–6406.
- (14) Chen, H.; Ogo, S.; Fish, R.H. *J. Am. Chem. Soc.* **1996**, 118, 4993–5001.
- (15) Escuder, B.; Martinus, A.E.R.; Feiters, M.C.; Nolte, R.J.M. *Tetrahedron* **2004**, 60, 291–300.
- (16) Konishi, K.; Yahara, K.; Toshishige, H.; Aida, T.; Inoue, S. *J. Am. Chem. Soc.* **1994**, 116, 1337–1344.
- (17) Lipkowitz, K.B.; Raghothama, S.; Yang, J.A. *J. Am. Chem. Soc.* **1992**, 114, 1554–1562.
- (18) Yang, Y.K.; Tae, J. *Org. Lett.* **2006**, 8, 5721–5723.
- (19) Garcia-Garrido, S.E.; Caltagirone, C.; Light, M.E.; Gale, P.A. *Chem. Commun.* **2007**, 72, 1450–1452.
- (20) Lin, C.; Simov, V.; Drueckhammer, D.G. *J. Org. Chem.* **2007**, 72, 1742–1746.
- (21) Thiagarajan, V.; Ramamurthy, P. *J. Lumin.* **2007**, 126, 886–892.
- (22) Thiagarajan, V.; Ramamurthy, P. *Spectrochim. Acta A* **2007**, 67, 772–777.
- (23) Mandl, C.P.; König, B. *J. Org. Chem.* **2005**, 70, 670–674.
- (24) Galán, A.; Andreu, D.; Echavarren, A.M.; Prados, P.; de Mendoza, J. *J. Am. Chem. Soc.* **1992**, 114, 1511–1512.
- (25) Wu, F.Y.; Li, Z.; Wen, Z.C.; Zhou, N.; Zhao, Y.F.; Jiang, Y.B. *Org. Lett.* **2002**, 4, 3203–3205.
- (26) Lee, D.H.; Lee, H.Y.; Hong, J.I. *Tetrahedron Lett.* **2002**, 43, 7273–7276.
- (27) Diverdi, L.A.; Topp, M.R. *J. Phys. Chem.* **1984**, 88, 3447–3451.
- (28) Duke, R.M.; Gunnlaugsson, T. *Tetrahedron Lett.* **2007**, 48, 8043–8047.
- (29) Kim, S.K.; Yoon, J. *Chem. Commun.* **2002**, 770–771.
- (30) Nishizawa, S.; Kato, Y.; Teramae, N. *J. Am. Chem. Soc.* **1999**, 121, 9463–9464.
- (31) Kovalchuk, A.; Bricks, J.L.; Reck, G.; Rurack, K.; Schulz, B.; Szumna, A.; Weibhoff, H. *Chem. Commun.* **2004**, 1946–1947.
- (32) Wu, F.-Y.; Jiang, Y.-B. *Chem. Phys. Lett.* **2002**, 355, 438–444.
- (33) Thiaganajan, V.; Ramamurthy, P.; Thirumalai, D.; Ramakrishnan, V. T. *Org. Lett.* **2005**, 7, 657–660.
- (34) Sauer, M. *Angew. Chem., Int. Ed. Engl.* **2003**, 42, 1790–1793.
- (35) Kanamura, N.; Lim, E.C. *J. Chem. Phys.* **1976**, 65, 4055–4060.
- (36) McGlynn, S.P.; Sunseri, R.; Christodouleas, N. *J. Chem. Phys.* **1962**, 37, 1818–1824.
- (37) Werner, R. *Essential of Modern Biochemistry*; Jones and Bartlett: Boston, MA, 1983.
- (38) Bourson, J.; Valeur, B. *J. Phys. Chem.* **1989**, 93, 3871–3876.
- (39) Becke, A.D. *Phys. Rev.* **1988**, A38, 3098–3100.
- (40) Lee, C.; Yang, W.; Parr, R.G. *Phys. Rev.* **1988**, B37, 785–789.
- (41) Frisch, M.J.; Trucks, G.W.; Schlegel, H.B.; Scuseria, G.E.; Robb, M.A.; Cheeseman, J.R.; Montgomery, Jr, J.A.; Vreven, T.; Kudin, K.N.; Burant, J.C.; et al. *Gaussian 03, Revision C.02*, Gaussian Inc., Wallingford, 2006.



Structural and conformational investigations of chiral bis(phenylamido)ferrocenes by X-ray crystallography and density functional calculations

Chomchai Suksai^a, Pannee Leeladee^b, Thawatchai Tuntulani^{b,*}, Vithaya Ruangpornvisuti^{b,*}, Narongsak Chaichit^c

^a Department of Chemistry and Center of Excellence for Innovation in Chemistry, Faculty of Science, Burapha University, Chonburi 20131, Thailand

^b Department of Chemistry, Faculty of Science, Chulalongkorn University, Bangkok 10330, Thailand

^c Department of Physics, Faculty of Science and Technology, Thammasat University, Patumthani 12121, Thailand

ARTICLE INFO

Article history:

Received 11 April 2009

Received in revised form 10 August 2009

Accepted 8 September 2009

Available online 11 September 2009

Keywords:

Bis(phenylamido)ferrocene
Structural and conformational analysis
Enantiomer
X-ray crystallography
DFT calculations

ABSTRACT

X-ray crystallographic structures of the synthesized bis(phenylamido)ferrocene, compound **1**, were determined in two forms: *cis*-conformer (**1a**) and *trans*-conformer (**1b**). Structures **1a** and **1b** possessed their enantiomeric pairs **1a'** and **1b'**, respectively in the crystal structures. B3LYP/LanL2DZ-optimized structures of all conformers of **1** were obtained as Z1, Z2 and E2 and their corresponding enantiomers Z4, Z3 and E2'. Conformers Z1 and E2 are found to be the most stable conformers. The structures of enantiomeric pairs Z1/Z4 and E2/E2' are in good agreement with crystal structures of **1a/1a'** and **1b/1b'**, respectively. Their relative energies are in order Z1 (Z4) < Z2 (Z3) < E2 (E2'). Their interconversion equilibria Z1 ↔ Z2, Z2 ↔ E2 and Z2 ↔ Z3 were found and their reaction energies, thermodynamic quantities, rate, and equilibrium constants were obtained. DFT calculations suggested that different conformations of bis(phenylamido)ferrocene could be ascribed to both thermodynamic and kinetic factors.

© 2009 Elsevier B.V. All rights reserved.

1. Introduction

Since the discovery of ferrocene, $\text{Fe}(\eta^5\text{-C}_5\text{H}_5)_2$, by Pauson in 1951 [1], its chemistry has been a subject of many studies in the past several decades. Numerous derivatives of ferrocene were used in homogeneous catalysis, materials and molecular devices [2]. During the last decades, ferrocene units appended with secondary amides have been used in anion recognition [3,4]. Bis(phenylamido)ferrocene, compound **1** (Scheme 1), was thus synthesized to be a controlled compound to compare anion binding and sensing abilities with the synthetic receptors and sensors containing amidoferrocene units [5].

Compound **1** was crystallized in various solvents and conditions. Interestingly, due to the rotation of the cyclopentadiene (Cp) rings and hydrogen bonding interactions, crystal structures of **1** were obtained in two forms: *cis* and *trans* forms. The *cis* and *trans* forms were found to have enantiomeric pairs in the crystal structures. We, therefore, used computational methods to investigate the possibility and stability of all structures of compound **1** that could possibly exist upon rotation of the Cp rings and their substituents.

In 1996, Oberhoff et al. found the X-ray crystallographic structure of **1a** (Fig. 1) from their study of the preparation of carboxamide-substituted cyclopentadienide–ligand systems and their respective metallocene complexes [6]. As the application of ferrocene-conjugates for the electrochemical detection of oligonucleotides on electrode surfaces is of importance, ferrocene–peptide conjugates were widely studied. Hirao and coworkers studied many amide derivatives of ferrocene dicarboxylic acid [7]. Heinze et al. studied amido-substituted ferrocenes in the crystal and in solution by X-ray crystallography, IR and NMR spectroscopy and DFT calculations [8]. Kraatz and colleagues used a new bioorganometallic approach for the detection of proteins using surface-bound ferrocene–peptide conjugates and a series of peptide conjugates of ferrocene amino acid [9,10].

2. Methodology

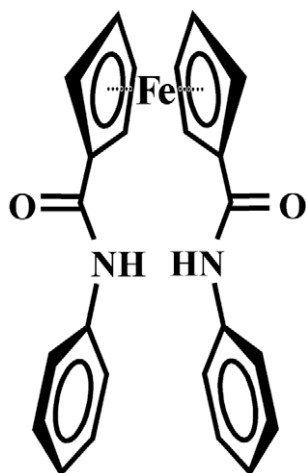
2.1. Experimental

2.1.1. Materials

All solvents were of reagent grade and purified with standard procedures. Compound **1**, bis(phenylamido)ferrocene, was prepared by the previously published procedure [5].

* Corresponding authors. Tel.: +66 2218 7644; fax: +66 2254 1309.

E-mail addresses: tthawac@chula.ac.th (T. Tuntulani), vithaya.r@chula.ac.th (V. Ruangpornvisuti).



Scheme 1. Compound 1.

2.1.2. Crystallization

Compound **1** was dissolved in a mixture of chloroform and heptane. The crystal of **1a** suitable for X-ray crystallography was obtained from the slow evaporation of the solvent at room temperature. Single crystals of polymorph **1b** were obtained from the slow evaporation of compound **1** in methanol in a refrigerator for 1 week.

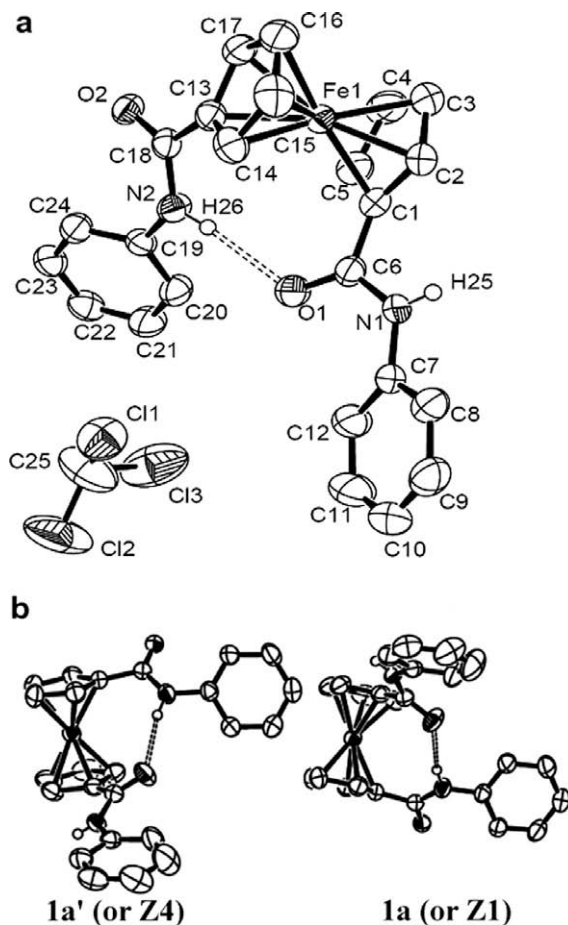


Fig. 1. (a) ORTEP plots of **1a** with 50% probability thermal ellipsoids and (b) showing an enantiomeric pair. Hydrogen atoms of phenyl rings and cyclopentadiene rings are omitted for clarity.

Table 1

Crystallographic data and structure refinement of solid state structures of compound **1**, **1a** and **1b**.

	1a	1b
Chemical formula	C ₂₅ H ₂₁ FeCl ₃ N ₂ O ₂	C ₂₄ H ₂₀ FeN ₂ O ₂
Molecular weight	543.63	424.27
Color	Orange	Orange
Temperature (K)	293(2)	293(2)
Crystal system	Monoclinic	Orthorhombic
Space group	P ₂₁ /n	P _{bn} 21
a (Å)	9.28180(10)	5.6007(2)
b (Å)	14.9540(2)	12.7730(3)
c (Å)	17.54530(10)	26.1521(7)
α (°)	90	90
β (°)	93.4870(10)	90
γ (°)	90	90
V (Å ³)	2430.78(4)	1870.86(9)
Z	4	4
F(000)	1108	880
D _{calc} (g cm ⁻³)	1.483	1.506
μ (mm ⁻¹)	0.976	0.83
θ Range for data collection	1.79–30.53	1.56–30.42
Index ranges	−10 ≤ h ≤ 13 −20 ≤ k ≤ 21 −23 ≤ l ≤ 24	−7 ≤ h ≤ 7 −17 ≤ k ≤ 17 −26 ≤ l ≤ 37
Reflections collected	17426	12758
Reflections observed	6959	4195
Parameters	338	302
Final R indices [I > 2σ(I)]	R ₁ = 0.0666, wR ₂ = 0.1502	R ₁ = 0.0357, wR ₂ = 0.0672
R indices (all data)	R ₁ = 0.1342, wR ₂ = 0.1858	R ₁ = 0.0498, wR ₂ = 0.0732
Goodness-of-fit	1.011	1.084
Maximum, minimum difference (e Å ⁻³)	0.938, −0.75	0.250, −0.299

Crystallographic data for structures **1a** and **1b** reported in this paper were deposited in the Cambridge Crystallographic Data Center as supporting information CCDC No. 679049 and 679178 for structures **1a** and **1b**, respectively.

2.1.3. X-ray crystal structure determinations

X-ray diffraction measurement for structures **1a** and **1b** were performed on a Bruker–Nonius Kappa CCD diffractometer with graphite-monochromated Mo Kα radiation (λ = 0.71073 Å). The structures were solved by direct method and all non-hydrogen atoms were refined with anisotropic thermal parameters by full-matrix least-squares calculations on F² using the SHELXL97 program [11] on the WinGX package [12]. Hydrogen atoms were inserted at calculated positions and constrained with isotropic thermal parameters, except for the hydrogen atoms of the NH amide protons which were located from a difference Fourier map and refined isotropically. Drawings were produced with MERCURY [13]. The crystallographic data and refinements of structures **1a** and **1b** are presented in Table 1.

2.2. Computational details

2.2.1. Structure optimization and potential energy surface

Structure optimizations of various conformers of bis(phenylamido)ferrocene, **1** and their corresponding transition states for all interconversion reactions were carried out using density functional theory (DFT) method. The calculations have been performed with hybrid density functional B3LYP, the Becke's three-parameter exchange functional [14] with the Lee–Yang–Parr correlation functional [15], using the Los Alamos LanL2DZ split-valence basis set [16–18]. All conformers of compound **1** were obtained from all possible conformations generated by clockwise rotation of one of the amidophenyl unit against the other (fixed) unit by 7°. All opti-

mized geometries of conformers and transition-state structures were characterized as minimum and first-order saddle points by analysis of computed frequencies. The zero-point vibrational energy (ZPVE) corrections were obtained from frequency calculations at the same theory level. All calculations were performed using GAUSSIAN 03 program [19].

2.2.2. Thermodynamic properties and formation constants

The standard enthalpy ΔH_{298}^0 and Gibbs free energy change ΔG_{298}^0 of an isomerization process have been derived from the zero-point vibrational energy (ZPVE) [20] computed at the same level of theory which has been employed for structure optimizations. The rate constants $k(T)$ for conversion reactions derived from the transition state theory were computed from activation energy (ΔE) using Eq. (1) [21–23].

$$k(T) = \kappa \frac{k_B T}{h} \frac{Q_{TS}}{Q_{REA}} \exp(-\Delta^\ddagger E/RT) = \kappa A \exp(-\Delta^\ddagger E/RT) \quad (1)$$

where k_B is the Boltzmann's constant, h is Planck's constant, T is the absolute temperature and R is the gas constant. Q_{TS} and Q_{REA} are the partition functions of the transition state (TS) and the reactant of compound **1** whose value is the product of the translational, rotational, vibrational, and electronic partition functions. These partition functions were obtained from their frequency calculations using the GAUSSIAN 03 program [19]. The tunneling coefficient (κ) can be computed with the Wigner method [24–26] using the equation $\kappa = 1 + \frac{1}{24} \left(\frac{h\nu_i}{k_B T} \right)^2$, where ν_i is the imaginary frequency of the transition-state structure that accounts for the vibrational motion along the reaction path. The pre-exponential factor (A) is defined as $A = \frac{k_B T}{h} \frac{Q_{TS}}{Q_{REA}}$. The equilibrium constant K at 298.15 K and 1 atm is computed using a thermodynamic equation $\Delta G^0 = -RT \ln K$.

3. Results and discussion

3.1. Cis and trans structures of compound **1**

We have tried to grow crystals of **1** in various solvents and conditions. Crystals of **1** could be grown in the mixture of chloroform and heptane. After 3 days, crystals of a *cis*-conformation structure of **1**, **1a**, were obtained. The structure **1a** was found in the $P_{21/n}$ space group of the monoclinic system, revealing one crystallographically independent molecule entity of **1a** and one chloroform molecule as shown in Fig. 1. The Cp rings were in fully eclipsed conformation, the distances between Fe atom and the centroids of the Cp rings were 1.63 Å and 1.64 Å with the angle of $\text{Cp}_{\text{centroid}}\text{--Fe--Cp}_{\text{centroid}}$ of 179.06°. The average $\text{Fe}\cdots\text{C}(\text{Cp})$ distance was 2.03 Å. As it can be seen from the crystal structure, the intramolecular hydrogen bonding between the amide group $\text{N}(2)\cdots\text{H}(26)\cdots\text{O}(1)$ showing $\text{N}(2)\cdots\text{O}(1)$ distance of 2.13(4) Å plays an important role to generate the *cis*-configuration. The structure **1a** has been previously reported by Erker et al. [6]. Erker found the supramolecular structure of the molecule occurred by intermolecular hydrogen bonding interactions. The structure **1a** also showed intermolecular hydrogen bondings with a $\text{H}(25)\cdots\text{O}(2)$ distance of 2.18(4) Å. Furthermore, we have also observed an enantiomeric pair of **1a** (**1a'**) in the crystal structure as shown in Fig. 1.

We anticipate that a polar solvent such as methanol can break the intramolecular hydrogen bonds in the structure of **1a** and give another polymorph. Therefore, we have attempted to grow crystals of compound **1** in methanol. The crystal of **1b** was obtained as orange rod. The structure of **1b** was packed into the orthorhombic P_{bn21} space group which possessed a Flack parameter of 0.013 after the final refinement [27]. As shown in Fig. 2, the phenyl side chains were pointing away from each other in which one of phenyl rings was coplanar and the other was perpendicular to the Cp ring. The

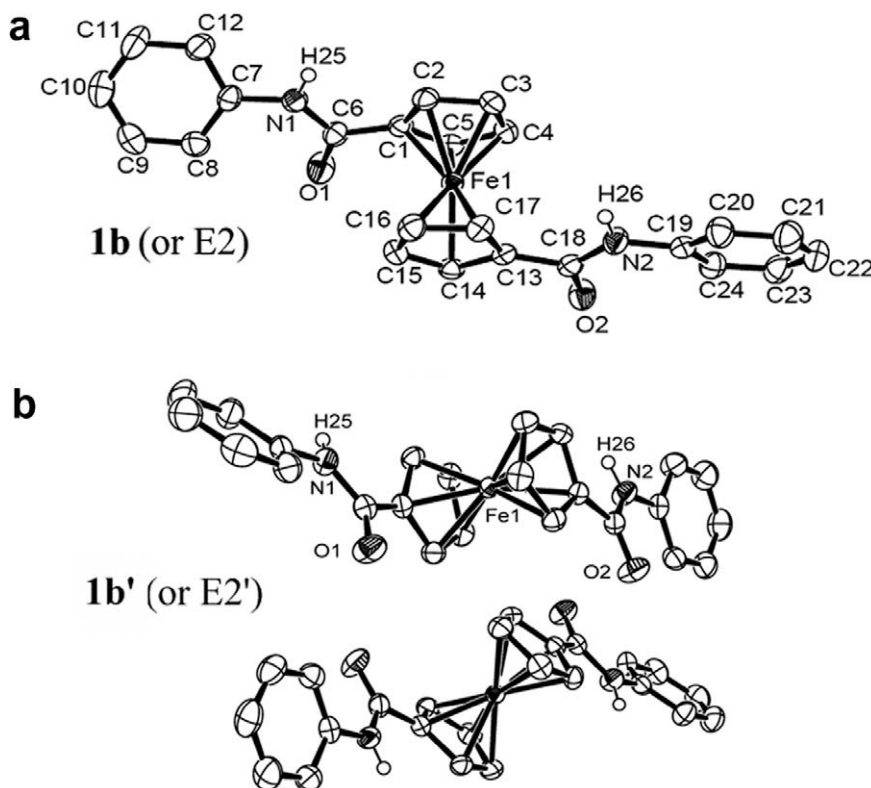


Fig. 2. (a) ORTEP plots of **1b** with 50% probability thermal ellipsoids and (b) showing an enantiomeric pair. Hydrogen atoms of phenyl rings and cyclopentadiene rings are omitted for clarity.

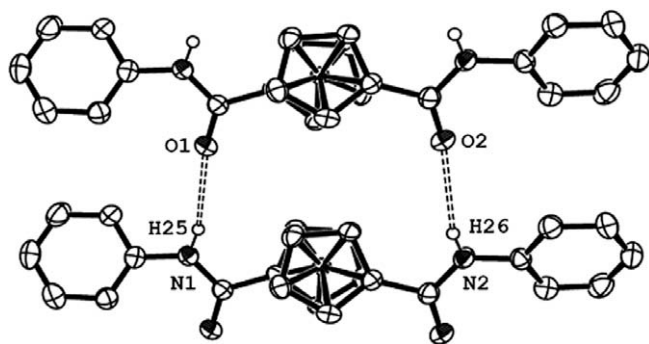


Fig. 3. ORTEP plots of **1b** with 50% probability thermal ellipsoids showing the dimeric structure. Hydrogen atoms of phenyl rings and cyclopentadiene rings are omitted for clarity.

average $\text{Fe} \cdots \text{C}(\text{Cp})$ distance was 2.05 Å which was identical to all previously studied ferrocenyl derivatives. The distances between Fe atoms and the centroids of the Cp rings were 1.65 Å and 1.66 Å with the angle of 179.0° and the distance between two Cp rings was 3.31 Å. Fig. 2b showed the crystal structure of an almost enantiomeric pair of **1b**, **1b'**. These crystallographically independent molecules are not perfect mirror images (as seen from bond lengths in Table 3).

It should be noted that there was a relationship between intramolecular hydrogen bonding and steric hindrance. In methanol the intramolecular hydrogen bonds were broken and the phenylamide side arms turned to *trans*-conformation in order to reduce the steric hindrance. Two weak intermolecular hydrogen bonds could be observed in $\text{N}(1)\text{--H}(25) \cdots \text{O}(1)\#1$ and $\text{N}(2)\text{--H}(26) \cdots \text{O}(2)\#1$ with distances of 2.64(3) and 2.63(4) Å, respectively, as shown in Fig. 3.

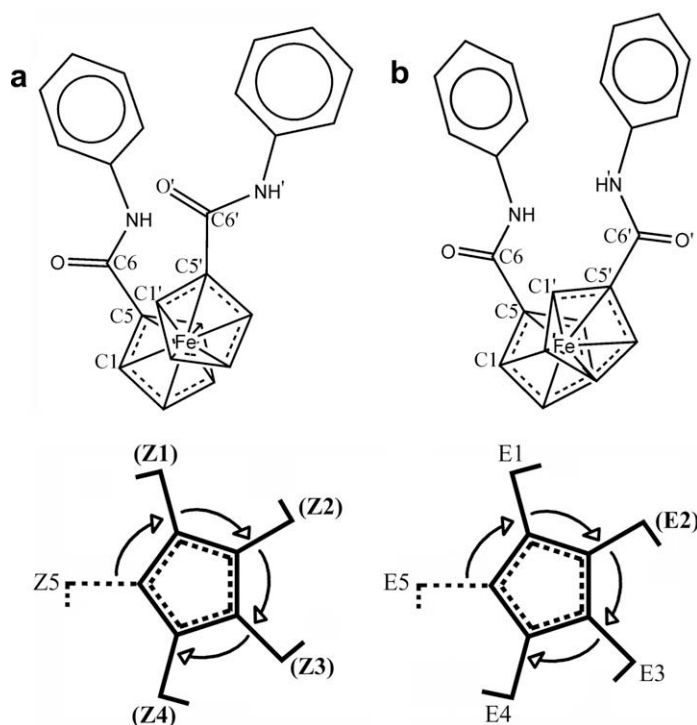


Fig. 4. Definition for (a) Z and (b) E conformers of compound **1** and their naming system shown at the bottom. Names of the existing conformers are highlighted as bold type in parenthesis.

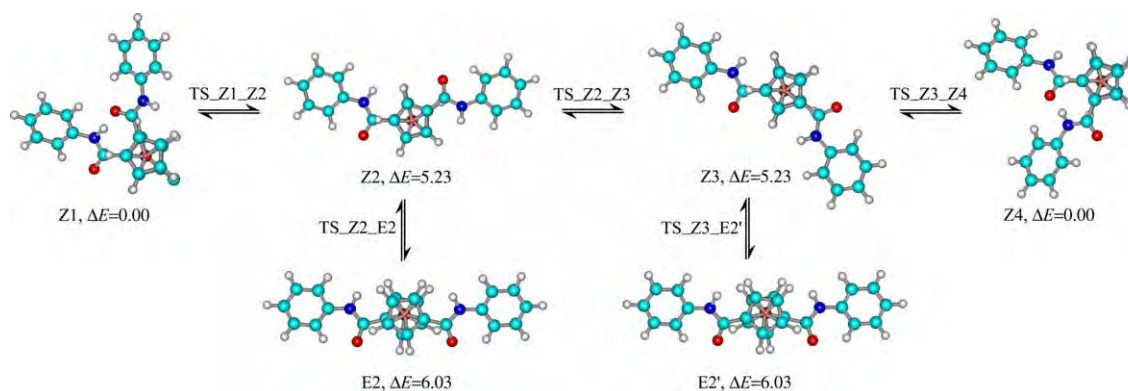


Fig. 5. The B3LYP/LanL2DZ optimized structures of **1** conformers and pathways of their interconversions in gas phase, relative energies based on the most stable conformer, Z1, in kcal/mol.

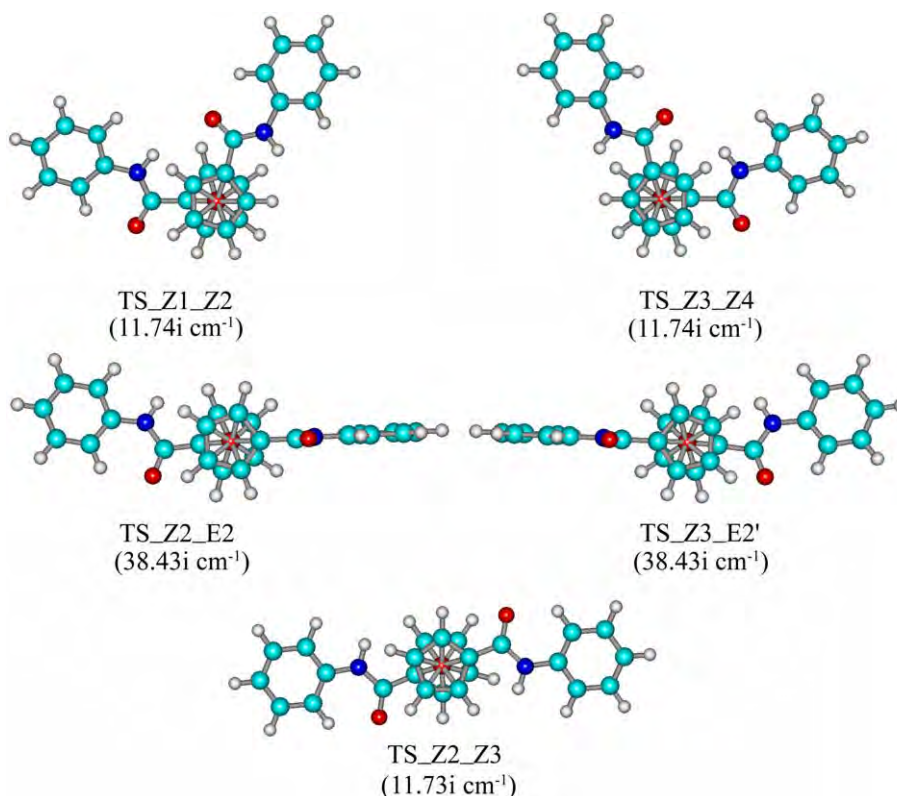


Fig. 6. The B3LYP/LanL2DZ optimized structures of transition states.

3.2. Conformation analysis and interconversion

Recently, Metzler-Nolte [28] and Heinze [29] have reported systematic evaluations of different hydrogen bonding patterns in unsymmetrical ferrocenyl peptides. In our case, it can be clearly seen from crystal structures **1a** and **1b** that the presence of amidophenyl units on the Cp rings provided intramolecular and intermolecular hydrogen bonding interactions. Although the substituents on both Cp rings are the same, rotation around the principal axis can lead to a number of chiral structures in the solid state. Therefore, all conformers and their interconversions from rotation of the Cp rings are studied and their energies are evaluated.

Conformers of compound **1** were obtained using the B3LYP/LanL2DZ calculations by rotating one of the amidophenyl groups

around the principal axis of ferrocene (solid line) against the fixed amidophenyl side-arm (broken line) as shown in Fig. 4. These conformers were defined as Z_n (for Z conformer, Fig. 4) and E_n (for E conformer, Fig. 4) where n referred to the n -fold ($n = 360/72$) rotation about the principal axis of ferrocene. All possible conformations for the Z conformer type (Z1, Z2, Z3 and Z4) and for the E conformer type (E1, E2, E3 and E4) were set as initial structures in optimization process and only conformers Z1, Z2, Z3, Z4, and E2 were obtained. The optimized structures and their stepwise interconversions were shown in Fig. 5.

It should be noted that Z1, Z2 and E2 conformers are enantiomers of Z4, Z3 and E2' (denoted as an enantiomer of E2) conform-

Table 2

Relative energies for conformers of compound **1**, computed at the B3LYP/LanL2DZ level of theory.

Reaction	E_{ZPE}^a	ΔE_{rel}^b
<i>E conformer</i>		
E2	−1309.4490550	6.03
<i>Z conformers</i>		
Z1 ^c	−1309.4586640	0.00
Z2 ^d	−1309.4503280	5.23
Z3 ^d	−1309.4503280	5.23
Z4 ^c	−1309.4586640	0.00
<i>Transition state</i>		
TS_Z1_Z2	−1309.4501520	5.34
TS_Z2_Z3	−1309.4483970	6.13
TS_Z2_E2	−1309.4414190	10.82

^a Total energies, computed with ZPVE corrections, in hartree.

^b Relative energies, computed with ZPVE corrections, in kcal/mol.

^c Conformers Z1 and Z4 are an enantiomeric pair.

^d Conformers Z2 and Z3 are an enantiomeric pair.

Table 3

Selected geometrical data for Z1 and E2 conformers.

Parameter ^a	Computed ^b	X-ray ^c	
		Enantiomer	Enantiomeric pair
<i>Z1 conformer</i>			
C1...C1'	3.389	3.272 ^d	3.272 ^e
O'...H	1.960	2.121 ^d	2.121 ^e
C1–C5–C6–O	−29.3	−32.8 ^d	−32.8 ^e
C1'–C5'–C6'–O'	−31.1	−27.4 ^d	−27.4 ^e
<i>E2 conformer</i>			
C1...C1'	3.411	3.271 ^f	3.271 ^g
O...H'	3.014	2.958 ^f	3.275 ^g
O'...H	3.197	3.841 ^f	3.827 ^g
O...O'	6.534	6.623 ^f	6.648 ^g
H...H'	7.902	7.187 ^f	7.402 ^g

^a Atomic numbering is shown in Fig. 4.

^b A single set of the optimized structure for each conformer was found.

^c The two X-ray crystallographic structures were found as enantiomeric pairs.

^d These values belong to the **1a** conformer.

^e These values belong to the **1a'** conformer.

^f These values belong to the **1b** conformer.

^g These values belong to the **1b'** conformer.

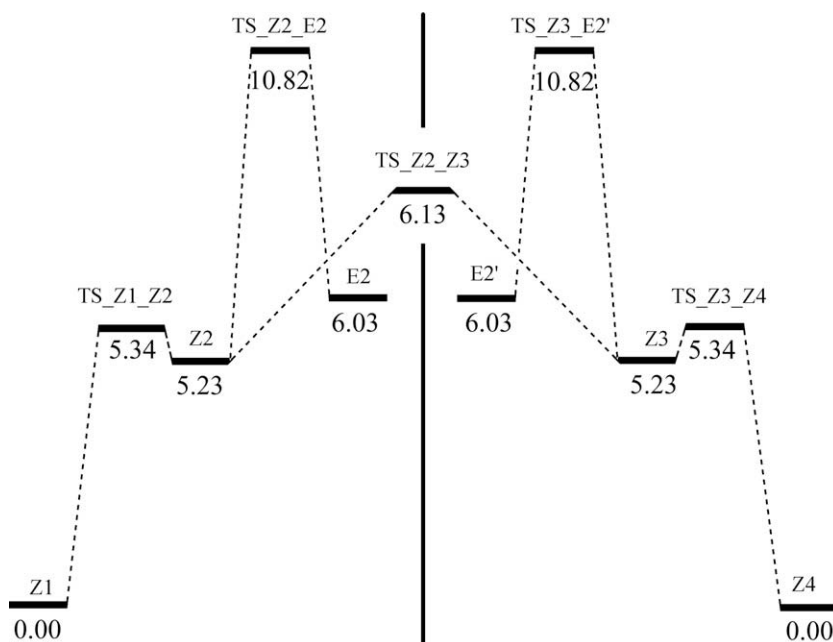


Fig. 7. Potential-energy profile of conversion pathways for all the conformers of compound **1** including their enantiomers, in kcal/mol.

ers, respectively. Conformers Z1, Z2, Z3 and Z4 are able to interconvert via three transition states TS_Z1_Z2, TS_Z2_Z3 and TS_Z3_Z4 (shown in Fig. 6). Conformers E2 and E2' are able to be converted from Z2 and Z3 conformers via transition states TS_Z2_E2 and TS_Z3_E2', respectively. Logically, the transition states TS_Z1_Z2 and TS_Z2_E2 are enantiomers of TS_Z3_Z4 and TS_Z2_E2', respectively. The transition state TS_Z2_E2 is located at an energy barrier for the conversion between Z2 and E2. Relative energies of all conformers and some transition states based on Z1 and Z4 (the most stable conformers) are shown in Table 2.

Conformers Z1 and Z4 co-exist as an enantiomeric pair Z1/Z4 which corresponds to the crystal structure of the enantiomeric pair **1a/1a'** (Fig. 1). As the E2 and E2' conformers are an enantiomeric pair, their total energies are, therefore, equivalent. The enantiomeric pair E2/E2' corresponds to the crystal structures **1b/1b'** (Fig. 2). The selected geometrical data for Z1 and E2 conformers and their enantiomeric pairs compared to their corresponding X-ray crystallographic data are shown in Table 3. The geometrical data for B3LYP/LanL2DZ optimized structures of Z1 and E2 conformers are in good agreement with the X-ray structures. However, we do not obtain the solid state structure of Z2/Z3 enantiomeric pair. Interestingly, Metzler-Nolte and colleagues have performed similar DFT calculations on conformations of disubstituted ferrocenyl amino acids and found that the most stable conformation possessed intramolecular hydrogen bonding while the least stable did not [30]. The calculations revealed that conformers with different H-bonding pattern have significantly different stabilities with a stabilization of the system by about 7 kcal/mol. Our calculations shown in Fig. 7 reveal that the differences in energy of Z1–Z2 and Z1–E2 are approximately 5 and 6 kcal/mol, respectively.

3.3. Rate, equilibrium constants and thermodynamics of conformation interconversion

The relative energies of all conformers of **1** in increasing order are Z1 (Z4) < Z2 (Z3) < E2 (E2'), where conformers in parentheses are their corresponding enantiomers. Three interconversion equilibria for all conformers namely Z1 ↔ Z2, Z2 ↔ E2 and Z2 ↔ Z3 are found. Energetics and thermodynamic properties of conver-

sions Z1 ↔ Z2 and Z2 ↔ E2 are equivalent to Z4 ↔ Z3 and Z3 ↔ E2', respectively. The interconversion diagram of all conformers of **1** and their enantiomers including their B3LYP/LanL2DZ optimized structures are shown in Fig. 5. As the logic of three enantiomeric pairs Z1/Z4, Z2/Z3 and E2/E2', their two equilibria Z1 ↔ Z2, and Z2 ↔ E2 are considered, the transition states TS_Z1_Z2 and TS_Z2_E2 are definitely enantiomers of TS_Z3_Z4 and TS_Z3_E2', respectively, as shown in Figs. 5 and 6.

Imaginary frequencies in cm^{-1} of all transition states obtained from frequency calculations are shown in Fig. 6. The transition state TS_Z2_Z3 belongs to the symmetry point group C_i and corresponds to the reaction path of interconversion between Z2 and its enantiomer, Z3. Geometries of all the transition states were confirmed by their single imaginary frequencies. Low imaginary frequencies of transition states TS_Z1_Z2 ($11.74i \text{ cm}^{-1}$) and TS_Z2_Z3 ($11.73i \text{ cm}^{-1}$) correspond to the rotation of their Cp rings and higher frequency of transition state TS_Z2_E2 ($38.43i \text{ cm}^{-1}$) corresponds to the rotation of amidophenyl side arm around its C5'–C6' axis. The imaginary frequencies of the Cp rings rotation are in the same order of magnitude of the Cp rings' rotation of previously reported ferrocene-peptides [31].

The reaction energies, thermodynamic quantities and equilibrium constants for conversions of Z1 ↔ Z2, Z2 ↔ Z3 and Z2 ↔ E2 are given in Table 4. These conformers can easily interconvert at

Table 4

Energies, thermodynamic properties and equilibrium constants of conversions between conformers of compound **1**, computed at the B3LYP/LanL2DZ level of theory.

Reaction	ΔE^a	$\Delta G_{298}^{a,b}$	$\Delta H_{298}^{a,b}$	K_{298}
Z1 ↔ Z2	5.23	3.32	5.48	3.68×10^{-3}
Z2 ↔ Z3 ^c	0	0	0	1.00×10^0
Z4 ↔ Z3 ^d	5.23	3.32	5.48	3.68×10^{-3}
Z2 ↔ E2	0.80	0.79	0.82	2.62×10^{-1}

^a In kcal/mol.

^b Obtained from the frequency calculations at 298.15 K, at the B3LYP/LanL2DZ level.

^c Conformers Z2 and Z3 are enantiomer.

^d Z4 ↔ Z3 is equivalent to Z1 ↔ Z2.

Table 5

Activation energies, tunneling coefficients, pre-exponential factor A and rate constants of conformers of compound **1**, computed at the B3LYP/LanL2DZ level of theory.

Reaction	k^a	Q_{TS}/Q_{REA}	A^b	$\Delta^\ddagger E^c$	k_{298}^d
Z1 \rightarrow Z2 path					
k_1 : Z1 \rightarrow TS_Z1_Z2	1.0	5.42×10^{-1}	3.37×10^{12}	5.34	4.09×10^8
k_{-1} : Z2 \rightarrow TS_Z1_Z2	1.0	2.16×10^{-2}	1.34×10^{11}	0.11	1.11×10^{11}
Z2 \rightarrow Z3 path					
k_2 : Z2 \rightarrow TS_Z2_Z3	1.0	1.01×10^{-2}	6.25×10^{10}	0.90	1.36×10^{10}
k_{-2} : Z3 \rightarrow TS_Z2_Z3	1.0	1.01×10^{-2}	6.25×10^{10}	0.90	1.36×10^{10}
Z2 \rightarrow E2 path:					
k_3 : Z2 \rightarrow TS_Z2_E2	1.0	1.15×10^{-1}	7.13×10^{11}	5.59	5.69×10^7
k_{-3} : E2 \rightarrow TS_Z2_E2	1.0	1.14×10^{-1}	7.07×10^{11}	4.79	2.18×10^8

$$^a k = 1 + \frac{1}{24} \left(\frac{h\nu}{k_B T} \right)^2.$$

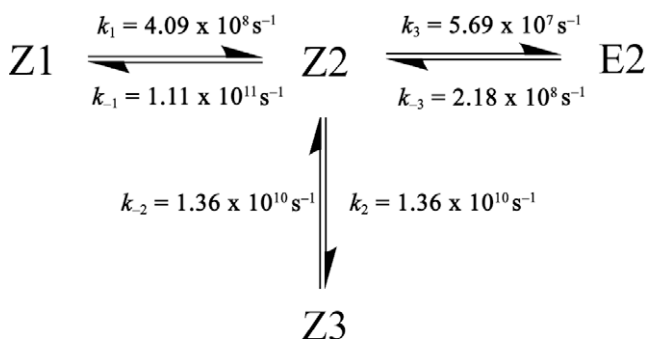
$$^b A = \frac{k_B T}{h} \frac{Q_{TS}}{Q_{REA}}, \text{ in } s^{-1}.$$

^c In kcal/mol.

^d Forward (k_1 , k_2 and k_3) and backward (k_{-1} , k_{-2} and k_{-3}) constants in s^{-1} , computed with ZPVE corrections, in kcal/mol.

higher temperature because activation energies for their corresponding equilibria are very low (less than 6 kcal/mol) as shown in Table 5. Both the forward and backward rate constants for these three conversions are fairly high being in the range of 5.69×10^7 – $1.11 \times 10^{11} s^{-1}$. The Z2 \leftrightarrow Z3 conversion is the equilibrium between enantiomeric pair and its forward and backward rate constants are therefore equivalent. The rate constants for conversion reactions between conformers Z1, Z2, E2 and enantiomer Z3 computed by Eq. (1) are presented in Scheme 2. Tunneling coefficients for these reactions are calculated to be 1.0 as shown in Table 5. This means that no tunneling effect has been detected.

It should be noted that conformer Z2 can undergo interconversion to conformer Z1 and E2 very fast and their energy differences are very small. Besides, the intramolecular hydrogen bonding interactions between O and H of the amide units should assist in stabilizing conformer Z1. Therefore, conformer Z1 is more favored in the crystallization liquor. This may be the reason why we could not obtain the solid state structure of conformer Z2. Only conformers Z1/Z4 and E2/E2' are observed in the crystal structures. The potential energy profile for interconversion of all conformers of **1**, Z1, Z2 and E2, and their respective enantiomers, Z4, Z3 and E2', is shown in Fig. 7. Therefore, the enantiomeric pair Z1/Z4 is the most stable chiral structure of compound **1** while chiral structures Z2/Z3 and E2/E2' are less stable, and their energies are comparable. As the conformer Z1 containing intramolecular hydrogen bonding comparing with relative energy of the conformer Z2 which contains no intramolecular hydrogen bonding, the intramolecular hydrogen bond energy in the conformer Z1 is approximately 5 kcal/mol.



Scheme 2. Rate constants for conversions of conformers Z1, Z2, E2 and enantiomer Z3.

4. Conclusion

X-ray crystallographic structures of synthesized bis(phenylamido)ferrocene, compound **1**, were determined in three forms: *cis*-conformer (**1a**) and *trans*-conformer. Structures **1a** and **1b** possessed their enantiomeric pairs **1a'** and **1b'**, respectively, in the crystal structures. B3LYP/LanL2DZ-optimized structures of all conformers of **1** were obtained as Z1, Z2 and E2 and their corresponding enantiomers Z4, Z3 and E2'. Conformers Z1 and E2 are found to be the most stable conformers. The structures of enantiomeric pairs Z1/Z4 and E2/E2' were in good agreement with crystal structures of **1a/1a'** and **1b/1b'**, respectively. Their relative energies were in order Z1 (Z4) < Z2 (Z3) < E2 (E2'). Three interconversion equilibria namely Z1 \leftrightarrow Z2, Z2 \leftrightarrow E2 and Z2 \leftrightarrow Z3 were found and their reaction energies, thermodynamic quantities and equilibrium constants were obtained. DFT calculations suggested that both thermodynamic and kinetic factors are involved in generating different conformations of bis(phenylamido)ferrocene.

Acknowledgments

Financial supports from the Thailand Research Fund (BRG5180016, RTA4880008 and RTA5080006) and the Center of Excellence for Innovation in Chemistry (PERCH-CIC), Commission on Higher Education, Ministry of Education are gratefully acknowledged.

Appendix A. Supplementary data

Cartesian coordinates of all the B3LYP/LanL2DZ optimized structures of conformers of compound **1** and related transition states. Supplementary data associated with this article can be found in the online version, at doi:10.1016/j.molstruc.2009.09.011.

References

- [1] T.J. Kealy, P.L. Pauson, *Nature* 168 (1951) 1039.
- [2] P. Štěpnička, *Ferrocenes; Ligands, Materials and Biomolecules*, John Wiley & Sons, Chichester, 2008.
- [3] P.D. Beer, J. Cadman, *Coord. Chem. Rev.* 205 (2000) 131.
- [4] P.D. Beer, E.J. Hayes, *Coord. Chem. Rev.* 240 (2003) 167.
- [5] C. Suksai, P. Leeladee, D. Jainuknan, T. Tuntulani, N. Muangsin, O. Chailapakul, P. Kongsaeere, C. Pakavatchai, *Tetrahed. Lett.* 46 (2005) 2765.
- [6] M. Oberhoff, L. Duda, J. Karl, R. Mohr, G. Erker, R. Fröhlich, M. Grehl, *Organometallics* 15 (1996) 4005.
- [7] A. Nomoto, T. Moriuchi, S. Yamazaki, A. Ogawa, T. Hirao, *Chem. Commun.* (1998) 1963.
- [8] K. Heinze, M. Schlenker, *Eur. J. Inorg. Chem.* (2004) 2974.
- [9] K.A. Mahmoud, H.B. Kraatz, *Chem. Eur. J.* 13 (2007) 5885.
- [10] H.B. Kraatz, *J. Inorg. Organomet. Polym. Mater.* 15 (2005) 83.
- [11] G.M. Sheldrick, *SHELXL-97; Program for the Refinement of Crystal Structures*, University of Göttingen, Germany, 1997.
- [12] L.J. Farrugia, *J. Appl. Crystallogr.* 32 (1999) 837.
- [13] I.J. Bruno, J.C. Cole, P.R. Edgington, M.K. Kessler, C.F. Macrae, P. McCabe, J. Pearson, R. Taylor, *Acta Crystallogr. B* 58 (2002) 389.
- [14] A.D. Becke, *J. Chem. Phys.* 98 (1993) 5648.
- [15] C. Lee, W. Yang, R.G. Parr, *Phys. Rev. B* 37 (1988) 785.
- [16] P.J. Hay, W.R. Wadt, *J. Chem. Phys.* 82 (1985) 270.
- [17] W.R. Wadt, P.J. Hay, *J. Chem. Phys.* 82 (1985) 284.
- [18] P.J. Hay, W.R. Wadt, *J. Chem. Phys.* 82 (1985) 299.
- [19] M.J. Frisch, G.W. Trucks, H.B. Schlegel, G.E. Scuseria, M.A. Robb, J.R. Cheeseman, J.A. Montgomery Jr., T. Vreven, K.N. Kudin, J.C. Burant, J.M. Millam, S.S. Iyengar, J. Tomasi, V. Barone, B. Mennucci, M. Cossi, G. Scalmani, N. Rega, G.A. Petersson, H. Nakatsuji, M. Hada, M. Ehara, K. Toyota, R. Fukuda, J. Hasegawa, M. Ishida, T. Nakajima, Y. Honda, O. Kitao, H. Nakai, M. Klene, X. Li, J.E. Knox, H.P. Hratchian, J.B. Cross, V. Bakken, C. Adamo, J. Jaramillo, R. Gomperts, R.E. Stratmann, O. Yazyev, A.J. Austin, R. Cammi, C. Pomelli, J.W. Ochterski, P.Y. Ayala, K. Morokuma, G.A. Voth, P. Salvador, J.J. Dannenberg, V.G. Zakrzewski, S. Dapprich, A.D. Daniels, M.C.O. Strain, Farkas, D.K. Malick, A.D. Rabuck, K. Raghavachari, J.B. Foresman, J.V. Ortiz, Q. Cui, A.G. Baboul, S. Clifford, J. Cioslowski, B.B. Stefanov, G. Liu, A. Liashenko, P. Piskorz, I. Komaromi, R.L. Martin, D.J. Fox, T. Keith, M.A. Al-Laham, C.Y. Peng, A. Nanayakkara, M. Challacombe, P.M.W. Gill, B. Johnson, W. Chen, M.W. Wong, C. Gonzalez, J.A. Pople, *Gaussian 03, Revision C.02*, Gaussian Inc., Wallingford, 2004.

- [20] J.W. Ochterski, Thermochemistry in Gaussian, Gaussian Inc., Pittsburgh, PA, 2000.
- [21] G. Bravo-Perez, J.R. Alvarez-Idaboy, A. Cruz-Torres, M.E. Ruiz, J. Phys. Chem. A 106 (2002) 4645.
- [22] V. Ruangpornvisuti, Int. J. Quant. Chem. 109 (2009) 275.
- [23] A. Suwattanamala, V. Ruangpornvisuti, Struct. Chem. 20 (2009) 619.
- [24] E.P. Wigner, Z. Phys. Chem. B 19 (1932) 203.
- [25] J.O. Hirschfelder, E. Wigner, J. Chem. Phys. 7 (1939) 616.
- [26] R.P. Bell, The Tunnel Effect in Chemistry, Chapman and Hall, London, 1980.
- [27] H.D. Flack, Acta Crystallogr. A 39 (1983) 876.
- [28] S.I. Kirin, U. Schatzschneider, S.D. Köster, D. Siebler, N. Metzler-Nolte, Inorg. Chim. Acta 362 (2009) 894.
- [29] J. Lapić, D. Siebler, K. Heinze, V. Rapić, Eur. J. Inorg. Chem. (2007) 2014.
- [30] S.I. Kirin, U. Schatzschneider, X. de Hatten, T. Weyhermüller, N. Metzler-Nolte, J. Organomet. Chem. 691 (2006) 3451.
- [31] K. Heinze, M. Beckmann, Eur. J. Inorg. Chem. (2005) 3450.



This article appeared in a journal published by Elsevier. The attached copy is furnished to the author for internal non-commercial research and education use, including for instruction at the authors institution and sharing with colleagues.

Other uses, including reproduction and distribution, or selling or licensing copies, or posting to personal, institutional or third party websites are prohibited.

In most cases authors are permitted to post their version of the article (e.g. in Word or Tex form) to their personal website or institutional repository. Authors requiring further information regarding Elsevier's archiving and manuscript policies are encouraged to visit:

<http://www.elsevier.com/copyright>



Contents lists available at ScienceDirect

Tetrahedron Letters

journal homepage: www.elsevier.com/locate/tetlet

Selective detection of pyrophosphate by new tripodal amine calix[4]arene-based Cu(II) complexes using indicator displacement strategy

Sarayut Watchasit^a, Arpadsara Kaowliw^a, Chomchai Suksai^{a,*}, Thawatchai Tuntulani^b, Wittaya Ngeontae^c, Chaveng Pakawatchai^d

^a Department of Chemistry and Center for Innovation in Chemistry, Faculty of Science, Burapha University, Chonburi 20131, Thailand

^b Department of Chemistry, Faculty of Science, Chulalongkorn University, Bangkok 10330, Thailand

^c Department of Chemistry and Center for Innovation in Chemistry, Faculty of Science, Khon Kean University, Khon Kean 40002, Thailand

^d Department of Chemistry and Center for Innovation in Chemistry, Faculty of Science, Prince of Songkla University, Songkhla 90112, Thailand

ARTICLE INFO

Article history:

Received 26 February 2010

Revised 12 April 2010

Accepted 23 April 2010

Available online 28 April 2010

ABSTRACT

Mono- and dinuclear Cu(II) complexes of *p*-tert-butylcalix[4]arene (**CuL1** and **CuL2**, respectively) were synthesized, and their anion recognition abilities were explored. Recognition is efficiently signaled through the displacement of pyrocatechol violet bound to the receptor. For **CuL2**, recognition selectivity is ascribed to the tuning of the distance between donor atoms of anion guests and their ability to encompass the Cu²⁺–Cu²⁺ distance within the cleft of **CuL2**. In addition, the preorganization of calix[4]arene in the cone conformation and steric hindrance of two bulky tripodal amine moieties are important factors in controlling the Cu²⁺–Cu²⁺ distance. These factors caused **CuL2** to recognize pyrophosphate selectively with respect to other inorganic anions in 80/20 (v/v%) MeCN/H₂O solution buffered with 10 mM HEPES at pH 6.4.

© 2010 Elsevier Ltd. All rights reserved.

Significant attention has been given to the development of anion sensing by indicator displacement assays (IDAs).¹ This method is a simple, convenient, and increasingly popular approach to naked-eye anion sensors because an indicator is bound to a receptor by non-covalent interactions. IDAs rely upon competition between the indicator and the analyte in the host cavity. Consequently, a receptor is designed to bind a target analyte with a desired affinity, and an indicator must have a weaker affinity with the receptor than the analyte. Importantly, the indicator must absorb or emit light differently upon binding to the host and being in free form in solution.

Generally, anion recognition in the aqueous system is very challenging due to the strong hydration effects of anions. The utilization of a metal complex as a binding site for anions has been found to be the most successful strategy.² Therefore, metal complexes are often used as IDA receptors.³ Normally, metal-bound ligands can bind anions more efficiently than water, allowing the detection of anions in aqueous solution. The metal center must have an unsaturated coordination sphere to accommodate the incoming anion guest.

IDA receptors for pyrophosphate (P₂O₇⁴⁻, PPI), the product of ATP hydrolysis and involved in DNA polymerization in biological reactions,⁴ have been developed by many research groups utilizing dinuclear zinc complexes of phosphotriesterase enzyme as the

receptor module.⁵ Recently, Hong and Fabbri reported that dinuclear Cu²⁺–DPA complexes can be employed as PPI fluorescence sensors using the IDA concept.⁶ The metal–metal distance is found to play a key role in analyte preference. In order to obtain the selectivity toward PPI over other anions, especially phosphate anion (PO₄³⁻), the metal–metal distance should not be less than 3.4 Å which is the Zn–Zn distance in phosphotriesterase.⁷

Our group is currently working on the synthesis of calix[4]arenes containing tripodal amine as the recognition unit for use as ionophores for ion selective electrodes (ISEs). The rigidity of calix[4]arenes in the cone conformation plays an important role by providing a specific cavity to recognize specific guest molecules, due to preorganization of its skeleton.⁸ The transannular distances in the lower rim of original calix[4]arene and its derivatives are in the range of 3.74–4.20 Å,⁹ which are longer than the Zn–Zn distance in the dinuclear zinc enzyme. Therefore, calix[4]arenes may be a suitable building block for PPI using IDA strategies. In addition, the side arms attached to the calix[4]arene can control the size and shape of the recognition cavity of calix[4]arene derivatives.¹⁰

In this work, calix[4]arenes containing a tripodal amine have been chosen as IDA receptors for PPI. Furthermore, we expected that steric interactions between the tripodal amine and the rigidity of the calix[4]arene framework would play crucial roles in optimizing the metal–metal distance and provide more selectivity toward PPI. Herein, we report the synthesis and characterization of ionophores based on calix[4]arenes **L1** and **L2** and their mononuclear and dinuclear complexes with CuCl₂ (**CuL1** and **CuL2**). We also

* Corresponding author. Tel.: +66 038 103067; fax: +66 038 393494.

E-mail address: jomjai@bua.ac.th (C. Suksai).

demonstrate that the dinuclear complex, **CuL2**, is a suitable receptor for indicator displacement assay of PPI.

Ionophores **L1** and **L2** were synthesized in two steps according to Scheme 1. The mono-calixaldehyde¹¹ and bis-calixaldehyde¹² (for **L1** and **L2**, respectively) were reacted with 2-[bis(2-pyridylmethyl)aminomethyl]aniline¹³ in dichloromethane, followed by in situ reduction with NaBH₄ in methanol to yield **L1** in 12% and **L2** in 20%, respectively. The HRMS-ESI spectra of **L1** and **L2** show parent peaks at *m/z* 1085.6671 and 1521.8715 assigned to the molecular ions [L+H]⁺ and provide evidence that the calix[4]arene derivatives are the 1:1¹⁴ and 1:2¹⁵ condensation products. The two calix[4]arene derivatives are in the cone conformation, as supported by their NMR spectra (Figs. S1–S4, Supplementary data). The ¹H NMR spectrum of **L1** was consistent with an asymmetric calix[4]arene structure. In particular, two pairs of doublets for the protons of the methylene bridges were observed.

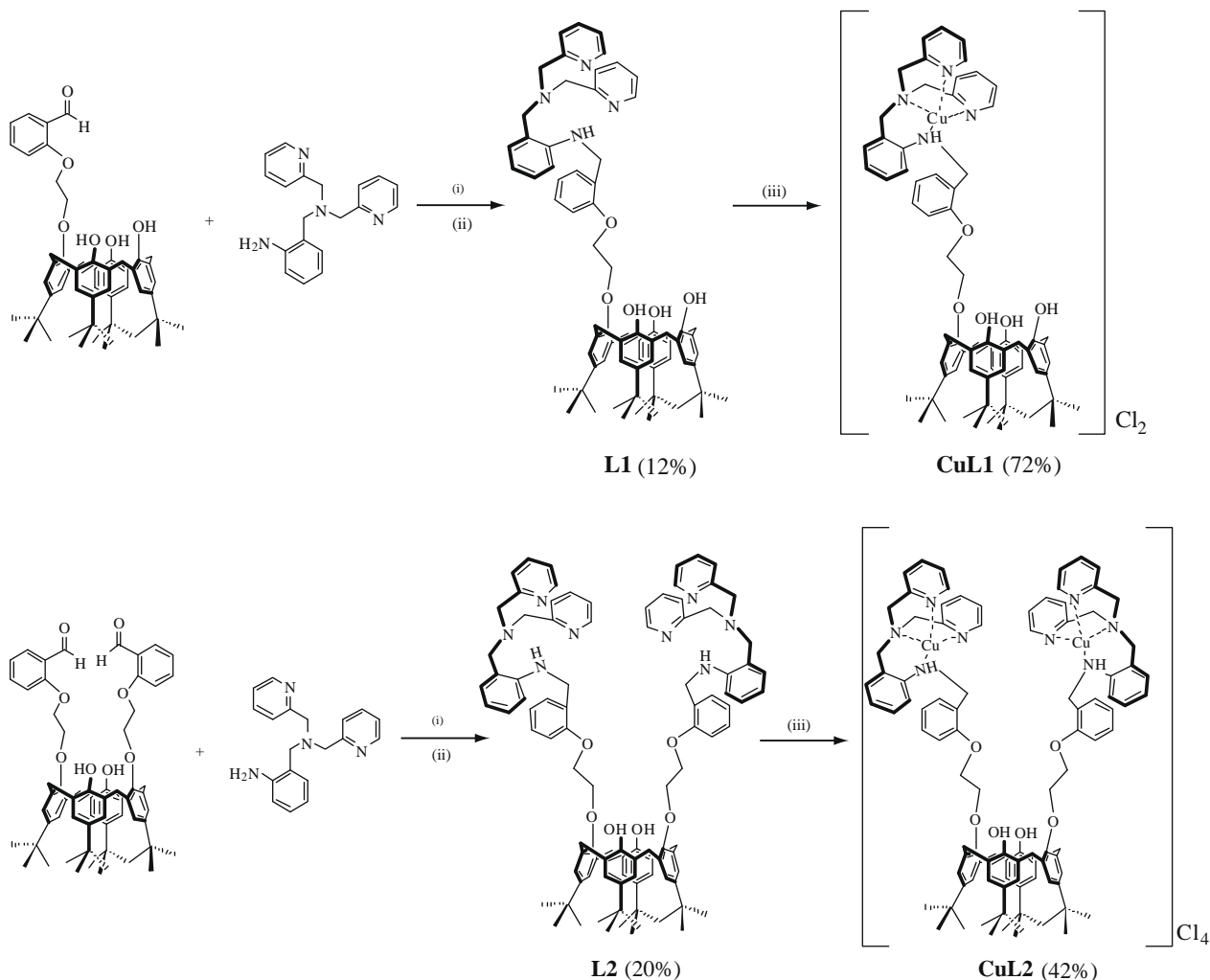
Two OH singlets were observed for **L1** at low field, 9.47 and 10.18 ppm (ratio 2:1). These strong downfield shifts for the OH protons are indicative of a circular hydrogen bond at the lower rim of these derivatives, in agreement with the results reported by Frkanec et al.¹⁶ The ¹H NMR spectrum of **L2** features a pair of doublets at 3.32 ppm and 4.43 ppm corresponding to the equatorial and the axial protons of the methylene bridging groups, respectively. We deduce that the cone structure is the major conformation of **L1** and **L2** in solution.

Addition of CuCl₂ to methanolic solutions of **L1** and **L2** gave green complexes of **CuL1** and **CuL2** in 72%¹⁷ and 42%¹⁸ yields,

respectively. The mass spectrum of **CuL1** shows the parent peak at *m/z* 1182.5424 which is assigned to the molecular ion of the mononuclear complex [CuL1Cl]⁺. For **CuL2**, the parent peak at *m/z* 1751.6365 corresponds to the molecular ion of the dinuclear complex [Cu₂L2Cl₃]⁺. A crystal of **CuL1** was obtained upon slow evaporation of a methanolic solution and the structure was determined by X-ray crystallography, Figure 1.¹⁹ It is clearly seen that the calixarene skeleton adopts a cone conformation. It should be noted that the phenolic hydrogen atoms are involved in strong intramolecular O–H...O hydrogen bonding with the neighboring oxygen atoms to stabilize the cone conformation, in agreement with the solution structure deduced from the ¹H NMR spectrum.

The crystal structure of **CuL1** also shows that two Cu(II) centers coordinate with four nitrogen donors from the tripodal amine unit and two chloride bridging ligands to give a distorted octahedral geometry. The substantial elongation of the axial Cu1–Cl1₂ and Cu1–N1 bonds [2.984 and 2.553(4) Å, respectively] compared to the equatorial Cu1–Cl1, Cu1–N2, Cu1–N3, and Cu1–N4 [2.278(12), 2.066(3), 1.977(4), and 1.994(4) Å, respectively] is caused by the active Jahn–Teller distortion of the Cu²⁺ ion. Interestingly, the mass spectrum of the **CuL1** complex suggests that it is a mononuclear complex in solution. This implies that the mononuclear complex of **CuL1** is the most stable species in solution while the dinuclear complex is the most stable species in the solid state.

In light of the crystal structure of **CuL1**, we expect that the dye and anions might occupy the bimetallic cleft of dinuclear complex **CuL2**. In this work, we chose pyrocatechol violet (PV) as a



Scheme 1. Synthetic procedures for **L1**, **L2**, **CuL1**, and **CuL2**. Reagents and conditions: (i) anhyd CH₂Cl₂, anhyd MgSO₄, rt; (ii) NaBH₄, CH₃OH, reflux; (iii) CuCl₂, MeOH, rt.

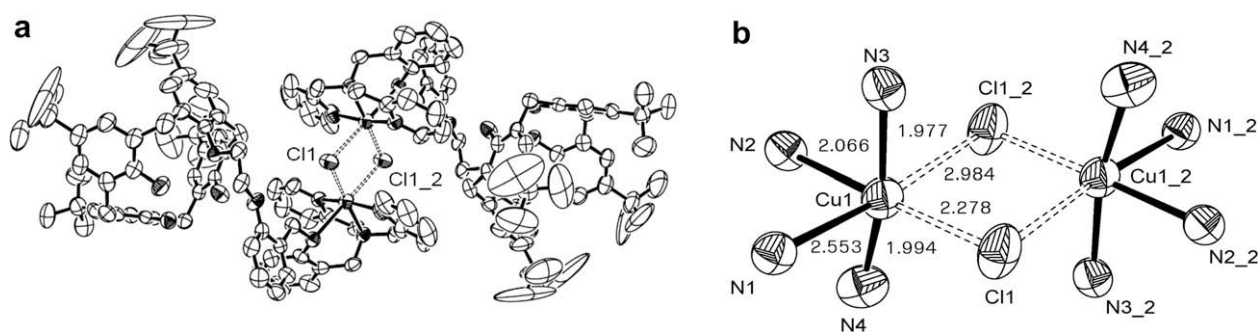


Figure 1. (a) ORTEP representation of the solid state structure of the dinuclear complex of **CuL1** with two bridging chloride ligands and (b) the coordination environment of Cu^{2+} in the complex. Thermal ellipsoids are drawn at 50% probability level (CCDC 767461).

competitive indicator.²⁰ The yellow solution of PV was prepared in 80% acetonitrile aqueous solution buffered with 10 mM HEPES pH 6.4, which was then titrated with increasing amounts of **CuL2** using the same solvent at 25 °C. It was found that addition of **CuL2** led to the disappearance of the absorption band of PV at 430 nm, with the simultaneous appearance of a new band at 670 nm and a color change from yellow to green (Fig. 2a). In addition, an isosbestic point was found at 488 nm, suggesting the presence of two equilibrium species. A Job plot (at 670 nm) was also obtained and suggested that the complex between **CuL2** and PV was formed with a 1:1 stoichiometry (inset of Fig. 2a). Using the Benesi–Hildebrand method, the association constant (K_a) between PV and **CuL2** was found to be $1.30 \times 10^4 \text{ M}^{-1}$.²¹

Upon addition of various anions (as tetrabutylammonium salts, 3 equiv) to the ensemble [**CuL2**·PV] solutions, only PPI was able to turn the color from green to yellow of the unbound dye, while other anions did not give rise to UV–vis spectral changes (Fig. 2b) or any color changes (Fig. 2c). Moreover, we also carried out displacement of PV from the **CuL2** cavity by phosphate containing biomolecules (AMP, ADP, and ATP). Results showed that both ADP and ATP were able to displace PV from the cleft of **CuL2**, whereas AMP was not (Fig. S5, Supplementary data). Therefore, **CuL2** possessed high selectivity toward PPI over other anions. We tried to change the dye from PV to fluorescein. However,

results of this ensemble did not show specific selectivity to any anions (Fig. S6, Supplementary data).

Titration of PPI with an ensemble solution [**CuL2**·PV] caused an absorbance increase around 430 nm and an absorbance decrease around 670 nm (hypsochromic shift), with a color change to yellow, revealing that the indicator was displaced from the cleft of **CuL2** by the analyte (Fig. 3). The UV–vis spectrum at 670 nm was completely saturated at 1.5 equiv of PPI. The binding constant between **CuL2** and PPI was estimated by the competitive spectrophotometric method²² and found to be $5.2 \times 10^5 \text{ M}^{-1}$. The electrospray ionization mass spectrum (positive mode) of **CuL2** complex with PPI showed a molecular ion peak at $m/z = 1824.57$ (Fig. S7, Supplementary data). The result thus confirmed the 1:1 complex species of **CuL2**:PPI.

Xu et al. have characterized crystallographically a ternary system complex of PPI with a mononuclear Cu^{2+} ion and a 2,2'-dipyridylamine (hdpa) ligand, $[\text{Cu}(\text{hdpa})]^{2+}$.²³ In this case, one PPI anion acted as the bridging ligand to bring two units of $[\text{Cu}(\text{hdpa})]$ together, forming a dinuclear complex. Simultaneously, two PPI ions coordinating to the oxygen atoms of a discrete dinuclear complex also acted as the bridging atoms to hold those two discrete dimeric species together to form a tetranuclear complex. Compared to our system, we assume that PPI is bound within the bimetallic cleft of **CuL2**. Two oxygen atoms on each phosphorus of PPI coordinated

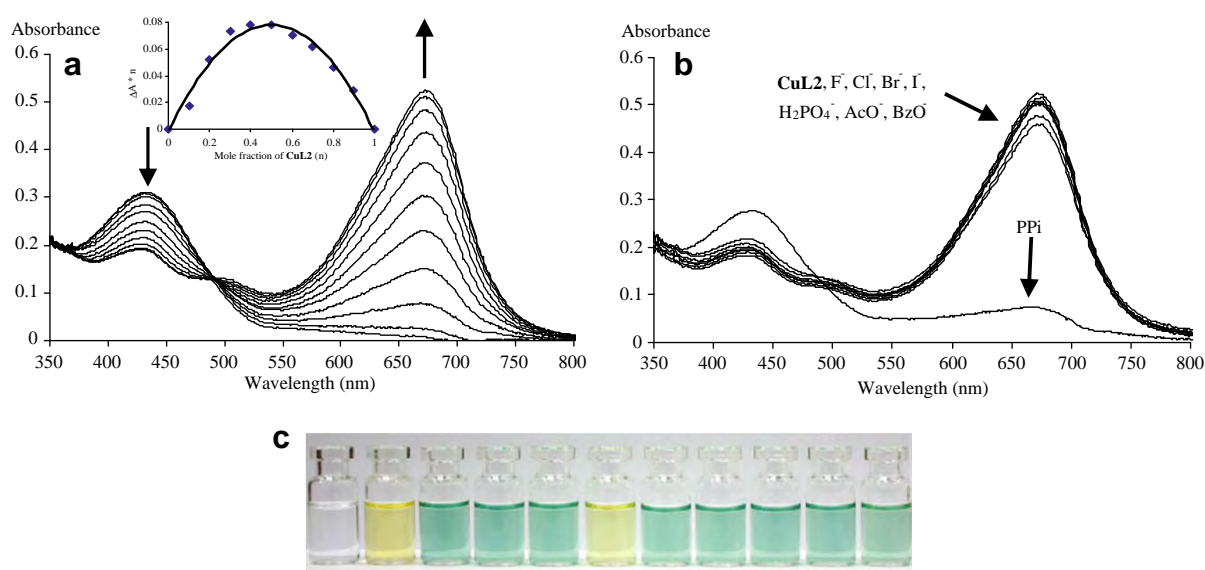


Figure 2. (a) UV–vis spectra obtained by addition of **CuL2** (400 μM) to PV (20 μM) solution; (b) UV–vis spectra obtained by addition of various anions (3 equiv of tetrabutylammonium salts) to an ensemble solution [**CuL2**·PV] (20 μM); and (c) color changes of the ensemble [**CuL2**·PV] 20 μM after addition of various anions (3 equiv of tetrabutylammonium salts). From left to right: **CuL2**, PV, [**CuL2**·PV], H_2PO_4^- , AcO^- , PPI, BzO^- , I^- , Br^- , Cl^- , and F^- . All experiments were carried out in 80/20 (v/v) MeCN/ H_2O solution buffered with 10 mM HEPES at pH 6.4.

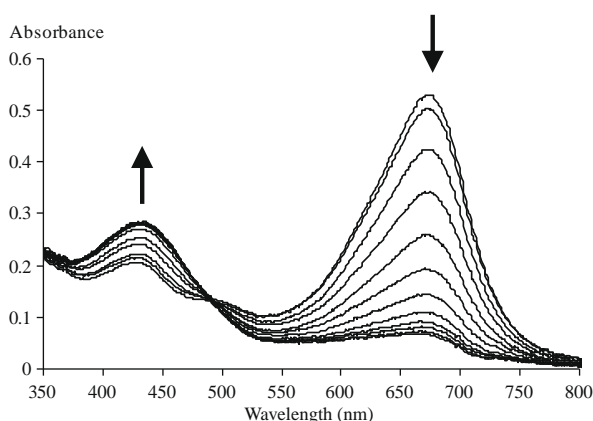


Figure 3. UV-vis spectra obtained by addition of PPI (400 μ M) to an ensemble solution of [CuL2-PV] (20 μ M) in 80/20 (v/v) MeCN/H₂O solution buffered with 10 mM HEPES at pH 6.4.

through one Cu²⁺ ion, which was similar to the binding mode of PPI with the dinuclear DPA-2Zn²⁺ derivatives reported by Yoon and co-workers²⁴ and Hong and co-workers.^{5b}

Similar experiments have been run with the mononuclear CuL1 complex. The results showed that in the presence of any anions in an ensemble solution of [CuL1-PV] the yellow solution of the unbound dye was not observed (Fig. S8, Supplementary data). This result strongly supports the fact that the cooperative action of two Cu²⁺ ions in solution is required for selective sensing of PPI.

In conclusion, we have successfully synthesized mono- and dinuclear Cu(II) complexes of calix[4]arene containing a tripodal amine, CuL1 and CuL2. CuL2 was demonstrated to be a remarkable IDA receptor for PPI. A rationale to account for the selectivity of CuL2 toward PPI requires matching of the distance between the donor atoms of PPI with the Cu²⁺–Cu²⁺ distance in the CuL2 cavity. In addition, the preorganization of calix[4]arene in the cone conformation and steric hindrance between the two bulky tripodal amine parts are the most important factors controlling the Cu²⁺–Cu²⁺ distance. This resulted in selective recognition of CuL2 toward PPI over other anions. Further studies are underway in our laboratory to prepare anion selective electrodes from CuL2.

Acknowledgments

Financial support from The Thailand Research Fund (MRG5380064 and RTA5080006), a Grant from the Faculty of Science, Burapha University, and Center for Innovation in Chemistry (PERCH-CIC) and Commission on Higher Education, Ministry of Education, are gratefully acknowledged.

Supplementary data

Supplementary data (additional ¹H and ¹³C NMR spectra of L1 and L2, and displacement results of CuL1 with various anions are available) associated with this article can be found, in the online version, at doi:10.1016/j.tetlet.2010.04.095.

References and notes

- (a) Wiskur, S. L.; Ait-Haddou, H.; Lavigne, J. J.; Anslyn, E. V. *Acc. Chem. Res.* **2001**, *34*, 963–972; (b) Nguyen, B. T.; Anslyn, E. V. *Coord. Chem. Rev.* **2006**, *250*, 3118–3127.
- (a) Kruppa, M.; König, B. *Chem. Rev.* **2006**, *106*, 3520–3560; (b) Suksai, C.; Tuntulani, T. *Chem. Soc. Rev.* **2003**, *32*, 192–202; (c) Martinez-Manez, R.; Sancenon, F. *Chem. Rev.* **2003**, *103*, 4419–4476; (d) Suksai, C.; Tuntulani, T. *Top. Curr. Chem.* **2005**, *255*, 163–198; (e) Kruppa, M.; Mandl, C.; Miltzschitzky, S.; König, B. *J. Am. Chem. Soc.* **2005**, *127*, 3362–3365; (f) Lim, M. H.; Wong, B. A.; Pitcock, W. H.; Mokshagundam, D.; Baik, M.-H.; Lippard, S. J. *Am. Chem. Soc.* **2006**, *128*, 14364–14373; (g) Salo, T. M.; Helaja, J.; Koskinen, A. M. P. *Tetrahedron Lett.* **2006**, *47*, 2977–2980; (h) Lee, D. H.; Im, J. H.; Son, S. U.; Chung, Y. K.; Hong, J.-I. *J. Am. Chem. Soc.* **2003**, *125*, 7752–7753; (i) Guo, Z.; Zhu, W.; Tian, H. *Macromolecules* **2010**, *43*, 739–744.
- (a) Amendola, V.; Bergamaschi, G.; Buttafava, A.; Fabbri, L.; Monzani, E. *J. Am. Chem. Soc.* **2010**, *132*, 264–268; (b) Zhang, T.; Anslyn, E. A. *Tetrahedron* **2004**, *60*, 11117–11124; (c) Hanshaw, R. G.; Hilbert, S. M.; Jiang, H.; Smith, B. D. *Tetrahedron Lett.* **2004**, *45*, 8721–8724; (d) Zhang, T.; Anslyn, E. V. *Org. Lett.* **2007**, *9*, 1627–1629; (e) Swamy, K. M. K.; Kwon, S. K.; Lee, H. N.; Kumar, S. M. S.; Kim, J. S.; Yoon, J. *Tetrahedron Lett.* **2007**, *48*, 8683–8686; (f) Jang, H. H.; Yi, S.; Kim, M. H.; Kim, S.; Lee, N. H.; Han, M. S. *Tetrahedron Lett.* **2009**, *50*, 6241–6243; (g) Zhang, S.; Glass, T. E. *Tetrahedron Lett.* **2010**, *51*, 112–114; (h) Yin, C.; Huo, F.; Yang, P. *Sens. Actuators, B* **2005**, *109*, 291–299; (i) Fabbri, L.; Marcotte, N.; Stomeo, F.; Taglietti, A. *Angew. Chem., Int. Ed.* **2002**, *41*, 3811–3814; (j) McDonough, M. J.; Reynolds, A. J.; Lee, W. Y. G.; Jolliffe, K. A. *Chem. Commun.* **2006**, 2971–2973.
- Ronaghi, M.; Karamohamed, S.; Pettersson, B.; Uhlén, M.; Nyrén, P. *Anal. Biochem.* **1996**, *242*, 84–89.
- (a) Kim, S. K.; Lee, D. H.; Hong, J.-I.; Yoon, J. *Acc. Chem. Res.* **2009**, *42*, 23–31; (b) Lee, J. H.; Park, J.; Lah, M. S.; Chin, J.; Hong, J.-I. *Org. Lett.* **2007**, *9*, 3729–3731; (c) Morgan, P. B.; He, S.; Smith, R. C. *Inorg. Chem.* **2007**, *46*, 9262–9266; (d) Cho, H. K.; Lee, D. H.; Hong, J.-I. *Chem. Commun.* **2005**, 1690–1692; (e) Mangalum, A.; Smith, R. C. *Tetrahedron* **2009**, *65*, 4298–4303; (f) Lee, D. H.; Kim, S. Y.; Hong, J.-I. *Tetrahedron Lett.* **2007**, *48*, 4477–4480.
- (a) Hong, J.-I.; Kim, S. Y. *Tetrahedron Lett.* **2009**, *50*, 1951–1953; (b) Fabbri, L.; Marcotte, N.; Stomeo, F.; Taglietti, A. *Angew. Chem., Int. Ed.* **2002**, *41*, 3811–3814.
- Benning, M. M.; Shim, H.; Raushel, F. M.; Holden, H. M. *Biochemistry* **2001**, *40*, 2712–2722.
- (a) Gutsche, C. D.; Reddy, P. A. *J. Org. Chem.* **1991**, *56*, 4783–4791; (b) Dijkstra, P. J.; Brunink, J. A. J.; Bugge, K.-E.; Reinhoudt, D. N.; Harkema, S.; Ungaro, R.; Ugozzoli, F.; Ghidini, E. *J. Am. Chem. Soc.* **1989**, *111*, 7567–7575; (c) Froidevaux, P.; Harrowfield, J. M.; Sobolev, A. N. *Inorg. Chem.* **2000**, *39*, 4678–4687.
- Lipkowitz, K. B.; Pearl, G. *J. Org. Chem.* **1993**, *58*, 6729–6736.
- (a) Scheeder, J.; van Duynhoven, J. P. M.; Engbersen, J. F. J.; Reinhoudt, D. N. *Angew. Chem., Int. Ed.* **1996**, *35*, 1092–1093; (b) Kim, S. K.; Kim, S. H.; Kim, H. J.; Lee, S. H.; Ko, J.; Bartsch, R. A.; Kim, J. S. *Inorg. Chem.* **2005**, *44*, 7866–7875; (c) Chang, K.-C.; Su, I. -H.; Senthilvelan, A.; Chung, W.-S. *Org. Lett.* **2007**, *9*, 3363–3366.
- Groenen, L. C.; Ruël, B. H. M.; Casnati, A.; Verboom, W.; Pochini, A.; Ungaro, R.; Reinhoudt, D. N. *Tetrahedron* **1991**, *47*, 8379–8384.
- Navakun, K.; Tuntulani, T.; Ruangpornvisuti, V. *J. Inclusion Phenom.* **2000**, *38*, 113–122.
- Burdette, S. C.; Frederickson, C. J.; Bu, W.; Lippard, S. J. *J. Am. Chem. Soc.* **2003**, *125*, 1778–1787.
- Ionophore L1, ¹H NMR (400 MHz, CDCl₃, ppm): δ 10.20 (s, 1H, –OH), 9.49 (s, 2H, –OH), 8.44 (d, 2H, J = 4.0 Hz, ArH), 7.49 (t, 2H, J = 6.0 Hz, ArH), 7.37 (d, 2H, J = 4.0 Hz, ArH), 7.34 (d, 2H, J = 8.0 Hz, ArH), 7.13 (s, 2H, ArH), 7.12 (s, 1H, ArH), 7.07 (d, 2H, J = 2.0 Hz, ArH), 7.05 (s, 2H, ArH), 7.03 (s, 2H, ArH), 7.02 (s, 2H, ArH), 6.94 (m, 2H, ArH), 8.82 (s, 1H, –NH–), 6.54 (t, 1H, J = 7.6 Hz, ArH), 6.40 (d, 1H, J = 8.0 Hz, ArH), 4.70 (d, 2H, J = 3.2 Hz, –CH₂–NH–), 4.64 (s, 4H, –O–CH₂–O–), 4.53 (d, 2H, J = 12.8 Hz, Ar–CH₂–Ar), 4.24 (d, 2H, J = 13.6 Hz, Ar–CH₂–Ar), 3.83 (s, 4H, –CH₂–N), 3.69 (s, 2H, –CH₂–N), 3.41 (dd, 4H, J = 7.6 Hz, J = 12.8, 13.6 Hz, Ar–CH₂–Ar), 1.23 (s, 36H, p -tert-butyl); ¹³C NMR (100 MHz, CDCl₃, ppm): δ 159.24, 156.11, 149.12, 149.04, 148.39, 148.29, 148.09, 147.85, 143.50, 143.12, 136.30, 133.61, 130.94, 128.74, 128.53, 128.12, 128.07, 127.75, 127.69, 126.56, 125.82, 125.71, 125.66, 123.18, 121.90, 121.51, 121.10, 115.32, 110.80, 110.20, 74.78, 60.13, 58.47, 41.73, 34.26, 33.99, 33.93, 33.00, 32.18, 31.50, 31.25; HRMS-ESI: [M+H]⁺ calcd for C₇₂H₈₄N₄O₈, 1085.6670; found 1085.6671.
- Ionophore L2, ¹H NMR (400 MHz, CDCl₃, ppm): δ 8.42 (d, 4H, J = 4.0 Hz, ArH), 7.65 (d, 2H, J = 2.4 Hz, ArH), 7.46 (m, 4H, ArH), 7.35 (d, 2H, J = 7.6 Hz, 2H, ArH), 7.30 (s, 4H, ArH), 7.19 (m, 2H, ArH), 7.06 (m, 8H, ArH), 7.05 (m, 2H, ArH), 6.95 (d, 4H, J = 8.4 Hz, ArH), 6.89 (s, 4H, ArH), 6.86 (d, 2H, J = 7.2 Hz, ArH), 6.72 (s, 2H, –NH–), 6.54 (m, 2H, ArH), 6.44 (d, 2H, J = 8.0 Hz, ArH), 4.53 (d, 4H, J = 4.8 Hz, –CH₂–NH–), 4.44 (d, 4H, J = 12.8 Hz, Ar–CH₂–Ar), 4.35 (s, 8H, –CH₂–O–), 3.80 (s, 8H, –CH₂–N), 3.68 (s, 4H, –CH₂–N), 3.33 (d, 4H, J = 13.2 Hz, Ar–CH₂–Ar), 1.26 (s, 18H, p -tert-butyl), 1.03 (s, 18H, p -tert-butyl); ¹³C NMR (100 MHz, CDCl₃, ppm): δ 159.23, 156.24, 150.35, 149.73, 149.07, 148.21, 147.34, 141.69, 136.29, 133.12, 130.97, 128.77, 128.56, 128.52, 127.93, 127.63, 125.72, 125.20, 123.20, 121.91, 121.55, 120.71, 115.35, 110.78, 110.32, 74.16, 66.65, 60.16, 58.47, 41.76, 34.04, 33.84, 31.83, 31.66, 31.10; HRMS-ESI: [M+H]⁺ calcd for C₁₀₀H₁₁₂N₈O₆, 1521.8705; found 1521.8715.
- Frkanec, L.; Višnjevac, A.; Kojić-Prodić, B.; Žinić, M. *Chem. Eur. J.* **2000**, *6*, 442–453.
- CuL1: A methanolic solution of CuCl₂·2H₂O (24 mg, 0.14 mmol) in 5 mL CH₃OH was added to a suspension of L1 (0.108 g, 0.09 mmol) in methanol giving a deep-green solution. The solution was allowed to stand at room temperature. After 1 week, green block-shaped X-ray diffraction quality single crystals of CuL1 were obtained (80 mg, 73%). HRMS-ESI: [M+Cl]⁺ calcd for C₇₂H₈₄ClCuN₄O₈, 1182.5426; found 1182.5424.
- CuL2: A methanolic solution of CuCl₂·2H₂O (26 mg, 0.15 mmol) was added to a methanolic suspension of ionophore L2 (110.9 mg, 0.06 mmol); the color of the solution changed to deep-green immediately. After standing the green solution at room temperature for 1 week, the deep-green solid appeared. This was filtered and washed with MeOH to give CuL2 in 42% yield (111 mg). HRMS-ESI: [M+Cl]⁺ calcd for C₁₀₀H₁₁₂Cl₃Cu₂N₈O₆, 1751.6362; found 1751.6365.

19. Crystal data for **CuL1**: $C_{146}H_{180}Cl_2Cu_2N_8O_{14}$, $M_r = 2539.99$, $T = 293(2)$ K, triclinic, space group $P\bar{1}$ $a = 13.3699(10)$, $b = 15.5074(12)$, $c = 17.9970(13)$ Å, $\alpha = 94.853^\circ$ (2), $\beta = 90.013^\circ$ (2), $\gamma = 99.694^\circ$ (2), $V = 3664.5(5)$ Å³, $\rho_{\text{calcd}} = 1.151$ g cm⁻³, $\mu = 0.422$ mm⁻¹, $Z = 1$, reflections collected: 50619, independent reflections: 17717 ($R_{\text{int}} = 0.0556$), final R indices [$I > 2\sigma I$]: $R1 = 0.0974$, $wR2 = 0.2936$, R indices (all data): $R1 = 0.1511$, $wR2 = 0.3344$. Crystallographic data for **CuL1** are available upon request from the Cambridge Crystallographic Data Base (CCDC 767461).
20. All spectrophotometric titrations were performed in 80/20 (v/v) MeCN/H₂O solution buffered with 10 mM HEPES at pH 6.4, thermostated at 25 °C. Receptor/indicator affinity constants were determined by adding aliquots of a 400 μM **CuL2** complex solution to a 20 μM solution of PV. After each addition, the UV–vis absorption spectra of the indicator solution were recorded in a quartz cuvette. Similar titration experiments were performed with PPI. In typical titrations, aliquots of PPI (400 μM) were added to an ensemble solution (20 μM) of [**CuL2**.PV].
21. Roy, P.; Dhara, K.; Manassero, M.; Ratha, J.; Banerjee, P. *Inorg. Chem.* **2007**, *46*, 6405–6412.
22. Niikura, K.; Bisson, A. P.; Anslyn, E. V. *J. Chem. Soc., Perkin Trans. 2* **1999**, 1111–1114.
23. Xu, J.-Y.; Tian, J.-L.; Zhang, Q.-W.; Zhao, J.; Yan, S.-P.; Liao, D.-Z. *Inorg. Chem. Commun.* **2008**, *11*, 69–72.
24. Jang, Y. J.; Jun, E. J.; Lee, Y. J.; Kim, Y. S.; Kim, J. S.; Yoon, J. J. *Org. Chem.* **2005**, *70*, 9603–9606.



Bulk optode sensors for batch and flow-through determinations of lead ion in water samples

Chantana Bualom^a, Wittaya Ngeontae^b, Sira Nitayanontakit^a, Passapol Ngamukot^a,
Apichat Imyim^a, Thawatchai Tuntulani^a, Wanlapa Aeungmaitrepirom^{a,*}

^a Department of Chemistry, Faculty of Science, Chulalongkorn University, Bangkok 10330, Thailand

^b Center for Innovation in Chemistry, Department of Chemistry, Faculty of Science, Khon Kaen University, Khon Kaen 40002, Thailand

ARTICLE INFO

Article history:

Received 23 March 2010

Received in revised form 11 May 2010

Accepted 12 May 2010

Available online 19 May 2010

Keywords:

Bulk optode

Lead ion

Lead IV

ETH 5294

ABSTRACT

A sensitive optode consisting of highly lead-selective ionophore (Lead IV), proton-selective chromoionophore (ETH 5294) and lipophilic anionic sites (KTPCIPB) in plasticized polyvinyl chloride (PVC) membrane was fabricated. The optode membranes were used for determination of Pb²⁺ by absorption spectrophotometry in batch and flow-through systems. The influence parameters such as pH, type of buffer solution, response time and concentration of regenerating solution were optimized. The membrane responded to Pb²⁺ by changing its color from blue to pinkish purple in Tris buffer containing different concentration of Pb²⁺ at pH 7.0. The optode provided the response range of 3.16×10^{-8} to 5.00×10^{-5} mol L⁻¹ Pb²⁺ with the detection limit of 2.49×10^{-8} mol L⁻¹ in the batch system within the response time of 30 min. The dynamic range of 1.26×10^{-8} to 3.16×10^{-5} mol L⁻¹ Pb²⁺ with detection limit of 8.97×10^{-9} mol L⁻¹ were obtained in the flow-through system within the response time of 15 min. Moreover, the proposed optode sensors showed good selectivity towards Pb²⁺ over Na⁺, K⁺, Mg²⁺, Cd²⁺, Hg²⁺ and Ag⁺. It was successfully applied to determine Pb²⁺ in real water samples and the results were compared with well-established inductively coupled plasma optical emission spectrometry (ICP-OES). No significant different value ($t_{\text{critical}} = 4.30 > t_{\text{exp}} = 1.00\text{--}3.42$, $n = 3$ at 95% of confidence level) was found.

© 2010 Elsevier B.V. All rights reserved.

1. Introduction

Many countries worldwide are increasing awareness of environmental problems and seeking the way to decrease environmental pollutions. In particular, the contamination of heavy metals in environment is one of the serious problems because even low contents of heavy metal can cause harmful effects to plants, animals and human. Among heavy metals, lead is a common toxic pollutant in the environment as a result of its use in storage batteries, cable sheath, gasoline antiknock products and paint pigments. The widespread uses cause environmental and health problems such as the cumulative poison and the retention of lead in the body for long periods [1].

The majority of lead determinations at the ppm–ppb levels are usually performed by using atomic absorption spectrometry (AAS). However, the detection limit of the instrument is not suitable with the presence of lead in environmental samples. Thus, the preconcentration step followed by spectrometric determinations and flow injection spectrometric methods have been employed [2–6]. Thus,

more sophisticated techniques such as inductively coupled plasma optical emission spectrometry (ICP-OES) and inductively coupled plasma-mass spectrometry (ICP-MS) have been employed due to higher sensitivity but these instruments are costly and need specific maintenance. In addition to the existing common methods, lead ion-selective electrodes (ISEs) based on neutral ionophores containing oxygen, nitrogen and sulphur donor atoms have been reported [7–14]. Nevertheless, most of ISEs possessed serious interferences from various cations. Therefore, the highly sensitive, selective and rapid method for determination of trace level of lead is desirable.

Chemical optical sensors (optode) offer advantages such as simple preparation and procedure, relatively fast response, wide response range, reasonable selectivity and high sensitivity [15–16]. Recently, reviews covering the principles and mechanisms of bulk optode have been published [17–19]. The immobilization in various sensing reagents of optode membranes have been developed for many analytically relevant ions, especially heavy metal ions. Examples of optode membranes are 2-(5-bromo-2-pyridylazo)-5-(diethylamino)phenol in Nafion for nickel ion [20], fatty hydroxamic acid in polymethylmethacrylate for vanadium ion [21], 2-hydroxy-1-(2-hydroxy-5-methylphenylazo)-4-naphthalenesulfonic acid in agarose membrane for copper ion

* Corresponding author. Tel.: +66 2 218 7607; fax: +66 2 254 1309.
E-mail address: wanlapa.a@chula.ac.th (W. Aeungmaitrepirom).

[22], zincon-tetraoctylammonium immobilized on triacetyl-cellulose membrane for zinc ion [23]. However, a few bulk optodes for determination of Pb^{2+} have been published to date. Examples of ionophores in optode membranes used for determination of Pb^{2+} by absorption spectrophotometry or reflectance techniques are dioxaoctanediamide derivative plus protonated Nile blue [24], dithizone [25], oxodiamide derivative [26], and 1,10-dibenzyl-1,10-diaza-18-crown-6 with 1-(2-pyridylazo)-2-naphthol as chromoionophore [27]. In addition, the detection using fluorescence and phosphorescence spectrophotometry was also reported. For example, compounds such as tetra-substituted aluminum 2,3-naphthalocyanine dyes [28], 3,3',5,5'-tetramethyl-*N*-(9-anthrylmethyl)benzidine [29], *tert*-butylcalix[4]arene-tetrakis(*N,N*-dimethylthioacetamide) [30], 4-hydroxysalophen [31], and quinolinesulphonic acid derivatives [32] have been employed as fluorophore and phosphorophore for metal ion detection.

Normally, a design of ion-selective optode membrane for lead ion is focused on the choice of ionophore/chromoionophore. However, the practical use of bulk optode membranes for lead in real water samples, especially in a flow-through system has rarely been seen. In this work, a Pb^{2+} selective thin film optode incorporating *tert*-butylcalix[4]arene-tetrakis(*N,N*-dimethylthioacetamide) or Lead IV as lead-selective ionophore, ETH 5294 as proton-selective chromoionophore and potassium tetrakis (4-chlorophenyl) borate as lipophilic anionic sites plasticized in PVC membrane was manually fabricated by a simple casting technique. The membranes were used in the quantification of Pb^{2+} in various types of water sample using a common UV–vis spectrophotometer combined with a simple lab-made flow-through cell. The validation result was also demonstrated in comparison with a standard method.

2. Experimental

2.1. Chemicals and reagents

For the membrane preparation, high molecular weight poly(vinyl chloride) or PVC, bis(2-ethylhexyl)sebacate (DOS), potassium tetrakis(4-chlorophenyl)borate (KTPClPB), *tert*-butyl calix[4]arene-tetrakis(*N,N*-dimethylthioacetamide) shown in Fig. 1(a), 9-(diethylamino)-5-(octadecanoylimino)-5H-benzo[a]phenoxazine (ETH 5294) shown in Fig. 1(b) and tetrahydrofuran (THF) were purchased from Fluka. The solvents were of analytical-reagent grade and used without further purification. All aqueous solutions were prepared using type quality water produced by Milli-Q purify-cation system (Millipore) with a specific resistivity of $18 \text{ M}\Omega \text{ cm}^{-1}$.

Buffer solutions ($1.0 \times 10^{-3} \text{ mol L}^{-1}$) used were (i) Tris buffer (tris(hydroxyl methyl)-aminomethane, adjusted with 0.01 mol L^{-1} HCl), (ii) acetate buffer (sodium acetate adjusted with 0.01 mol L^{-1} NaOH) and (iii) citrate buffer (tri sodium citrate adjusted with 0.01 mol L^{-1} citric acid).

A stock solution of $1.0 \times 10^{-2} \text{ mol L}^{-1} \text{ Pb}^{2+}$ was prepared by dissolving $\text{Pb}(\text{NO}_3)_2$ in Milli-Q water in an appropriate volume. Test solutions were prepared by serial dilution of the stock solution with the buffer solution. The Pb^{2+} solutions were buffered in order to provide nearly constant ionic strength. The activity coefficients in the aqueous solution were assumed to be constant so that the total concentration of measuring ions was used for calculations. The glassware was pretreated with 5% HNO_3 overnight before used.

2.2. Apparatus

The visible spectra and absorbance measurements were recorded on a Hewlett Packard diode array spectrophotometer, model 8453 (USA). Inductively coupled plasma optical emission spectrometric measurements were performed on Perkin Elmer, model PLASMA-1000 (USA). The pH values of sample solutions were determined with a pH glass electrode, Orion 2 star, model 9162BNWP and a pH meter, Orion, OR3557 (Taiwan).

A lab-made flow-through cell (Fig. 2) consisted of a rectangular $38 \text{ mm} \times 30 \text{ mm}$ acrylic block of 10 mm height with cylindrical opening of 12 mm diameter in the middle (a), rectangular $38 \text{ mm} \times 30 \text{ mm}$ acrylic block of 10 mm height as optical window with inlet (b) and outlet tubes (c), rectangular $20 \text{ mm} \times 25 \text{ mm}$ vacuum plastic sheet as seal gasket with elliptical opening of 17 mm (d), cover glass slide as support for optode membranes (e). All parts of the flow-through cell were fixed with screws for clamping the block (f). The flow-through cell system consisted of a peristaltic pump Ismatec model ISM 827, the lab-made flow-through cell, the connecting Tygon tube R3607 (2.79 mm i.d.), and a Teflon FEP tube (0.50 mm i.d.). Experiments were performed by setting the flow-through cell in the optical path of the spectrophotometer. The reference of the flow-through cell consisted of a glass slide without the membrane. Prior to analysis, the flow-through cell system was cleaned sequentially using $1.0 \text{ mol L}^{-1} \text{ HNO}_3$ and Milli-Q water for 5 min.

2.3. Optode membrane preparation

A mixture of membrane cocktail solution containing 0.95 mg (10 mmol kg^{-1}) of lead-selective ionophore, 0.22 mg (5 mmol kg^{-1}) of KTPClPB, 0.12 mg (2.5 mmol kg^{-1}) of ETH 5294, 29.57 mg of PVC and 59.14 mg of DOS was dissolved in 2.0 mL THF in a glass vial. The mixture was immediately shaken to obtain a clear homogeneous solution.

An aliquot of 50 μL cocktail solution was spread on a square microscope cover glass ($22 \times 22 \text{ mm}$) using micropipette. Prior to spread, the microscope cover glasses were cleaned with THF to remove organic impurities and dust. The membranes were dried at $23 \pm 1^\circ \text{C}$ and $40 \pm 4\%$ humidity for at least 30 min before use. The homogenous, transparent and pinkish purple membranes were obtained. The fabricated membranes were kept in a desiccator.

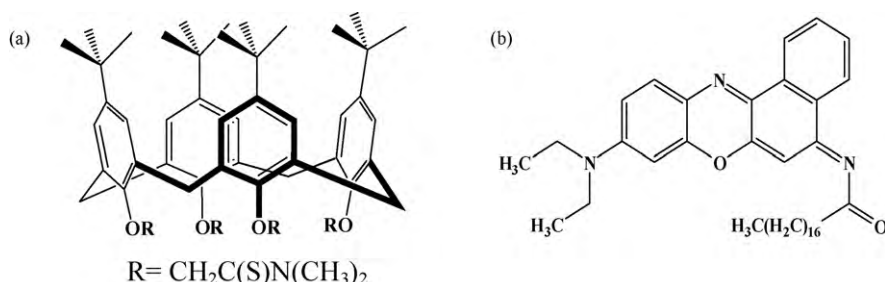


Fig. 1. Structures of (a) lead-selective ionophore and (b) chromoionophore.

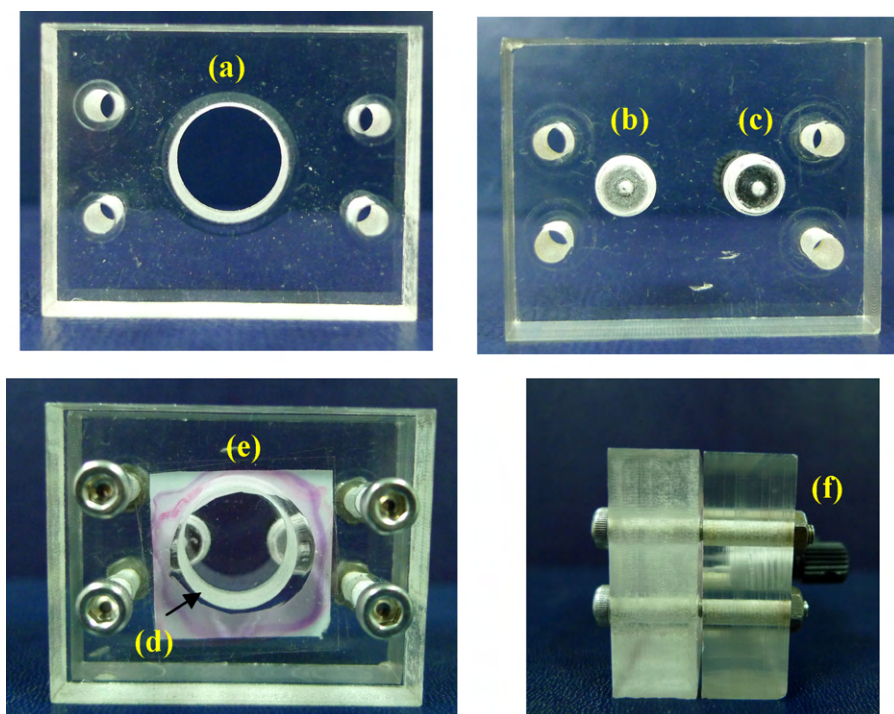


Fig. 2. Parts of lab-made flow-through cell (a) acrylic block, (b) and (c) inlet and outlet tubes on optical window, (d) seal gasket, (e) optode membrane and (f) fixing screws.

2.4. Absorbance measurements

The absorbance measurements of the optode membrane were performed over the wavelength range of 400–800 nm in three steps as follows:

Step 1. An optode membrane was conditioned by immersing in a 0.01 mol L^{-1} HCl as conditioning solution for 5 min to obtain fully protonated chromoionophore and then rinsed with Milli-Q water. The absorbance of the conditioned optode membrane (A_{prot}) was recorded when a cover glass without membrane was used as blank [24,33–34].

Step 2. The conditioned optode membrane was rinsed with Milli-Q water and then exposed to a Pb^{2+} solution for 30 min or until reach equilibrium and then rinsed with Milli-Q water. The absorbances of the optode membrane were measured.

Step 3. This optode membrane was regenerated by immersing in a regenerating solution to elute Pb^{2+} from the membrane and then rinsed with Milli-Q water. The same process was repeated for 3 times ($n=3$).

A fully deprotonated chromoionophore membrane was prepared by immersing in a 0.01 mol L^{-1} NaOH for 5 min and then rinsed with Milli-Q water. The absorbance of this optode membrane (A_{deprot}) was also recorded.

The measured absorbance is directly related to the membrane response [19], thus

$$\alpha = \frac{A_{\text{prot}} - A}{A_{\text{prot}} - A_{\text{deprot}}} \quad (1)$$

where α is the degree of deprotonation of chromoionophore, A is the absorbance of the chromoionophore for a giving equilibrium, A_{prot} and A_{deprot} are the absorbance values of the fully protonated ($\alpha=0$) and fully deprotonated ($\alpha=1$) forms of the chromoionophore, respectively.

The condition, measurement and regeneration steps for the flow-through measurement were investigated by passing 0.01 mol L^{-1} HCl, Tris buffer solution containing Pb^{2+} and 0.10 mol L^{-1} HNO_3 , respectively, through the membrane.

2.5. Sample preparation

Water samples (pond water, tap water and drinking water) were collected in the polyethylene bottles and adjusted to pH 2 with nitric acid. Pond water sample was filtered to remove particles before use. Determinations of Pb^{2+} in water samples were carried out with spiked method. Standard Pb^{2+} was spiked into 50.0 mL of the water sample. The water samples were diluted with Tris buffer (pH 7.0) to a final volume of 100 mL. The absorbance measurements of the optode membrane were performed in both batch and flow-through systems under the optimum conditions. The experiments were performed in triplicate ($n=3$).

3. Result and discussions

3.1. Effect of pH and type of buffer

The response characteristics of optode such as sensitivity, response range and detection limit depend on pH [26]. The optode response is based on the exchange of Pb^{2+} and H^+ between the membrane and aqueous phases. Therefore, the pH of the test solution has to be kept constant by buffering. Thus, the buffer solution in the experiment should not interfere the measurement of Pb^{2+} .

Fig. 3 illustrated the degree of deprotonation (α) in a function of pH. The absorbance of the optode membrane was recorded at 660 nm after equilibration for 30 min. The maximum response, which is the highest sensitivity, was experimentally found at pH 7. The decreased response at lower pH was probably due to the extraction of proton (H^+) from the aqueous solution into the membrane. At $\text{pH} > 7.0$, the reduced response may be due to the hydrolysis reaction of Pb^{2+} giving $\text{Pb}(\text{OH})^+$ resulting in the decreasing of the actual concentration of Pb^{2+} in the solution. Moreover, we also studied the responses of the optode at pH 5.0, 6.0, 7.0 in various concentrations of Pb^{2+} (Fig. 4). It was found that the maximum response and widest response range were obtained at pH 7. Therefore, pH 7 was chosen as the working pH. An appropriate buffer solution was examined by using $1.00 \times 10^{-3} \text{ mol L}^{-1}$ of acetate, citrate and

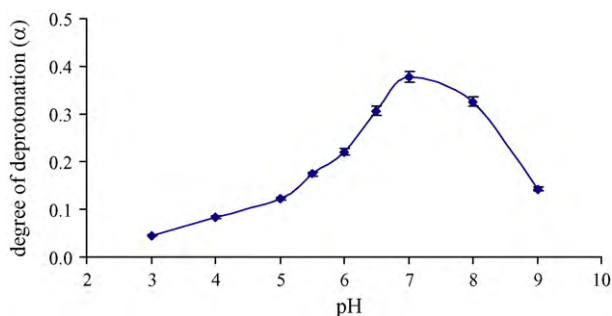


Fig. 3. The pH effect on the optode response at 660 nm in the presence of $3.16 \times 10^{-6} \text{ mol L}^{-1} \text{ Pb}^{2+}$.

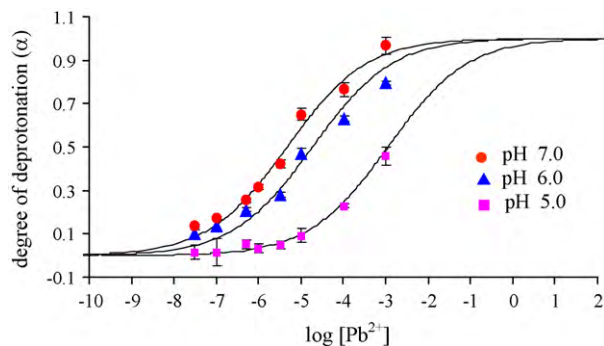


Fig. 4. The response of lead-selective optode at pH 5.0, 6.0, 7.0 in various concentrations of Pb^{2+} .

Tris buffers adjusted to pH 7.0. The optode response in Tris buffer had a greater response range than that of acetate buffer and citrate buffer.

3.2. Response time

The response time of the optode was controlled by the time required for the analyte to diffuse from bulk solution to the membrane adducting by the ionophore. The response time of the fabricated optode membrane was defined as the time required to reach 99% (t_{99}) of steady signal absorbance. It would be desirable for the optode to have a short response time. The response time of the optode depended on the membrane thickness, membrane composition, activity of the measuring ion and the pH of the measurement [35].

The observation of 99% steady signal absorbance was found within 15–30 min depending on the concentration of Pb^{2+} .

3.3. Response behavior

The diversities of the optodes in plasticized PVC membrane with high selectivity for lead have been described [24]. The response of the proposed optode was based on a cation-exchange mechanism. Ionophore (L) induced the extraction of Pb^{2+} into the membrane, at the same time hydrogen ion of the chromoionophore (CH^+) was released from the membrane to maintain the electroneutrality of the system. Then, Pb^{2+} in the membrane phase formed a complex with an ionophore. Therefore, the absorption spectra of the membrane changed with the concentration change of Pb^{2+} in solution.

The absorption spectra of the optode membrane were recorded after equilibration in Tris buffer solution (pH 7.0) containing different concentrations of Pb^{2+} in the range of 3.16×10^{-8} – $5.00 \times 10^{-3} \text{ mol L}^{-1}$ in comparison with the absorption spectrum of fully protonated chromoionophore ($0.01 \text{ mol L}^{-1} \text{ HCl}$) and the absorption spectrum of fully deprotonated chro-

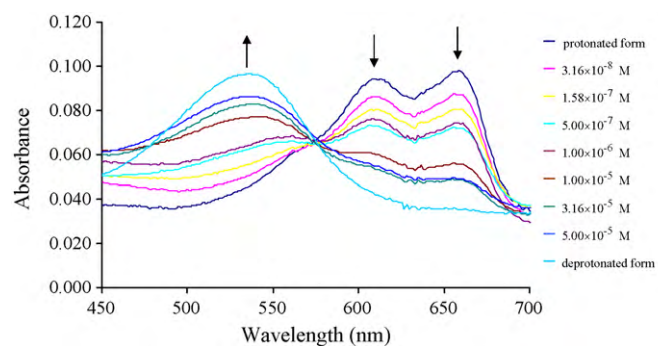
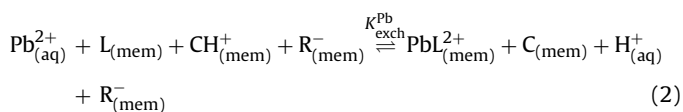


Fig. 5. Absorption spectra of the optode membranes after equilibrium in Tris buffer solutions containing different concentrations of Pb^{2+} (pH 7.0).

moionophore ($0.01 \text{ mol L}^{-1} \text{ NaOH}$). The results were shown in Fig. 5.

The absorption spectrum of the fully protonated membrane showed two absorption bands at 616 and 660 nm which correspond to the protonated form of the chromoionophore (CH^+), and the color of the membrane was blue. When the concentration of Pb^{2+} increased, the deprotonation of the chromoionophore occurred, resulting in a change from blue to pinkish purple. Thus, a reduction in the absorption band at 616 and 660 nm and an increase in the absorption band at 545 nm were observed.

If a 1:1 stoichiometry was assumed for the complexation of Pb^{2+} in the membrane phase, the equilibrium between the membrane phase (mem) and the sample solution phase (aq) can be described by Eq. (2):



The ion-exchange constant ($K_{\text{exch}}^{\text{Pb}}$) corresponding to the upper equilibrium was expressed by Eq. (3):

$$K_{\text{exch}}^{\text{Pb}} = \frac{[\text{PbL}^{2+}][\text{H}^+][\text{C}]}{[\text{Pb}^{2+}][\text{CH}^+][\text{L}]} \quad (3)$$

where PbL^{2+} and CH^+ represented the ionophore–lead complex and the protonated chromoionophore, respectively.

The response function for Pb^{2+} can be derived as shown in Eq. (4): [17]

$$[\text{Pb}^{2+}] = \frac{1}{K_{\text{exch}}^{\text{Pb}}} \left(\frac{\alpha[\text{H}^+]}{1-\alpha} \right)^z \left[\frac{R_{\text{tot}}^- - (1-\alpha)C_{\text{tot}}}{z(L_{\text{tot}} - \frac{n}{2}(R_{\text{tot}}^- + (1-\alpha)C_{\text{tot}}))} \right]^n \quad (4)$$

where $1-\alpha$ is the degree of protonation of the chromoionophore, R_{tot}^- is the total concentration of anionic sites, L_{tot} is the total concentration of ionophore, and C_{tot} is the total concentration of chromoionophore in the membrane. z is the charge of Pb^{2+} ($z=2$) and n is the ion–ionophore complex stoichiometry ($n=1$). The logarithmic form of Eq. (4) shows the dependence between the concentration of Pb^{2+} and the degree of protonation of chromoionophore ($1-\alpha$) since all the other terms are constant for each analytical system. When plotting $1-\alpha$ versus $\log[\text{Pb}^{2+}]$, a sigmoidal curve is obtained. All calculated curves are fitted to the experimental data by varying $K_{\text{exch}}^{\text{Pb}}$ in Eq. (4). This confirms the validity of Eq. (2) in explaining the response mechanism of the fabricated optode membrane towards Pb^{2+} and stoichiometry obtained in the solution phase.

3.4. Repeatability and reproducibility

The repeatability of the optode membrane was performed by repetitive exposure of the single optode membrane ($n = 10$), which was prepared from the same cocktail solution. The reproducibility of the optode membrane was evaluated by measuring the absorbance of twelve membranes. Therefore, the regeneration process is an important step in these studies. The efficiency of the regenerating solution was counted on the regeneration time which was defined as the time taken for reaching the baseline signal (the signal observed in 0.01 mol L^{-1} HCl as conditioning solution), where the minimum absorbance has been reached at the wavelength of 545 nm.

When 0.01 mol L^{-1} HCl solution was used, the color of the regenerated membrane did not change after immersing in Pb^{2+} solution at any response time. Therefore, HCl solution was not a good regeneration solution. However, 0.10 mol L^{-1} HNO_3 could fully regenerate optode membrane within 5 min.

The relative standard deviation (R.S.D.) of the absorbance for repeatability and reproducibility, 2.3% and 4.1% respectively, were obtained. These R.S.D. values were acceptable for the fabricated membrane to operate in the condition described.

3.5. Short-term stability and lifetime

The short-term stability of the optode membrane was defined in term of the stability of absorbance of the optode membrane. The absorbance was recorded at 660 nm over a period of at least 6 h [36–38] by recording the UV–vis spectrum every 30 min intervals ($n = 12$), giving 1.0% R.S.D. This indicated a satisfied short-term stability.

The lifetime of the optode membrane described by the stability of the absorbance of the optode membrane at 545 nm in the ambient conditions on recording for a period of 30 days [36–37] in comparison with the absorbance at 545 nm of a freshly prepared optode membrane. The observed absorption changes are 1.7%, 3.9%, 4.8% and >10% after 7, 15, 20 and 30 days, respectively. The R.S.D was 1.6% for 20 absorption values. Therefore, the lifetime of optode membrane which stored in ambient condition was at least 20 days before use. However, the fabricated membrane could be used efficiently within 7 days.

3.6. Flow-through measurement

A membrane was placed in the flow-through measuring cell. Then, 0.01 mol L^{-1} HCl and milli-Q water were consecutively passed through the membrane at a flow rate of 1.6 mL min^{-1} for 3 min. Tris buffer solution at pH 7.0 containing $1.00 \times 10^{-6} \text{ mol L}^{-1}$ Pb^{2+} was passed through the membrane at different flow rates from 0.9 to 7.5 mL min^{-1} for 30 min. The absorbance of each optode membrane was recorded at 660 nm. The response of the membrane in various flow rates was then determined. Fig. 6 showed that the optode response decreased as the flow rate increased in the range of $3.8\text{--}7.5 \text{ mL min}^{-1}$ because of less contact time between Pb^{2+} and the optode membrane. The maximum degree of deprotonation was obtained at a flow rate of 1.6 mL min^{-1} with high response and less time-consuming of sampling solutions.

The response time of the optode membrane to reach 99% of steady signal absorbance was 15 min. The response time in the flow-through system was better than that in the batch system probably due to the faster mass transfer rate of a solute between solution/membrane interfaces which the concentration gradient in the flow system is higher than that in the batch system. The repeatability and reproducibility of the optode membrane in the flow-through system were evaluated in the same manner as

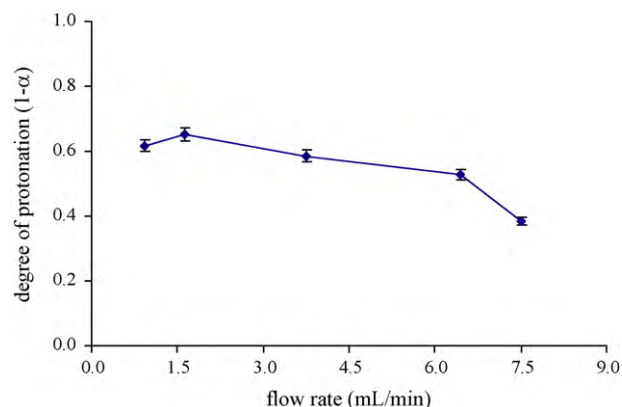


Fig. 6. Responses of the optode membrane for $1.00 \times 10^{-6} \text{ mol L}^{-1}$ Pb^{2+} at different flow rates of $0.9\text{--}7.5 \text{ mL min}^{-1}$.

described in the batch system. The R.S.D. values of responses were 1.2% ($n = 10$) and 2.7% ($n = 9$), respectively.

3.7. Analytical performance of proposed method

The linearity of the sigmoidal response curve is usually employed for analysis, defined as a linearity between a lower and an upper detection limit. The lower detection limit can be estimated from different approximates [9,18,24,33]. In order to determine the detection limit, two series of Pb^{2+} standard solutions were prepared. A maximum slope zone (8 standards, 3.16×10^{-8} to $5.00 \times 10^{-5} \text{ mol L}^{-1}$) was obtained with linear functions of $1 - \alpha = -0.2346 \log [\text{Pb}^{2+}] - 0.8243$ (Fig. 7). The lower detection limit was defined as the concentration at the intersection of two linear functions of the maximum slope and the minimum slope. The interception of both functions gave a detection limit (DL) of $2.49 \times 10^{-8} \text{ mol L}^{-1}$. A practical upper detection limit obtained from the intercept of the linear calibration function with the axis of abscissa was found at $1.00 \times 10^{-3} \text{ mol L}^{-1}$. The central zone of the sigmoidal curve showed a straight line that was a dynamic range of the optode. A dynamic range of 3.16×10^{-8} to $5.00 \times 10^{-5} \text{ mol L}^{-1}$ was obtained in the batch system.

In the flow-through system, the linear equations were $1 - \alpha = -0.1994 \log [\text{Pb}^{2+}] - 0.6294$. The lower and upper detection limit values were 8.97×10^{-9} and $3.16 \times 10^{-3} \text{ mol L}^{-1}$, respectively. A dynamic range of 1.26×10^{-8} to $3.16 \times 10^{-5} \text{ mol L}^{-1}$ was obtained.

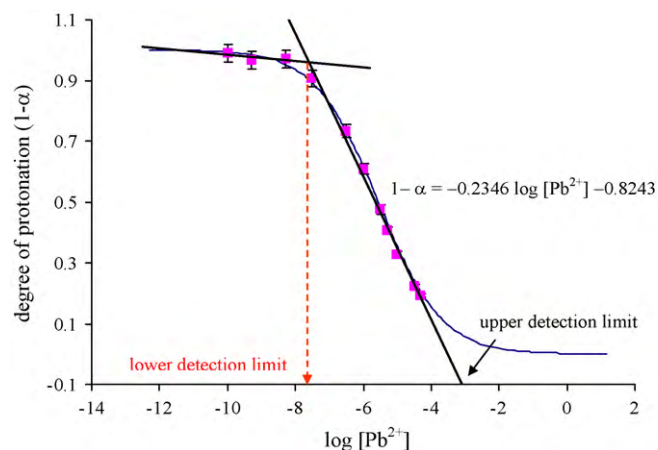


Fig. 7. Sigmoidal response curves of the optode membrane with the intersection of two linear functions for determination of detection limit in the batch system.

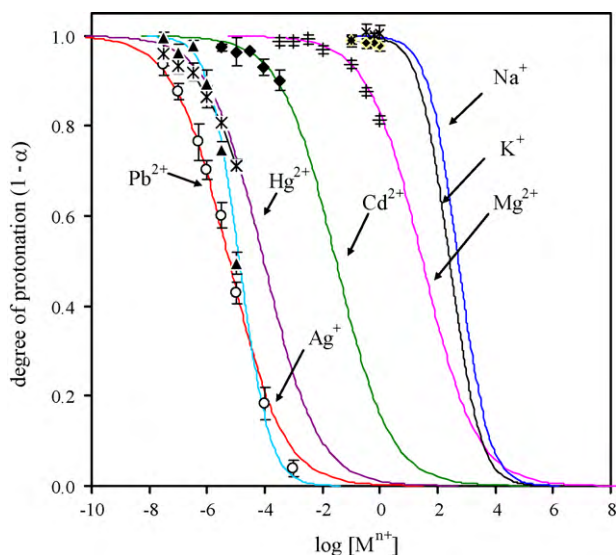


Fig. 8. Response curves of the optode membrane in various interfering ions at pH 7.0.

3.8. Selectivity

The influence of the common interfering ions on the optode response of the proposed Pb^{2+} optode membrane was investigated. The selectivity coefficient depended on the pH and the degree of protonation of the chromoionophore [26]. The optical selectivity of the fabricated optode membrane over common interfering ions was carried out by separated sample solution method (SSM) [19]. The response of optode membrane in the presence of different concentrations of each interfering ion was measured and selectivity coefficients ($K_{\text{Pb},\text{M}}^{\text{opt}}$) were determined by graphically plotting the corresponding $(1 - \alpha)$ versus log concentration of interfering ions ($\log C_{\text{M}}$) shown in Eq. (5).

$$K_{\text{Pb},\text{M}}^{\text{opt}} = \frac{z^{\text{M}} K_{\text{exch}}^{\text{M}}}{z^{\text{Pb}} K_{\text{exch}}^{\text{Pb}}} \left(\frac{\alpha[\text{H}^+]}{1 - \alpha} \right)^{z^{\text{Pb}} - z^{\text{M}}} \frac{\left([L_{\text{tot}}] - \frac{n_{\text{M}}}{z^{\text{M}}} \{ [R_{\text{tot}}^-] - (1 - \alpha)[C_{\text{tot}}] \} \right)^{n_{\text{M}}}}{\left([L_{\text{tot}}] - \frac{n_{\text{Pb}}}{z^{\text{Pb}}} \{ [R_{\text{tot}}^-] - (1 - \alpha)[C_{\text{tot}}] \} \right)^{n_{\text{Pb}}}} \quad (5)$$

where $z^{\text{M}}, z^{\text{Pb}}$ are the charge of the interfering ion M and Pb^{2+} , $n_{\text{M}}, n_{\text{Pb}}$ are the ion interfering–ionophore complex stoichiometry and lead–ionophore complex stoichiometry ($n = 1$), respectively.

The response curves of the optode membrane in various interfering ions are illustrated in Fig. 8 and the selectivity coefficients ($K_{\text{Pb},\text{M}}^{\text{opt}}$) were calculated at the highest sensitivity ($\alpha = 0.5$). $\log K_{\text{Pb},\text{M}}^{\text{opt}}$ values of Ag^+ , Hg^{2+} , Cd^{2+} , Mg^{2+} , K^+ and Na^+ were -0.35 , -1.20 , -3.70 , -6.70 , -7.65 and -7.95 , respectively. The strong preference of Pb^{2+} over Na^+ , K^+ , Mg^{2+} , Cd^{2+} and Hg^{2+} was due to its specific binding capability [14].

Some characteristics of the optodes used for determination of Pb^{2+} by absorption spectrophotometry are compared with other optodes listed in Table 1. Although, the insignificant difference of the working range and the detection limit were observed but our optode showed high preference to Pb^{2+} over alkali, alkaline earth metals, especially over Cd^{2+} and Hg^{2+} . This indicated that the fabricated optode could apply to determine Pb^{2+} in natural water. Moreover, regeneration of the fabricated optode was achieved within only 5 min in comparison with that reported by Alizadeh et al. [27].

3.9. Application to real water samples

This proposed method was successfully applied to determine Pb^{2+} in different real water samples under the optimum conditions either batch or flow-through systems with the satisfied recover-

Table 1
Comparison of some characteristics of lead optode in plasticized PVC membranes.

Ionophore	Response time	Working range (mol L^{-1})	Detection limit (mol L^{-1})	Remarks	Ref.
ETH 5435 (flow-through system)	Order of minutes, up to 220 min if lower concentration	5.0×10^{-9} – 5.0×10^{-3} at pH 5.68	3.2×10^{-12}	Cd^{2+} , Ag^+ and Cu^{2+} interfere, Hg^{2+} irreversible change in membrane	[24]
ETH 5493 (flow-through system)	–	1.0×10^{-7} – 1.0×10^{-2} at pH 5.0	–	Cd^{2+} interfere, Cu^{2+} causes drifting signals	[26]
DBzDA18C6 (batch system)	20 min	1.0×10^{-8} – 5.0×10^{-5} at pH 5.0	1.0×10^{-8}	Use long time to regenerate (2 h)	[27]
Lead IV	30 min	3.2×10^{-8} – 5.0×10^{-5} at pH 7.0	2.5×10^{-8}	Ag^+ slightly interfere lifetime = 7 days, regenerate time = 5 min	This work
	Flow-through system	1.3×10^{-8} – 3.2×10^{-5} at pH 7.0	9.0×10^{-9}		

Table 2The determination of Pb²⁺ in real water samples in batch and flow-through systems.

Sample	Batch system			Flow-through system		
	Added (mg L ⁻¹)	Found ± SD (mg L ⁻¹) ^a	Recovery (%)	Added (mg L ⁻¹)	Found ± SD (mg L ⁻¹) ^a	Recovery (%)
Pond water	–	<DL	–	–	<DL	–
	3.16 × 10 ⁻⁶	(3.06 ± 0.02) × 10 ⁻⁶	97	3.16 × 10 ⁻⁷	(2.88 ± 0.01) × 10 ⁻⁷	91
	1.00 × 10 ⁻⁵	(0.97 ± 0.01) × 10 ⁻⁵	97	1.00 × 10 ⁻⁶	(0.93 ± 0.01) × 10 ⁻⁶	93
	3.16 × 10 ⁻⁵	(2.95 ± 0.02) × 10 ⁻⁵	93	3.16 × 10 ⁻⁶	(2.88 ± 0.01) × 10 ⁻⁶	91
Tap water	–	<DL	–	–	<DL	–
	3.16 × 10 ⁻⁶	(3.02 ± 0.01) × 10 ⁻⁶	96	3.16 × 10 ⁻⁶	(2.87 ± 0.01) × 10 ⁻⁶	91
	1.00 × 10 ⁻⁵	(0.96 ± 0.01) × 10 ⁻⁵	96	1.00 × 10 ⁻⁵	(0.91 ± 0.01) × 10 ⁻⁵	91
	3.16 × 10 ⁻⁵	(3.05 ± 0.01) × 10 ⁻⁵	97	3.16 × 10 ⁻⁵	(3.19 ± 0.01) × 10 ⁻⁵	101

^a Mean value of three determinations.**Table 3**The comparison results of the proposed method (flow-through system) and ICP-OES for determination of Pb²⁺ in real water samples.

Sample	Added	Optode method		ICP-OES		<i>t</i> -statistics (<i>t</i> _{0.05,3} = 4.30)
		Found ± SD (mol L ⁻¹) ^a	Recovery (%)	Found ± SD (mol L ⁻¹) ^a		
Drinking water (1)	–	<DL	–	<DL	–	–
	3.16 × 10 ⁻⁶	(3.19 ± 0.01) × 10 ⁻⁶	101	(3.16 ± 0.02) × 10 ⁻⁶		2.61
	5.01 × 10 ⁻⁶	(4.82 ± 0.01) × 10 ⁻⁶	96	(4.66 ± 0.01) × 10 ⁻⁶		1.86
Drinking water (2)	–	<DL	–	<DL	–	–
	3.16 × 10 ⁻⁶	(3.13 ± 0.01) × 10 ⁻⁶	99	(3.36 ± 0.03) × 10 ⁻⁶		1.90
	5.01 × 10 ⁻⁶	(4.99 ± 0.02) × 10 ⁻⁶	97	(5.06 ± 0.02) × 10 ⁻⁶		1.00
Pond water	–	<DL	–	<DL	–	–
	1.00 × 10 ⁻⁶	(0.92 ± 0.01) × 10 ⁻⁶	92	(1.01 ± 0.02) × 10 ⁻⁶		3.24
	3.16 × 10 ⁻⁶	(2.89 ± 0.01) × 10 ⁻⁶	91	(3.25 ± 0.02) × 10 ⁻⁶		3.42
Tap water	–	<DL	–	<DL	–	–
	1.00 × 10 ⁻⁶	(0.91 ± 0.02) × 10 ⁻⁶	91	(1.08 ± 0.02) × 10 ⁻⁶		1.11
	3.16 × 10 ⁻⁶	(2.87 ± 0.02) × 10 ⁻⁶	91	(3.18 ± 0.02) × 10 ⁻⁶		1.01
	1.00 × 10 ⁻⁵	(9.33 ± 0.01) × 10 ⁻⁶	93	(9.75 ± 0.02) × 10 ⁻⁶		1.06
	1.00 × 10 ⁻⁵	(9.66 ± 0.02) × 10 ⁻⁶	97	(9.55 ± 0.02) × 10 ⁻⁶		1.74

^a Mean value of three determinations.

ies (Table 2). Sample throughput in flow-through system was 4 samples h⁻¹.

The results obtained from flow-through measurements were compared with the results determined by ICP-OES. The statistical *t*-test was used to compare the experimental means obtained from the proposed optode membrane and ICP-OES. The results were summarized in Table 3. No significant different value (*t*_{critical} = 4.30 > *t*_{exp} = 1.00–3.42, *n* = 3, 95% of confidence level) was found in both flow-through method and ICP-OES.

4. Conclusions

We have successfully fabricated the bulk optode by a simple casting technique for the determination of Pb²⁺. In the batch system, the response range of 3.16 × 10⁻⁸ to 5.00 × 10⁻⁵ mol L⁻¹ Pb²⁺ with the detection limit of 2.49 × 10⁻⁸ mol L⁻¹ and the response time of 30 min were obtained. In the flow-through system, the dynamic range of 1.26 × 10⁻⁸ to 3.16 × 10⁻⁵ mol L⁻¹ Pb²⁺ with detection limit of 8.97 × 10⁻⁹ mol L⁻¹ were obtained at a flow rate of 1.6 mL min⁻¹. The response time of the flow-through system was 15 min. The proposed optode showed high preference to Pb²⁺ over Na⁺, K⁺, Mg²⁺, Cd²⁺, Hg²⁺ and Ag⁺. Moreover, the application of the proposed optode to determine Pb²⁺ in real water samples, pond water, tap water and drinking water, provided high accuracy and high precision.

Acknowledgements

This work was supported by the Thailand Research Fund (RTA 5080006) and Ratchadaphiseksompoj Endowment Fund, Chulalongkorn University (GRU51-017-23-008 and GRU52-007-23-002)

under Environmental Analysis Research Unit and Supramolecular Chemistry Research Unit, Department of Chemistry, Faculty of Science, Chulalongkorn University

References

- [1] S.E. Manahan, Environmental Chemistry, Missouri University Willard grant Press, Boston, 1984, pp. 154–155.
- [2] M.S. Di Nezio, M.E. Palomeque, B.S. Fernandez Band, Talanta 63 (2004) 405.
- [3] O. Cankur, D. Korkmaz, O.Y. Ataman, Talanta 66 (2005) 789.
- [4] M. Tuzen, K. Parlar, M. Soyulak, J. Hazard. Mater. 121 (2005) 79.
- [5] S. Baytak, A.R. Turker, J. Hazard. Mater. 129 (2006) 130.
- [6] R.M. Cespon-Romero, M.C. Yebra-Biurrun, Anal. Chim. Acta 600 (2007) 221.
- [7] A. Michalska, M. Wojciechowski, E. Bulska, J.Z. Mieczkowski, K. Maksymiuk, Talanta 79 (2009) 1247.
- [8] S.Y. Kazemi, M. Shamsipur, H. Sharghi, J. Hazard. Mater. 172 (2009) 68.
- [9] X.G. Li, X.L. Ma, M.R. Huang, Talanta 78 (2009) 498.
- [10] V.K. Gupta, A.K. Jain, P. Kumar, Sens. Actuators B: Chem. 120 (2006) 259.
- [11] J. Lu, R. Chen, X. He, J. Electroanal. Chem. 528 (2002) 33.
- [12] A. Ceresa, E. Bakker, B. Hattendorf, D. Günther, E. Pretsch, Anal. Chem. 73 (2001) 343.
- [13] T. Sokalski, T. Zwickl, E. Bakker, E. Pretsch, Anal. Chem. 71 (1999) 1204.
- [14] E. Bakker, M. Willer, E. Pretsch, Anal. Chim. Acta 282 (1993) 265.
- [15] H. Hisamoto, K. Suzuki, TrAC, Trends Anal. Chem. 18 (1999) 513.
- [16] J. Jantana, M. Josowicz, P. Vanysek, D.M. DeVney, Anal. Chem. 70 (1998) 179.
- [17] K. Seiler, W. Simon, Anal. Chim. Acta 266 (1992) 73.
- [18] K. Seiler, W. Simon, Sens. Actuators B: Chem. 6 (1992) 295.
- [19] E. Bakker, W. Simon, Anal. Chem. 64 (1992) 1805.
- [20] M.K. Amini, T. Momeni-Isfahani, J.H. Khorasani, M. Pourhossein, Talanta 63 (2004) 713.
- [21] A. Isha, N.A. Yusof, M. Ahmad, D. Suhendra, W.M.Z.W. Yunus, Z. Zainal, Sens. Actuators B: Chem. 114 (2006) 344.
- [22] P. Hashemi, M.M. Abolghasemi, K. Alizadeh, R.A. Zarjani, Sens. Actuators B: Chem. 129 (2008) 332.
- [23] S. Rastegarzadeh, V. Rezaei, Sens. Actuators B: Chem. 129 (2008) 327.
- [24] M. Lerchi, E. Bakker, B. Rusterholz, W. Simon, Anal. Chem. 64 (1992) 1534.
- [25] W.A. de Oliveira, R. Narayanaswamy, Talanta 39 (1992) 1499.

- [26] E. Antico, M. Lerchi, B. Rusterholz, N. Achermann, M. Badertscher, M. Valiente, E. Pretsch, *Anal. Chim. Acta* 388 (1999) 327.
- [27] N. Alizadeh, A. Moemeni, M. Shamsipur, *Anal. Chim. Acta* 464 (2002) 187.
- [28] G.A. Casay, N. Narayanan, L. Evans Iii, T. Czuppon, G. Patonay, *Talanta* 43 (1996) 1997.
- [29] W.H. Chan, R.H. Yang, T. Mo, K.M. Wang, *Anal. Chim. Acta* 460 (2002) 123.
- [30] M. Telting-Diaz, E. Bakker, *Anal. Chem.* 74 (2002) 5251.
- [31] A.A. Ensafi, A.K. Far, S. Meghdadi, *J. Hazard. Mater.* 172 (2009) 1069.
- [32] B.S.V. de la Riva, J.M. Costa-Fernandez, R. Pereiro, A. Sanz-Medel, *Anal. Chim. Acta* 395 (1999) 1.
- [33] M. Lerchi, E. Reitter, W. Simon, E. Pretsch, D.A. Chowdhury, S. Kamata, *Anal. Chem.* 66 (1994) 1713.
- [34] M. Bochenska, J. Inclusion Phenom. *Macrocyclic Chem.* 22 (1995) 269.
- [35] S. O'Neill, S. Conway, J. Twellmeyer, O. Egan, K. Nolan, D. Diamond, *Anal. Chim. Acta* 398 (1999) 398.
- [36] A. Safavi, M. Sadeghi, *Talanta* 71 (2007) 339.
- [37] B. Kuswandi, H.H. Nuriman, D.N. Dam, W. Reinhoudt, Verboom, *Anal. Chim. Acta* 591 (2007) 208.
- [38] M. Shamsipur, K. Alizadeh, M. Hosseini, C. Caltagirone, V. Lippolis, *Sens. Actuators B: Chem.* 113 (2006) 892.



Synthesis, photophysical properties, and cyanide detection in aqueous solution of **BF₂-curcumin** dyes

Anusak Chaicham^a, Sirinan Kulchat^a, Gamolwan Tumcharern^b, Thawatchai Tuntulani^a, Boosayarat Tomapatanaget^{a,*}

^aSupramolecular Chemistry Research Unit, Department of Chemistry, Faculty of Science, Chulalongkorn University, Bangkok, 10330, Thailand

^bNational Nanotechnology Center, National Science and Technology Development Agency, Pathumthani 12120, Thailand

ARTICLE INFO

Article history:

Received 8 February 2010

Received in revised form 4 May 2010

Accepted 24 May 2010

Available online 4 June 2010

ABSTRACT

Derivatives of difluoroboron curcumin (**BF₂-curcumin**, **BF₂-cur(OMe)₂**, **BF₂-cur(OTs)₂**, and **BF₂-curOTs**), were synthesized. All compounds possessed electron donor moieties at both ends of the conjugated π system and an electron acceptor moiety in the middle of the molecules (D–A–D system) and should exhibit different optical properties depending on substituents on the benzene rings. Photophysical properties of curcumin and difluoroboron curcumin derivatives were explored. The electron-withdrawing substituent could decrease the electron acceptability of BF₂-acceptor moiety resulting in the hypsochromic shift of both absorption and emission bands. **BF₂-curcumin** and **BF₂-cur(OMe)₂** displayed the positive solvatochromic effect relying predominantly on polarity and polarizability of the solvent. Interestingly, **BF₂-curcumin** showed high selectivity and sensitivity towards cyanide with the detection limits of 22 μ M and 0.14 μ M measured by visual detection and UV–vis spectrophotometry, respectively. Compared to the original curcumin, **BF₂-curcumin** offered a remarkably promising detection of cyanide with 66-fold enhancement in aqueous media (4:1 of CH₃CN/H₂O).

Crown Copyright © 2010 Published by Elsevier Ltd. All rights reserved.

1. Introduction

In recent years, chemists have employed a number of dyes and their derivatives in colorimetric detection of toxic substances.¹ Curcumin, obtained by extraction of the rhizomes of *Curcuma Longa*, is a natural yellow-orange dye with low toxicity. Turmeric root is a well-known spice, cosmetic and medicine² due to its interesting multiple pharmacological effects, for examples, *anti-oxidant*, *anti-cancer*, *anti-inflammatory*, and potent *anti-Alzheimer's* disease activity.^{3–9} Curcumin consists of two methoxy phenols conjugated through α,β -unsaturated β -diketone linker, which can perform a keto–enol tautomerism. A few investigations concerning photophysical properties of curcumin for medicinal chemistry have been reported.^{10–12} Curcumin surprisingly exhibits many interesting photophysical and photochemical properties. The absorption band is approximately 408–430 nm in most organic solvents while the fluorescence spectrum is solvent-sensitive with emission wavelengths ranging from 460 to 560 nm.¹³ Considering the fluorescent responses of curcumin, the emission quantum yield decreases on going from solvents of low polarity to those of high polarity. Recently, fluorescent borondifluoride dyes, such as

bodipy^{14–19} and boron/diketones^{20–24} have offered the advantages of optical properties including high emission quantum yields, large molar extinction coefficients and high sensitivity upon changes in solvent polarity.²⁵ In 1993, Montellano et al.²⁶ pioneered the addition of the difluoroboron moiety on the enolate group of curcumin and studied the inhibition of HIV-1 and HIV-2 proteases. Difluoroboron-curcumin displayed HIV-1 inhibition with IC₅₀ of 24 μ M while the typical curcumin showed HIV-1 inhibition with IC₅₀ of 100 μ M.

Cyanide, which was released in a widespread way from industrial uses, was found to cause severe toxicity in physiological system and environments. In the last decades, many efforts have been devoted to design various chemosensors specific for CN[−] detection^{27–30} since this method is outstanding in terms of inexpensive cost and rapid implementation. Yoon et al.³¹ have collected and summarized researches involving optical sensors for cyanide based on a covalently linked binding site and signaling unit,^{32,33} displacement approach of Cu complex and CN[−]^{34,35} and chemodosimeter of cyanide-substitution.^{36,37} However, a significant visual change for cyanide sensing employing a deprotonation approach is still rare. Here, we aim to investigate the photophysical and photochemical properties of derivatives of **BF₂-curcumin**. Addition of BF₂ on the carbonyl group can inhibit the keto–enol tautomerization possibly resulting in an improvement in the photophysical properties and stability of curcumin.

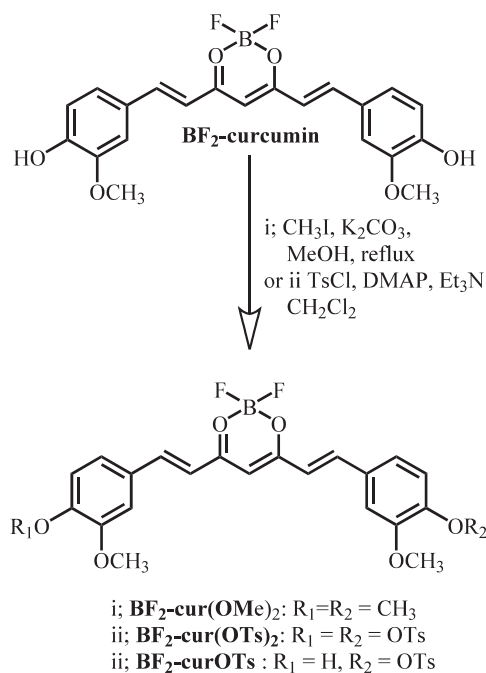
* Corresponding author. Tel.: +662 2187642; fax: +662 2541309; e-mail address: tboosayarat@gmail.com (B. Tomapatanaget).

The **BF₂-curcumin** complexes consist of two methoxy phenol as electron donor parts conjugated to the difluoroboron enolate as the electron acceptor part resulting in a D–A–D system. In our design, the substituents on the OH moiety of **BF₂-curcumin** were synthetically modified to **BF₂-cur(OMe)₂**, **BF₂-cur(OTs)₂**, and **BF₂-cur OTs** in order to evaluate the effect of substituents on the photophysical properties of **BF₂-curcumin**. We explored the solvatochromic behavior of **BF₂-curcumin** and **BF₂-cur(OMe)₂** in various solvents. Moreover, we also investigated the cyanide sensing property of **BF₂-curcumin** in aqueous media compared with the original curcumin.

2. Results and discussion

2.1. Synthesis

All difluoroboron curcumin derivatives, **BF₂-cur(OMe)₂**, **BF₂-cur(OTs)₂**, and **BF₂-curOTs** were prepared from curcumin obtained by extraction of the rhizomes of *C. longa*. The synthesis of all compounds was illustrated in Scheme 1. **BF₂-curcumin** was prepared by the addition of borontrifluoride diethyletherate to the enolate unit of curcumin.²⁵ **BF₂-cur(OMe)₂** was obtained by methylating **BF₂-curcumin** with methyl iodide using potassium carbonate as base. The ¹H NMR spectrum of **BF₂-cur(OMe)₂** displayed the methoxy protons at 3.82 ppm. The methoxy group in this compound was a representative of an electron-donating group.



Scheme 1. Synthesis of **BF₂-cur(OMe)₂**, **BF₂-cur(OTs)₂** and **BF₂-curOTs**.

Mono and di-tosylated (**BF₂-curOTs** and **BF₂-cur(OTs)₂**) were prepared by the reaction between **BF₂-curcumin** and tosyl chloride. ¹H NMR spectra showed significantly different patterns between di- and mono-tosylation indicating by the ratio of 2:1 for the aromatic protons of the tosyl groups. The mono-tosyl compound displayed two non-equivalent methyl protons at different positions of 3.50–4.00 ppm. The purity of all prepared compounds was assured by the good agreement of elemental analysis except for **BF₂-curOTs**, which readily decomposed in air.

2.2. Photophysical properties of all difluoroboron curcumin derivatives

The photophysical behavior of all D–A–D molecules, **BF₂-cur(OMe)₂**, **BF₂-curOTs**, and **BF₂-cur(OTs)₂**, exhibited a strong

absorption and emission band in CH₂Cl₂ as shown in Table 1. It was found that when the OH group was replaced with the electron-donating group such as OMe in **BF₂-cur(OMe)₂**, the maximum absorption spectrum of **BF₂-cur(OMe)₂** showed a small red shift at 502.1 nm ($\Delta\lambda_{\text{max(ex)}}=5.1$ nm in CH₂Cl₂) compared to that of **BF₂-curcumin**. This red shift is less than Moore's **CRANAD 2** ($\lambda_{\text{max(ex)}}=760$ nm in MeOH) containing a *N,N*-dimethyl moiety instead of OH group on the ends of benzene rings leading to a large bathochromic shift.³⁸ Conversely, a blue shift of the absorption band was observed when the hydroxyl groups in **BF₂-curcumin** were modified with an electron-withdrawing group such as OTs in **BF₂-cur(OTs)₂** (Fig. 1a). Therefore, the substituted group influenced the electron accepting ability of the BF₂-part. Their relative transition energies should be dependent on the relative electron affinity of the donor fragment (curcumin part).³⁹ An electron-withdrawing group on the donor fragment will decrease the electron accepting ability of BF₂-part inducing the blue shift of the absorption band, while the electron-donating group will promote the electron accepting ability of the BF₂-part resulting in a red-shifted absorption band.

Table 1
Photophysical properties of **BF₂-curcumin**, **BF₂-cur(OMe)₂**, **BF₂-curOTs** and **BF₂-cur(OTs)₂** in CH₂Cl₂ at a concentration of 1.0×10^{-6} M

Compound	Absorption (nm)	Emission (nm)	Quantum yield	Molar absorptivity ($\times 10^5$ cm ⁻¹ mol ⁻¹ L)
BF₂-curcumin	497	557.01	0.62	0.82
BF₂-cur(OMe)₂	502.1	570.00	0.61	1.29
BF₂-curOTs	492.0	562.00	0.22	0.33
BF₂-cur(OTs)₂	436.0, 460.1	505.07	0.48	0.34

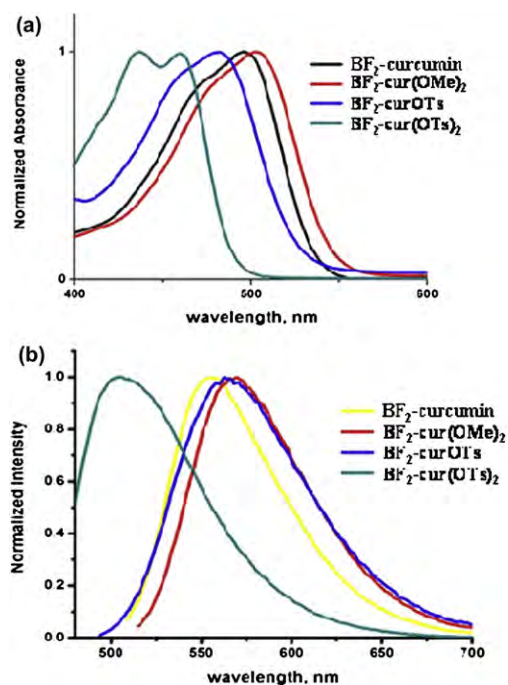


Figure 1. The normalized UV–vis spectra (a) and fluorescence spectra (b) of **BF₂-curcumin**, **BF₂-cur(OMe)₂**, **BF₂-curOTs** and **BF₂-cur(OTs)₂** in CH₂Cl₂ at a concentration of 1.0×10^{-3} mM.

Compared to **BF₂-curcumin**, the emission spectra of **BF₂-curOTs** and **BF₂-cur(OMe)₂** demonstrated a trend of a small red shift depending on the electron accepting ability of the BF₂-part. **BF₂-curOTs**, however, showed the maximum emission wavelength of 562 nm, which is higher than that of **BF₂-curcumin** (557.10 nm) (Fig. 1b). The unsymmetrical structure of **BF₂-curOTs** with different

substituents on both ends of benzene rings causes a higher relaxation of electrons resulting in the bathochromic shift compared to **BF₂-curcumin**.

2.3. Studies of solvatochromic effects of difluoroboron curcumin derivatives

BF₂-curcumin and **BF₂-cur(OMe)₂** are soluble in several common organic solvents and exhibit solvent-dependent photophysical properties in selected common organic solvents (Fig. 2). It was worth noting that the color of the solutions changed ranged from yellow to red on going from solvents of low polarity to those of high polarity. **BF₂-curcumin** in selected solvents exhibited different colors with a red color-shade upon increasing the solvent polarity and a very bright fluorescent emission with low solvent polarity (Fig. 2a and Fig. 2b). The normalized UV–vis and fluorescence spectra of **BF₂-curcumin** in several organic solvents are shown in Figures 3a and b. The fluorescent quantum yields of **BF₂-curcumin** and **BF₂-cur(OMe)₂** were collected in Tables S1 and S2. The results can be rationalized that the increase of the electron accepting ability of the BF₂-acceptor enhanced the charge separation or dipole-moment of the molecule. Therefore, the different solvent polarities yielded different colors of the solution.

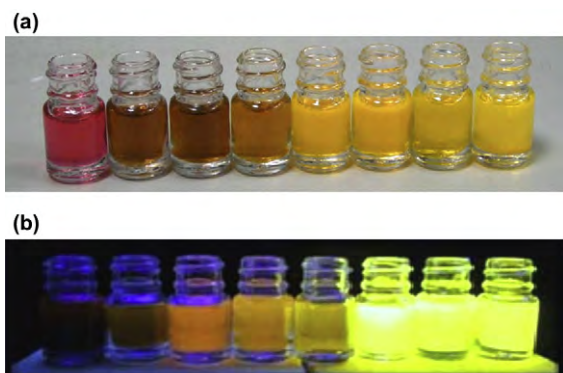


Figure 2. The photographs of **BF₂-curcumin** in organic solvents (from left to right, DMSO, CH₃OH, CH₃Cl, C₂H₅OH, CH₃CN, CH₂Cl₂, EtOAc, and *o*-C₆H₄Cl₂) under illumination of (a) white light and (b) black light ($\lambda=365$ nm).

To explain the solvent effect on the photophysical properties of **BF₂-curcumin** and **BF₂-cur(OMe)₂**, the linear solvation energy relationships (LSER) based on the Kamlet–Taft equation were examined. The solvatochromic parameters involving π^* (polarity/polarizability factor), α (solvent hydrogen bond donor ability, HBD), and β (solvent hydrogen bond acceptance ability, HBA) are used in the Kamlet–Taft relationship as shown in Eq. 1.⁴⁰

$$y = y_0 + a\alpha + b\beta + c\pi^* \quad (\text{Kamlet – Taft}) \quad (1)$$

The coefficients (y_0 , a , b , and c), and correlation coefficients (R^2) were evaluated by multiple linear regression fit to the Kamlet–Taft relationship of the absorption spectra of **BF₂-curcumin** and **BF₂-cur(OMe)₂**, and summarized in the Supplementary data. The solvents used in this study were CH₃OH, DMSO, C₂H₅OH, CHCl₃, C₆H₆, CH₃C₆H₅, and (CH₃CH₂)₂O. The solvatochromic parameters expressed in Eqs. 2 and 3 were obtained from the best linear regression fits⁴⁰ between the calculated and measured

ν_{\max} with R^2 values of 0.991 and 0.997 for **BF₂-curcumin** and **BF₂-cur(OMe)₂**, respectively (Fig. 4 and Fig. S5).

$$\tilde{\nu}_{\max} \text{BF}_2 - \text{curcumin} (\times 10^{-3}) = 20.97 + 0.23\alpha - 0.70\beta - 1.39\pi^* \quad (2)$$

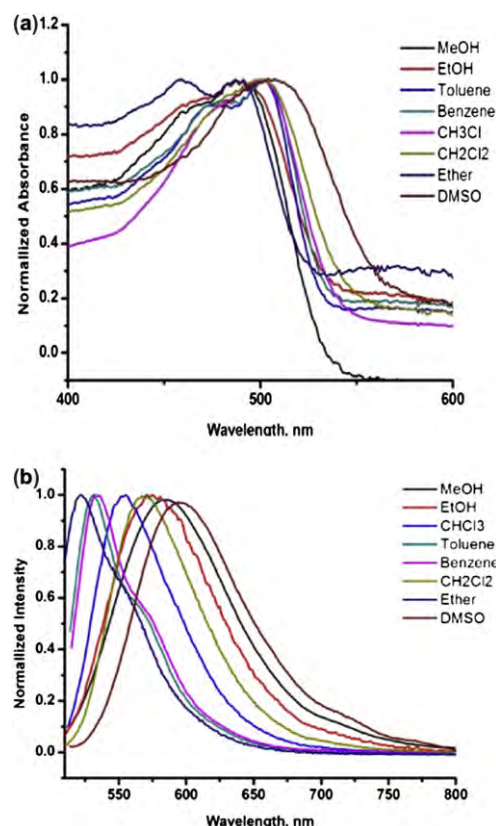


Figure 3. The normalized UV–vis spectra (a) and fluorescence spectra (b) of **BF₂-curcumin** in various organic solvents.

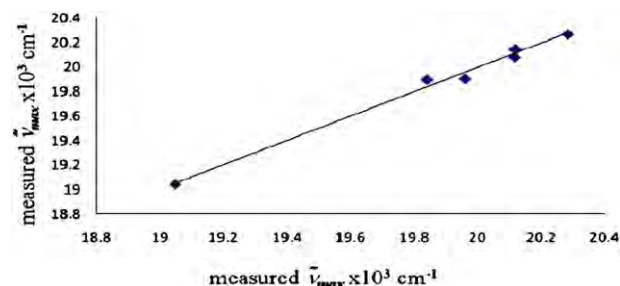


Figure 4. Multi-parameter linear regression analysis between calculated and measured absorption of **BF₂-curcumin**.

$$\tilde{\nu}_{\max} \text{BF}_2 - \text{curcumin} (\times 10^{-3}) = 20.61 + 0.39\alpha + 0.20\beta - 1.32\pi^* \quad (3)$$

From Eqs. 2 and 3, the polarity/polarizability factors (π^*) play the most important role on the photophysical properties of **BF₂-curcumin** and **BF₂-cur(OMe)₂**. Additionally, hydrogen bond accepting abilities (β) followed by hydrogen bond donating abilities (α) play a minor effect for the former derivative. This result implied that the dipole/dipole interaction between the curcumin derivatives and the medium is markedly larger than the hydrogen bonding between the solute and the solvent. The ' c ' values are minus for **BF₂-curcumin** and **BF₂-cur(OMe)₂**, indicating the electronically excited state of these molecules with a stronger solvate stabilized upon increasing the solvent's dipolarity/polarizability resulting in a good agreement with bathochromic shift of UV–vis absorption maxima on going from benzene to DMSO. Considering in each coefficient, ' a ' and ' c ' are approximately the same in both **BF₂-curcumin** and **BF₂-cur(OMe)₂** systems, while ' b ' displays large difference. This result suggested that

HBA plays a larger role than HBD in the photophysical properties of both curcumin derivatives in organic solvents. It is also worth mentioning that the negative value of HBA of **BF₂-curcumin** in organic solvent indicates the favorable hydrogen bonding towards a protophilic solvent leading to the bathochromic shift of the absorption band.⁴¹ On the contrary, the coefficient of the HBA part in the Kamlet–Taft equation of **BF₂-cur(OMe)₂** system means unfavorable hydrogen bond interaction in a protic solvent. Undoubtedly, the maximum absorption of **BF₂-cur(OMe)₂** in methanol and ethanol illustrated a blue shift of ~13 nm compared with the solution in benzene (see in [Supplementary data](#)). The unfavorable hydrogen bond interaction in a protic solvent of **BF₂-cur(OMe)₂** related to the fluctuation of the maximum absorption in the optical spectra with an increase of the solvent polarity. However, **BF₂-curcumin** and **BF₂-cur(OMe)₂** generally displayed a positive solvatochromism under the effect of solvent dipolarity/polarizability factor.

2.4. Anion sensing of **BF₂-curcumin** and curcumin

The complexed properties of **BF₂-curcumin** towards anions, in comparison with **curcumin**, were investigated. All optical and emission spectrum were measured in CH₃CN/H₂O (4:1 v/v), since deprotonation by a strongly basic anion might occur at the hydroxyl group of both compounds. Anion sensing ability of **BF₂-curcumin** was examined with various anions (F[−], Cl[−], Br[−], I[−], CN[−], AcO[−], and BzO[−], and H₂PO₄[−]) by UV–vis and fluorescence spectrophotometry.

Upon addition of CN[−], the color transitions from red to blue of **BF₂-curcumin** and from yellow to red of **curcumin** were observed by naked-eye ([Fig. 5](#)). For other anions, the color of solution remained unchanged. The photophysical properties were further examined by UV–vis spectrophotometry. The absorption band of **BF₂-curcumin** at 507 nm decreased concurrently with the appearance of a new strong absorption band at 649 nm in the presence of CN[−] ([Fig. 6](#)). In the case of AcO[−] and BzO[−], the maximum absorption at 507 nm slightly decreased, and a weak absorption band at 625 nm intensified. No spectrum change was observed for F[−], Cl[−], Br[−], I[−], and H₂PO₄[−]. The addition of CN[−] in the **curcumin** solution led to a bathochromic shift (from 460 to 510 nm). In the case of the other anions, the UV–vis spectrum remained unchanged (shown in [S7](#)).

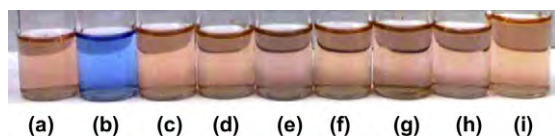


Figure 5. Color transition of **BF₂-curcumin** (1.0×10^{-6} M) in CH₃CN/H₂O (4:1, v/v) solution in the presence of 100 equiv of various anions (a) none, (b) CN[−], (c) F[−], (d) Br[−], (e) Cl[−], (f) I[−], (g) BzO[−], (h) AcO[−], and (i) H₂PO₄[−].

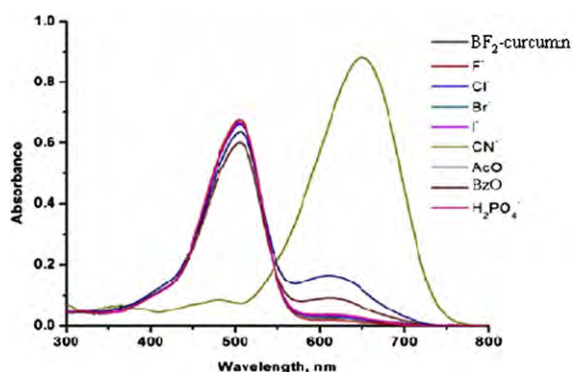


Figure 6. UV–vis spectra of **BF₂-curcumin** (5 μM) in CH₃CN/H₂O (4:1, v/v) in the presence of 100 equiv of various anions.

Photoemission properties of **BF₂-curcumin** and curcumin were also investigated. The fluorescent spectrum of **BF₂-curcumin** showed a strong emission band at 600 nm while that of curcumin displayed a very weak emission band at 543 nm as shown in [Figure 7](#). Compared to curcumin, a large red shift and high quantum yield of **BF₂-curcumin** could stem from the electron transition from π to π^* from oxygen to the empty orbital of boron.⁴² The incorporation of BF₂ on the curcumin structure resulted in a more rigid structure and extended π -conjugation and consequently facilitated electron transfer through the conjugated system.

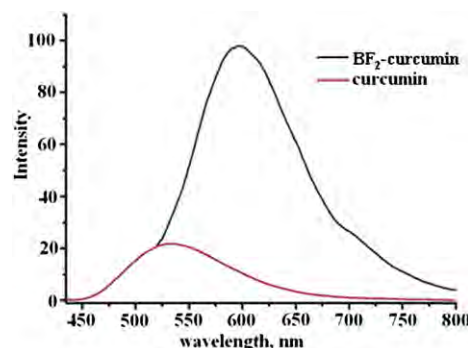


Figure 7. Fluorescent spectra of **BF₂-curcumin** and **curcumin** in CH₃CN/H₂O (4:1 v/v).

The emission spectra of **BF₂-curcumin** and **curcumin** in the presence of various anions are illustrated in [Figure 8](#). Interestingly, excitation wavelength dependent fluorescence spectra were observed. The emission bands of **BF₂-curcumin** in the presence of CN[−] were markedly changed. The excitation wavelength of 507 nm resulted in a complete quenching at the emission wavelength of 600 nm. On the other hand, a new emission band at 750 nm of the cyanide complex appeared upon changing the excitation wavelength to 649 nm ([Fig. 8](#), inset). In the case of other anions, the emission bands at 649 nm slightly change without the appearance of a new emission band at 750 nm when excited at 649 nm. The fluorescence responses of **curcumin** towards various anions were also investigated.

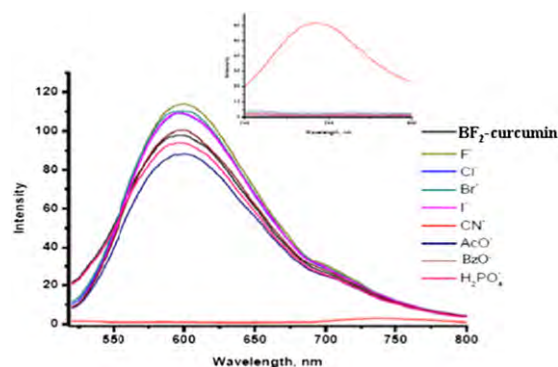


Figure 8. Fluorescent spectra of **BF₂-curcumin** with various anions ($\lambda_{\text{ex}}=507$ nm, Inset: $\lambda_{\text{ex}}=649$ nm).

The presence of cyanide in the solution of curcumin caused a complete quenching of the emission band at 543 nm without the appearance of a new emission band. No changes were observed with other anions. ([Fig. S14 in Supplementary data](#)).

The photophysical and photochemical phenomena of **BF₂-curcumin** in the presence of cyanide were assumed to undergo the deprotonation of hydroxyl groups by CN[−]. NMR spectra showed a strong evidence to support this assumption ([Fig. 9](#)). According to ¹H NMR spectra of **BF₂-curcumin** and CN[−], the hydroxyl protons

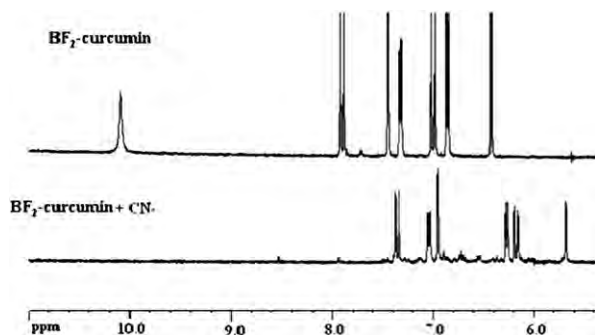
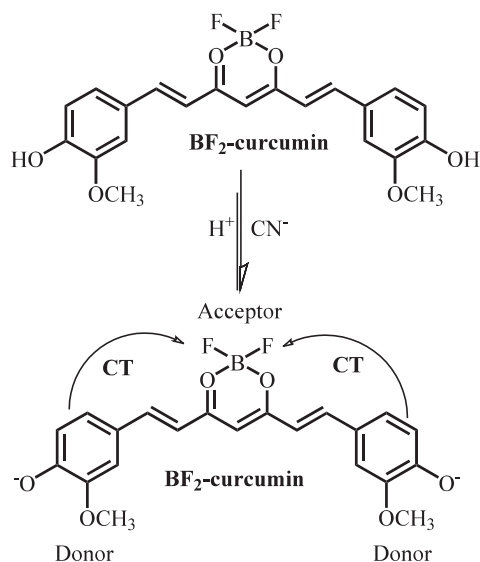


Figure 9. ^1H NMR spectrum of $\text{BF}_2\text{-curcumin}$ and $\text{BF}_2\text{-curcumin}+\text{CN}^-$ in $\text{DMSO-}d_6$.

(10.09 ppm) completely disappeared with a concomitant of the large upfield shifts of aromatic and alkene protons from 7.90–6.42 to 7.28–5.64 ppm. This indicated that the aromatic protons were shielded by the negative charge of the deprotonated hydroxyl group.

This deprotonation caused a high charge separation between acceptor and donor unit in $\text{BF}_2\text{-curcumin}$, and consequently excellent electron delocalization to BF_2 unit. The excited states in the complexes were stabilized upon the binding of CN^- , resulting in a bathochromic shift in the absorption band with $\Delta\lambda=142$ and 92.9 nm for $\text{BF}_2\text{-curcumin}$ and curcumin , respectively. Moreover, a new emission band at 750 nm for $\text{BF}_2\text{-curcumin}$ and CN^- was observed. The red shift of $\text{BF}_2\text{-curcumin}$ is larger than that of curcumin , possibly caused by a large charge separation between BF_2 unit and the aromatic rings resulting in a strong intramolecular charge transfer (ICT).^{43–46} A schematic illustration is shown in Scheme 2.



Scheme 2. The ICT process of $\text{BF}_2\text{-curcumin}$ upon adding CN^- .

The selective binding properties of $\text{BF}_2\text{-curcumin}$ and curcumin towards CN^- can be described by the basicity of anions. The charge transfer process could not occur in the case of fluoride ion due to its high hydration enthalpy and low basicity ($\Delta H_{\text{hyd}}^0 = -504$ kJ/mol, $\text{p}K_{\text{a}} = 3.18$) in an aqueous system.⁴⁷ Furthermore, the binding constants of $\text{BF}_2\text{-curcumin}$ or curcumin towards CN^- were carried out by UV–vis and fluorometric titrations. Logarithm ($\log \beta_2$)⁴⁸ of overall stability constants of the deprotonation of $\text{BF}_2\text{-curcumin}$ are 8.8 and those of curcumin are 7.7.

The interference of foreign substances; such as, F^- , Cl^- , Br^- , I^- , AcO^- , BzO^- , and H_2PO_4^- against cyanide detection of $\text{BF}_2\text{-curcumin}$

and curcumin was evaluated by fluorescence methods. Compared to curcumin , the presence of the BF_2 part in $\text{BF}_2\text{-curcumin}$ showed a benefit on the reduction of the interference effect from other anions (Fig. 10). The fluorescence signal of the solution of curcumin and cyanide were seriously disturbed by other anions. In the case of $\text{BF}_2\text{-curcumin}$, the miscellaneous competitive anions did not perturb the emission signal, except for F^- , AcO^- , and H_2PO_4^- . The tolerance of cyanide sensing against other interference anions, in which the relative error are fixed at $\pm 10\%$,⁴⁹ was listed in Table S5. The presence of F^- , AcO^- , and H_2PO_4^- at molar ratios of 100, 470, and 6, respectively, could interfere the cyanide sensing of $\text{BF}_2\text{-curcumin}$.

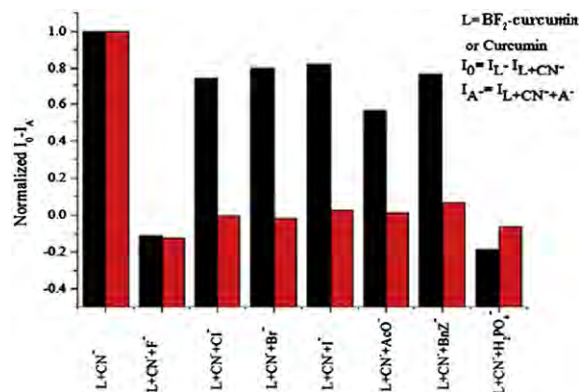


Figure 10. Fluorescence responses of $\text{BF}_2\text{-curcumin}$ (black bar) and curcumin (red bar) (7.5 μM) to CN^- (0.5 mM) in the presence of foreign anions in $\text{CH}_3\text{CN}/\text{H}_2\text{O}$ (4:1) ($\text{BF}_2\text{-curcumin}$: $\lambda_{\text{ex}}=507$ nm, $\lambda_{\text{em}}=600$ nm, and curcumin : $\lambda_{\text{ex}}=417.1$ nm, $\lambda_{\text{em}}=543$ nm).

Colorimetric and UV–vis detection limits of $\text{BF}_2\text{-curcumin}$ and curcumin for CN^- were also evaluated (Fig. 11). In $\text{CH}_3\text{CN}/\text{H}_2\text{O}$ (4:1 v/v), the visual detection limit of $\text{BF}_2\text{-curcumin}$ (10 μM) towards CN^- is 22 μM while in the case of curcumin (10^{-4} M), the color change can be detected visually at the concentration of $\text{CN}^- \geq 75$ μM . Compared to the UV–vis detection limit, the absorption changes (Fig. 12), calculated on the basis of $3\sigma/K$,^{50,51} could extend the limit of detection down to 0.14 and 9.33 μM for $\text{BF}_2\text{-curcumin}$ and curcumin , respectively (Fig. 11).

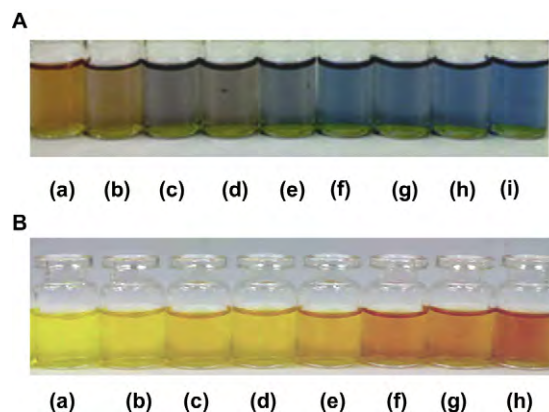


Figure 11. Colorimetric changes of A. $\text{BF}_2\text{-curcumin}$ (0.01 mM) in $\text{CH}_3\text{CN}/\text{H}_2\text{O}$ (4:1, v/v) upon the addition of (a) 0, (b) 15, (c) 22, (d) 24, (e) 29, (f) 36, (g) 43, (h) 50, and (i) 57 μM of CN^- . B. curcumin (0.1 mM) in $\text{CH}_3\text{CN}/\text{H}_2\text{O}$ (4:1, v/v) upon the addition of (a) 0, (b) 50, (c) 75, (d) 99, (e) 109, (f) 124, (g) 149, and (h) 172 μM of CN^- .

This is indicative of a higher detectable sensitivity of $\text{BF}_2\text{-curcumin}$ than that of curcumin for cyanide sensing. Therefore, $\text{BF}_2\text{-curcumin}$ is a promising sensor for cyanide. For $\text{BF}_2\text{-curOTs}$, we did not study the cyanide detection properties of this compound because it readily decomposed in air.

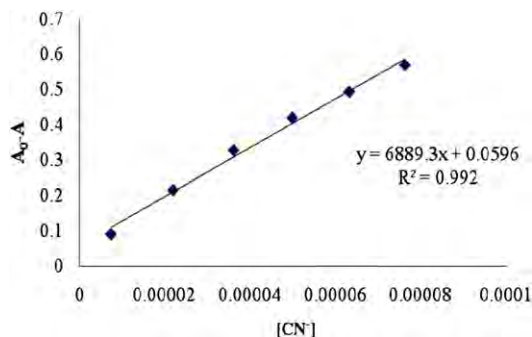


Figure 12. Linear plot between absorbance of **BF₂-curcumin** (7.5 μM) versus concentration of CN⁻.

3. Conclusions

In summary, D–A–D molecular sensors employing derivatives of **BF₂-curcumin** with different substituents on hydroxyl groups were successfully synthesized, and their photo-physical and -chemical properties were examined. Electron-withdrawing substituted groups attached to the donor part of **BF₂-curcumin** induced a hypsochromic shift in both absorption and emission spectra. Conversely, electron-donating groups stabilized a higher energy level of the molecules resulting in the bathochromic shift of UV–vis and fluorescence spectra. The photophysical properties of **BF₂-curcumin** and **BF₂-cur(OMe)₂** exhibited a positive solvatochromic effect, mainly depending on the solvent polarity/polarizability factor. The incorporation of BF₂ on the curcumin structure gave a cyanide sensor with excellent selectivity and sensitivity. The sensing approach relied on the deprotonation of the hydroxyl group of **BF₂-curcumin** by CN⁻ leading to an extended π-conjugated system. **BF₂-curcumin** thus serves as a promising chemical sensor for cyanide detection by either naked-eye for on-site detection or spectrophotometry when a better resolution is required.

4. Experimental

4.1. Materials and methods

Nuclear magnetic resonance (NMR) spectra were recorded in DMSO-*d*₆, CDCl₃ and CD₃CN on a Varian 400 MHz spectrometer. Electrospray mass spectra were determined on a Micromass Platform quadrupole mass analyzer with an electrospray ion source using acetonitrile as solvent. Elemental analyses were carried out on a Perkin–Elmer CHON/S analyzer (PE 2400 series II). Absorption spectra were measured by a Varian Cary 50 UV–vis spectrophotometer. Fluorescence spectra were performed on a Varian eclipse spectrofluorometer. Unless otherwise specified, the solvents and all materials were reagent grades without further purification. Commercial grade solvents such as acetone, dichloromethane, hexane, methanol, and ethyl acetate were purified by distillation. Acetonitrile, dimethylformamide, and dichloromethane were dried over calcium hydride and THF was dried over benzoquinone and sodium and freshly distilled under nitrogen prior to use.

4.2. Synthesis

4.2.1. Preparation of methylated curcumin borondifluoride (BF₂-cur(OMe)₂). In a 250 mL two-necked round bottom flask equipped with a magnetic bar and a reflux condenser, a solution of **BF₂-curcumin** (0.416 g, 1 mmol) and anhydrous potassium carbonate in

methanol (100 mL) was stirred for 10 min. Methyl iodide (1.5 mL, 2 mmol) in methanol (4 mL) was added dropwise into the reaction mixture, which was refluxed at 60 °C overnight. The solvent was removed by rotary evaporator to obtain a crude product. The crude product was dissolved in ethyl acetate and washed with water. The organic layer was dried over anhydrous sodium sulfate and evaporated to dryness under reduced pressure. The desired product (**BF₂-cur(OMe)₂**) was obtained as a purple crystalline solid (73% yield) after recrystallization in hexane/ethyl acetate. ¹H NMR (400 MHz, DMSO) δ (in ppm)=7.954 (*J*=16.0 Hz, d, –ArH, 2H), 7.477 (*s*, –ArH, 2H), 7.450 (*J*=8.4 Hz, d, –ArH, 2H), 7.086 (*J*=15.6 Hz, d, –olifinic-H, 2H), 7.077 (*s*, –ArH, 2H), 6.487 (*s*, –ArH, 1H), 3.822 (*s*, –OCH₃, 12H). ¹³C NMR (100.6 MHz, CDCl₃) δ (in ppm)=56.11, 56.22, 102.20, 111.63, 112.23, 119.30, 125.64, 127.54, 147.28, 149.55, 153.01, 179.50; ESI MS: *m/z*=445.63 [M⁺]. Anal. Calcd for C₂₃H₁₅N₃O₃: C, 62.18; H, 5.22. Found: C, 62.53; H, 5.32.

4.2.2. Preparation of monotosylation curcumin borondifluoride (BF₂-curOTs) and ditosylation curcumin borondifluoride (BF₂-cur(OTs)₂). In a 100 mL two-neck round bottom flask, a solution of **BF₂-curcumin** (0.277 g, 0.67 mmol), DMAP (4-Dimethylaminopyridine), and triethylamine (0.084 mL, 2.01 mmol) was stirred for 30 min in dichloromethane (30 mL) at 0 °C under nitrogen. A solution of *para*-toluenesulfonyl chloride (0.284 g, 1.49 mmol) in dichloromethane (10 mL) was added dropwise into the mixture over 30 min. Upon completion of the reaction, a solution of HCl (3 M) was added into the mixture to adjust the pH to 1 and stirred for 30 min. The reaction was extracted with water, and the organic solvent was dried over Na₂SO₄ and then evaporated in vacuo. The crude product was purified by column chromatography using 5% ethyl acetate in dichloromethane to afford **BF₂-curOTs** (*R_f*=0.65) and **BF₂-cur(OTs)₂** (*R_f*=0.83) in 23% and 71% yields, respectively.

4.2.2.1. BF₂-curOTs. ¹H NMR (400 MHz, DMSO-*d*₆) δ (in ppm)=7.97 (*J*=15.6 Hz, d, olifinic-H, 1H), 7.85 (*J*=15.2 Hz, d, olifinic-H, 1H), 7.70 (*J*=8.0 Hz, d, –ArH, 2H), 7.26 (*J*=8 Hz, d, –ArH, 2H), 7.07 (d, –ArH, 2H), 7.03 (*s*, –ArH, 1H), 6.93 (d, –ArH, 1H), 6.90 (*s*, –ArOH, 1H), 6.54 (*J*=15.6 Hz, d, –CH=CH–, 3H), 6.01 (*J*=17.2 Hz, d, –CH=CH–, 2H), 3.90 (*s*, –OCH₃, 3H), 3.56 (*s*, –OCH₃, 3H), 1.98 (*s*, –CH₃, 3H). ¹³C NMR (100.6 MHz, CDCl₃) δ (in ppm)=29.71, 55.72, 56.07, 110.82, 112.83, 115.46, 121.39, 121.62, 124.46, 124.69, 128.61, 129.50, 133.93, 139.24, 145.03, 147.13, 148.82, 180.01; ESI MS: *m/z*=570.87 [M⁺] (C₂₃H₂₃BF₂O₆)

4.2.2.2. BF₂-cur(OTs)₂. ¹H NMR (400 MHz, DMSO-*d*₆) 7.91 (*J*=16 Hz, d, olifinic-H, 2H), 7.70 (*J*=8.4 Hz, d, –ArH, 4H), 7.26 (*J*=8.0 Hz, d, –ArH, 4H), 7.15 (d, –ArH, 4H), 6.96 (*s*, –CH=CH–, 2H), 6.59 (*J*=15.6 Hz, d, –CH=CH–, 2H), 6.04 (*s*, –CH=CH–, 1H), 3.57 (*s*, –OCH₃, 6H), 2.40 (*s*, –CH₃, 6H). ¹³C NMR (100.6 MHz, CDCl₃) δ (in ppm)=21.76, 55.74, 102.56, 112.91, 121.34, 121.67, 124.74, 128.59, 129.55, 133.0, 133.73, 140.92, 145.48, 146.38, 152.35, 180.06; HRMS (positive ESI) *m/z* calcd for C₂₃H₂₃BF₂O₆Na (M+Na⁺) 747.1420, found 747.1396.

4.3. Studies of solvent effects of BF₂-curcumin and BF₂-cur(OMe)₂

The solutions of **BF₂-curcumin** and **BF₂-cur(OMe)₂** (1.0 mM) were prepared in organic solvents (spectroscopic grade), such as methanol, ethanol, toluene, benzene, chloroform, dichloromethane, diethyl ether, ethyl acetate, and DMSO and were placed in 10.0 mm width quartz cell. Fluorescence spectra (excitation at 497.1 and 503.0 nm for **BF₂-curcumin** and **BF₂-cur(OMe)₂**, respectively) and UV–vis spectra were recorded at room temperature.

4.4. UV–vis titrations and fluorescent titrations to determine the binding constants of BF₂-curcumin and curcumin towards CN[−]

All UV–vis and fluorescent titrations of **BF₂-curcumin** (7.5×10^{-3} mM) and **curcumin** (5.0×10^{-3} mM) in the presence of cyanide ion were recorded in CH₃CN/H₂O (4/4 v/v) using of [Bu₄N] [PF₆] (0.01 M) as a supporting electrolyte. The solutions of CN[−] were prepared and gradually added into the solution of receptor (2 mL). Absorption and emission spectra of solution were recorded after each addition until absorbance of a new peak at 649 nm and 510 nm and emission quenching at 600 nm and 543 nm for **BF₂-curcumin** and **curcumin**, respectively, were constant. The stability constants (log β) of cyanide complexes of receptors were evaluated by fitting the titration curves to the non-linear relation using the following equations (Eqs. 4 and 5 for fluorescence and UV–vis techniques, respectively).

$$I = \frac{I_0 + I_{\infty} \beta_n [\text{CN}^-]^n}{1 + \beta_n [\text{CN}^-]^n} \quad (4)$$

$$A = \frac{A_0 + A_{\infty} \beta_n [\text{CN}^-]^n}{1 + \beta_n [\text{CN}^-]^n} \quad (5)$$

Acknowledgements

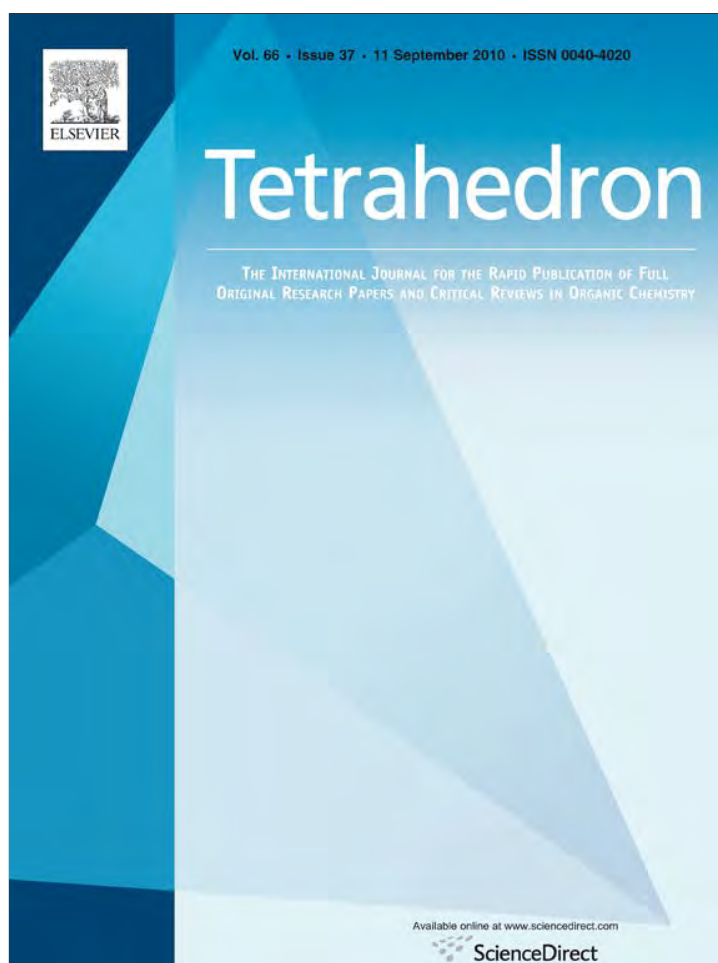
AC is a M.Sc. student supported by Thailand Graduate Institute of Science and Technology (TGIST) and SK is a M.Sc. student supported by Junior Science Talent Project (JSTP). The authors wish to thank the grants provided by National Nanotechnology Center (NN-B-22-b15-94-49-55) and the Thailand Research fund (RTA5080006). The authors also appreciate THAI-CHINA FLAVORS & FRAGRANCES INDUSTRY CO., LTD for providing the turmeric extract (curcumin powder).

Supplementary data

The analysis of the synthesized compounds including NMR spectra, UV–vis and fluorescent experiments are provided. Supplementary data associated with this article can be found in online version at doi:10.1016/j.tet.2010.05.088.

References and notes

- Tomasulo, M.; Raymo, M. F. *Org. Lett.* **2005**, *7*, 4633–4636.
- Chattopadhyay, I.; Biswas, K.; Bandyopadhyay, U.; Banerjee, R. K. *Curr. Sci.* **2004**, *87*, 44–53.
- Aggarwal, B. B.; Shishodia, S. *Biochem. Pharmacol.* **2006**, *71*, 1397–1421.
- Leyon, P. V.; Kuttan, G. *J. Exp. Clin. Cancer Res.* **2003**, *22*, 77–83.
- Nurfinal, A. N.; Reksodiprodjo, M. S.; Timmerman, H. U.; Jenie, A.; Sugiyant, D.; van der Goot, H. *Eur. J. Med. Chem.* **1997**, *32*, 321–328.
- Shishodia, S.; Sethi, G.; Aggarwal, B. B.; Ann, N. Y. *Acad. Sci.* **2005**, *1056*, 206–217.
- Siwak, D. R.; Shishodia, S.; Aggarwal, B. B.; Kurzrock, R. *Cancer* **2005**, *104*, 879–890.
- Aggarwal, B. B.; Shishodia, S.; Takada, Y.; Banerjee, S.; Newman, R. A.; Bueso-Ramos, C. E.; Price, J. E. *Clin. Cancer Res.* **2005**, *11*, 7490–7498.
- Aggarwal, S.; Ichikawa, H.; Takada, Y.; Sandur, S. K.; Shishodia, S.; Aggarwal, B. B. *Mol. Pharmacol.* **2006**, *69*, 195–206.
- Garcia-Alloza, M.; Borrelli, L. A.; Rozkalne, A. B.; Hyman, T. B.; Bacska, J. J. *Neurochem.* **2007**, *102*, 1095–1104.
- Yang, F.; Lim, G. P.; Begum, A. N.; Ubeda, O. J.; Simmons, M. R.; Ambegaokar, S. S.; Chen, P. P.; Kaye, R.; Glabe, C. G.; Frautschi, S. A.; Cole, G. M. *J. Biol. Chem.* **2005**, *280*, 5892–5901.
- Ryu, E. K.; Choe, Y. S.; Lee, K. H.; Choi, Y.; Kim, B. T. *J. Med. Chem.* **2006**, *49*, 6111–6119.
- Barik, A.; Priyadarsini, K. I.; Mohan, H. *Photochem. Photobiol.* **2003**, *77*, 597–603.
- Priyadarsini, K. I. *J. Photochem. Photobiol. C: Photochem. Revs.* **2009**, *10*, 81–95.
- Loudet, A.; Burgess, K. *Chem. Rev.* **2007**, *107*, 4891–4932.
- Fana, J.; Guoa, K.; Penga, X.; Dua, J.; Wangb, J.; Suna, S.; Li, H. *Sens. Actuators, B* **2009**, *142*, 191–196.
- Meng, G.; Velayudham, S.; Smith, A.; Luck, R.; Liu, H. *Macromolecules* **2009**, *42*, 1995–2001.
- Donuru, V. R.; Vegesna, G. K.; Velayudham, S.; Green, S.; Liu, H. *Chem. Mater.* **2009**, *21*, 2130–2138.
- Lai, R. Y.; Bard, A. J. *J. Phys. Chem. B* **2003**, *107*, 5036–5042.
- Ma, G.; Cheng, Q. *Langmuir* **2006**, *22*, 6743–6745.
- Chow, Y. L.; Johansson, C. I.; Zhang, Y.-H.; Gautron, R.; Yang, L.; Rassat, A.; Yang, S.-Z. *J. Phys. Org. Chem.* **1996**, *9*, 7–16.
- Hales, J. M.; Zheng, S.; Barlow, S.; Marder, S. R.; Perry, J. W. *J. Am. Chem. Soc.* **2006**, *128*, 11362–11363.
- Chow, Y. L.; Johansson, C. I. *J. Phys. Chem.* **1995**, *99*, 17558–17565.
- Cogne'-Laage, E.; Allemand, J.-F.; Ruel, O.; Baudin, J.-B.; Croquette, V.; Blanchard-Desce, M.; Jullien, L. *Chem.—Eur. J.* **2004**, *10*, 1445–1455.
- Pfister, A.; Zhang, G.; Zareno, J.; Horwitz, A. F.; Fraser, C. L. *ACS Nano* **2008**, *2*, 1252–1258.
- Suai, Z.; Salto, R.; Li, J.; Craik, C.; Ch-tizde Montellano, P. R. *Bioorg. Med. Chem.* **1993**, *1*, 415–422.
- Li, Z.; Lou, X.; Yu, H.; Li, Z.; Qin, J. *Macromolecules* **2008**, *41*, 7433–7439.
- Sessler, J. L.; Cho, D.-G. *Org. Lett.* **2008**, *10*, 73–75.
- Ho, H. A.; Leclerc, M. *J. Am. Chem. Soc.* **2003**, *125*, 4412–4413.
- Powell, S. C. *Anal. Chem.* **2009**, *81*, 9535.
- Xu, Z.; Chen, X.; Kim, H. N.; Yoon, J. *Chem. Soc. Rev.* **2010**, *39*, 127–137.
- Anzenbacher, P., Jr.; Tyson, D. S.; Jurskova, K.; Castellano, F. N. *J. Am. Chem. Soc.* **2002**, *124*, 6232–6233.
- Kim, Y.-H.; Hong, J.-I. *Chem. Commun.* **2002**, 512–513.
- Ganesh, V.; Sanz, M. P. C.; Mareque-Rivas, J. C. *Chem. Commun.* **2007**, 5010–5012.
- Zeng, Q.; Cai, P.; Li, Z.; Qina, J.; Tang, B. Z. *Chem. Commun.* **2008**, 1094–1096.
- Kim, Y. K.; Lee, Y.-H.; Lee, H.-Y.; Kim, M.-K.; Cha, G. S.; Ahn, K. H. *Org. Lett.* **2003**, *5*, 4003–4006.
- Ekmekci, Z.; Yilmaz, M. D.; Akkaya, E. U. *Org. Lett.* **2008**, *10*, 461–464.
- Ran, C.; Xu, X.; Raymond, S. B.; Ferrara, B. J.; Neal, K.; Bacska, B. J.; Medarova, Z.; Moore, A. J. *Am. Chem. Soc.* **2009**, *131*, 15257–15261.
- Lakowicz, J. R. *Principles of Fluorescence Spectroscopy*; Springer Science+Business Media, LLC: New York, NY, USA, 2006.
- Marcus, Y. *Chem. Soc. Rev.* **1993**, *22*, 409–416.
- Schreiter, K.; Spange, S. J. *Phys. Org. Chem.* **2008**, *21*, 242–250.
- Roth, H. J.; Miller, B. *Arch. Pharm. Ber. Dtsch. Pharm. Ges.* **1964**, *297*, 660–673.
- Huh, J. O.; Do, Y.; Lee, M. H. *Organometallics* **2008**, *27*, 1022–1025.
- Marcotte, N.; Plaza, P.; Lavabre, D.; Fery-Forgues, S.; Martin, M. M. J. *Phys. Chem. A* **2003**, *107*, 2394–2402.
- Jamkratoke, M.; Ruangpornvisuti, V.; Tumcharern, G.; Tuntulani, T.; Tomapatanaget, B. *J. Org. Chem.* **2009**, *74*, 3919–3922.
- Fery-Forgues, S.; Le Bris, M.-T.; Mialocq, J.-C.; Pouget, J.; Rittig, W.; Valuer, B. J. *Phys. Chem. A* **1992**, *96*, 701–710.
- Hudnall, T. W.; Gabbai, F. P. *J. Am. Chem. Soc.* **2007**, *129*, 11978–11986.
- Cooper, C. R.; Spencer, N.; James, T. D. *Chem. Commun.* **1998**, 1365–1366.
- Shen, Y.; Yang, X.-F.; Wu, Y.; Li, C. J. *Fluoresc.* **2008**, *18*, 163–168.
- Ono, A.; Togashi, H. *Angew. Chem., Int. Ed.* **2004**, *43*, 4300–4302.
- Liu, J.; Lu, Y. *Angew. Chem., Int. Ed.* **2007**, *46*, 7587–7590.



This article appeared in a journal published by Elsevier. The attached copy is furnished to the author for internal non-commercial research and education use, including for instruction at the authors institution and sharing with colleagues.

Other uses, including reproduction and distribution, or selling or licensing copies, or posting to personal, institutional or third party websites are prohibited.

In most cases authors are permitted to post their version of the article (e.g. in Word or Tex form) to their personal website or institutional repository. Authors requiring further information regarding Elsevier's archiving and manuscript policies are encouraged to visit:

<http://www.elsevier.com/copyright>



Contents lists available at ScienceDirect

Tetrahedron

journal homepage: www.elsevier.com/locate/tet

A steroid-based receptor for unprotected amino acids: the enantioselective recognition of L-tryptophan

Anchalee Sirikulajorn^{a,b}, Thawatchai Tuntulani^a, Vithaya Ruangpornvisuti^a,
Boosayarat Tomapatanaget^{a,*}, Anthony P. Davis^{b,*}

^aSupramolecular Chemistry Research Unit, Department of Chemistry, Faculty of Science, Chulalongkorn University, Bangkok 10330, Thailand

^bSchool of Chemistry, University of Bristol, Bristol, BS8 1TS, UK

ARTICLE INFO

Article history:

Received 5 April 2010

Received in revised form 16 June 2010

Accepted 28 June 2010

Available online 7 July 2010

ABSTRACT

A cholapod receptor possessing urea binding sites at C3, C7, and C12 positions and with an intrinsic chiral structure was synthesized, and the binding abilities toward amino acids in both L- and D- forms (Trp, Phe, Leu, and Ala) were studied using ¹H NMR spectroscopy, UV–vis spectroscopy and computer simulation. Changes in ¹H NMR spectra of the receptor revealed that complexation with amino acids occurred via hydrogen bonding and CH–π interactions. Binding to tryptophan was especially strong, and was found to be enantioselective ($K_a=480\text{ M}^{-1}$ for L-Trp, 260 M^{-1} for D-Trp). NOESY and computer simulations were used to investigate the structures of the diastereomeric complexes between the receptor and the tryptophan enantiomers. In the case of L-Trp the carboxylate group bound at the two ureas adjacent to C7 and C12, while D-Trp was positioned closer to the urea adjacent to C3.

© 2010 Elsevier Ltd. All rights reserved.

1. Introduction

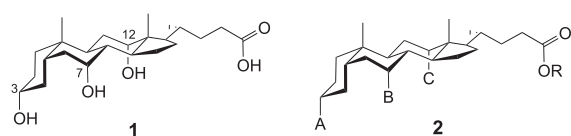
The molecular recognition of biological targets has formed a major part of host–guest chemistry. Amino acids and their derivatives are especially important substrates,¹ due to their central role in natural living systems. However, the molecular recognition of unprotected α-amino acids presents distinctive challenges, due to the requirement for polar solvents to dissolve the substrates and the suppression of polar interactions in such solvents. Amino acids are also relevant as archetypal chiral substrates. Much effort has been devoted to the design and synthesis of receptors for chiral recognition.² However, success has not been easy to achieve, and not many have shown good selectivities. There are only a few receptor systems giving enantioselectivities of more than 90% ee³.

To obtain good enantioselectivity, a receptor must be designed carefully for 3D complementarity to its intended substrate. The steroidal framework derived from cholic acid **1** affords many advantages; (i) a large rigid unit able to span a substrate, (ii) chirality, and (iii) preorganized codirected functional groups, which can be elaborated into ‘legs’ to contact the substrate. This combination of

properties has lead to various applications of steroids in the construction of receptors,⁴ including enantioselective receptors for amino acid derivatives.⁵ A successful strategy has been the conversion of cholic acid **1** into cholapods of general form **2**, in which groups A–C include NH groups for hydrogen bonding with the substrate. The NH unit is more versatile than the native OH in **1**, appearing in amides, sulfonamides, carbamates, ureas thioureas, and guanidinium groups.

Although cholapods have been used for the recognition of peptides^{4a} and N-acetyl amino acids,⁵ they have not been applied to unprotected amino acids.⁶ In the present work, our target was a receptor capable of enantioselective recognition of the less polar α-amino acids (L-Trp, D-Trp, L-Phe, D-Phe, L-Leu, D-Leu, L-Ala, and D-Ala) in a polar organic solvent. Our design **8** was based on the cholapod architecture with urea units attached to C-3, C-7, and C-12. Urea groups were known to interact strongly with anionic species through hydrogen bonding interactions,⁷ and would be especially suitable as binding sites for the carboxylate groups of zwitterionic amino acids. By employing three ureas we would maximise the chance of binding in the polar, competitive solvent, which would be needed to dissolve the substrates. Cholapods with three urea groups had been used to bind inorganic anions,^{7k} but not organic substrates. The aromatic groups terminating the ‘legs’ could assist binding through CH–π interactions with substrate side-chains, while the nitroazobenzene unit was included as a chromophore, which might provide an optical response to binding.

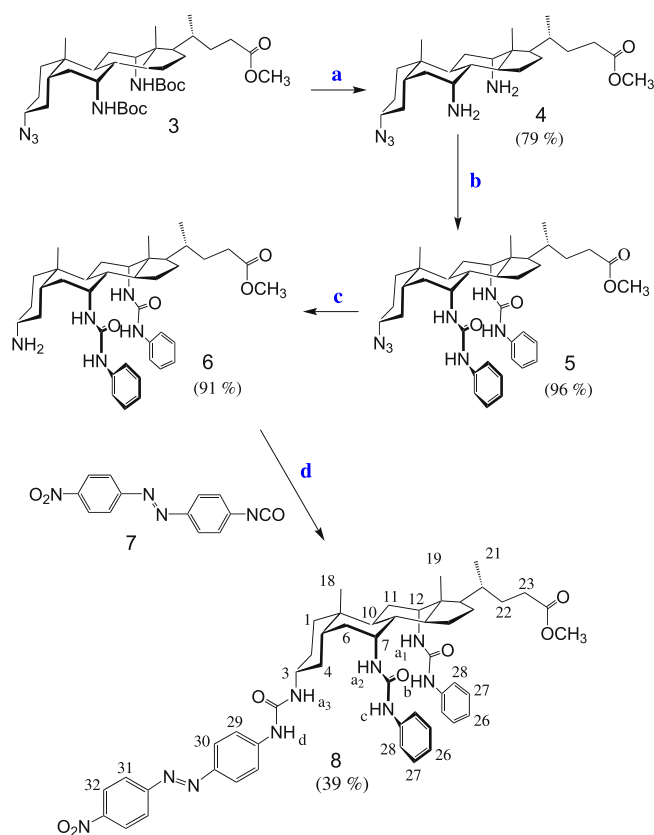
* Corresponding authors. E-mail address: tboosayarat@gmail.com (B. Tomapatanaget).



2. Results and discussion

2.1. Synthesis

The synthetic pathway to receptor **8** is summarized in Scheme 1. The synthesis of azide **3**, a key intermediate for the synthesis of steroidal podands with multiple NH groups, has been previously reported.⁸ Diamine **4** was prepared by reaction of **3**⁸ with TFA. Treatment of **4** with 2 equiv of phenyl isocyanate afforded 7,12-bis-urea **5**⁹ in 96% yield. The third amino group was then unmasked through reduction of the azide group, giving **6**.⁹



Scheme 1. Synthesis and numbering system for receptor **8**. Reagents and conditions: (a) TFA, DCM; (b) PhNCO, Et₃N, DMAP, THF, 50 °C; (c) activated zinc, HOAc; (d) DMAP, THF.

Treatment of **6** with nitroazobenzene isocyanate **7**¹⁰ in the presence of DMAP as a catalyst gave the desired product **8** in 39% yield.

2.2. Binding studies using ¹H NMR spectroscopy

The recognition of unprotected α -amino acids by **8** was investigated first by ¹H NMR spectroscopy. The amino acids were added in fourfold excess to the receptor in DMSO-*d*₆, and the resulting changes in the spectrum of the receptor were recorded to provide preliminary information on complex formation. The results are shown in Figure 1 and Table 1. Addition of the amino acids produced substantial downfield movements of the urea NH signals (H_a, H_b, H_c, and H_d), consistent with complex formation via

hydrogen bonding interactions between the urea moieties and the carboxylate groups of the zwitterionic substrates. Small shifts of some aromatic protons (H₂₇, H₂₈, H₂₉, and H₃₀) were also observed, suggestive of interactions between amino acid side-chains and aromatic moieties in **8**.

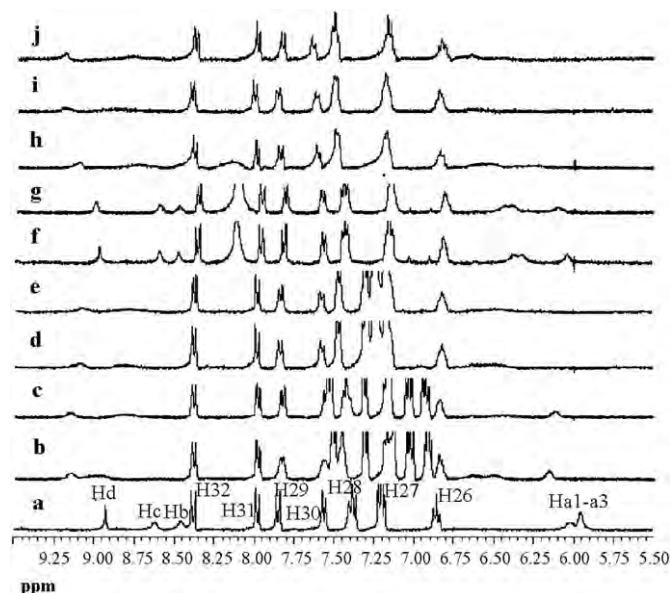


Figure 1. Partial ¹H NMR spectra in DMSO-*d*₆ of **8** (a) and the complexes of **8** with 4 equiv of L-Trp (b) D-Trp (c) L-Phe (d) D-Phe (e) L-Leu (f) D-Leu (g) D-Ala (h) Gly (i) Gly (j).

Table 1

Chemical shifts (ppm) of ligand **8** (4 mM) in DMSO-*d*₆ and the changes observed upon addition of various amino acids (4 equiv)^a

	H ₂₆	H ₂₇	H ₂₈	H ₂₉	H ₃₀	NH _a	NH _b	NH _c	NH _d
8	6.86	7.20	7.38	7.84	7.56	6.00	8.46	8.23	8.93
8 ·L-Trp	−0.02	−0.03	+0.08	−0.02	−	+0.48	+0.50	+0.34	+0.21
8 ·D-Trp	−0.01	−0.03	+0.04	−0.03	−	+0.31	+0.36	+0.20	+0.22
8 ·L-Phe	−0.03	−0.04	+0.08	−	−	−	+0.35	+0.19	+0.17
8 ·D-Phe	−0.03	−0.04	+0.08	−0.02	+0.02	−	−	−	+0.22
8 ·L-Leu	−0.03	−0.04	+0.08	−0.02	+0.03	+0.30	+0.04	−	+0.08
8 ·D-Leu	−	−	+0.09	−	+0.05	+0.31	+0.06	+0.02	+0.09
8 ·L-Ala	−0.03	−0.04	+0.09	−0.02	+0.05	−	−	−	+0.25
8 ·D-Ala	−0.03	−0.04	+0.09	−0.02	+0.05	−	−	−	+0.25
8 ·Gly	−0.03	−0.05	+0.12	−0.02	+0.07	−	−	−	+0.25

−: Values could not be determined due to signal broadening.

^a Positive values represent downfield shifts and negative values represent upfield shifts.

The movements of the urea NH signals varied considerably depending on the amino acid added, giving preliminary indications of differential complexation properties. Especially, large movements were observed in the complex between **8** and L-Trp (**8**·L-Trp). In this case, the signals for H_a, H_b, and H_c were shifted downfield by +0.48, +0.50, and +0.34 ppm, respectively. The corresponding values for the diastereomeric complex **8**·D-Trp were significantly smaller. The shifts of urea protons (H_d) and aromatic protons (H₂₆–H₃₀) were less sensitive to the structure of the amino acid.

Complex formation was further investigated through ¹H NMR titrations. The results from the addition of aliquots of L-Trp to **8** in DMSO-*d*₆ are shown in Figure 2. Corresponding data from the experiments employing D-Trp, L-Phe, and D-Phe are shown in the Supplementary data.

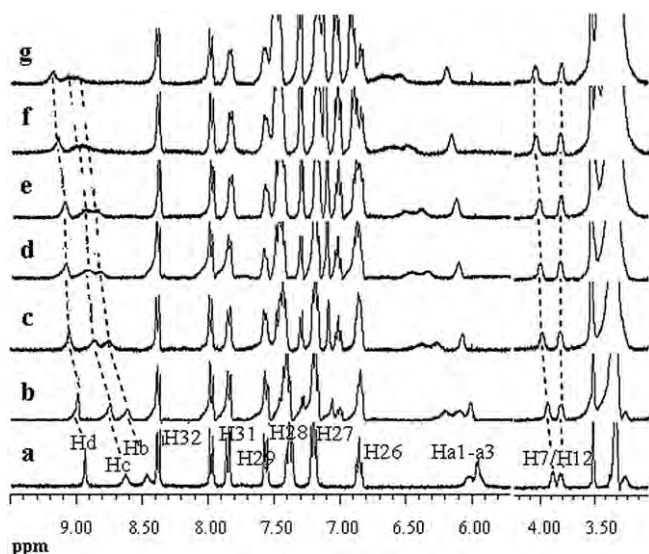


Figure 2. Partial ^1H NMR titration spectra of (a) **8** (4.0×10^{-3} M) upon adding L-Trp in equivalent of (b) 0.4 (c) 0.8 (d) 1.6 (e) 2.0 (f) 3.0 and (g) 4.0 in $\text{DMSO}-d_6$.

Initially, the NH_a urea protons in **8** appeared as two signals, one due to the NH proton adjacent to the C3 position and the other due to the two NH protons adjacent to C7 and C12. Addition of L-Trp caused all the NH_a resonances to move downfield, although the signals due to C7/C12-NH moved considerably further than those due to C3-NH. A similar pattern was observed for the ArNH urea protons, where NH_b and NH_c (from the C7 and C12 ureas) were shifted further than the C3 urea proton NH_d .

It thus seems that complex formation between **8** and L-Trp occurs mainly through hydrogen bonding to the C7 and C12 ureas. Downfield shifts were also observed for all the NH protons of **8** on addition of the other amino acids. However, in these cases the signals became broadened so that detailed interpretations were problematic.

The broadening of the NH signals precluded accurate analysis to obtain binding constants. However small movements of the C7 and C12 protons at $\delta=3.60\text{--}3.80$ ppm were also observed, and these could be followed reliably. In the case of D/L-Phe, D/L-Leu, and D/L-Ala, the changes in chemical shift were almost linear with substrate concentrations, over the range of concentrations accessible so that binding was too weak to be quantified by this methodology. In contrast, the movements of the C7-H signal caused by addition of L-Trp or D-Trp showed significant curvature when plotted against the concentrations of added guest (see Fig. 3). The shifts could be analyzed by non-linear curve-fitting according to a 1:1 binding model, to give association constants K_a of 480 M^{-1} for L-Trp and 260 M^{-1} for D-Trp. The formation of simple 1:1 complexes was confirmed by Job's plot analysis (see Supplementary data).

UV–vis titration experiments were also carried out in DMSO, in the hope of detecting binding through an optical signal. Unfortunately, the UV–vis spectrum of **8** showed only very small changes on addition of amino acids (see Supplementary data), and no significant color change was observed. Although disappointing, this was consistent with the NMR and modeling studies, which did not imply significant interactions between substrate and chromophore. We thus could not refine and investigate the binding properties of host **8** with amino acids by UV–vis spectrophotometry. If the azo group is not involved in binding, it is probable that the simpler analogues with three identical urea groups^{7k} would show similar affinities and enantioselectivities.

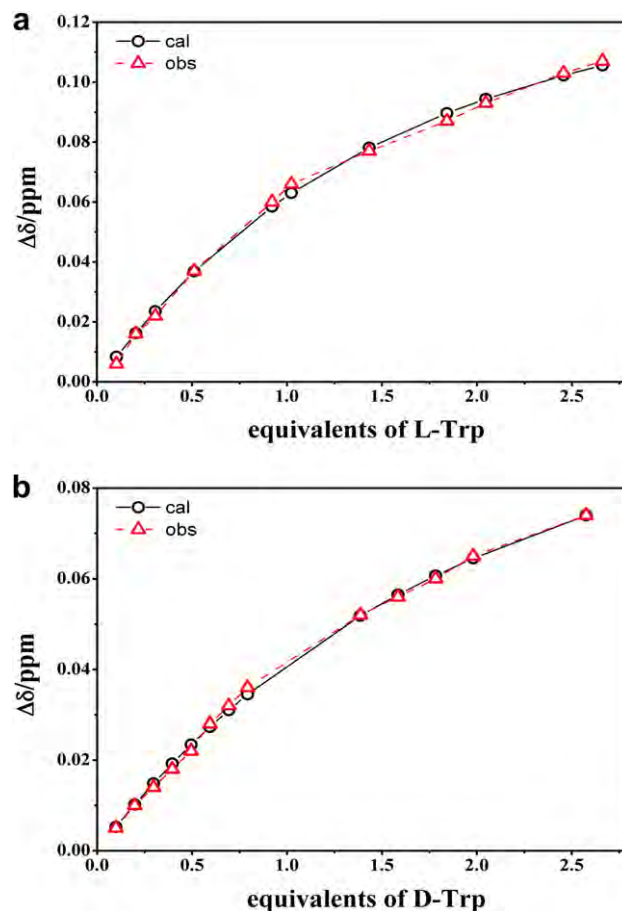


Figure 3. Theoretical (O) and experimental (Δ) binding curves for NMR titrations of **8** (4.0×10^{-3} M) with tryptophan enantiomers in $\text{DMSO}-d_6$. In each case the signal followed was due to 7 β H. (a) L-Trp, $K_a=480\text{ M}^{-1}$. (b) D-Trp, $K_a=260\text{ M}^{-1}$.

2.3. NOESY results and computer simulation of the complex of Trp and host **8**

The NMR results described above showed clearly that **8** binds both D- and L-Trp in DMSO, with selectivity over other amino acids and significant enantioselectivity in favor of L-Trp. We were interested in the origins of this selectivity and therefore investigated the structures of the complexes through intermolecular NOESY and computational chemistry. NOESY spectra of **8** with D- and L-Trp suggested that the structures of the diastereomeric complexes were significantly different from each other. In the case of **8** and L-Trp, several correlation peaks between protons on the phenyl rings of **8** (denoted H_x) and protons on Trp (denoted T_x) were observed (H_{28} to T_1 , T_2 , T_3 , T_5 ; H_{27} to T_4 ; see Supplementary data and Fig. 4a). These connections suggest that the L-Trp indole unit lies in the cleft between the C7 and C12 phenylurea groups. In the case of **8**+D-Trp, the NOESY spectrum again showed correlations between Trp aryl protons (T_5 and T_2) and receptor phenylurea protons (H_{27} , H_{28}) (see Supplementary data and Fig. 4b). However cross-peaks also appeared between the D-Trp aryl protons T_2/T_5 and the azobenzene proton H_{29} . It thus seems that, while the D-Trp indole unit spends part of its time in the cleft between the C7/C12 phenylurea groups, it can also take up a position near the C3 substituent.

The correlations between the receptor phenyl protons and the tryptophan indole protons (both enantiomers) may help to explain the selectivity of **8** for Trp. The close approach of these aromatic units may be driven by $\text{CH}-\pi$ interactions, which would contribute to the overall binding energies. To obtain further insight into the

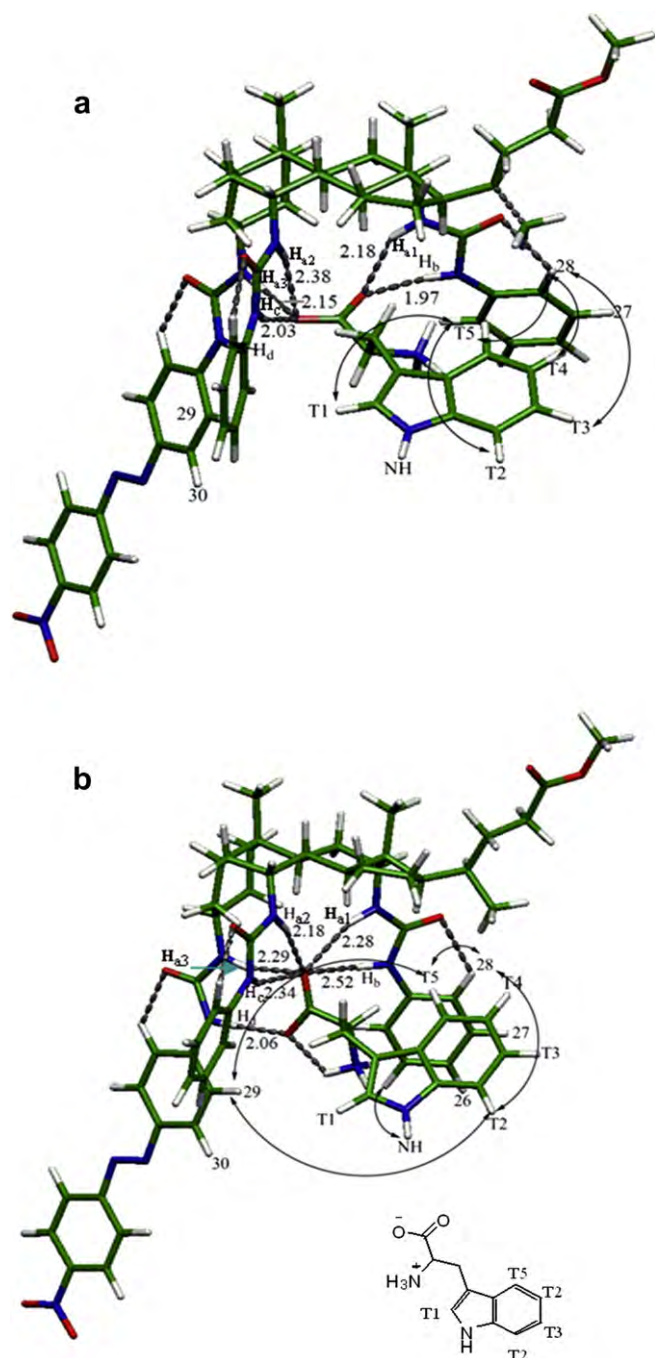


Figure 4. Structures of the (a) **8**⊂L-Trp and (b) **8**⊂D-Trp complexes derived from computer-based molecular modeling using Density Functional Theory: DFT (B3LYP/6-31G(d)) in Gaussian03 Program. Arrows represent the correlation peaks observed from NOESY spectra. Intramolecular and intermolecular hydrogens are shown as broken lines. Atoms H, C, N, and O represent in white, green, blue, and red, respectively. Inset: formula for Trp substrates with numbering used in discussion.

structures of [**8**⊂L-Trp] and [**8**⊂D-Trp], modeling studies were carried out using Density Functional Theory (B3LYP/6–31G(d) in the Gaussian03 program). Starting conformations were randomised and independent of the NOESY analyses. The lowest energy minima obtained for the diastereomeric complexes are shown in Figure 4. For [**8**⊂L-Trp] the carboxylate group is located close to all four C7/12 urea NH, apparently forming four strong hydrogen bonds (donor–acceptor distances of $d[\text{NH}_{a1}, \text{NH}_{a2}, d\text{NH}_b$ and $\text{NH}_c \cdots \text{O}] = 2.18, 2.38 \text{ \AA}, 1.97$ and 2.03 \AA , respectively). A fifth hydrogen bond is formed to the C3–NH (H_{a3}) group (2.15 \AA). In

contrast, the carboxylate group in D-Trp was found to make two hydrogen bonds to the C3 urea group (donor–acceptor distances $d[\text{NH}_{a3}$ and $\text{NH}_d \cdots \text{O}] = 2.29$ and 2.06 \AA , respectively), as well as four hydrogen bonds to the C7/12 ureas (donor–acceptor distances of $d[\text{NH}_{a1}, \text{NH}_{a2}, \text{NH}_b$, and $\text{NH}_c \cdots \text{O}] = 2.28, 2.18, 2.52$, and 2.34 \AA). However, these last four protons involve a single carboxylate oxygen. This oxygen makes five H-bonds in total (including one to the proximal C3 urea) while the second carboxylate oxygen binds only to the distal C3 urea NH. This asymmetric arrangement results in longer H-bond distances, presumably due to crowding and competition around the multiply-bonded oxygen. Such over-coordination is probably unfavorable and may account for the weaker binding of D-Trp compared to L-Trp. The movements of the C7/12 urea NH signals (Table 1) are consistent with this analysis. The signals for [**8**⊂L-Trp] are generally more downfield of those for [**8**⊂D-Trp], implying more effective H-bonding in the former case. For both structures, the modeling places the Trp indole unit between the C7 and C12 phenylurea groups as implied by the NOESY analysis. The correlations between T_2/T_5 and H_{29} in [**8**⊂D-Trp] are assumed to arise from an alternative conformation.

3. Conclusion

Previous research has shown that cholapods can serve as receptors for anions in non-polar solvents, and can distinguish between enantiomers of chiral carboxylates. In the present work we have shown that amino acid zwitterions can also be bound enantioselectively, even in a highly polar organic solvent (DMSO). Receptor **8** shows interesting selectivity for one particular amino acid, tryptophan, which may be ascribed to aromatic–aromatic interactions. The enantioselectivity is modest, but significant considering that the main interactions between host and guest (H-bonds) are strongly attenuated by the solvent. Improvements in scope and selectivity could result from the engineering of a more enclosed binding site, and this will be the subject of future research.

4. Experimental

4.1. Materials and methods

All reagents and solvents were obtained from commercial suppliers and used without further purification unless otherwise stated. Methanol was distilled over calcium chloride, magnesium, and iodine. DMF was obtained from Aldrich. THF and DCM were obtained from an Anhydrous Engineering Solvent Purification System (AESPS). Analytical TLC was carried out on DC-Alufolien Kieselgel 60F₂₅₄ 0.2 mm plates (Merck) and compounds were visualized by UV fluorescence, ninhydrin solution or by charring over a Bunsen burner flame. Flash chromatography of reaction products was carried out using Silica 60A, particle size 35–70 μ (Fischer Scientific). IR spectra were recorded on a Perkin–Elmer Spectrum One spectrometer. ^1H NMR and ^{13}C NMR spectra were recorded on Jeol Delta/GX270 or Delta/GX400 spectrometers, using deuterated solvents and were referenced internally to the residual solvent peak or TMS ($\delta_{\text{H}} = 0.00 \text{ ppm}$, $\delta_{\text{C}} = 0.00 \text{ ppm}$) signal. UV absorption spectra were obtained on a Varian Cary 50 Probe UV-Visible spectrophotometer. Unless otherwise specified, the solvents were spectroscopic grade without further purification. Samples were contained in 10 mm path length quartz cuvettes (3.5 mL volume).

4.2. Synthesis

4.2.1. Methyl 3 α -azido-7 α , 12 α -bis-[(phenylaminocarbonyl) amino]-5 β -cholan-24-oate (5**)⁹.** Azido-bis-carbamate **3**⁸ (2.27 g, 3.52 mmol) was dissolved in dry dichloromethane (55 mL) and placed in an ice bath. Trifluoroacetic acid (34 mL) was added

dropwise, and the mixture was stirred at 0 °C for 1 h then at room temperature for 4 h. The solvent was evaporated under reduced pressure and the residue was redissolved in dichloromethane. The solution was washed with satd aq NaHCO₃, dried over magnesium sulfate, and evaporated under reduced pressure to give a yellow crude product. Precipitation from DCM/hexane gave diamine **4**⁹ (1.24 g, 79%) as a white solid. **4**: ¹H NMR (CDCl₃, 400 MHz) δ =0.71 (3H, s, 18-H₃), 0.91 (3H, s, 19-H₃), 0.96 (3H, d, J =6.32 Hz, 21-H₃), 2.02–2.15 (2H, m), 2.18–2.27 (1H, m), 2.32–2.52 (2H, m), 3.07–3.21 (3H, m, 3 β -H+7 β -H+12 β -H), 3.66 (3H, s, COOCH₃).

To a solution of diamine **4** (1.27 g, 2.84 mmol) in dry THF (30 mL) were added DMAP (0.33 g, 2.70 mmol), triethylamine (0.74 mL, 5.30 mmol), and phenyl isocyanate (620 μ L, 5.68 mmol). The reaction mixture was stirred at 50 °C for 24 h and the solvent was evaporated under reduced pressure. The crude product was purified by flash column chromatography (eluent DCM/methanolic ammonia 99:1) to provide azido-bis-urea **5** (1.86 g, 96%) as a white solid. **5**: ¹H NMR (CDCl₃, 400 MHz) δ =0.75 (3H, s, 18-H₃), 0.85 (3H, d, J =6.36 Hz, 21-H₃), 0.91 (3H, s, 19-H₃), 1.96–2.06 (1H, m), 2.25–2.32 (1H, m), 3.15 (1H, br s, 3 β -H), 3.93 (1H, br s, 7 β -H), 4.05 (1H, br s, 12 β -H), 5.33 (1H, br s, NH), 5.63 (1H, br s, NH), 6.85 (1H, br s, NH), 6.98–7.06 (2H, m, Ar–CH), 7.25–7.39 (8H, m, Ar–CH). lit.⁹ ¹H NMR δ =3.15 (1H, br s), 3.92 (1H, br s), 4.07 (1H, br s).

4.2.2. Methyl 3 α -amino-7 α , 12 α -bis-[(phenylaminocarbonyl) amino]-5 β -cholan-24-oate (6**)⁹.** Activated zinc powder (3.77 g, 58.74 mmol) was added to a solution of azide **5** (2.00 g, 2.93 mmol) in glacial acetic acid (120 mL) and the mixture was stirred vigorously for 24 h. Acetic acid was completely removed by the addition of toluene followed by evaporation, repeated as necessary. The residue was dissolved in satd aq NaCl (60 mL), which was then basified with triethylamine and extracted with EtOAc. The organic phase was dried over magnesium sulfate, and the solvent was evaporated under reduced pressure. The residue was purified by flash column chromatography (eluent DCM/methanolic ammonia 97:3 to 9:1) to give amine **6** (1.76 g, 91%) as a white solid. **6**: ¹H NMR ((CD₃)₂CO) δ =0.88 (3H, s, 18-H₃), 0.90 (3H, d, J =9.76 Hz, 21-H₃), 1.04 (3H, s, 19-H₃), 3.16 (1H, br s, 3 β -H), 3.54 (3H, s, COOCH₃), 4.04 (1H, br s, 7 β -H), 4.15–4.21 (1H, br s, 12 β -H), 5.86 (1H, br s, CH–NH–CO), 5.94 (1H, br s, CH–NH–CO), 6.86–6.94 (2H, m, Ar–CH), 7.18–7.26 (4H, m, Ar–CH), 7.51 (4H, d, J =5.88 Hz, Ar–CH), 8.10 (2H, d, J =8.30 Hz, Ar–NH–CO). lit.⁹ ¹H NMR δ =3.24–3.34 (1H, br s), 3.96–4.02 (1H, br s), 4.17–4.23 (1H, br s).

4.2.3. 4-Isocyanato-4'-nitroazobenzene (7**)¹⁰.** Disperse orange **3**⁸ (4-(4-nitrophenylazo)-aniline) (0.20 g, 0.83 mmol) was dried under high vacuum then dissolved in dry THF (15 mL). Triphosgene (2 equiv) was dried by dissolution in toluene followed by evaporation under reduced pressure, then redissolved in dry THF (15 mL) and added into the solution of disperse orange 3. The red-brown reaction mixture was stirred at room temperature for 2 h, monitoring the progress of the reaction using FT-IR (disappearance of the band at 1734 cm⁻¹ due to –NHCOCl). A band due to the product **7** appeared at 2257 cm⁻¹ (lit.¹⁰ 2259 cm⁻¹). The solution was employed in the following step without purification.

4.2.4. Methyl 3 α -[(4-nitroazobenzene-4'-aminocarbonyl)amino]-7 α , 12 α -bis-[(phenylaminocarbonyl)amino]-5 β -cholan-24-oate (8**).** To the above solution of compound **7** in dry THF was added a solution of amino compound **6** (0.5 g, 0.83 mmol) and DMAP (0.13 g, 1.08 mmol) in THF. The mixture was heated for 2 h after which the solvent was evaporated under reduced pressure. The crude product was purified by column chromatography using dichloromethane/methanolic ammonia 94:6 as eluent to provide tris-urea **8** (0.30 g, 39%) as a red solid. **8**: IR (KBr, cm⁻¹) 3385, 2941, 2867, 1676, 1544, 1439, 1341, 1228, 1139; ¹H NMR ((CD₃)₂CO) δ =0.81 (6H, s,

18-H₃+21-H₃), 0.99 (3H, s, 19-H₃), 3.26 (1H, m, 3 β -H), 3.48 (3H, s, COOCH₃), 3.99 (1H, br s, 7 β -H), 4.09 (1H, br s, 12 β -H), 5.56 (1H, d, J =5.85 Hz, CH–NH_a–CO), 5.79 (1H, m, CH–NH_a–CO), 6.82–6.86 (2H, m, Ar_{phenyl}–CH₂₆), 7.21–7.15 (4H, m, Ar_{phenyl}–CH₂₇), 7.40–7.44 (4H, s, Ar_{phenyl}–CH₂₈), 7.56–7.58 (2H, d, J =9.0 Hz, Ar_{org3}–C₂₉), 7.79–7.83 (3H, d, J =4.8 Hz, Ar_{org3}–CH₃₀+Ar_{phenyl}–NH_c–CO), 7.96–7.98 (2H, d, J =9.0 Hz, Ar_{org3}–CH₃₁), 8.03 (1H, br s, Ar_{phenyl}–NH_b–CO), 8.16 (1H, br s, Ar_{org3}–NH_d–CO), 8.33–8.35 (2H, d, J =9.0 Hz, Ar_{org3}–CH₃₂); ¹³C {¹H} NMR (100 MHz, (CD₃)₂CO, 25 °C, TMS) δ =12.27, 15.71, 21.82, 22.31, 25.74, 26.17, 26.86, 29.45, 29.80, 31.92, 33.78, 34.15, 34.73, 35.56, 36.45, 41.14, 43.65, 43.78, 45.22, 47.28, 49.67, 50.44, 51.84, 116.73, 116.86, 120.29, 120.36, 122.14, 123.82, 127.75, 139.98, 144.26, 146.11, 147.42, 153.18, 153.41, 153.59, 155.13, 172.62. Anal. Calcd for C₅₂H₆₃N₉O₇+1.5H₂O: C, 65.54; H, 6.93; N, 13.24. Found C, 65.48; H, 6.87; N, 13.03; MS (ESI): m/z for C₅₂H₆₃N₉O₇=948 [M+Na]⁺, 926 [M+H]⁺.

4.3. ¹H NMR titrations of host **8** and amino acids

Typically, a 4.0 mM solution of the ligand **8** (1.4 \times 10⁻³ mmol) in DMSO-*d*₆ (0.35 mL) was prepared in a 5-mm NMR tube. An initial ¹H NMR spectrum of the solution of the ligand was recorded. A stock solution of guest compound (7.48 \times 10⁻³ mmol, 18 mM) in DMSO-*d*₆ (0.4 mL) was prepared in a vial. The solution of guest (0.3 mL) was added portionwise via microsyringe (10 and 50 μ L portions) to the NMR tube. After each addition the sample was shaken to ensure mixing and the ¹H NMR spectrum was recorded.

4.4. UV–vis titrations of host **8** and amino acids

All UV–vis experiments were carried out in DMSO with tetrabutylammoniumhexafluorophosphate as supporting electrolyte. The solution of **8** (2.00 \times 10⁻⁴ mmol, 0.02 mM) was prepared and gradually added with the solution of guests (1.067 \times 10⁻² mmol, 1.067 mM) until the system reached the equilibrium point observed by a small change in UV–vis spectrum. Each addition was recorded from 300 to 550 nm at room temperature.

Acknowledgements

A.S. is a Ph.D. student supported by Development Science Talent Project. We thank the Thailand Research Fund and Commission on Higher Education (RTA5080006), the National Center of Excellence for Petroleum, Petrochemical, and Advanced Materials (NCE-PPAM) and the Project for Establishment of Comprehensive Center for Innovative Food, Health Products and Agriculture (PERFECTA) UK EPSRC (EP/E021581/1) for financial support.

Supplementary data

The synthetic procedure of **8** and the analysis of the synthesized compounds including of ¹H NMR titration, 2D NMR spectra and Job's plots of complexes are provided as supplementary data. Supplementary data associated with this article can be available in the online version at doi:10.1016/j.tet.2010.06.069.

References and notes

- (a) Lehn, J.-M.; Sirlin, C. *J. Chem. Soc., Chem. Commun.* **1978**, 949–951; (b) Peacock, S. C.; Domeier, L. A.; Geata, F. C. A.; Helgeson, R. C.; Timko, J. M.; Cram, D. J. *J. Am. Chem. Soc.* **1978**, *100*, 8190–8202; (c) Sogah, G. D. Y.; Cram, D. J. *J. Am. Chem. Soc.* **1979**, *101*, 3035–3042; (d) Newcomb, M.; Toner, J. L.; Helgeson, R. C.; Cram, D. J. *J. Am. Chem. Soc.* **1979**, *101*, 4941–4947; (e) Peacock, S. S.; Walba, D. M.; Gaeta, F. C. A.; Helgeson, R. C.; Cram, D. J. *J. Am. Chem. Soc.* **1980**, *102*, 2043–2052; (f) Davidson, R. B.; Bradshaw, J. S.; Jones, B. A.; Dalley, N. K.; Christensen, J. J.; Izatt, R. M.; Morin, F. G.; Grant, D. M. *J. Org. Chem.* **1984**, *49*, 353–357; (g) Naemura, K.; Fukunaga, R.; Yamanaka, M. *J. Chem. Soc., Chem. Commun.* **1985**, 1560–1561; (h) Murakami, Y.; Ohno, T.; Hayashida, O.; Hiseada,

- Y. J. Chem. Soc., Chem. Commun.* **1991**, 950–952; (i) Behr, J.-P.; Lehn, J.-M. *J. Am. Chem. Soc.* **1973**, 95, 6108–6110; (j) Tsukube, H. *Tetrahedron Lett.* **1981**, 22, 3981–3984; (k) Echavarren, A.; Galan, A.; Lehn, J.-M.; de Mendoza, J. *J. Am. Chem. Soc.* **1989**, 111, 4994–4995; (l) Konishi, K.; Yahara, K.; Toshishige, H.; Aida, T.; Inoue, S. *J. Am. Chem. Soc.* **1994**, 116, 1337–1344; (m) Sunamoto, J.; Iwamoto, K.; Mohri, Y.; Kominato, T. *J. Am. Chem. Soc.* **1982**, 104, 5502–5504; (n) Rebek, J., Jr.; Askew, B.; Nemeth, D.; Parris, K. *J. Am. Chem. Soc.* **1987**, 109, 2432–2434; (o) Galan, A.; Andreu, D.; Echsbttrm, S. M.; Prados, P.; de Mendoza, J. *J. Am. Chem. Soc.* **1992**, 114, 1511–1512; (p) Kuroda, Y.; Kato, Y.; Higashioji, T.; Hasegawa, J.-Y.; Kawanami, S.; Takahashi, M.; Shiraishi, N.; Tanabe, K.; Ogoshi, H. *J. Am. Chem. Soc.* **1995**, 117, 10950–10958.
2. (a) Pinkhassik, E.; Stibor, I.; Casnati, A.; Ungaro, R. *J. Org. Chem.* **1997**, 62, 8654–8659; (b) Zheng, Y. S.; Zhang, C. *Org. Lett.* **2004**, 6, 1189–1192; (c) Erdemir, S.; Tabakci, M.; Yilmaz, M. *Tetrahedron: Asymmetry* **2006**, 17, 1258–1263; (d) Karakucuk, A.; Durmaz, M. S. A.; Yilmaz, M.; Demirel, A. *Tetrahedron: Asymmetry* **2006**, 17, 1963–1968; (e) Yakovenko, A. V.; Boyko, V. I.; Kalchenko, V. I.; Baldini, L.; Casnati, A.; Sansone, F.; Ungaro, R. *J. Org. Chem.* **2007**, 72, 3223–3231; (f) Webb, T. H.; Wilcox, C. S. *Chem. Soc. Rev.* **1993**, 22, 383–395; (g) Zhang, X. X.; Bradshaw, J. S.; Izatt, R. M. *Chem. Rev.* **1997**, 97, 3313–3362; (h) Ogoshi, H.; Mizutani, T. *Acc. Chem. Res.* **1998**, 31, 81–89; (i) Schmuck, C. Chem.—*Eur. J.* **2000**, 6, 709–718; (j) Andrisano, V.; Gottarelli, G.; Masiero, S.; Hejjine, E. H.; Pieraccini, S.; Spada, G. P. *Angew. Chem., Int. Ed.* **1999**, 38, 2386–2388; (k) Henley, P. D.; Kilburn, J. D. *Chem. Commun.* **1999**, 1335–1336; (l) Chin, J.; Lee, S. S.; Lee, K. J.; Park, S.; Kim, D. H. *Nature* **1999**, 401, 254–257; (m) Gavin, J. A.; Garcia, M. E.; Benesi, A. J.; Mallouk, T. E. *J. Org. Chem.* **1998**, 63, 7663–7669; (n) Lewandowski, K.; Murer, P.; Svec, F.; Frechet, J. M. J. *Chem. Commun.* **1998**, 2237–2238; (o) Sawada, M.; Shizuma, M.; Takai, Y.; Adachi, H.; Takeda, T.; Uchiyama, T. *Chem. Commun.* **1998**, 1453–1454.
 3. (a) Jeong, K. S.; Muehldorf, A. V.; Rebek, J. *J. Am. Chem. Soc.* **1990**, 112, 6144–6145; (b) Hong, J.-I.; Namgoong, S. K.; Bernardi, A.; Still, W. C. *J. Am. Chem. Soc.* **1991**, 113, 5111–5112; (c) Yoon, S. S.; Still, W. C. *J. Am. Chem. Soc.* **1993**, 115, 823–824; (d) Pirkle, W. H.; Murray, P. G.; Rausch, D. J.; McKenna, S. T. *J. Org. Chem.* **1996**, 61, 4769–4774; (e) Martin, M.; Raposo, C.; Almaraz, M.; Crego, M.; Caballero, C.; Grande, M.; Morán, J. R. *Angew. Chem., Int. Ed. Engl.* **1996**, 35, 2386–2388; (f) Botana, E.; Ongeri, S.; Arienzo, R.; Demarcus, M.; Frey, J. G.; Piarulli, U.; Potenza, D.; Gennari, C.; Kilburn, J. D. *Chem. Commun.* **2001**, 1358–1359.
 4. (a) Boyce, R.; Li, G.; Nestler, H. P.; Suenaga, T.; Still, W. C. *J. Am. Chem. Soc.* **1994**, 116, 7955–7956; (b) Cheng, Y.; Suenaga, T.; Still, W. C. *J. Am. Chem. Soc.* **1996**, 118, 1813–1814; (c) Broderick, S.; Davis, A. P.; Williams, R. P. *Tetrahedron Lett.* **1998**, 39, 6083–6086; (d) Wallimann, P.; Marti, T.; Furer, A.; Diederich, R. *Chem. Rev.* **1997**, 97, 1567–1608; (e) Li, Y. X.; Dias, J. R. *Chem. Rev.* **1997**, 97, 283–304.
 5. (a) Davis, A. P.; Lawless, L. J. *Chem. Commun.* **1999**, 9–10; (b) Lawless, L. J.; Blackburn, A. G.; Ayling, A. J.; Pérez-Payán, M. N.; Davis, A. P. *J. Chem. Soc., Perkin Trans. 1* **2001**, 1329–1341; (c) Baragaña, B.; Blackburn, A. G.; Breccia, P.; Davis, A. P.; de Mendoza, J.; Padron-Carrillo, J. M.; Prados, P.; Riedner, J.; de Vries, J. G. *Chem.—Eur. J.* **2002**, 8, 2931–2936; (d) Siracusa, L.; Hurley, F. M.; Dresen, S.; Lawless, L. J.; Pérez-Payán, M. N.; Davis, A. P. *Org. Lett.* **2002**, 4, 4639–4642.
 6. Sirikulkajorn, A.; Duanglaor, P.; Ruangpornvisuti, V.; Tomapatanaget, B.; Tuntulani, T. *Supramol. Chem.* **2009**, 21, 486–494.
 7. (a) Bondy, C. R.; Gale, P. A.; Loeb, S. J. *J. Am. Chem. Soc.* **2004**, 126, 5030–5031; (b) Jose, D. A.; Kumar, D. K.; Ganguly, B.; Das, A. *Org. Lett.* **2004**, 6, 3445–3448; (c) Hughes, M. P.; Shang, M.; Smith, B. D. *J. Org. Chem.* **1996**, 61, 4510–4511; (d) Calderon-Kawasaki, K.; Kularatne, S.; Li, Y. H.; Noll, B. C.; Scheidt, W. R.; Burns, D. H. *J. Org. Chem.* **2007**, 72, 9081–9087; (e) Esteban-Gomez, D.; Fabbrizzi, L.; Licchelli, M. *J. Org. Chem.* **2005**, 70, 5717–5720; (f) Hughes, M. P.; Smith, B. D. *J. Org. Chem.* **1997**, 62, 4492–4499; (g) Amendola, V.; Boiocchi, M.; Colasson, B.; Fabbrizzi, L. *Inorg. Chem.* **2006**, 45, 6138–6147; (h) Turner, D. R.; Paterson, M. J.; Steed, J. W. *J. Org. Chem.* **2006**, 71, 1598–1608; (i) Oton, F.; Tarraga, A.; Espinosa, A.; Velasco, M. D.; Molina, P. *J. Org. Chem.* **2006**, 71, 4590–4598; (j) Davis, A. P.; Joos, J.-B. *Coord. Chem. Rev.* **2003**, 240, 143–156; (k) Clare, J. P.; Ayling, A. J.; Joos, J. B.; Sisson, A. L.; Magro, G.; Pérez-Payán, M. N.; Lambert, T. N.; Shukla, R.; Smith, B. D.; Davis, A. P. *J. Am. Chem. Soc.* **2005**, 127, 10739–10746.
 8. (a) Davis, A. P.; Pérez-Payán, M. N. *Synlett* **1999**, 991–993; (b) del Amo, V.; Siracusa, L.; Markidis, T.; Baragaña, B.; Bhattarai, K. M.; Galobardes, M.; Naredo, G.; Pérez-Payán, M. N.; Davis, A. P. *Org. Biomol. Chem.* **2004**, 2, 3320–3328.
 9. Sisson, A. L.; Sanchez, V. d. A.; Magro, G.; Griffin, A. M. E.; Shah, S.; Charmant, J. P. H.; Davis, A. P. *Angew. Chem., Int. Ed.* **2005**, 44, 6878–6881.
 10. Masse, C. E.; Vanderwiede, K.; Kim, W. H.; Jiang, X. L.; Kumar, J.; Tripathy, S. K. *Chem. Mater.* **1995**, 7, 904–908.

A Selective Spectrofluorometric Determination of Micromolar Level of Cyanide in Water Using Naphthoquinone Imidazole Boronic-Based Sensors and a Surfactant Cationic CTAB Micellar System

Matinee Jamkratoke · Gamolwan Tumcharern ·
Thawatchai Tuntulani · Boosayarat Tomapatanaget

Received: 21 July 2010 / Accepted: 28 December 2010 / Published online: 19 January 2011
© Springer Science+Media, LLC 2011

Abstract We developed a new spectrofluorometric method for qualitative and quantitative determination of cyanide in water using the incorporation of naphthoquinone imidazole boronic-based sensors (*m*-NQB and *p*-NQB) and a cationic surfactant, cetyltrimethyl ammonium bromide (CTAB). This micellar system exhibited great selectivity for cyanide detection with an assistance of the cationic surface of micelle. The interaction of boronic acid of the sensor toward cyanide in CTAB micellar media gave a quantitative measure of cyanide concentration in the micromolar level. Under the optimal condition, fluorescence intensity at 460 nm of *m*-NQB and *p*-NQB provided two sets of linear ranges, 0.5–15 μ M and 20–40 μ M and the limit of cyanide detection of 1.4 μ M. Hence, both sensors in CTAB aqueous micellar system offered a considerably promising cyanide detection with 1000-fold enhancement of the detection limit compared to those studied in DMSO: H₂O. The proposed sensors could also be used to determine cyanide in water with good analytical characteristics.

Keywords Naphthoquinone imidazole · Boronic acid · Micromolar cyanide detection · CTAB · Micellar system

Introduction

Cyanide ion is extremely toxic substance due to metabolic asphyxiation. The World Health Organization (WHO) has suggested that an acceptable cyanide concentration for drinking water is 0.07 mg/L [1]. Recently, cyanide level in blood for fire victim has been reported to be *ca.* 20 μ M [2]. Any potential cyanide determination methods should offer the detection limit in micromolar concentration level. As described in previous reports, low concentration cyanide detection in water can be accomplished by various instrumental methods such as voltammetry [3], ion selective potentiometry [4], indirect atomic absorption spectrometry [5], spectrofluorimetry in flow systems [6, 7]. However cyanide determination by spectrofluorimetry methods often needed complicated separation steps such as liquid chromatography [8, 9]. In the field of supramolecular chemistry, the development of cyanide sensors has been widely considered due to its simple procedure and reasonable cost with high selectivity and sensitivity [10–26]. During the past decade, synthetic cyanide chemosensors utilized H-bonding interactions [10], metal coordination [11–14] and nucleophilic substitution of cyanide [15–24] for cyanide recognition events have been reported. However, most of them showed excellent characteristic of cyanide probes in organic solvents [10–12, 15–18, 20–22, 24] especially, in the cases of non-covalent based sensors. Regarding to the remarkable nucleophilic properties of cyanide, many organic reagents were used to serve as cyanide probes for low concentration of cyanide detection in water [15, 22–28]. Recently, boronic acid probes have shown an excellent characteristic of

M. Jamkratoke · T. Tuntulani · B. Tomapatanaget (✉)
Supramolecular Chemistry Research Unit, Department of
Chemistry, Faculty of Science, Chulalongkorn University,
10330, Bangkok, Thailand
e-mail: tboosayarat@gmail.com

G. Tumcharern
National Nanotechnology Center,
National Science and Technology Development Agency,
Pathumthani 12120, Thailand

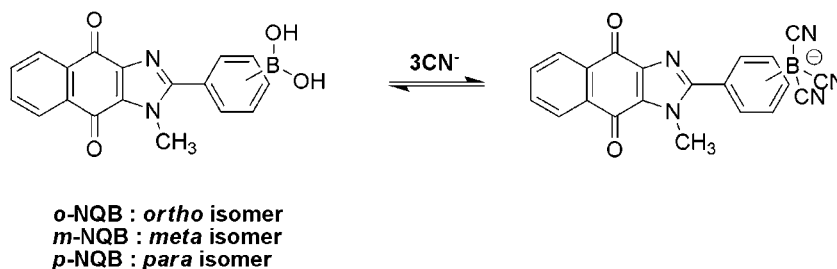
fluorometric probes for detecting micromolar concentration of cyanide in water [25–29].

In our previous work [29], we successfully synthesized new acceptor-donor-acceptor (A-D-A) type of fluorescence sensors for cyanide (Scheme 1) possessing naphthoimidazolidione as a main donor site and boronic acid as an acceptor site. The results showed that *m*-NQB and *p*-NQB offered a good characteristic of fluorescence probes for cyanide in terms of selectivity and sensitivity in the mixture of DMSO and water (1:1).

Upon interacting with cyanide, fluorescence spectra of these sensors showed a new emission band at 460 nm due to the intramolecular charge transfer (ICT) mechanism. The alternation of the boron center from the electron deficient sp^2 boron, R-B(OH)₂, to the electron rich sp^3 boron, R-B(CN)₃[−], resulted in the switching on of the ICT band at 460 nm with a large Stoke shift ($\Delta\lambda_{\text{ex-emiss}}$ =120 nm) as well as a large blue shift of *ca.* 100 nm. Unfortunately, this approach gave a low detection limit, a slow rate of cyanide-substitution on the boron center and a poor solubility in water. It is very challenging to improve the efficiency of neutral boronic acid based receptors, *o*-NQB, *m*-NQB and *p*-NQB, for micromolar detection of cyanide in water without any synthetic modification. Previously, a number of the micellar systems were used to improve the efficiency of the synthetic chemosensors for detecting cations [30–35] but anion detections were rarely studied [36–39]. The incorporation of our sensors into a micellar system was expected to not only increase solubility of sensors in water but also enhance the cyanide complexation ability of sensors.

Herein, we describe a protocol for optimum micellar system in detecting micromolar concentration of cyanide in water by the incorporation of the synthesized receptors (*o*-NQB, *m*-NQB and *p*-NQB) into a cationic surfactant (CTAB). We evaluate the stability constants of the tri-substitution of cyanide on the boron centers of *m*-NQB or *p*-NQB in the CTAB micellar system, while such a stability constant of this approach could not be obtained in DMSO:H₂O. The validation of our sensing approach has also been carried out to determine cyanide in drinking water samples.

Scheme 1 Equilibrium involved in the interaction between naphthoimidazolidione and boronic acid based sensors, *o*-NQB, *m*-NQB and *p*-NQB and cyanide



Experimental

Apparatus

All of fluorescence spectra were recorded on a Varian Cary Eclipse spectrophotometer (Australia) with excitation and emission slits at 10.0 nm, λ_{ex} =344 nm and scan rate 120 nm/min.

Reagent and Materials

Analytical grade surfactants, cetyltrimethylammonium bromide (CTAB), dodecyltrimethylammonium bromide (DTAB), tetradecyltrimethylammonium bromide (TTAB), sodium dodecyl sulfate (SDS), and Triton X-100 (TX-100) were purchased from Merck (Germany). Spectroscopic grade ethanol was purchased from Merck (Germany). Water used for the experiment was purified with a Milli-Q filtration system (Millipore). Sensors, *m*-NQB, *p*-NQB, and *o*-NQB were prepared according to the literature [29].

Stock Solutions

A sensor stock solution of *m*-NQB, *p*-NQB, and *o*-NQB (2.5×10^{-4} mol/L) was prepared in spectroscopic grade ethanol. A surfactant stock solution CTAB, DTAB, TTAB, TX-100 and SDS (1.25×10^{-2} mol/L) was prepared in Milli-Q water. A 2.5×10^{-3} mol/L standard stock solution of potassium salts of anions including KCN, KF, KAcO, KBzO, KH₂PO₄, KNO₃, KClO₄, KCl, KBr, KSCN, and KI was prepared in Milli-Q water.

Procedure

Construction of Calibration Graphs

In a 5.0 mL volumetric flask, 1.0 mL of stock solution of a sensor was mixed with 2.0 mL of stock solution of CTAB. Aliquots of the stock solution of KCN were then added to the mixture to give the final concentration of CN[−] in the range of 0–250 μ M upon the volume adjustment with Milli-Q water. After standing at room temperature for

30 min, the sample mixture was transferred to a 10.0 mm width quartz cell and then fluorescence spectra were recorded with excitation wavelength at 344 nm. Calibration graphs were obtained by the plot of fluorescence intensity at 460 nm and KCN concentrations.

Cyanide Sensing with Various Surfactants

Into a 5.0 mL volumetric flask, 1.0 mL of stock solution of a sensor was mixed with a stock solution of surfactants (CTAB, SDS, TX-100) and 0.1 mL of stock solution of KCN to give a final concentration of 5×10^{-5} mol/L cyanide ion, 5×10^{-5} mol/L sensor and 5×10^{-3} mol/L surfactant with Milli-Q water. After standing at room temperature for 30 min, the sample mixture was transferred to a 10.0 mm width quartz cell and then fluorescence spectra were recorded with the excitation wavelength at 344 nm.

Anion Sensing with Excess Anions in the CTAB Micellar System

In a 5.0 mL volumetric flask, 1.0 mL of stock solution of a sensor was mixed with 2.0 mL of stock solution of CTAB. Then, 0.10 mL of stock solution of potassium salts of anions was added to the mixtures. Upon the volume adjustment with Milli-Q water, the final concentration of the anion, the sensor and the surfactant are 5×10^{-5} mol/L, 5×10^{-5} mol/L and 5×10^{-3} mol/L, respectively. After standing at room temperature for 30 min, the sample mixture was transferred to a 10.0 mm width quartz cell and then fluorescence spectra were recorded with the excitation wavelength at 344 nm.

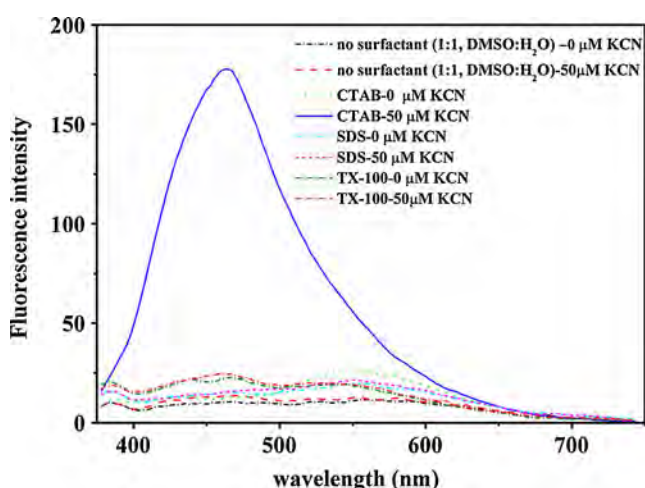


Fig. 1 Fluorescence spectra of *m*-NQB and *m*-NQB + 50 M KCN with various types of surfactants (5.0×10^{-5} mol/L of *m*-NQB, 5.0×10^{-3} mol/L of surfactant in 1:4 ethanol:H₂O)

Table 1 Fluorescence enhancement (I/I_0 at 460 nm) in different media of *m*-NQB

Medium	I/I_0 at 460 nm
1:1 DMSO-H ₂ O	1.30
5.0×10^{-3} mol/L of CTAB	14.74
5.0×10^{-3} mol/L of TX-100	1.02
5.0×10^{-3} mol/L of SDS	1.12

Fluorescence Titrations with CN⁻ in Optimum Conditions of the Micellar System

In a 5.0 mL volumetric flask, 1.0 mL of ethanol solution of the sensors was mixed with 2.0 mL of the stock solution of CTAB. Then, the mixture was added with portions of the stock solution of KCN to give final concentrations of CN⁻ ranging from 0 to 250 μM after the volume adjustment with MilliQ water. After standing at room temperature for 30 min, the sample mixture was transferred to a 10.0 mm width quartz cell and then fluorescence spectra were recorded with the excitation wavelength at 344 nm.

Effect of Interference Anions on Cyanide Sensing under Optimum Condition of Micellar System

In a 5.0 mL volumetric flask, 1.0 mL of ethanol solution of the sensors and 2.0 mL of the stock solution of CTAB was mixed with 0.10 mL of stock solution of KCN to give the final concentration of 1.3 μg/mL of CN⁻. Then, the mixture was added with portions of the stock solution of interference anion salts after the volume adjustment with MilliQ water. After standing at room temperature for 30 min, the sample mixture was transferred to a 10.0 mm width quartz cell and then fluorescent spectra were recorded with excitation wavelength at 344 nm.

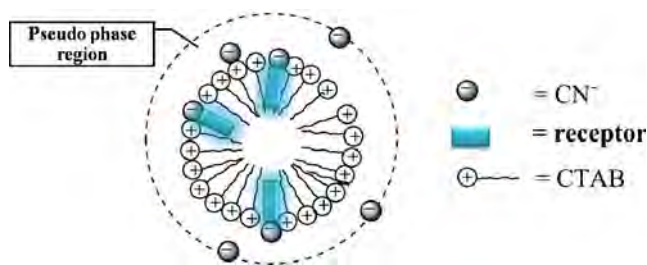


Fig. 2 The proposed model of the reaction of receptors and cyanide in the CTAB micellar system

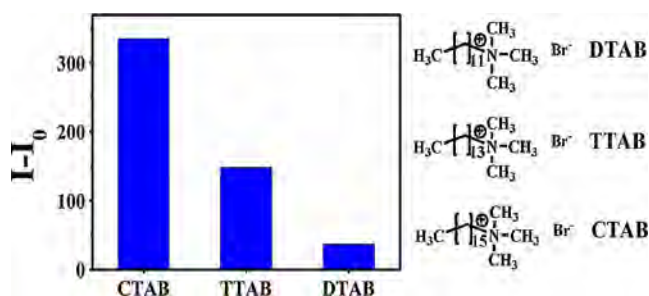


Fig. 3 Fluorescence responses ($I-I_0$ at 460 nm) of *m*-NQB and *m*-NQB + 50 μ M KCN with various types of cationic surfactants (5.0×10^{-5} mol/L of *m*-NQB, 5.0×10^{-3} mol/L of surfactant in 1:4 ethanol: H_2O)

Cyanide Detection of Drinking Water Sample

In a 5.0 mL volumetric flask, 1.0 mL of stock solution of a sensor and 2.0 mL of stock solution of CTAB. Then the commercially drinking water sample was used for the volume adjustment to give the final concentration of 40%(V/V) of the sample. The portion of KCN stock solution was spiked to the mixture to give the final concentration of 5–40 μ M of CN^- . After standing at room temperature for 30 min, the sample mixture was transferred to a 10.0 mm width quartz cell and then fluorescent spectra were recorded with excitation wavelength at 344 nm.

Results and Discussion

Effect of Surfactant Types

Three types of surfactants, neutral (TX-100), anionic (SDS) and cationic (CTAB) surfactants were first examined for fluorescence response in the presence of 50 μ M cyanide ion (50 μ M of a sensor in 5 mM of surfactant

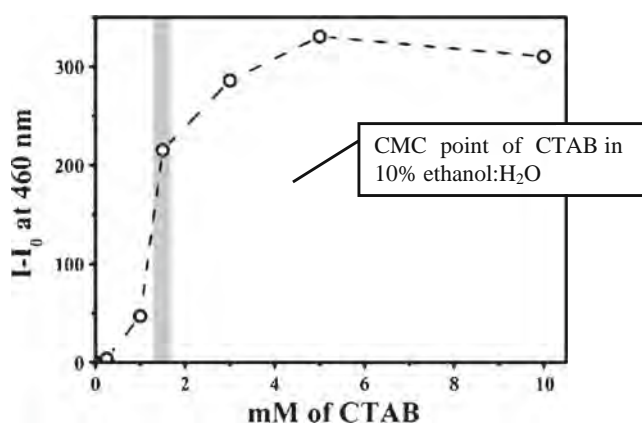


Fig. 4 Fluorescence response ($I-I_0$ at 460 nm) of *m*-NQB (5.0×10^{-5} mol/L) + 50 μ M KCN in various concentrations of CTAB and CMC of CTAB in 10% ethanol: H_2O shown as gray area [43]

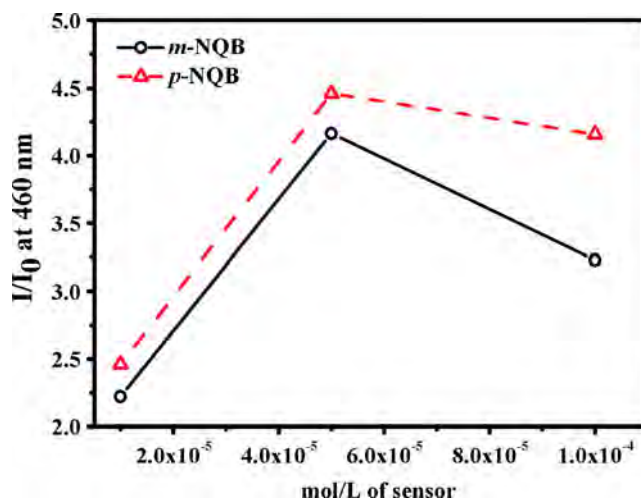


Fig. 5 Fluorescence response of *m*-NQB + 25 μ M KCN and *p*-NQB + 25 μ M KCN with various concentrations of sensors (100 equivalents of CTAB compared to sensors in 1:4 ethanol: H_2O)

in 1:4 ethanol: H_2O). Due to the sustainable pH under micromolar concentration of the cyanide (50 μ M) in water, the pH control using buffer was not required in these studies.

All types of surfactants, cationic, anionic, and neutral surfactants were able to improve the solubility of the sensors, *o*-NQB, *m*-NQB and *p*-NQB, in water. Emission spectra of free sensors in three micellar systems exhibited similar features with emission maxima at 560 nm. Fluorescence spectra of *m*-NQB in different media are shown in Fig. 1. The fluorescence spectra showed that the characteristic of sp^3 band of *m*-NQB upon binding with CN^- at 460 nm was remarkably affected in the CTAB system while

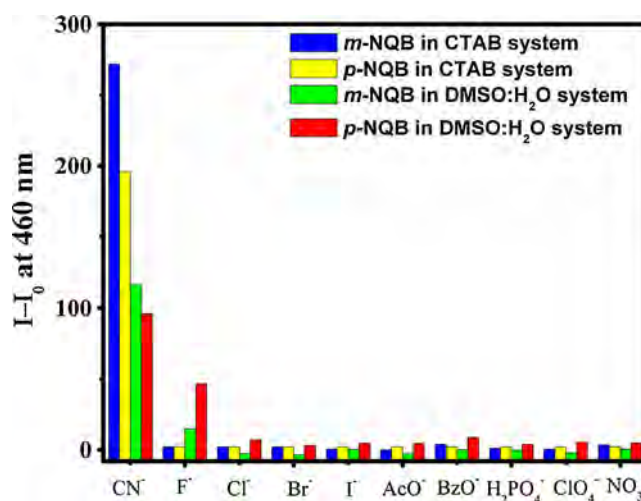


Fig. 6 Fluorescence responses ($I-I_0$ at 460 nm) of *m*-NQB and *p*-NQB in the CTAB micellar system in the presence of 50 μ M (1 equiv.) of various anions (5.0×10^{-5} mol/L of sensors, 5.0×10^{-3} mol/L of CTAB in 1:4 ethanol: H_2O) and fluorescence responses ($I-I_0$ at 460 nm) of *m*-NQB and *p*-NQB in DMSO: H_2O system with 25 mM (500 equiv.) of various anions (5.0×10^{-5} mol/L of sensor in 0.1 mol/L of NaCl in 50% DMSO: HEPES pH 7.4)

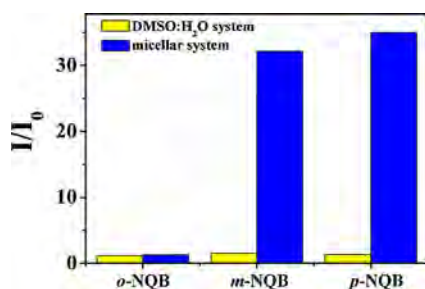


Fig. 7 Fluorescence responses (I/I_0 at 460 nm) of *o*-NQB, *m*-NQB and *p*-NQB with 0.25 mM of cyanide for 30 min of DMSO:H₂O system (5.0×10^{-5} mol/L of sensor in 0.1 mol/L of NaCl in 50% DMSO:HEPES pH 7.4) and micellar system (5.0×10^{-5} mol/L of sensors, 5.0×10^{-3} mol/L of CTAB in 1:4 ethanol:H₂O)

in other types of the media including TX-100, SDS and DMSO-H₂O showed slightly response of this emission band upon the addition of $50 \mu\text{M}$ CN⁻. As illustrated in Table 1, the fluorescence enhancement of the band at

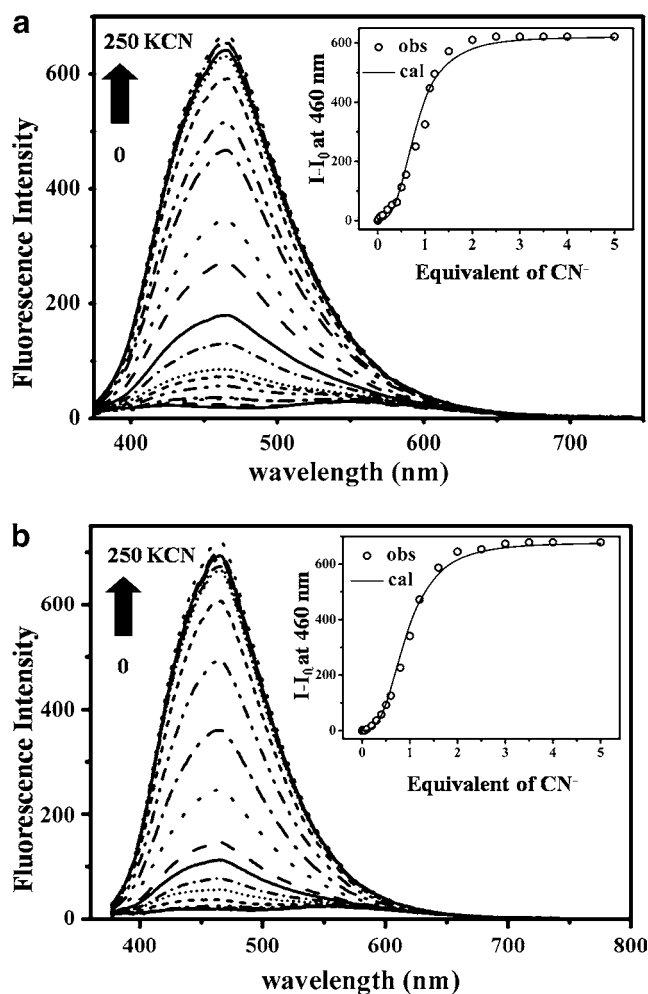


Fig. 8 **a** Fluorescence titration spectra of *m*-NQB and **b** fluorescence titration spectra of *p*-NQB upon the addition of cyanide ion in CTAB micellar system (5.0×10^{-5} mol/L of sensors, 5.0×10^{-3} mol/L of CTAB in 1:4 ethanol:H₂O)

460 nm (I/I_0) revealed that CTAB micellar system could improve the complexation ability of the sensor with CN⁻. In the case of SDS anionic micelle, the fluorescence response of the ICT band (460 nm) remained unchanged in both sensors suggesting that interactions between sensors and cyanide did not occur in this system. This result implied that the complexation ability of sensors toward cyanide was interrupted by the electrostatic repulsion between the anionic micellar surface and cyanide. Therefore, neutral and anionic surfactants improved only the solubility of the sensors in water but did not promote the cyanide-substitution on the boron center.

According to the previous literature, the model of the reaction between sensors and cyanide in the micellar system was proposed in Fig. 2 [34, 40–42]. The improvement of cyanide complexation ability in CTAB probably stemmed from electrostatic interactions between the cationic surface of the CTAB micelle and the negative charge of cyanide. In the pseudo-phase region of the micelle surface, the local concentrations of the sensors and cyanide increased resulting in the enhancing of interactions between both species. Subsequently, the boronic acid sensor was easily converted to the cyanide-adduct species. The anionic R-B(CN)₃⁻ species produced fluorescence enhancement at 460 nm as described previously. Additionally, this method improved the emission properties of R-B(CN)₃⁻ due to a good distribution of the sensors in hydrophobic region of the micellar system. This distribution could prevent the solvation of sensors by water and polar solvents, which probably caused a low quantum yield of the fluorophore in aqueous system due to non-emissive relaxation by polar solvents.

The effect of the chain length of cationic surfactants was also explored. Figure 3 showed the fluorescence responses ($I-I_0$ at 460 nm) of *m*-NQB and *m*-NQB + $50 \mu\text{M}$ KCN in

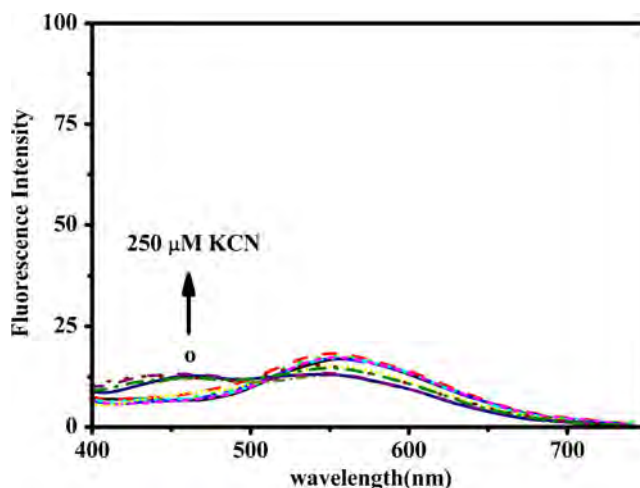


Fig. 9 **a** Fluorescence titration spectra of *o*-NQB upon the addition of cyanide ion in the CTAB micellar system (5.0×10^{-5} mol/L of *o*-NQB, 5.0×10^{-3} mol/L of CTAB in 1:4 ethanol:H₂O)

Table 2 Effect of interference anions on the determination of CN^- ($C_{\text{CN}}=1.3 \mu\text{g/mL}$)

Interference ions	Tolerance limit ($\mu\text{g/mL}$)	
	<i>m</i> -NQB	<i>p</i> -NQB
F^-	0.48	1.90
Cl^-	1.78	3.55
Br^-	11.99	5.99
OAc^-	8.85	4.43
NO_3^-	3.10	3.10

DTAB, TTAB and CTAB. It was clearly seen that incorporated sensors in a longer chain micelles, CTAB, gave remarkable cyanide sensing properties compared to that in shorter chain micelles. Regarding to the high CMC point of a shorter chain cationic surfactant, DTAB could not be aggregated in a micellar form at $5.0 \times 10^{-3} \text{ mol/L}$ in 1:4 ethanol: H_2O . Thus, the improvement of cyanide sensing could not occur in this condition for DTAB [42]. On the other hand, the longer chain CTAB presumably gave a larger surface area than DTAB did. Therefore, CTAB offered a higher concentration of the sensor and the cyanide at the pseudo-phase region resulting in a strong fluorescence response [42]. The results shown in Fig. 3 also agreed well with the proposed model in Fig. 2.

Effect of CTAB Concentrations

The effect of CTAB concentrations was also studied as shown in Fig. 4. The concentration of CTAB at $1.5 \times 10^{-3} \text{ mol/L}$ showed a large change of fluorescence response of *m*-NQB and *p*-NQB. These results agreed well with critical micelle concentration (CMC) of CTAB reported in the literature (the CMC of CTAB is 1.5 mM in 10% of ethanol in water) [43]. However, the concentration of CTAB at $5.0 \times 10^{-3} \text{ mol/L}$ provided the highest response. Therefore, this concentration of CTAB was used in all preparations of the micellar system. (100 equivalents of CTAB compared to the sensor)

Effect of Sensor Concentrations

The effect of sensor concentrations was also examined in the presence of 100 equivalents of CTAB compared to the sensor concentration and $25 \mu\text{M}$ of KCN. Fluorescence responses of *m*-NQB and *p*-NQB were displayed in Fig. 5. I/I_0 of the detection system showed the highest response at $5.0 \times 10^{-5} \text{ mol/L}$ of sensors and $5.0 \times 10^{-3} \text{ mol/L}$ of CTAB. At low concentration of the sensor, the accessibility of the molecular probes toward cyanide was disturbed by the competitive interaction between CTAB and cyanide. At high concentration of the sensor ($1.0 \times 10^{-4} \text{ mol/L}$), fluorescence responses were slightly decreased probably due to a low amount of cyanide and an excessive amount of the sensor incorporated in the micelle. Therefore, the optimum condition selected for the cyanide detection was $5.0 \times 10^{-5} \text{ mol/L}$ of the sensor and $5.0 \times 10^{-3} \text{ mol/L}$ of CTAB.

Selectivity and Sensitivity of Sensors in the Micellar System

The selectivity of sensors, *m*-NQB and *p*-NQB, with various anions was evaluated under the optimum conditions as shown in Fig. 6. Both sensors in the CTAB micellar system exhibited a dramatically selective response at 460 nm for CN^- while other anions gave slight changes in fluorescence enhancement. In addition, the micellar system can improve much greater selectivity than the DMSO: H_2O (1:1) system [29].

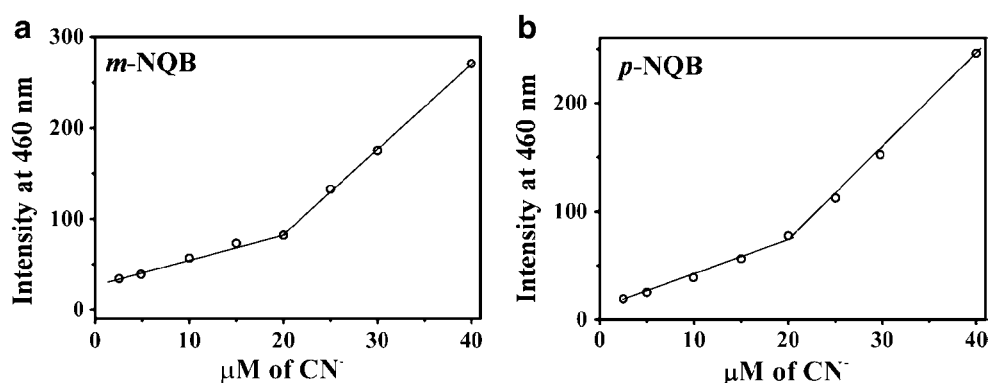
To compare the sensitivity of *m*-NQB and *p*-NQB for cyanide detection in the micellar system and in the solution of DMSO: H_2O in the same period of time (30 min), the fluorescence responses (shown in Fig. 7) of *m*-NQB and *p*-NQB with 0.25 mM CN^- in the micellar system showed remarkably higher sensitivity than that in the solution of the mixed DMSO: H_2O . As described in our previous work, the sensors in DMSO: H_2O system showed responses in a millimolar level of CN^- while in the micellar system, the sensors exhibited the working range in a micromolar level of CN^- [29]. Furthermore, the sensors in the CTAB micellar system showed the complete emission change

Table 3 Analytical characteristics of *m*-NQB and *p*-NQB sensors in the optimal condition of CTAB micellar system ($50 \mu\text{M}$ of *m*-NQB, $5.0 \times 10^{-3} \text{ mol/L}$ of surfactant in 1:4 of ethanol: H_2O)

Sensor	Linear range (μM)	Linear regression equation (μM)	Correlation coefficient (R)	Detection limit ^a (μM)
<i>m</i> -NQB	2.5–15	$I=3.15C_{\text{CN}} + 25.47$	0.9956	1.4
	20–40	$I=11.22C_{\text{CN}}-135.12$	0.9920	
<i>p</i> -NQB	2.5–15	$I=2.37C_{\text{CN}} + 15.09$	0.9970	1.4
	20–40	$I=6.84C_{\text{CN}}-72.46$	0.9963	

^a Detection limits were calculated from the concentration at which the fluorescence intensity is 3 times of standard deviation of the blank ($n=10$) [45]

Fig. 10 Calibration graphs of cyanide 2.5–40.0 μM for **a** *m*-NQB and **b** *p*-NQB in optimum condition (5.0×10^{-5} mol/L of sensors, 5.0×10^{-3} mol/L of CTAB in 1:4 ethanol in H_2O)



upon the addition of 0.25 mM of CN^- whereas the sensors in DMSO: H_2O gave insignificant response ($I/I_0=1$).

Stability Constants for Sensor-Cyanide Adducts

Fluorescence titration was carried out to elucidate the cyanide binding properties of the sensors in the cationic micellar optimum condition. From our attempts in the previous work, binding constants of sensor-cyanide adducts in DMSO:HEPES (pH 7.4) system could not be obtained. This disadvantage was possibly stemmed from the interference of hydroxide ion which was generated by a very high concentration of cyanide in the solution of 50% DMSO:HEPES (pH 7.4). Regarding the micellar system, the fluorescence titration was performed at low concentration of cyanide (0–250 μM) without any buffer because the pH of solution remained at pH 7 even adding excess cyanide. Therefore, the interference from hydroxide ion could be neglected. As illustrated in Fig. 8, the emission intensity at 460 nm progressively increased upon the increment of the cyanide concentration. Interestingly, the fluorescence intensity was saturated at 3 equivalents (150 μM) of KCN. It was indicative of the *tri*-substitution of cyanide on the boron center as described in previous report [27]. The overall stability constants (β_3) of *tri*-cyanide complexes of sensors, *m*-NQB or *p*-NQB, in the CTAB micellar media (5×10^{-5} mol/L of sensors, 5×10^{-3} mol/L of CTAB in 1:4 ethanol: H_2O) were evaluated by fitting the titration curves

using equations 1 and 2, where $n=3$. The intensities I_{\min} and I_{\max} are the initial and the final fluorescence intensities of the titration curves, respectively [44].

$$I = \frac{I_0 + I_{\infty}\beta_n[\text{CN}^-]^n}{1 + \beta_n[\text{CN}^-]^n} \quad (1)$$

$$\beta_n = \frac{[\text{RB}(\text{OH})_{3-n}(\text{CN})_n^-]}{[\text{RB}(\text{OH})_2][\text{CN}^-]^n} \quad (2)$$

Overall stability constants of the *tri*-cyano substituted complex ($\log \beta_3$) of *m*-NQB and *p*-NQB obtained from the best fit of the curves were 4.16 ± 0.09 and 3.99 ± 0.05 , respectively. These results showed that *meta* and *para* isomers possessed similar binding abilities towards cyanide in the CTAB micellar system. Therefore, the position of the boronic acids at *meta* and *para* does not give a different influence on cyanide substitution on the boron center.

Sensitivity of the *ortho* isomer, *o*-NQB, was also measured in the CTAB micellar system. However, in the mixture of DMSO: H_2O , *o*-NQB showed insignificant fluorescence response toward cyanide substitution due to steric hindrance [27]. As shown in Fig. 9, *o*-NQB also showed a poor response toward cyanide in the optimal CTAB micellar system. It indicated that the steric hindrance between hydroxyl groups of boronic acid played an important factor for cyanide substitution on this isomer

Table 4 Analysis of CN^- in drinking water

Added CN^- (μM)	<i>m</i> -NQB		<i>p</i> -NQB	
	Found (μM)	% Recovery	Found (μM)	% Recovery
5	5.32	106	5.08	102
10	10.19	102	10.48	105
15	14.82	99	15.53	104
25	25.09	100	24.91	100
30	33.12	110	30.52	102
40	40.61	102	39.50	99

resulting in a poor photophysical changes upon the addition of cyanide in both systems [29].

Effect of Interference Anions

The effect of interference anions was evaluated in the determination of $1.3\text{ }\mu\text{g/mL}$ of CN^- . The tolerance amounts of five common anions were considered at less than 5% relative error compared to the fluorescence intensity at 460 nm in the presence of $1.3\text{ }\mu\text{g/mL}$ of CN^- . As listed in Table 2, the tolerance limit of various anions revealed that most common anions did not affect the cyanide detection in this system for both sensors especially, ***p*-NQB** (Table 2).

Calibration Curves and the Limit of Detection

Under optimum condition of the CTAB micellar system, the calibration curves of cyanide detection were obtained from plots between fluorescence intensity at 460 nm and CN^- concentration. At below $50\text{ }\mu\text{M}$ cyanide concentration corresponding to the level in practical application for high toxic substance as cyanide, the emission intensities at 460 nm of ***m*-NQB** and ***p*-NQB** versus the cyanide concentration provided two well linear ranges of cyanide detections, $2.5\text{--}15\text{ }\mu\text{M}$ and $20\text{--}40\text{ }\mu\text{M}$. As illustrated in Fig. 10, the analytical data (Table 3) of both sensors clearly demonstrated that both sensors in CTAB micellar media gave excellent limits of detection of cyanide at $1.4\text{ }\mu\text{M}$.

The proposed spectrofluorometric method was applied to determine CN^- in commercial drinking water, and results were shown in Table 4. Average%recoveries of the spike samples of ***m*-NQB** and ***p*-NQB**, were 103 and 102, respectively. Our method thus gave good analytical characteristics of cyanide detection.

Conclusion

In summary, we have successfully developed a new effective determination system for cyanide by the incorporating naphthoquinone boronic based sensors, ***m*-NQB** and ***p*-NQB**, into a cationic surfactant (CTAB). The optimized condition used in this proposed method is $5.0\times 10^{-5}\text{ mol/L}$ of sensors and $5.0\times 10^{-3}\text{ mol/L}$ of CTAB in 1:4 ethanol: H_2O . Compared to the cyanide detection studied in the 1:1 DMSO: H_2O solution, the cationic micellar system provided significant improvement in sensitivity and selectivity resulting in 1000-fold enhancement of the detection ability. The proposed sensing system could also be used to determine cyanide in drinking water with good analytical characteristics.

Acknowledgements M.J. is a Ph.D student supported by the Royal Golden Jubilee Program (PHD/0049/2550) of the Thailand Research Fund (TRF) and Commission on Higher Education (CHE). We gratefully acknowledge the National Nanotechnology Center (NN-B-22-b15-94-49-55), the TRF and CHE (RTA5080006) and Project for Establishment of Comprehensive Center for Innovative Food, Health Products and Agriculture (PERFECTA) for financial support.

References

- Guidelines for Drinking-Water Quality. World Health Organization, Geneva, (1996)
- Ishii A, Watanabe-Suzuki H, Suzuki O, Kumazawa T (1998) Determination of cyanide in whole blood by capillary gas chromatography with cryogenic oven trapping. *Anal Chem* 70:4873–4876
- González LaFuente JM, Fernández Martínez E, Vicente Pérez JA, Fernández Fernández S, Miranda Ordiores AJ, Sánchez Uría JE, Fernández Sánchez ML, Sanz-Medel A (2000) Differential-pulse voltammetric determination of low $\mu\text{g/L}^{-1}$ cyanide levels using EDTA, Cu(II) and a hanging mercury drop electrode. *Anal Chim Acta* 410:135–142
- Vallejo-Pecharrómán B, Luque de Castro MD (2002) Determination of cyanide by a pervaporation–UV photodissociation–potentiometric detection approach. *Analyst* 127:267–270
- López Gómez AV, Martínez Calatayud J (1998) Determination of cyanide by a flow injection analysis-atomic absorption spectrometric method. *Analyst* 123:2103–2107
- Miralles E, Prat D, Compañó R, Granados M (1997) Assessment of different fluorimetric reactions for cyanide determination in flow systems. *Analyst* 122:553–558
- Recalde-Ruiz DL, Andrés-García E, Díaz-García ME (2000) Fluorimetric flow injection and flow-through sensing systems for cyanide control in waste water. *Analyst* 125:2100–2105
- Miralles E, Compañó R, Granados M, Prat MD (2000) Determination of metal-cyanide complexes by ion-interaction chromatography with fluorimetric detection. *Anal Chim Acta* 403:197–204
- Gamoh K, Imamichi S (1991) Postcolumn liquid chromatographic method for the determination of cyanide with fluorimetric detection. *Anal Chim Acta* 251:255–259
- Miyaji H, Sessler JL (2001) Off-the-shelf colorimetric anion sensors. *Angew Chem Int Ed* 40:154–157
- Jr Anzenbacher P, Tyson DS, Jursiková K, Castellano FN (2002) Luminescence lifetime-based sensor for cyanide and related anions. *J Am Chem Soc* 124:6232–6233
- Kim Y-H, Hong J-I (2002) Ion pair recognition by Zn–porphyrin/crown ether conjugates: visible sensing of sodium cyanide. *Chem Commun* 512–513
- Chow C-F, Lam MHW, Wong W-Y (2004) A heterobimetallic ruthenium(II)-copper(II) Donor-acceptor complex as a chemodosimetric ensemble for selective cyanide detection. *Inorg Chem* 43:8387–8393
- Chung S-Y, Nam S-W, Lim J, Park S, Yoon J (2009) A highly selective cyanide sensing in water via fluorescence change and its application to in vivo imaging. *Chem Commun* 2866–2868
- Chung Y, Lee H, Ahn KH (2006) N-acyl triazines as tunable and selective chemodosimeters toward cyanide ion. *J Org Chem* 71:9470–9474
- Chen C-L, Chen Y-H, Chen C-Y, Sun S-S (2006) Dipyrrole carboxamide derived selective ratiometric probes for cyanide ion. *Org Lett* 8:5053–5056

17. Tomosulo M, Sortino S, White AJP, Raymo FM (2006) Chromogenic oxazines for cyanide detection. *J Org Chem* 71:744–753
18. Lee K-S, Kim H-J, Shin I, Hong J-I (2008) Fluorescence chemodosimeter for selective detection of cyanide in water. *Org Lett* 10:49–51
19. Ekmekci Z, Yilmaz MD, Akkaya EU (2008) A monostyryl-boradiazaindacene (BODIPY) derivative as colorimetric and fluorescence probe for cyanide ions. *Org Lett* 10:461–464
20. Yang Y-K, Tae J (2006) Acridinium salt based fluorescence and colorimetric chemosensor for the detection of cyanide in water. *Org Lett* 8:5721–5723
21. Ros-Lis JV, Matinez-Manez R, Soto J (2002) A selective chromogenic reagent for cyanide determination. *Chem Commun* 2248–2249
22. Hudnall TW, Gabbaï FP (2007) Ammonium boranes for the selective complexation of cyanide or fluoride ions in water. *J Am Chem Soc* 129:11978–11986
23. Sun Y, Wang G, Guo W (2009) Colorimetric detection of cyanide with N-nitrophenyl benzamide derivatives. *Tetrahedron* 65:3480–3485
24. Huh JO, Do Y, Lee MH (2008) A BODIPY-Borane dyad for the selective complexation of cyanide ion. *Organometallics* 27:1022–1025
25. Badugu R, Lakowicz JR, Geddes CD (2005) Anion sensing using quinolinium based boronic acid probes. *Curr Anal Chem* 1:157–170
26. Badugu R, Lakowicz JR, Geddes CD (2005) Cyanide-sensitive fluorescence probes. *Dyes Pigments* 64:49–55
27. Badugu R, Lakowicz JR, Geddes CD (2005) Enhanced fluorescence cyanide detection at physiologically lethal levels: reduced ICT-based signal transduction. *J Am Chem Soc* 127:3635–3641
28. Badugu R, Lakowicz JR, Geddes CD (2004) Fluorescence intensity and lifetime-based cyanide sensitive probes for physiological safeguard. *Anal Chem Acta* 522:9–17
29. Jamkratoke M, Ruangpornvisuti V, Tumcharern G, Tuntulani T, Tomapatanaget B (2009) A-D-A sensors based on naphthoimidazole-dione and boronic acid as Turn-On cyanide probes in water. *J Org Chem* 74:3919–3922
30. Fernandez YD, Gramateges AP, Amendola V, Foti F, Mangano C, Pallavicini P, Patroni S (2004) Using micelles for a new approach to fluorescence sensors for metal cations. *Chem Commun* 1650–1651
31. Nakahara Y, Kida T, Nakatsuji Y, Akashi M (2004) A novel fluorescence indicator for Ba^{2+} in aqueous micellar solutions. *Chem Commun* 224–225
32. Nakahara Y, Kida T, Nakatsuji Y, Akashi M (2005) Fluorometric sensing of alkali metal and alkaline earth metal cations by novel photosensitive monoazacryptand derivatives in aqueous micellar solutions. *Org Biomol Chem* 3:1787–1794
33. Vargas LV, Sand J, Brãno TAS, Fiedler HD, Quina FH (2005) Determination of environmentally important metal ions by fluorescence quenching in anionic micellar solution. *Analyst* 130:242–246
34. Mallick A, Mandal MC, Haldar B, Charabarty A, Das P, Chattopadhyay N (2006) Surfactant-induced modulation of fluorosensor activity: a simple way to maximize the sensor efficiency. *J Am Chem Soc* 126:3126–3127
35. Pallavicini P, Dias-Fernandez YA, Foti F, Mangano C, Patroni S (2007) Fluorescence sensors for Hg^{2+} in micelles: a new approach that transforms an ON–OFF into an OFF–ON response as a function of the lipophilicity of the receptor. *Chem Eur J* 13:178–187
36. Cuccovia IM, Chaimovich H (1982) Determination of micromolar concentrations of iodine with aqueous micellar hexadecyltrimethylammonium bromide. *Anal Chem* 54:789–791
37. Kunda S, Ghosh SK, Manadal M, Pal T (2002) Micelle bound redox dye marker for nanogram level arsenic detection promoted by nanoparticles. *New J Chem* 26:1081–1084
38. Hayakawa K, Kanda M, Satake I (1979) The determination of formation constant of triiodide ion in micellar solution of dodecyltrimethylammonium chloride. *Bull Chem Jpn Soc* 52:3171–3175
39. Grosh SK, Kundu S, Mandal M, Pal T (2002) Silver and gold nanocluster catalyzed reduction of methylene blue by arsine in a micellar medium. *Langmuir* 18:8756–8760
40. Button CA, Nome F, Quina FH, Romsted LS (1991) Ion binding and reactivity at charged aqueous interfaces. *Acc Chem Res* 24:357–364
41. Mallick K, Jewraka S, Pradhan N, Pal T (2001) Micelle-catalysed redox reaction. *Curr Sci* 80:1408–1412
42. Matzinger S, Hussey DM, Fayer MD (1998) Fluorescence probes solubilization in the headgroup and core regions of micelles: fluorescence lifetime and orientational relaxation measurement. *J Phys Chem B* 102:7216–7224
43. Wei L, Ming Z, Jinli Z, Yongcai H (2006) Self-assembly of cetyl trimethylammonium bromide in ethanol-water mixtures. *Front Chem China* 4:438–442
44. Cooper CR, Spencer N, James TD (1998) Selective fluorescence detection of fluoride using boronic acids. *Chem Commun* 1365–1366
45. Ingle JD Jr, Wilson RL (1976) Difficulties with determining the detection limit with nonlinear calibration curves in spectrometry. *Anal Chem* 48:1641–1642